0/29/91gs (1)

PNL-7830 Vol. 1
UC-245

Subcontractor Report

Development of an Extruder-Feeder Biomass Direct Liquefaction Process

Final Report, Volume 1: Parts 1 - 3

October 1991

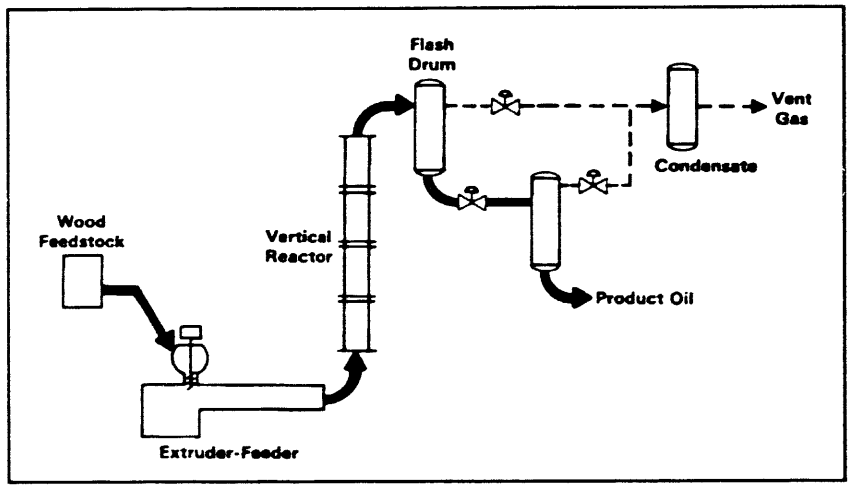

Prepared for the U.S. Department of Energy
under Contract DE-AC06-76RLO 1830

Pacific Northwest Laboratory
Operated for the U.S. Department of Energy
by Battelle Memorial Institute

Battelle

PNL-7830

DISTRIBUTION OF THIS DOCUMENT IS UNLIMITED

DISCLAIMER

This report was prepared as an account of work sponsored by an agency of the United States Government. Neither the United States Government nor any agency thereof, nor Battelle Memorial Institute, nor any of their employees, makes **any warranty, expressed or implied, or assumes any legal liability or responsibility for the accuracy, completeness, or usefulness of any information, apparatus, product, or process disclosed, or represents that its use would not infringe privately owned rights.** Reference herein to any specific commercial product, process, or service by trade name, trademark, manufacturer, or otherwise does not necessarily constitute or imply its endorsement, recommendation, or favoring by the United States Government or any agency thereof, or Battelle Memorial Institute. The views and opinions of authors expressed herein do not necessarily state or reflect those of the United States Government or any agency thereof.

PACIFIC NORTHWEST LABORATORY
operated by
BATTELLE MEMORIAL INSTITUTE
for the
UNITED STATES DEPARTMENT OF ENERGY
under Contract DE-AC06-76RLO 1830

Printed in the United States of America

Available to DOE and DOE contractors from the Office of Scientific and Technical Information, P.O. Box 62, Oak Ridge, TN 37831; prices available from (615) 576-8401. FTS 626-8401.

Available to the public from the National Technical Information Service, U.S. Department of Commerce, 5285 Port Royal Rd., Springfield, VA 22161.

PNL--7830-Vol.1

DE92 003845

DEVELOPMENT OF AN EXTRUDER-FEEDER BIOMASS DIRECT LIQUEFACTION PROCESS

Final Report; Volume 1: Parts 1-3

Work Period: 1978 - 1988

D. H. White and D. Wolf

Department of Chemical Engineering
University of Arizona
Tucson, Arizona 85721

G. F. Schiefelbein, PNL Project Manager

October 1991

Prepared by the University of Arizona for
Pacific Northwest Laboratory Under Contract
DE-AC06-76RLO 1830 with the U.S. Department
of Energy under Agreement 006249-A-Q

Pacific Northwest Laboratory
Richland, Washington 99352

MASTER

DISTRIBUTION OF THIS DOCUMENT IS UNLIMITED

DEVELOPMENT OF AN EXTRUDER-FEEDER BIOMASS DIRECT LIQUEFACTION PROCESS

ABSTRACT

As an abundant, renewable, domestic energy resource, biomass could help the United States reduce its dependence on imported oil. Biomass is the only renewable energy technology capable of addressing the national need for liquid transportation fuels. Thus, there is an incentive to develop economic conversion processes for converting biomass, including wood, into liquid fuels. Through research sponsored by the U.S. Department of Energy's Biomass Thermochemical Conversion Program, managed by Pacific Northwest Laboratory (PNL)[(a)], the University of Arizona has developed a unique biomass direct liquefaction system. The system features a modified single-screw extruder capable of pumping solid slurries containing as high as 60 wt% wood flour in wood oil derived vacuum bottoms at pressures up to 3,000 psi. By comparison, conventional pumping systems are capable of pumping slurries containing only 10-20 wt% wood flour in wood oil under similar conditions.

The extruder-feeder has been integrated with a unique reactor by the University of Arizona to form a system which offers potential for improving high pressure biomass direct liquefaction technology. The extruder-feeder acts simultaneously as both a feed preheater and a pumping device for injecting wood slurries into a 3,000 psi pressure reactor in the biomass liquefaction process.

An experimental facility was constructed at the University during 1983-84. Following shakedown operations, wood crude oil was produced by mid-1985. During the period January 1985 through July 1988, a total of 57 experimental continuous biomass liquefaction runs were made using White Birch wood feedstock. Good operability was achieved at slurry feed rates up to 30 lb/hr, reactor pressures from 800 to 3,000 psi and temperatures from 350°C to 430°C under conditions covering a range of carbon monoxide feed rates and

(a) Operated for the U.S. Department of Energy by Battelle Memorial Institute under Contract DE-AC06-76RLO 1830

sodium carbonate catalyst addition. Crude wood oils containing as little as 6-10 wt% residual oxygen were produced.

The work is reported in two volumes. Volume 1 contains the Executive Summary, Parts 1 through 3 which cover development and scale-up of the extruder-feeder, and Appendices A through C. Volume 2 contains Parts 4 through 8 covering the design, construction and operation of the continuous liquefaction unit, characterization of the wood oils produced and conclusions and recommendations. Volume 2 also contains Appendix D, which presents experimental data on the test runs conducted in the experimental liquefaction facility.

ACKNOWLEDGEMENTS

This research project and final report was produced by a research team in the Department of Chemical Engineering, University of Arizona, Tucson, Arizona, supplemented by subcontract research at the University of Lowell and special tests by other organizations. The material in this report is the result of efforts by many team members and we wish to express our gratitude. We wish to thank the sponsors for their wholehearted support over the 11-year period, especially Simon Friedrich of the U.S. Department of Energy and Gary Schiefelbein and Don Stevens of Pacific Northwest Laboratory.

PART 1

Major Investigators: Dr.. Don H. White, Dr. David Wolf, Dr. Nick R. Schott, A. Homaidan, I. Iregbulem.

Other Contributors: M. Ghoddoussi, A. Haddad, J. Hagen, L. Hampel, V. Joshi, D. Kaufman, D. Schott, S. Gonzales.

PART 2

Major Investigators: Dr. Don H. White, Dr. David Wolf, Dr. Nick R. Schott, M. Chehab, A. Haddad, A. Lezzar, L. Yang.

Other Contributors: L. Hampel, D. Schott, S. Gonzales.

PART 3

Major Investigators: Dr. Don H. White, Dr. David Wolf, Dr. Nick R. Schott.

Other Contributors: A. Homaiden, M. Chehab, A. Lezzar.

PART 4

Major Investigators: Dr. Don H. White, Dr. David Wolf, Dr. Nick R. Schott, M. Moghaddan, M. Khan, N. Andrews, D. Joshi, B. Reyes, J. Wong.

Other Contributors: H. Elliott (Construction Supervisor), J. Southwell (Plant Supervisor), D. Arbo, J. Arrizon, B. Benard, R. Robles, P. Wood.

PART 5

Major Investigators: Dr. Don H. White, Dr. David Wolf, D. Joshi, B. Reyes, J. Wong, G. Davenport, S. Mathews, Y. Zhao.

Other Contributors: P. Wood (Plant Supervisor), D. Arbo, J. Arrizon, B. Benard, T. Bingham, F. Holmes, J. Southwell, M. Porter, L. York, M. Folkerts, G. Hopper, J. Risser, K. Stuffle.

PART 6

Major Investigators: Dr. Don H. White, Dr. David Wolf, J. Wong, B. Reyes, D. Joshi, G. Davenport, S. Mathews, Y. Zhao.

Other Contributors: M. Porter (Plant Supervisor), S. Risser, K. Stuffle, L. York, R. Felty, W. Clemons, C. Chen, R. Felty, A. Maya, T. Kuhl, J. Hawkins, D. Sabalesky.

PART 7

Major Investigators: Dr. Don H. White, Dr. David Wolf, Y. Zhao, R. Cranford.

Other Contributors: Dr. Don H. White, Dr. David Wolf.

CONTRIBUTING ORGANIZATIONS

1. University of Lowell

   Scale-up data and calculations, experimental data upon Plasticorder work, viscous dissipation and Instron capillary rheology for model PE fluids and wood flour slurries.

2. Pacific Northwest Laboratory

   Analysis and properties of Albany TR-9 and TR-12 crude wood oils, analytical assistance.

3. Rensselaer Polytechnic Institute

   Surface friction coefficients for wood flour slurries and related materials.

4. HPM Corporation

   Experimental scale-up data on a larger single screw extruder for wood flour slurries, operating and cost data on large single screw extruders.

5. Werner & Pfleiderer Corporation

   Evaluation of wood flour slurry extrusion in a twin screw extruder.

6. Solar Energy Research Institute

   Pyrolysis mass spectroscopy upon University of Arizona wood oils and Albany vacuum bottoms.

7. Berstorff Corporation

   Operating and cost data on large single screw extruders.

8. Davis-Standard Division, Crompton & Knowles Corporation

   Operating and cost data on single screw extruders.

9. Farrel Corporation

   Operating and cost data on large single screw extruders.

10. Midland Ross Company

    Operating and cost data on large single screw extruders.

11. Welex, Inc.

    Operating and cost data on large single screw extruders.

12. Exxon Chemical Company

    Sharing information on high-pressure liquefaction equipment.

13. Hydrocarbon Research, Inc.

    Sharing information on high-pressure liquefaction equipment.

14. Sandia Laboratories

    Supported Dr. White as a visiting professor for two summers to assist and exchange technology on laboratory pilot plant scale for coal liquefaction.

15. U.S. DOE North Dakota Laboratory

    Sharing information on high-pressure liquefaction equipment.

16. Colorado School of Mines

    Sharing information on high-pressure liquefaction equipment.

17. Laramie Bureau of Mines

    Sharing information on high-pressure liquefaction processes.

18. University of Utah

    Sharing information on high-pressure liquefaction equipment.

19. University of California LBL Laboratories

    Sharing information on biomass liquefaction processes.

20. Rust Engineering

    Sharing information on biomass liquefaction processes.

21. Autoclave Engineers, Inc.

    Sharing information on high-pressure liquefaction equipment, especially autoclaves, valves and seals.

22. Fluor Corporation

    Review of extruder-feeder biomass liquefaction unit design.

23. Union Oil Company

    Sharing information on vacuum distillation of heavy oils to produce vacuum bottoms.

24. Chevron Oil Company

    Sharing information on vacuum distillation of heavy oils to produce vacuum bottoms.

25. National Institute for Petroleum and Energy Research

    Sharing information on vacuum distillation of heavy oils in Pope Vacuum Stills.

DISCLAIMER

The contents of this report are offered as information. The University of Arizona and all technical sources referenced in this report do not (a) make any warranty or representation, expressed or implied, with respect to the accuracy, completeness, or usefulness of the information contained in this report, or that the use of any information, apparatus, method, or process disclosed in this report may not infringe on privately owned rights; (b) assume any liabilities with respect to the use of, or for damages resulting from the use of, any information, apparatus, method, or process disclosed in this report. This report does not reflect official views or policy of the above-mentioned institution. Mention of trade names or commercial products does not constitute endorsement or recommendation for use.

CONTENTS

Volume 1

Volume 2

EXECUTIVE SUMMARY

DEVELOPMENT OF EXTRUDER-FEEDER BIOMASS DIRECT LIQUEFACTION PROCESS

DEVELOPMENT OF EXTRUDER-FEEDER BIOMASS DIRECT LIQUEFACTION PROCESS

EXECUTIVE SUMMARY

Biomass, including wood, could provide liquid fuels on a regional basis if an economic liquefaction process can be developed. Through research sponsored by the U.S. Department of Energy (DOE), under its Thermochemical Conversion Program managed by Pacific Northwest Laboratory (PNL), the University of Arizona has developed a unique method of pumping concentrated, viscous biomass slurries, characteristic in biomass direct liquefaction systems. A modified single-screw extruder has now been shown to be capable of pumping solid slurries as high as 60 wt. % wood flour in wood oil derived vacuum bottoms, as compared to only 10-20 wt. % wood flour in wood oil by conventional pumping systems (White and Wolf, 1981).

A Phase II program has integrated the extruder-feeder pumping system with a unique reactor which offers potential for further improving direct biomass liquefaction technology (White, 1983). An experimental facility was constructed during 1983-84, shakedown operations were conducted, and wood crude oil produced by Mid-1985 (White and Wolf, 1985). During the period January, 1985-July, 1988, a total of 57 experimental continuous biomass liquefaction runs were made using White Birch wood feedstock. Good operability with feed rates up to 30 lb/hr covering a range of carbon monoxide, sodium carbonate catalyst, pressures from 800 to 3,000 psi and temperatures from 350°C to 430°C was achieved. Crude wood oils containing 6-10 wt.% residual oxygen were reported by Zhao (1987). Other wood oil characteristics were reported. During the period May, 1987 through September, 1988, an All-Arizona wood oil was produced, using no outside source of materials.

INTRODUCTION

The modified extruder-feeder has now been shown to be capable of pumping slurries as high as 60 wt. % wood flour. The ability to handle such concentrated slurries which are in solid form at ambient temperatures is expected to improve direct liquefaction wood oil quality and process economics. Various preliminary process design and economic studies indicate that the utilization of the newly-developed extruder-feeder in biomass direct liquefaction processes could lead to one or more of the process improvements listed below:

1. Elimination of recycle wood oil (or dramatically reducing it), which should result in less coke formation and better quality wood oil.

2. Attainment of reactor temperature almost instantaneously, by the preheating in the extruder-feeder and then injecting superheated steam at the inlet of the vertical reactor.

3. Attainment of near-plug flow in the reactor with or without the use of static mixers.

The extruder-feeder acts simultaneously as both a feed preheater and a pumping device into a 3,000 psi pressure reactor in the biomass liquefaction process. It could prove to be of importance in other processes where high concentration of solids in liquids are to be handled.

This DOE-sponsored project was temporarily shut down and partially-mothballed on June 30, 1989, due to lack of funding.

I. DEVELOPMENT OF EXTRUDER-FEEDER

This project was initiated on January 1, 1978 to prove the feasibility of pumping 50 to 70 weight percent wood flour slurries into 3,000 psi direct liquefaction systems. The fundamental principle involved recycling 30-40 high-viscosity wood oil vacuum bottoms (properties similar to petroleum asphalt) with the 50-60 wt.% wood flour (WF) of fresh feedstock, by means of a modified single-screw plasticating extruder. The high drag flow generated by this system generated the necessary outlet pressure of 3,000 psi or higher.

An existing plasticating extruder in the Department of Chemical Engineering, University of Arizona was utilized to prove this principle, (a) using polyethylenes as model feedstock components in place of real wood oil vacuum bottoms, and (b) using a pressure let-down valve at the extruder outlet in place of a real biomass liquefaction reactor. The feasibility was achieved within the first nine months and work was immediately initiated to obtain detailed rheology data.

The first two years of work were sponsored by the DOE by Contract through the DOE Contracts office at Oak Ridge, Tennessee. This work was completed during the calendar year 1980 under the DOE-funding of a second contract, namely, Subcontract B-96249-A-Q, managed by Pacific Northwest Laboratory, Richland, Washington.

II. ECONOMIC ANALYSIS OF PRELIMINARY WORK

Technical data and cost estimations were prepared to show the economic potential of the biomass extruder-feeder under development for use in biomass liquefaction processes. It became evident early in this work, that it was necessary to consider the entire feeder-preheater-reactor system in order to see the full potentials of the extruder-feeder. It was called a system, rather than a process, because it is only part of a process.

In summary, it was shown that the extruder-feeder-preheater-reactor system has the following technical and economic advantages (White and Wolf, 1981):

1. It reduces the heating load on the liquefaction preheater and reactor from the range of 65,000 to 91,000 Btu per unit of 52.4 pounds crude wood oil product, compared with 160,000 to 200,000 Btu for the PERC system and about 350,000 Btu per 52.4 pounds product for the LBL system. This means that only a small fraction of the fuel value energy of the feedstock wood flour is needed for this critical heating load.

2. The estimated capital investment for the extruder-feeder-preheater-reactor system for a 3,000 barrel per day crude wood oil commercial plant is about $12,000,000, compared with $14,000,000 for the PERC system and $21,840,000 for the LBL system (based on 1981 economics).

The technical feasibility and operability of the extruder-feeder was proven as follows:

1. The vacuum bottoms from the Albany fractionator have been shown to be an excellent carrier for the wood flour feedstock.

2. The viscous dissipation of the vacuum bottoms (internal friction) was shown to be some 20 to 30-fold less than viscous plastics, and hence require less than half of the horsepower (Hp) needed for low-density polyethylene. In fact, only about one-fourth as much Hp is needed for pumping the wood flour slurry into a 3,000 psi pressure reactor and the other one-fourth is used to preheat the slurry from 25°C to 150°C.

3. Due to the viscous dissipation of 50 to 60 wt. % WF/vacuum bottom slurries being so much less than plastics, the extruder can be operated at a much higher screw rpm. This means that a given extruder can have a much higher capacity for a given capital investment. Only a small fraction of this potential was scaled to the commercial size units for the preliminary economy study.

4. The extruder feeder-preheater-reactor system is the only known system which has the potential of circulating hot reactor effluent back to the feedstock without reducing pressure, because it does not need a low-viscosity oil to dilute the wood flour slurry for proper pumping.

5. The extruder-feeder has proven to have much flexibility, both in design factors and operating factors. Design factors include extruder size (sizes available up to 24-inch diameter), screw compression, screw pitch, channel depth and screw speed. Operating factors include screw speed, temperature profile, slurry concentration and carrier oil viscosity. In other words, a choice can be made of several different combinations of these factors, for a given process for oils from biomass.

6. The extruder-feeder-preheater-reactor system is the only known system that can recycle the heavy ends of liquefaction products, and thus offer the potential of converting these ends to a lighter, less-viscous, more-useful product. Exxon has recently discovered that this is advantageous in coal liquefaction, resulting in higher overall yields of light oils.

7. The operability of the extruder-feeder has proven to be very reliable. There is no plugging from even concentrated slurries, and outlet pressures and temperatures can be closely controlled. Thus, this system appears to be well-adapted for a continuous process, especially where temperature and residence time should be closely controlled.

III. DESIGN OF SMALL-SCALE CONTINUOUS BIOMASS EXTRUDER-FEEDER LIQUEFACTION SYSTEM

During the period November 1, 1981 - January 31, 1982, a detailed design was completed for a system to operate the extruder-feeder with a reactor for biomass liquefaction. The unit was designated the Extruder-Feeder-Preheater-Reactor System.

DESIGN APPROACH

The detailed design was made by the Biomass Extruder-Feeder Research Group at the University of Arizona, under the direction of Dr. Don H. White. However, the approach was to take advantage of the expertise of many other groups.

A summary of this approach is as follows:

1. A thorough review of the biomass liquefaction data in reports and the literature, especially by Rust Engineering and Bechtel in operating the Albany, Oregon facility, and also Pacific Northwest Laboratory, LBL at Berkeley, SRI International and Econergy Associates, as well as the exploratory data of the University of Arizona.

2. A review of critical items developed by various coal liquefaction projects, especially EDS by Exxon, SRC-I and SRC-II by Gulf Oil and others, H-Coal by Hydrocarbon Research, Inc. and the laboratory studies by Sandia Labs, North Dakota DOE Labs, Laramie Bureau of Mines and the University of Utah.

3. Worked closely with three key University of Arizona groups, namely, the High-Pressure Laboratory personnel, the design section of the Division of Physical Resources and the Department of Risk Management and Safety.

4. Visitations by Dr. White to LBL laboratory biomass liquefaction facilities, Berkeley, California and Exxon coal liquefaction pilot plant and laboratory facilities, Baytown, Texas.

5. Consultations in Tucson with two key engineers from Autoclave Engineers, Inc., design engineers and manufacturer of high-pressure systems.

6. Consultation by Dr. White with the Fluor Corporation, a major design and construction company in the process industries. This meeting was held in Los Angeles on September 14, 1981.

OVERALL DESIGN BASIS

The major objective of the project was to connect the extruder-feeder to a laboratory reactor, operating with wood flour feedstock to produce a wood oil product by liquefaction. Therefore, it was desirable to design and construct a unit that would demonstrate the feasibility of the Extruder-Feeder-Preheater-Reactor System.

The overall design premises are summarized herein. Details on assumptions and design premises were listed. The general premises which constitute the basis of the design were as follows:

1. Use much of the existing extruder-feeder equipment and related facilities, existing at the University of Arizona.

2. Place the operating system in the University High-Pressure Laboratory, which is in an off-campus building but within five miles of the Department of Chemical Engineering.

3. Keep the operating system as simple as possible to enhance operability. It was limited basically to the extruder-feeder, preheater, reactor, hot recycle pump, CO compression and two automatic process control valves.

4. Operate the unit in a continuous mode (but each run in terms of hours, not days) behind the barrier separating the bunker room from the rest of the building in the High Pressure Laboratory.

5. Design for start-ups using Albany wood oil, but providing startup oils in case there is not sufficient Albany wood oil on hand.

6. Select a vertical reactor, similar to those developed in coal liquefaction, first by Exxon, and later on by Gulf Oil and others.

7. Design the system so that two important features can be demonstrated, namely:

   a. The feasibility of the extruder feeding a real reactor, and
   b. The feasibility of recycling hot oil for 2-fold to 3-fold energy savings, which inherently can be achieved only by a device such as the extruder that can pump 50 to 60 wt. % wood flour into a pressure system.

DETAILED DESIGN OF EXTRUDER FEEDER-PREHEATER-REACTOR SYSTEM

The simple design described above went through several iterations and interactions with Battelle PNL personnel. Eventually the design evolved to that described below (White, 1983).

Design Criteria

The objective was to design a reactor in conjunction with the University of Arizona extruder to produce a pilot plant system capable of making wood oil and heavy vacuum bottom fuel products from a wood flour feedstock. Under continuous funding since 1978, the University of Arizona has shown that a modified single screw plasticating extruder is a good pressure feeding and preheating device for wood flour slurries.

The design was based on the following requirements: The reactor must be mounted to the University extruder and it must be scaled for a residence time based on the minimum and maximum output rates of the extruder. These flow rates are approximately 7 lb/hr to 40 lb/hr. The unit must be capable of generating pressures up to 3,000 psi and the reactor temperature must be maintained at 310 to 370°C. The main factors governing the size of the system is the average residence time of the reactor. This time is based on the average volumetric flow rate of the wood flour, vacuum bottom carrier, chemical additives, and wood oil diluent to control reactor viscosity. Residence times of 18 minutes to 2 hours were estimated for the mass flow rates encountered. The times are based on a single size reactor volume of 1.0 ft^3 which would accommodate various modes of operation, within the range of residence time.

SUMMARY PROCESS DESCRIPTION

Overall Description

An advanced extruder-feeder biomass liquefaction reactor system was designed to experimentally convert wood flour to liquid wood oil fuels by direct liquefaction. The extruder-feeder system developed at the University of Arizona is incorporated into the system to develop 3,000 psi pressure at its discharge and preheat the slurry prior to entering the vertical reactor, as shown in Figure ES-1. As the wood flour slurry of up to 60 wt% solids in a liquid carrier enters the reactor it is mixed with superheated steam and carbon monoxide. The following carriers were used in the course of this work (a) asphalt, (b) Albany vacuum bottoms (c) Albany TR-9 and TR-12, and (d) recycle of our let-down liquid product effluent. The superheated steam is used to heat the wood flour slurry to the reaction temperature of 350°C which is then maintained by the use of electrical band heaters surrounding the reactor. Steam and carbon monoxide serve as (a) reactants for the liquefaction process, and (b) react via the water-gas shift reaction to provide hydrogen for the liquefaction process. The liquefaction products are split into the vapor phase which is condensed by the condenser in the off-gas line where an oil condensate is obtained and liquid fractions cooled down and brought to atmospheric pressure by means of the let-down pressure system. This liquid product is then vacuum distilled to produce the major wood oil product. Computer control and real-time data acquisition have been implemented for the unit.

The various equipment components as shown in Figure ES-1 for the process are as follows (White and Wolf, 1985):

1. Feedstock drum with mixer.
2. Screw conveyer, 2-in. Dia. x 12 ft long, steel, 100 rpm.
3. Crammer-Feeder, 5 hp (DC Drive), 3.4 ft^3 total volume, 2.6 ft^3 operating capacity.
4. Extruder-Feeder, single screw 1.75" diameter, 15 hp, 3-phase, 220V, 5-160 rpm.
5. 10 cylinder battery rack and manifold, 175 SCF/cylinder; 1650 psig at 70°F.
6. Over-pressure relief valve, 2000 psig.
7. CO compressor, 2 stage, 10 hp, 3 phase, 220V, maximum discharge pressure 5250 psig, maximum flow rate 9 scfm.
8. Surge tank, 600 ft3.
9. Over-pressure relief valve, 5000 psig.
10. Masonelian Micropack 29000 series control valve and Omniflo turbine flow meter, C_v = 0.002 at 3200 psi, 700°F with electropneumatic transducer, Masonelian 8006A series, 4-20 mA input, 3-15 psig output.
11. Heat exchanger, 5.0 ft^2 double-pipe both sides high pressure, CO inlet 60°C, outlet 360°C.
12. Two distilled water holding drums, 55 gal. and 16 gal., steel.
13. Ion exchange column.
14. De-aerator, 8.5 gal. tank, 1.6 kw heater, 110 volt, 7 phase.
15. Treated water holding tanks, 10 gal. and 30 gal., SS.
16. Metering pump, 1 hp, 6.6 GPH at 4450 psi, 240V, 3-phase.

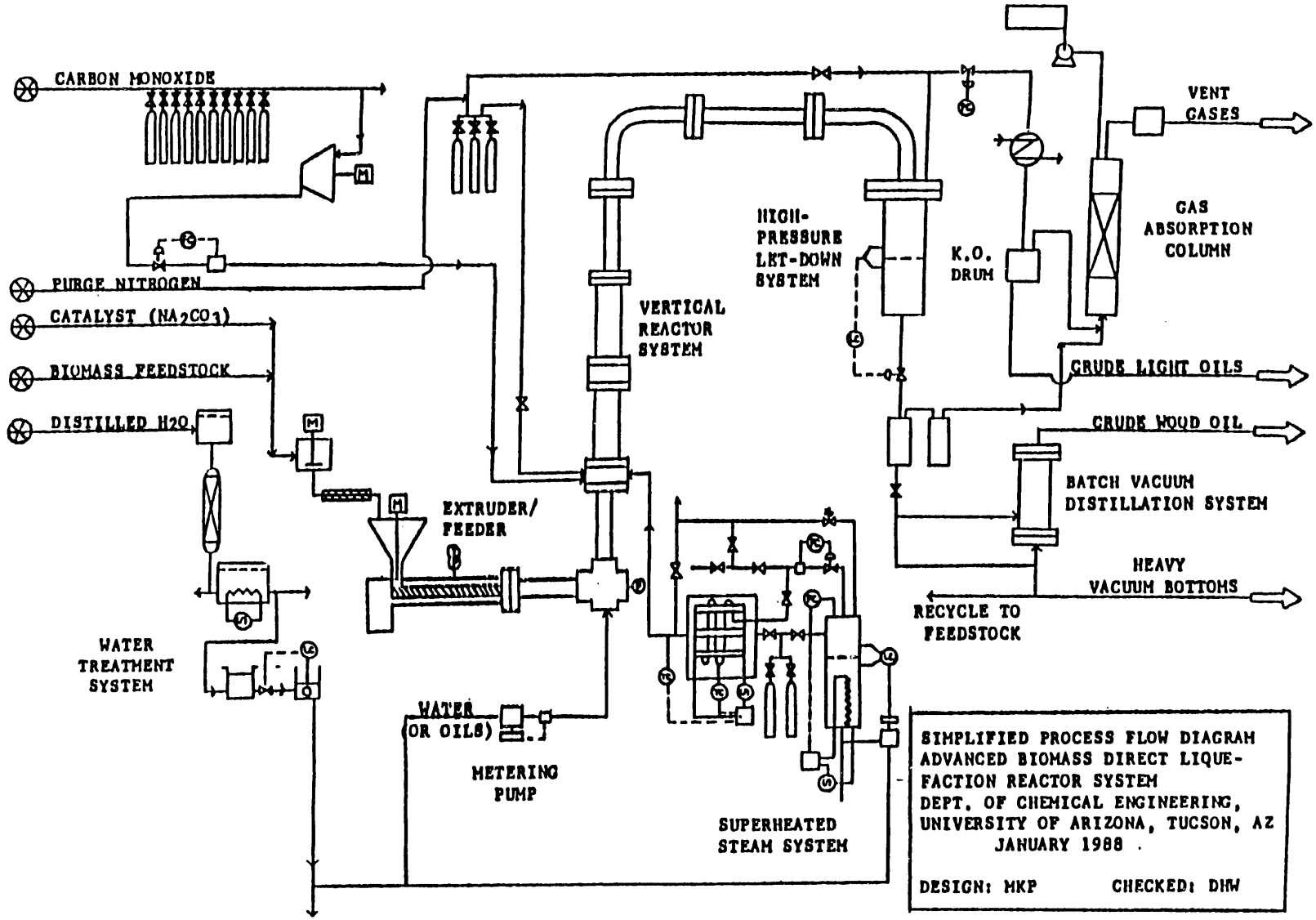

Figure ES-1. Process Flow Diagram of Extruder-Feeder Biomass Liquefaction Unit.

17. Vaporizer, Xalloy-lined steel, 3.5" ID, 3.5 gal., 3100 psia, 372°C, 15 kw heaters, 240 volt, 3-phase.
18. Argon purge system, 2 cylinders, 285 SCF/cylinder, 270°F, with rack and regulator.
19. Control valve, Masonelian model Wee Willie 6051, C_V 0.00001 to 0.01 at 32000 psi, 372°C, driven by Omniflo turbine flow meter and controller.
20. Steam Superheater, 1.0 ft^2 316 stainless steel/inconel 625 coil, 3100 psi, SiC heaters, 17kw, 240V, 3-phase and 120V, 1-phase.
21. Catalyst holding tank with mixer.
22. Metering pump, 3 hp, 3000 psig delivery pressure.
23. Solvent holding tank.
24. Metering pump, 3 hp, 3000 psig.
25. Flanged tee with static mixer elements, 1.75" ID with sparger, 316 stainless steel, 28" length, 18" offshoot, 3000 psig, 550°C.
26. Reactor consisting of, 4 flanged, Xalloy-line steel sections with static mixer elements, heaters and insulation. 1.75" ID; 3000 psig, 350°C.
27. High pressure let-down vessel, Xalloy-lined steel, 3000 psig, 350°C, 3.5' x 3.5" ID with differential pressure transducer for liquid level control.
28. Gas let-down control valve, Masonelian micropack 2900 series, Class 1500, C_V = 0.001.
29. Vapor condenser, double-pipe coiled type, 1.5 ft^2, inlet 350°C outlet 40°C.
30. Low pressure overhead flash drum, 6.5 gal. stainless steel class 150 flanged connections.
31. Control valve, 300 psi inlet, atmospheric pressure outlet.
32. Cold trap.
33. Product tank.
34. Liquid let-down control valve, Masonelian 3660-61 angle body control valve, Class 2500, C_V = 0.6.
35. Heat exchanger, inlet 350°C.
36. Low pressure flash drum, 100 gal., carbon steel, (Vessel 100°F, 875 psig) or at 200°C, 750°F, 495 psig) 400 psi.
37. Control valve, 400 psi inlet, atmos. pressure outlet.
38. Vapor condenser, 200°C inlet, 30°C.
39. Product tank.
40. Sampling system, dual in-line off/on solenoid valves, downstream normally closed, upstream normally open, stainless steel sample cylinders.
41. 4 flanged reactor spools, 6" long, 1.75" I.D. 7" O.D. with sampling and injector ports.

Extruder-Feeder System

The feeding section of the system consisted of mixing equipment, a screw conveyer, and an extruder-feeder. A feedstock drum mixes the wood flour and the brittle granular vacuum bottoms carrier into a solid mixture which is then transported by a screw conveyer to the extruder-feeder at a continuous feeding rate. The single screw extruder of 1.75-inch diameter and 24:1 L to D ratio is designed to generate 3,000 psi with flow rates over a range of about 5 to 30 lb./h. The extruder-feeder also acts as a preheater, normally to 150°C, but if desired up to 250°C. The preheating temperature is a function of the feedstock composition.

Carbon Monoxide System

The carbon monoxide section is a bank of CO cylinders with a booster compressor to obtain the desired pressure. The carbon monoxide from the multi-cylinder battery is being fed to a two-stage, 10 hp compressor which provides up to 40 lb./h of CO at approximately 5,000 psi. The high-pressure CO is then fed to the bottom of the reactor. A unique and novel control system which we have developed in the course of this work and which is operated by the computer regulates the CO flow rate to the reactor.

Super heated Steam System

The steam superheater system is composed of a section that provides high-purity water, a vaporizer and a superheater. The steam superheater is designed to deliver 40 lb./h of superheated steam at around 800°C and 3,100 psi. Distilled water is purified by ion-exchange and degassed before feeding it to the vaporizer. Steam flows through a control valve to the superheater where it is heated to above 800°C. High-temperature corrosion is minimized by keeping an argon atmosphere in the superheater "furnace" chamber. The flow control system for the steam is similar to that developed and used by the CO flow control system. The level of water in the vaporizer is controlled by a nuclear level controller self designed and constructed of University of Arizona available equipment.

Sodium Carbonate Catalyst System

The sodium carbonate catalyst injection system provides flexibility for experimental purposes. Three systems for introduction of Na_2CO_3 were tested: (1) One is soaking the wood flour with a Na_2CO_3 solution; (2) introduction of solid Na_2CO_3 with the solid feedstock; (3) direct injection system of an aqueous solution of Na_2CO_3 using a high-pressure metering pump. The first method was finally chosen and used during the majority of the experiments made.

Solvent Flush System

A solvent flush system has been considered for use during shutdown to flush the reactor with solvent in order to clean it for the next run. Alternatively, hold-up of the reactor can be emptied just by heating the reactor and blowing out the contents. However the method finally adopted was to replace the reactor hold-up at the end of the experiments by a lower viscosity feedstock which would enable an easy restart of the unit after heating it up to the operational temperatures.

Gas Dispersion System

A series of gas dispersion elements have been tested to disperse superheated steam and carbon monoxide into the viscous wood flour slurry. The initial design was a mixing tee, connecting the vertical reactor with the extruder-feeder. However the various ports in the spools between reactor sections were also tested as feeding options. Finally the introduction of these gases were made through ports in the bottom flange of the reactor.

Vertical Reactor Systems

A vertical reactor system of about 11 feet in height has been constructed of two used extruder barrels of 1.75" diameter. These are steel flanged sections with Xalloy-lining and can withstand pressures of 10000 psi and more. The flanged sections connect the unit to the extruder-feeder on one end and to the let-down vessel on the other. The two sections are interconnected by spools which allow gas injection and reactor sampling. Electrical heater bands are utilized in order to maintain the required reaction temperature in the reactor. In order to increase the reactor throughput and to study a wider range of residence times, two more flanged sections are available which could be added to the reactor system at a later date.

Pressure Let-down System

The pressure let-down system consists of two stages of lowering the pressure. However, only the first stage was installed. The first stage is a used extruder barrel with 3.5" inside diameter and 12:1 L to D ratio. The let-down system has two purposes: (a) to regulate the reactor pressure at 3,000 psi, and (b) to split the product into its vapor and liquid fractions to be collected at atmospheric pressure. The pressure of the reactor and the let-down vessel is controlled at 3,000 psi by the rate of release of gases. The gases are released through a computer controlled valve in the off-gas line located after the condenser and before the gas absorber. The non-condensed gases are metered, prior to venting to the stack. The liquid level in the let-down vessel is maintained by the withdrawal of liquid products through a control valve at the bottom of the vessel.

Product and Process Sampling

Liquid product sampling could be taken from the ports of the spools of the reactor but basically they were taken from the let-down product effluent. Also liquid product in form of condensate was taken from the condenser effluent. The gas samples were taken from the vent lines of the let-down system and were collected in evacuated sampling bottles. Special badges were worn for CO monitoring and for radioactive measurements. Also a CO alarm system was installed.

Real-Time Microprocessor Control System

A real-time digital microprocessor control system was designed and installed, so that the experimental unit can be operated remotely. It consists of an IBM PC and OPTO-22 hardware interface. The software used was the FIX program acquired from the Intelution Corporation. The selection of this system was based on our initial development of the control algorithms and the experiences gained with them. The let-down system control valves, the steam superheater flow control valve, the CO flow control valve, the reactor temperature control heaters and reactor pressure are controlled by this real-time control system. The input signals are feeding the computer from various pressure, temperature and flow transducers for the control and data acquisition purposes. Provision has been made for eventual flow control of feed by adjustment of the extruder-feeder screw rpm. The extruder-feeder is presently fixed at a desired RPM and is monitored by an ampermeter available on the unit and in the control room. The RPM of the

screw can also be set remotely from the control room. The computer controlled system is presently configured for 16 PID controllers and real-time data acquisition.

Feedstock preparation

The wood flour is being pretreated before mixing it with the carrier as follows. Some 20-25 wt% of water is being mixed with 75-80 wt% of wood flour and then heated in an oven for about 24 hrs. The water usually contains some 5 wt% of sodium carbonate based on the dry wood flour. The pretreated wood flour is then mixed with the carrier at the desired proportions. Sometimes this mixture is being run through the extruder-feeder in order to obtain homogeneity of the feedstock.

IV. MODIFIED DESIGN AND ESTIMATION OF CAPITAL REQUIREMENTS

During the first part of 1983, the conceptual design of the direct biomass liquefaction experimental unit was finalized and documented (White, 1984). As the groundwork for the experimentation area continued, the basic equipment for the experimental unit was ordered and parts of the unit started to arrive during the second half of 1983. This phase II of work on the project also included changes and improvements in the conceptual design as well as detailed design of the various parts of the experimental unit, especially as more experience was gained during preliminary operations with the laboratory Prodex extruder-feeder and more details were obtained on the availability of equipment and instrumentation. Also, some more process simulation experiments were made in the laboratory in order (a) to supply design data not available in the literature or (b) to back-up some of the literature data that were obtained at somewhat different conditions than those prevailing at our process. Details on these various aspects of studies can be found in the M.S. thesis by Quevedo (1981), Iregbulem (1982), Chehab (1982), and Joshi (1983). Among the model compounds we used, we should mention some viscous oils like glycerol and especially the low viscosity polyethylenes that simulate quite well the feedstock material to be used in the experimental stages of the project. This preliminary work was especially important for the development of the pumping conditions of the highly concentrated wood flour slurries by the extruder-feeder and for the determination of the pressures to be developed by the extruder-feeder during the various operating conditions and various feedstock compositions and slurry concentrations. More details on an extruder-feeder operation can be found in the M.Sc. thesis by Homaidan (1984). The Rheological properties of various materials can be found in the M.Sc. thesis by Haddad (1983), Chehab (1982), and Lezzar (1983).

Analytical work was also done in parallel with the detailed mechanical designs, especially on the process control, instrumentation and data-acquisition aspects of the project. The first goal of these studies was to understand the dynamics of the system so as to be able to write the proper control algorithm for the control strategy and data acquisition. A full description of this work can be found in the M.Sc. thesis by Andrews (1984). Additional analytical work was done (a) on the mixing theory for various mixing devices, (b) on the residence time distribution effects, and (c) on the mechanisms of bubble formation and gas dispersion, including mathematical simulation, especially in highly-viscous medium. A complete study of the mechanism of bubble formation and gas dispersion can be found in the M.Sc. thesis by Kahn (1984).

One of the major parts of the experimental unit is the steam superheater. At the end of 1983, the design was completed and documented and procurement of equipment was started. Also, a computer simulation program was run on the steam superheated system in order to check the design and performance. The full design of the description of the superheated steam unit can be found in the M.Sc. thesis by Reyes (1985). Another major part of the unit is, of course, the reactor. A revised reactor system design was made before it was finalized and the equipment, like reactor sections, spools, and flanges, were ordered. During 1984, much of the equipment arrived and construction, as well as shake-downs, have started. This refers to units like the extruder-feeder, the crammer-feeder, the CO compressor, and the steam superheater. The shake-downs were possible as the required additional electrical power of 3-phase, 240-volt and 200 amp was finally supplied at the high-pressure laboratory. Also, all the necessary wiring and power distribution panel inside the control room was accomplished. At this stage of the project, experimental work was also done on viscosity measurement of oxidized TR-12 Albany wood oil, which was to be used as carrier for the feeding of wood flour. The measurements were made using a Hooke Rotovisco RV-3 and viscosities vs. shear rates were obtained. Upon the arrival of the Killion-type extruder-feeder and its installation at the high-pressure lab, experimentation with this unit was started in order to establish its operability. Flow rates as a function of rpm and pressures developed at various operating conditions were determined. These preliminary tests were made with low-density polyethylene and with mixtures of wood flour and polyethylene. Also, a revision of the let-down system was made. Also, at this stage of the project, a review was done on the operational procedures and safety consideration for the experimental unit including start-ups, steady state operation, and shut downs. This was a revised version of the procedures suggested in 1982 and it was based on the new data, final design, and experimental experience to this date.

A literature review study on the structure of wood was made at this point for better understanding the process which we were to use in our experiments. Important data on wood and its characteristics were summarized. Data on Solvolysis of biomass can be found in the M.Sc. thesis by Moghaddam (1984). In order to be able to start the experimentation and characterize the feedstock and products, sampling and analysis methods were established in addition to the viscosity measurements mentioned above. Also, the equipment available in the teaching laboratory for control systems at the Department of Chemical Engineering at the UA was used to test by means of simulation the microprocessor control system and the PID algorithm derived. Details on the revised control system and algorithm can be found in the thesis by Joshi (1985) and by Wong (1986).

VI. SHAKE-DOWN OPERATIONS

With the start of the shake-down operation, procedures were established first for testing individual units and parts before the complete experimental unit was to be tested (White and Wolf, 1985). The various tests were made from relatively mild condition to the very harsh operating conditions to be used for the system, like 3,000 psi pressures and 375°C temperatures. The units tested were the extruder-feeder, the CO compressor, the control system and the steam superheater. Based on the experience gained during the shake-down stage, operating procedures and safety regulations were again reviewed for the general and overall approach to safety and especially with regard to mechanical, chemical, and health hazards. At the first stages of operation of the unit, only one stage of the let-down system was designed. This first stage of

let-down system is more critical than the second stage that was also introduced some time in the future. Parallel work was still proceeding with the gas dispersion simulation systems and experimental data were obtained on the effect of various parameters of the system on the dispersion. Also, additional theoretical work was done in order to understand better the water-gas shift reaction, the mechanics of biomass liquefaction and the kinetics of liquefaction. The shake-down of the whole system started in early 1985 and this included calibration of equipment, interaction between the various units, testing the dynamics of the system and making variations in the feedstock and the concentration of solids. Upon completion of the major aspects of the shake-down operation, experiments were started with petroleum asphalts as the initial carrier for the wood flour. Adaptation of the asphalt to the system was necessary due to its low softening point. This was achieved by cooling down the asphalt to freezing temperatures, thus making it brittle and thus operable. The first highlight occurred on March 26, 1985, when 3,000 psi pressures were obtained with the asphalt as a carrier and with a wood flour concentration of 50 wt.%. The shake-down experiments A1-A6 and the initial experiments B1-B3 and C1-C2 proved the feasibility of the process for the direct biomass liquefaction and the operability of the unit, although several improvements to the system were still necessary and were made at various times during the continuation of the project. Of special interest was the incorporation of a cooling system for the feeding part of the extruder-feeder and for the off-gas condensation heat exchanger. Tap water temperatures were not low enough for cooling purposes. More elements that needed improvements were heaters to the reactor, heating tracing on various lines, extruder-feeder operation in connection with the crammer-feeder, piping and connecting tubes and the let-down system. Also, several methods for feedstock preparation were considered.

VII. PRELIMINARY BIOMASS LIQUEFACTION RUNS

Supplements to Subcontract B-96249-A-Q were awarded in June, 1985, consisting of $1,000,000. This involved about $900,000 from Battelle PNL under its DOE Contract and about $100,000 of cost-sharing by the University of Arizona. However, due to the unavailability of full funding by the DOE/Battelle, the budgets were "spread out" over the period June 1985 through September 1988 with some of the funding never provided prior to when the experimental work was terminated.

Since flow conditions in the extruder-feeder and reactor are of great importance, a radioactive tracer technique was used to obtain information on the flow conditions in the system. As experience was gained with the operation of the system, experiments were made in order to study the effect of several parameters on the operation and wood oil production. Experiments D1-D2 are in this category and operational data were carefully recorded. At this stage, we decided to move to the Albany wood oil vacuum bottoms as the carrier for the wood flour. The first all-wood oil experiment was made on August 29, 1985 designated as experiment E1 and this was considered as another technical highlight of the project. For this experiment, full data was recorded and analytical work was done on the products such as heat of combustion, ultimate analysis, soxhlet extraction with THF and viscosity measurements. Additional experiments (F1 and F2) were made for testing some of the changes made in the system and in the operational conditions, especially with the aim to find ways to restart the unit after shut-down and cooling-down without having to clean-out the reactor (White and Wolf, 1985). During these experiments and also at later experiments, we progressively made the conditions harsher and harsher, and as

a consequence we had to constantly make changes and improvements in the experimental unit in order to overcome the various obstacles we faced.

VIII. PROVING PROCESS OPERABILITY UNDER FULL PRESSURES AND TEMPERATURES

The preliminary runs under Section VII were made at atmospheric pressure, with occasional operations with pressures up to 1,000 psi. This was necessary in order to make certain all process step were operable.

During 1986, the unit was in full operation and many sets of experiments were designed and performed (White and Wolf, 1987). Good operational conditions were achieved and reasonable data was obtained. Several parameters were checked during experiments G1-G4 and H1-H5 and good results were obtained, including acceptable material balances (White and Wolf, 1988). Also, gas chromatographic analysis of the off-gases were added to the analytical tests as well as analysis of the Sodium Carbonate and analysis of moisture. At this point, we had the experience and confidence to run the unit continuously for several days. Indeed, experiment I1 lasted 50 consecutive hours and it ran without problems until all the feedstock was exhausted. This was considered another important milestone in this project. Two additional experiments, J1 and J2, were made during 1985, winding up quite a significant number of experimental runs during this year. At this stage, vacuum distillation for obtaining distillate wood oil became important, and indeed the vacuum distillation unit which was acquired from Pope Scientific became available.

In order to complement the work done with the experimental unit, and especially to check specific problems, an autoclave unit was installed and experiments were made with this autoclave. More details on the autoclave work will be found in the M.Sc. thesis by Mathews. An additional type of analysis was used at this stage, namely NMR spectrometer for aromatic and aliphatic carbon determination. Runs J1 and J2 were made with asphalt as the carrier due to the lack of availability of other feedstock material and since the main objectives being the determination of flow conditions and flow rates, especially with regard to increased capacity of the unit.

As Arizona wood oil became available during the extensive runs of 1986, the characterization of the wood oil obtained was made in cooperation with Doug Elliott of Battelle and Thomas Milne of SERI. Again, IR and GC/MS measurements were added to the other type of analysis done so far. Full details on the various analytical methods used in this project can be found in the M.Sc. thesis by Zhao (1987). These analysis would supply data in Aromatic and aliphatic C-H bonds and the identification of the various compounds in the product. Also, work was started on Separation of phenolic fractions of the wood oil product for improved economics of the process. Details on this work will be found in the M.Sc. thesis by Cranford (1989).

IX. PREPARATION OF AN ALL-ARIZONA WOOD OIL

During 1987, an effort was started to produce a pure UA oil. For that purpose, the Pope vacuum distillation unit was put in operation in order to produce UA vacuum bottoms to be used as the carrier for the wood flour. Unfortunately, the glass-made distillation part of the unit broke beyond repair and another unit had to be built, this time out of metal, in order to be able to do

the vacuum distillation. Therefore, in the meantime experiments were scheduled and made with Albany TR-9 crude wood oil as the carrier, and the product of these runs to be used as is as carrier for second, third, and fourth recycle of the products. Experiments K1-K2, L1-L2, M1-M4 were all made for testing pumpabilities of this feedstock and for making the first round of product for the recycle purposes (White et al. 1987a,b,c,d). At this point, there was an opportunity to check the corrosion/erosion problems of the unit and embrittlement due to Hydrogen attack. Basically, no problems were detected from this point of view. Runs M1-M3 could be seen as a milestone since in these experiments we have achieved mass balance closures of around 95 percent (White and Wolf, 1988).

Experiments N1-N2 were long runs and they were made in order to produce large amounts of product for the recycling of this material as carrier for the second round (White et al. 1987c). The product of N1-N2 runs were used as the carrier for runs O1-O2, thus obtaining a second round of the material through the reactor or a first recycle of the product (White et al. 1987d). Not only were these runs successful and ran for long periods of time, but the continuation of Run O2 was a restart of the operation with the reactor full with material from Run O1 (White et al. 1987d).

The third round or second recycle with product of runs O1-O2 as carrier was then made and this run P1 lasted for 10 hours. Again the unit was restarted with material in it left from experiment O2. A fourth round or third recycle was attempted during 1987, and trial experiments P2-P4 were made. However, although it appeared to be operable, a good run could not be achieved, probably due to feeding problems of the very high concentration of solids. However, oil distilled from the product of run P1 could already be considered a good UA wood oil.

X. PRODUCTION OF WOOD OIL FOR EXPERIMENTS ON UPGRADING BY HYDROTREATING

Since we wanted more material and more recycles a thorough upgrading and improvement of the experimental system was made during the last part of 1987 and during the first part of 1988. This included a unique feeding system for CO and H_2, an upgraded computer control system with the "FIX" program as the software, the installation of a gas absorption unit, the improvement of the feeding system using a screw feeder, and the incorporation of a second let-down barrel. Details on the improved feeding system, the FIX program and the upgraded control hardware will be found in the M.Sc. thesis by Davenport (1988).

Experiments Q1-Q4 and R1-R3 were made as shake-down runs to test the unit after these changes were made. With this improved system, we made run R4 that lasted 17.5 hours and was a basic run with TR-9 as the carrier, so that more reactor effluent could be accumulated in order to be able to produce around 2-3 gallons of all UA wood oil, to be sent later to Battelle Laboratories for upgrading. Thus, the reactor effluent of run R4 was vacuum distilled with the newly constructed vacuum distillation unit and the vacuum bottoms after releasing some 10 wt.% of the light oil was mixed with reactor effluent of run P1 (which was three rounds in the system) and this mixture was the carrier for the wood flour. Thus, we accomplishing the fourth round or third recycle, which failed in 1987. Runs S1 and S2 processed successfully this feedstock and a reactor effluent with All-Arizona wood oil was obtained. Two gallons of wood oil were

obtained by vacuum distillation of this reactor effluent. Oxygen content of this oil was found to be of an average of 7 wt.%, which is another achievement of the project. At this stage we proved the feasibility of the technology that we have suggested for direct biomass liquefaction and a second phase of research and development is necessary in order to obtain fundamental data on the process, and the technology and optimum design data for this direct biomass liquefaction system.

REFERENCES

Andrews, N. A., "Microprocessor-based Real-Time Process Control of Biomass Liquefaction," M.S. Thesis in Chemical Engineering, University of Arizona, Tucson, Arizona. (1984).

Chehab, M., "The Rheology of concentrated Cellulosics Slurries", M.S. Thesis in Chemical Engineering, University of Arizona, Tucson, Arizona. (1982).

Cranford, R. J., "Separation of a Phenolic Fraction Concentrate from Biomass Liquefaction Oils," M.S. Thesis in Chemical Engineering, University of Arizona, Tucson, Arizona. (1989).

Davenport, G., "Development of Continuous Real-Time Computer-Control of a Biomass Liquefaction Process," M.S. Thesis in Chemical Engineering, University of Arizona, Tucson, Arizona. (1988).

Haddad, A., "Rheology and Extrusion Characteristics of L-LDPE", M.S. Thesis in Chemical Engineering, University of Arizona, Tucson, Arizona. (1983).

Homaidan, A., "Modified Extruder for Feeding Fine-Ground Cellulosic Slurries to Pressure Systems", M.S. Thesis in Chemical Engineering, University of Arizona, Tucson, Arizona. (1984).

Iregbulem, I. A., "On-Line Data Acquisition and Energy Balances for a Single-Screw Extruder", M.S. Thesis in Chemical Engineering, University of Arizona, Tucson, Arizona. (1982).

Joshi, V. H., "Acid-Hydrolysis of Biomass in an Extruder-Reactor", M.S. Thesis in Chemical Engineering, University of Arizona, Tucson, Arizona. (1983).

Joshi, D., "Real-time Digital Control for Biomass Liquefaction System", M.S. Thesis in Chemical Engineering, University of Arizona, Tucson, Arizona. (1985).

Khan, M. B., "Gas Dispersion in Highly Viscous Non-Newtonian Fluids using Extruder-Feeder", M.S. Thesis in Chemical Engineering, University of Arizona, Tucson, Arizona. (1984).

Lezzar, A., "Effect of Void volume on the Friction and Rheology of Concentrated Slurries", M.S. Thesis in Chemical Engineering, University of Arizona, Tucson, Arizona. (1983).

Mathews, S., "Laboratory Correlation of Experimental Parameters in Biomass Liquefaction", M.S. Thesis in Chemical Engineering, University of Arizona, Tucson, Arizona. (1990).

Moghaddam, M. G., "Solvolysis of Biomass at Elevated Temperatures", M.S. Thesis in Chemical Engineering, University of Arizona, Tucson, Arizona. (1984).

Quevedo, J. A., "Development of Stirred Near-Plug Flow High-Pressure Extruder-Reactor", M.S. Thesis in Chemical Engineering, University of Arizona, Tucson, Arizona. (1981).

Reyes, B. F., "Development of a High-Pressure, High-Temperature Superheated Steam System", M.S. Thesis in Chemical Engineering, University of Arizona, Tucson, Arizona. (1985).

White, D.H., D. Wolf, et al., "Modified Extruder for Feeding Fine-Ground Cellulosic Slurries to Pressure Systems," Proceedings of the 13th Biomass Thermochemical Conversion Contractor's Meeting, CONF-8110115, October 27-29, 1981 Arlington Virginia.

White, D.H., "Advanced laboratory-Scale Extruder-Reactor Biomass Liquefaction Unit," Proceedings of the 15th Biomass Thermochemical Conversion Contractors' Meeting, CONF-830323, March 16-17, 1983, Atlanta, Georgia.

White, D.H., "Development of Extruder-Feeder Biomass Liquefaction System," Proceedings of the 16th Biomass Thermochemical Conversion Contractors Meeting, CONF-8405157, May 8-9, 1984, Portland, Oregon.

White, D.H., "An Advanced Extruder-Feeder Biomass Liquefaction Reactor System," Proceedings of the 1985 Biomass Thermochemical Conversion Contractors' Meeting, CONF-8510167, October 15-16, 1985, Minneapolis, Minnesota.

White, D.H., D. Wolf, et al., "An Advanced Extruder-Feeder Biomass Liquefaction Reactor System," Proceedings of the 1987 Biomass Thermochemical conversion contractors' Review Meeting, CONF-8705212, May 20-21, 1987, Atlanta, Georgia.

White, D.H., and D. Wolf, "Advances in Direct Biomass Liquefaction by the Extruder-Feeder Method," Thermochemical Conversion Program Annual Meeting, SERI/CP-231-3355, June 21-22, 1988, Denver, Colorado.

Wong, J. M., "A Non-Plugging Annulus Control Valve for Extrusion of Polymers and Slurries", M.S. Thesis in Chemical Engineering. (1986).

Zhao, Y., "Characterization of Crude Wood Oils from Wood Liquefaction", M.S. Thesis in Chemical Engineering. (1987).

PART 1

Development of a Biomass Extruder-Feeder

TABLE OF CONTENTS

LIST OF TABLES

LIST OF FIGURES

PART 1

DEVELOPMENT OF A BIOMASS EXTRUDER-FEEDER

1.1 INTRODUCTION

The U.S. Department of Energy authorized the construction of a Waste-to-Energy direct liquefaction facility at Albany, Oregon in the mid-1970's. Rust Engineering designed the unit and Bechtel Corporation constructed the unit and conducted its initial operations. The design was based on the laboratory work conducted by the U.S. Bureau of Mines, Pittsburgh, wherein biomass was converted to a crude oil under high pressure/high temperature in the presence of carbon monoxide and sodium carbonate catalyst (Appell et al. 1970, 1975).

In early 1976, Dr. Don White of the University of Arizona suggested that an improved solids feeding system for the Albany direct liquefaction facility could be developed, based upon a modified single-screw plasticating extruder. Upon his return from Sabbatical leave at Imperial College, London, he visited the Albany facility in mid-1977 and subsequently submitted a research proposal to the Thermochemical conversion Branch, Solar Energy Division, U.S. Department of Energy (White and Wolf, 1981).

1.2 BASIS FOR DEVELOPMENT OF EXTRUDER-FEEDER

A plasticating single-screw extruder can generate high pressures at its outlet when pumping a very high viscosity fluid. It can also pump a high concentration of solids in a high-viscosity carrier fluid, with the slurry mixture acting like a pseudo-homogeneous fluid.

1.2.1 Basic Extruder Concept

An extruder consists of a helical screw conveying solids, liquids or a slurry through a barrel, typified in Figure 1.1. It has been proven experimentally and theoretically that an extruder is a good conveyor of solids, as long as the friction of the solids on the screw surface is not excessively greater than the friction of the solids on the barrel surface. A typical single screw section is shown on Figure 1.2.

The helical geometry results in a *"plug of solids"* moving down the channel, due both to an axial translation and rigid rotation. In addition, the frictional force that the barrel exerts on the solid plug is composed of axial and tangential components. The axial components can be shown as a single force balance, although the mathematics becomes somewhat complicated due to the screw and barrel geometry. Similarly, the tangential components can be expressed as a torque balance. It is the fact that the torque balance must be satisfied that the screw extruder is an efficient conveyor of solids.

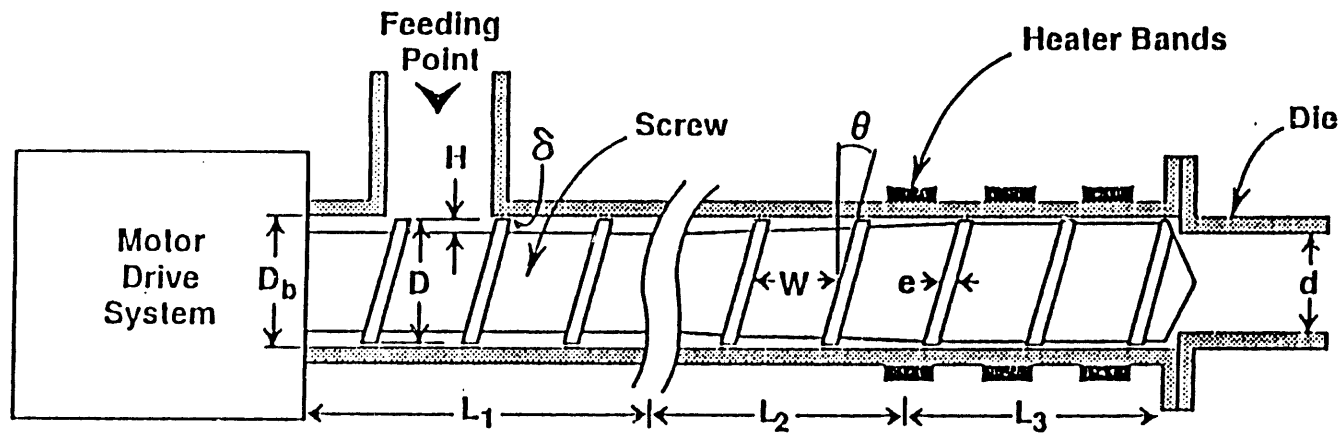

Figure 1.1. Schematic of Extruder-Feeder.

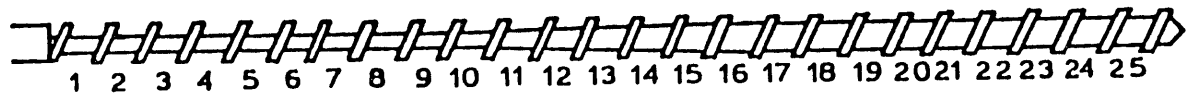

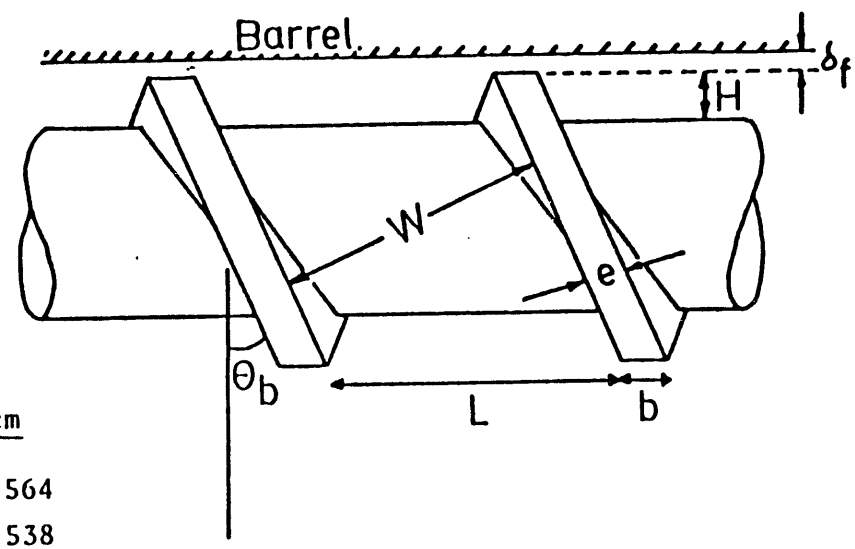

	in	cm
b_b	0.222	0.564
e	0.212	0.538
W_b	1.46	3.71
L	1.75	4.45
D_b	1.75	4.45

$\theta_b = 17.7°$

Channel 1 located in hopper zone

Figure 1.2. Geometry of the Extruder Square Pitched Screw.

The angle of movement of the solid plug determines the flow rate. In turn, the angle is related to the geometrical variables of screw and barrel, the physical properties of the material being conveyed, the friction factors f_s and f_b on the screw and barrel, and the pressure drop across the solids conveying zone. Therefore, given the flow rate, the screw geometry and the coefficients of friction one can calculate the pressure drop across any given length of solids conveying zone. Similarly, given the pressure drop, the screw geometry and the coefficients of friction, one can calculate the flow rate of solids.

1.2.2 Importance of Friction

The solid flow equation in the solid conveying zone is given by Tadmor and Klein (1970) as follows:

$$Q_s = V_{pl}\left[\frac{\pi}{4}\left(D_b^2 - D_s^2\right) - \frac{peH}{\sin\bar{\theta}}\right] \tag{1.1}$$

where Q_s = volumetric flow of solids.
D_b = diameter of screw at the channel surface
D_s = diameter of screw at the channel root
$\bar{\theta}$ = average helix angle
p = Number of flights in parallel
e = flight width
H = depth of channel
and V_{pl} = plug velocity in the axial direction.

A diagrammatic presentation of the solid plug movement was also given by Tadmor and Klein (1978) as shown in Figure 1.3. Tadmor and Klein are summarizing this phenomenon as follows: "If the frictional force between polymer and screw is so large that the polymer in effect adheres to the screw, the plug does not move with respect to the screw, i.e. $Q_s = 0$ and $V_{pl} = 0$, as well as the angle ϕ will be zero. If the frictional force between polymer and screw is negligible it can be shown below that the plug acquires a down channel velocity which equals that of the barrel surface. Here, the velocity of a solid plug in the down channel direction at the barrel surface is $V_{pz} = V_{pl}/\sin\theta_b$. Normally this results in the maximum flow rate and the angle $\phi = 90 - \theta$. Higher flow rates can be achieved in principle, if the friction coefficient between barrel and plug in the tangential direction is very large (no slip), compared to that in axial direction. This would be the case if the barrel has longitudinal grooves. The theoretical upper limit of the flow rate would occur at $\phi = 90°$. The tangential components of the velocity of the plug equals then the velocity of the barrel surface. This would be a case when a plug slides toward the exit as a nut held in a wrench. Thus, maximum flow rate can be achieved by polishing or coating the screw, thereby minimizing the friction of the screw surface."

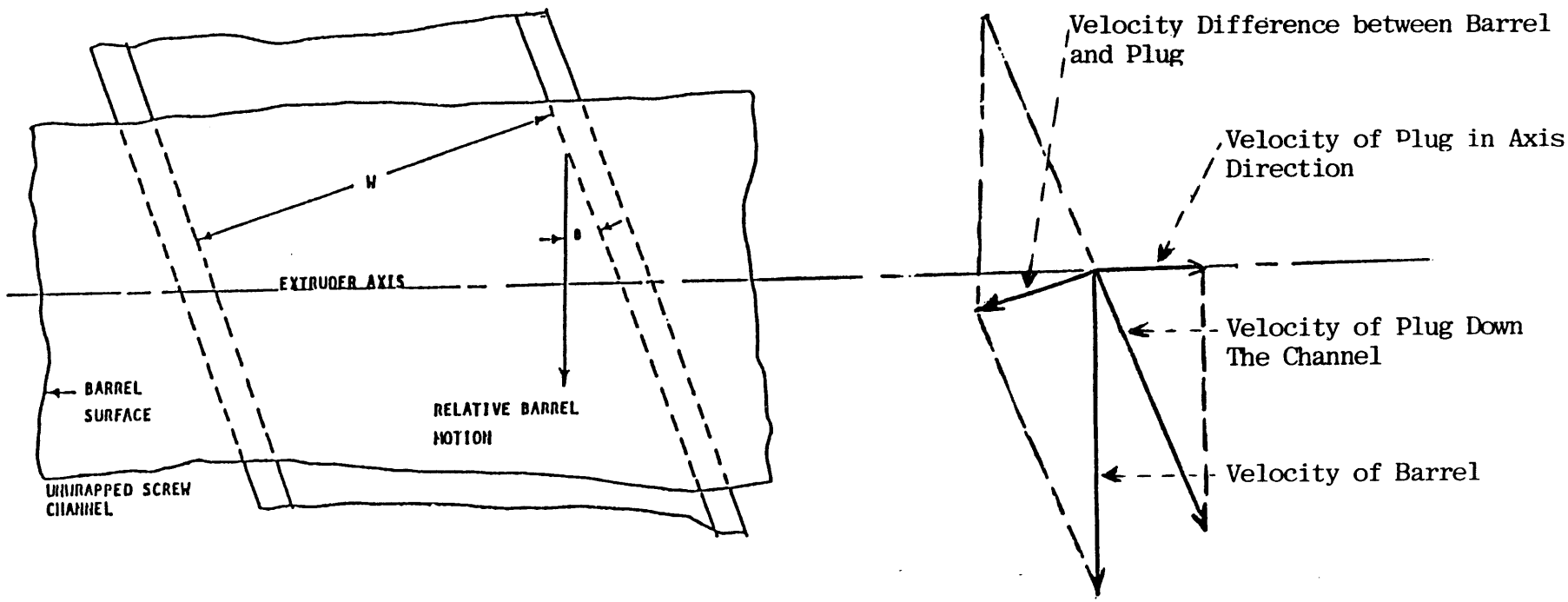

Figure 1.3. Diagram of Flow Velocity Vectors in Extruders for Solid Pumping.

A complete derivation of the force and torque balances in the extruder can be found in Tadmor and Klein (1978). A modified version of these balances will be utilized as an overall correlation in the present work, provided sufficient slurry property data and extruder performance data are obtained.

1.2.3 Importance of Cellulosic Slurry Properties

Obviously, the key objective of developing a pressure head in the extruder depends upon both sawdust slurry properties and the extruder performance. In turn, the slurry properties depend upon the solids and liquid properties individually and in combination, as follows:

Solids

- Particle size
- Proper size distribution for minimum void volume
- Increased friction by solids compression
- Increased friction by solids surface
- Particle swelling
- Particle wettability

Liquid Phase

- Viscosity
- Higher viscosity due to compressibility
- Temperature dependence of viscosity
- Shear-rate dependence of viscosity

Slurry

- Slurry concentration
- Increased flow (of liquid) resistance due to compression
- Increased or decreased friction between particles due to carrier fluid.

Extruder Variables

Extruder operating variables are very limited in scope, with the major ones leading to higher differential pressure development being:

- Higher screw speed
- Lower temperature in feed section
- Heating screw and/or cooling barrel
- Granulated (pelletized) feed form
- Masterbatched feedstock

However, the extruder machine design has many dependent factors that affect the pressure head, as follows:

- Screw design
- Barrel wall design
- Feed section design, especially for additional compression
- Feed compactor
- Heating/cooling of the barrel and/or screw
- Internal mixing devices
- Internal grinding devices

1.3 EXTRUDER-FEEDER OPERATING CORRELATIONS

The derivation of the extruder-feeder flow rate equation in the metering section can be found elsewhere (Tadmor and Klein 1978, Bernhardt 1959, McKelvey 1962). The assumptions made in its derivation are:

1. Steady state, laminar, fully developed flow.
2. No slip at walls.
3. Gravity forces are neglected.
4. Shallow prismatic channels.
5. Constant channel depth as applied in the metering section of the screw.
6. Flight width is negligible.
7. Newtonian fluid.
8. Isothermal conditions.
9. Leakage flow across the screw flights is neglected.

The equation under these conditions is:

$$Q = \frac{V_{bz} W H F_d}{2} + \frac{W H^3}{12 \mu} \frac{\Delta P}{\Delta Z} F_p$$

where

$$F_d = \frac{16W}{\pi^3 H} \sum_{i=1,3,5}^{\infty} \frac{1}{i^3} \tanh \frac{i\pi H}{2W}$$

$$F_p = 1 - \frac{192H}{\pi^5 W} \sum_{i=1,3,5}^{\infty} \frac{1}{i^5} \tanh \frac{i\pi H}{2W}$$

V_{bz}	=	velocity in the z direction of the barrel
	=	π DN COS θ
W	=	width of one turn
H	=	depth of channel
D	=	diameter of screw
μ	=	viscosity
N	=	rotational speed of screw
ΔP	=	pressure drop across the metering section
ΔZ	=	length of metering section
θ	=	helix angle

One should note that in theory both F_d and F_p are functions only of the screw geometry, independent of the nature of the fluid and the machine operating condition.

Equation (1.2) is often expressed in the simplified form:

$$Q = AN - \frac{B\Delta P}{\mu} = \textit{Drag flow} - \textit{Pressure flow} \qquad (1.3)$$

The theoretical values of F_d and F_p can be found elsewhere (McKelvey 1962). For our screw we have: $F_d = F_p = 0.95$.

The single screw extruder-feeder consists of one screw which rotates inside a close-fitting barrel of constant diameter and is normally divided into three zones. These zones are the feeding zone, the compression zone and the metering zone. There is also a circulation across the screw channel, the leakage flow, and across the depth of the screw channel, the transverse flow, generated by the force and torque balances on the rotating screw with respect to the stationary barrel. The function of the various zones are similar to those of a plasticating extruder and are described elsewhere (McKelvey, 1962; Tadmor and Klein, 1978). The most efficient solids pumping occurs when the coefficient of friction with respect to the barrel is maximized and the coefficient with respect to the screw is minimized, for example by polishing its surface (Chan, 1975). A helix angle of 7-17° lies within the optimum range for many plastic materials and the channel depth of the feed zone may be approximately three times that of the metering zone. The most general theory of extrusion is based on the plastic melt flow.

The compression zone (also called transition or melting zone) typically receives an unmelted bulky material from the feed zone and converts it to a dense melt of uniform temperature and viscosity for delivery to the metering zone. The compression or compaction of material is accomplished by a gradual decrease in the channel depth along the zone length.

The metering or mixing zone is the portion of the screw that acts as a metering pump to provide the extruder head with a constant pressure and flow rate. It is in this zone that the quantitative calculations of *"drag flow,"* Q_d, *"pressure flow,"* Q_p, and *"leakage flow,"* Q_l are applied. For idealized calculations, all of the pressure that builds up along the screw should occur within this zone.

The basic equation found in the literature for calculating the net flow rate Q is as follows:

$$Q = Q_d - Q_p - Q_l = AN + B\frac{\Delta P}{\mu} + C\frac{\Delta P}{\mu} \tag{1.4}$$

The transverse flow is not included in Equation (1.4) since it does not contribute to the net flow output. For the very small flight clearances between the barrel and screw that normally exist in extruders or even for higher clearances developed due to wear and for the very high viscosities that we deal with in extrusion, leakage flow over the flights can be neglected in Equation (1.4) (Schenkel, 1966; Glanvill, 1971; Wolf and White, 1975).

The more fundamental equation for the melting section that neglects leakage flow and flight width but takes into account various screw parameters and operational conditions is:

$$Q = Q_d - Q_p = AN - B\frac{\Delta P}{\mu} - \frac{V_{bz}WH}{2}F_d - \frac{WH^3\Delta P}{12\mu\Delta Z}F_p \tag{1.5}$$

where $V_{bz} = \pi DN\cos\theta$, $W = D\cos\theta$, $\Delta Z = L/\sin\theta$ and $\Delta P = P_2 - P_1$.

To obtain the pressure flow term in Equation (1.5) it is necessary to know the pressure drop across the metering section and the viscosity of the melt. The viscosity is a function of both shear rate and temperature and it must, therefore, be determined for each experimental condition separately. For the extruder-feeder, the shear rate is obtained from:

$$\dot{\gamma} = (\pi DN)/H \tag{1.6}$$

For the different materials used as feedstock, the apparent viscosities were measured by either a Hooke RV_2 viscometer, Instron Rheometer, or a Brookfield viscometer (Chehab, 1982; Lezzar, 1983; Yang, 1981). From the shear stress versus shear rate plots for several temperatures, the apparent viscosities are calculated and plotted versus shear rate for constant temperature or versus temperature for constant shear rate. Bernhardt (1959) has presented such graphs for a series of thermoplastic materials that he has compiled.

Also, apparent viscosities were determined indirectly from the data obtained from the extruder-feeder outputs or from data found in the literature (Bernhardt, 1959; McKelvey, 1962).

An analytical expression for the apparent viscosity as a function of temperature and at a given shear rate is:

$$\eta = Me^{E\dot{\gamma}/RT} \tag{1.7}$$

The activation energy, $E_{\dot{\gamma}}$, is a function of the shear rate for non-Newtonian fluids. From experimental data a relationship between the shear rate and activation energy can be obtained for constant temperatures (McKelvey, 1962).

The extruder-feeder die valve can be opened and closed to adjust for the desired output rates and pressures. When the die valve is open, the output rate, Q_v, is at a maximum while the output pressure is at a minimum, and the drag flow is dominating. When the die valve is partially open, the output rate is lower, the output pressure is higher, and both drag and pressure flows prevail.

The flow rate through the die valve can be obtained separately from the following equation which is commonly used for flows through orifices and valves:

$$Q_v = K_d \frac{\Delta P}{\eta} \tag{1.8}$$

By combining Equations (1.5) and (1.8) (McKelvey 1962) and eliminating $\Delta P/\eta$ we get:

$$Q = \frac{ANK_d}{B + K_d} \tag{1.9}$$

while by eliminating Q from Equations (1.5) and (1.8), we obtain:

$$\Delta P = \frac{\eta AN}{B + K_d} \tag{1.10}$$

If the characteristic coefficient for the restriction K_d is known and Q_v and ΔP can be measured, the apparent viscosity of the fluid can also be determined from Equation (1.8).

1.4 EXPERIMENTAL WORK

An existing Prodex single screw extruder, which had been used extensively for plastics research in the Department of Chemical Engineering, University of Arizona, was utilized in the experimental work.

The Prodex unit was well-equipped with measuring devices and a microprocessor data acquisition unit. A variable speed unit in the range of 0 to 200 min^{-1} attached to the extruder-feeder enabled one to change the screw rotational speed.

1.4.1 Experimental Equipment

The heart of the experimental equipment is the Prodex extruder-feeder and its data acquisition system (DAS). The extruder is a 1-3/4 inch (4.45 cm) diameter model with a barrel of 24:1 length to diameter ratio. The location of thermocouples and pressure transducers along the extruder barrel are given in Table 1.1 and in a schematic form in Figure 1.4. Data on the geometry of the screw is given in Table 1.2. Other information about instrumentation, calibration and Data Acquisition System are discussed in detail by Iregbulem (1982). A plastic scrap grinder with heavy right-angled blades was utilized to prepare the *"regrind"* feedstock. It produces granular scrap with a wide particle size distribution and rough edges.

1.4.2 Experimental Materials

It was necessary to use model materials, mainly polyethylenes from mid-1978 to mid-1981, due to the unavailability of crude wood oil vacuum bottoms from the DOE Albany, Oregon experimental unit. Vacuum bottoms finally were made available to the University of Arizona in mid-1981. Fortunately, the performance of wood flour in polyethylenes proved to be excellent, and the results correlated very well with later data using wood oil vacuum bottoms.

Table 1.1. Distance of Thermocouples and Transducers from Start of Feed Section.

Thermocouple	Distance from Start of Feed Section in.	cm.	Pressure Transducer	Distance from Start of Feed Section in.	cm.
T1	49.4	125.4	P1	45.0	114.2
T2	45.0	114.2	P2	42.2	107.2
T3	42.2	107.2	P23	37.2	94.5
T4	37.2	94.5	P4	32.8	83.3
T5	32.8	83.3	P5	24.3	61.7
T6	24.3	61.7			
T7	11.9	30.2			
T8	7.1	18.0			
T9	0.8	2.0			
TB1	44.7	113.5			
TB2	37.4	95.0			
TB3	30.7	77.9			
TB4	24.4	62.0			
TB5	19.4	49.3			
TB6	14.4	36.6			

Table 1.2. Geometry of the Extruder Square Pitched Screw.

Channel Number	Channel Depth, H		Screw Diameter, D_s		Helix Angle, θ_s	Channel Width, W_s	
	in.	cm.	in.	cm.	degrees	in.	cm.
1*	0.31	0.79	1.13	2.87	26.2	1.36	3.45
2 . . 10	0.30	0.76	1:15	2.92	25.8	1.36	3.46
11	0.28	0.71	1.19	3.02	25.1	1.37	3.49
12	0.24	0.61	1.27	3.23	23.7	1.39	3.53
13	0.21	0.53	1.33	3.38	22.7	1.40	3.56
14	0.17	0.43	1.41	3.58	21.6	1.42	3.59
15	0.13	0.33	1.49	3.78	20.5	1.43	3.63
16	0.09	0.23	1.57	3.99	19.5	1.44	3.65
17 . . 25	0.08	0.20	1.59	4.04	19.3	1.44	3.66

* Located in Hopper Zone.

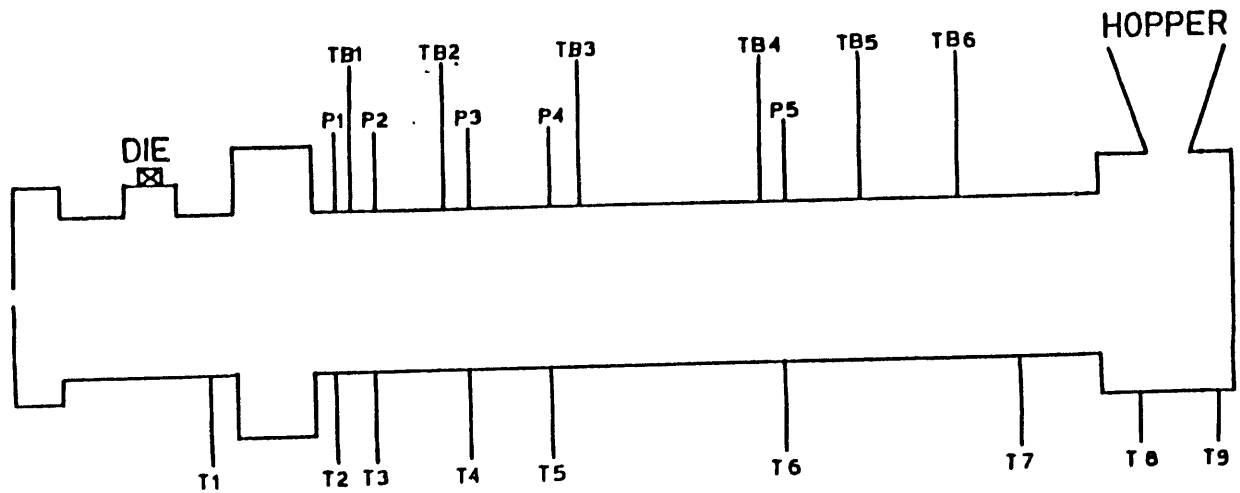

Figure 1.4. Location of Thermocouples and Transducers.

The materials used for the development of the extruder-feeder are described below.

1.4.2.1 Wood Flour

Douglas Fir, obtained from DOE Liquefaction Plant, Albany, Oregon, 4 wt.% moisture, ground in a hammer mill. Particle size distributions and aspect ratio shown in Figure 1.5. An equivalent diameter D_{e1} or D_{e2} to a cube of the same volume can be defined:

$$D_{e1} = \sqrt[3]{L \cdot W \cdot T} \tag{1.11}$$

$$D_{e2} = (L + B + T)/3$$

where:

D_{e1} = equivalent diameter
D_{e2} = equivalent diameter
L = length of particle
W = width of particle
T = thickness of particle

The density of Albany Wood Flour was found to be 1.45 g/cm^3.

1.4.2.2 Low Density Polyethylene (LDPE)

Grade LDPE 515, manufactured by Dow Chemical Company, 0.92 g/cm^3 density, 1/8-inch solid pellets. Schott (1981) reported the density a given in the following equation:

$$\delta = \frac{0.92}{1+6x10^{-4}\ (T°C-20)} \tag{1.12}$$

The Softening Point of LDPE is 97°C (208°F).

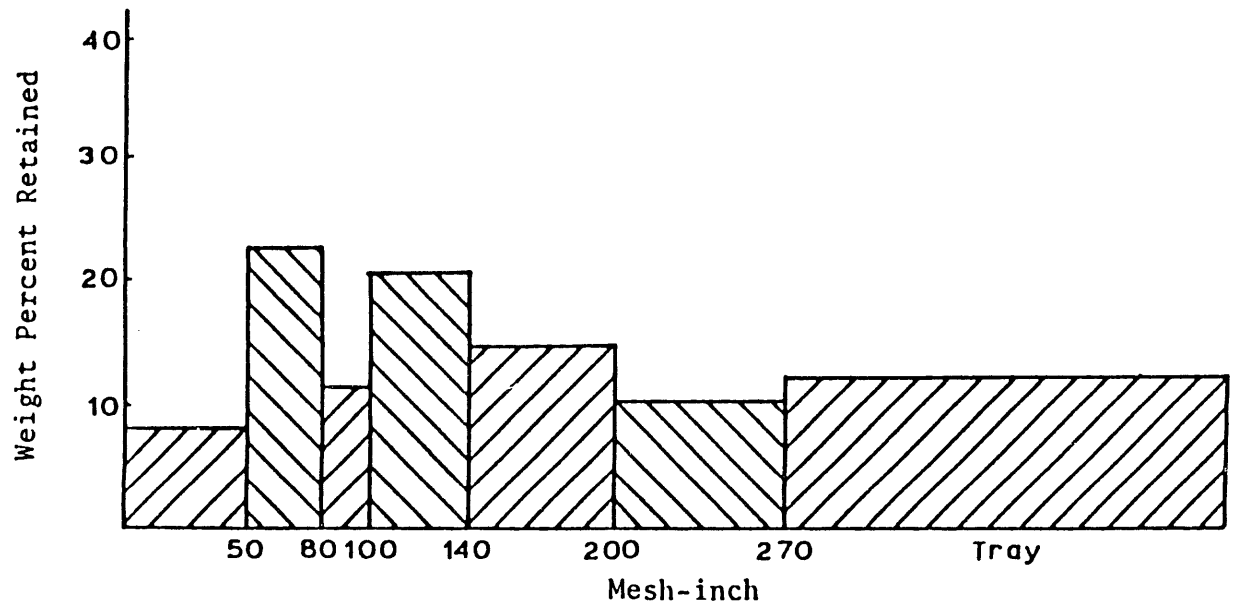

Figure 1.5. Bar Histogram of Particle Size Distribution for Albany Wood.

1.4.2.3 Low Molecular Weight Polyethylene

The low molecular weight polyethylene was grade AC-6, manufactured by Allied Chemical Company, fine white powder, waxy in nature.

1.4.2.4 Crude Wood Oil Vacuum Bottoms

Crude wood oil vacuum bottoms was experimental product obtained from Rust Engineering Company, DOE Liquefaction Facility, Albany, Oregon; a black, brittle solid at room temperature. The data and analysis (Courtesy Rust Engineering Company) are as follows:

Density: 1.31 g/cm^3
Softening Point: 102°C
Melting Point: 115-120°C
Initial Flash Point: 250°C

Carbon	83.9%	
Hydrogen	7.1%	
Oxygen	5.6%	
Nitrogen	0.1%	
Sodium	0.9%	
Sulfur	< 0.4	ppm
Nickel	5.1 ± 0.6	ppm
Chromium	26.0 ± 3	ppm
Titanium	110 ± 30	ppm

1.4.2.5 Petroleum Asphalt and Albany Crude Wood Oils

A roofing grade asphalt was used, purchased from local suppliers. Two grades of Albany crude wood oils were used, namely, TR9 and TR12. Data on these materials were reported by Rust Engineering and Battelle PNL. The viscosities of TR12 are given in Part 2 of this report; TR9 is a much more viscous oil than TR12.

1.4.3 Advanced Data Acquisition

Fortunately, in 1978 the Department of Chemical Engineering, University of Arizona, had a fully-operational state-of-the-art Mini-Computer Data Acquisition system, as shown in Figure 1.6. It was available for several research projects, including those utilizing the Prodex single screw extruder. Further, the latter was well instrumented to provide temperature and pressure profiles along the 24/1 L/D barrel (see Table 1.3).

In addition, a special computer program provided the means of automatically determining when the Prodex extruder has reached steady state at some given screw rpm

Table 1.3. Channel Allocation.

Channel	Data Collected
1	T1
2	T2
3	T3
4	T4
5	T5
6	T6
7	T7
8	T8, Outlet cooling water
9	T9, Inlet cooling water
10	Screw speed
11	Voltage
12	Amperage
13	P1
14	P2
15	P3
16	P4
17	P5

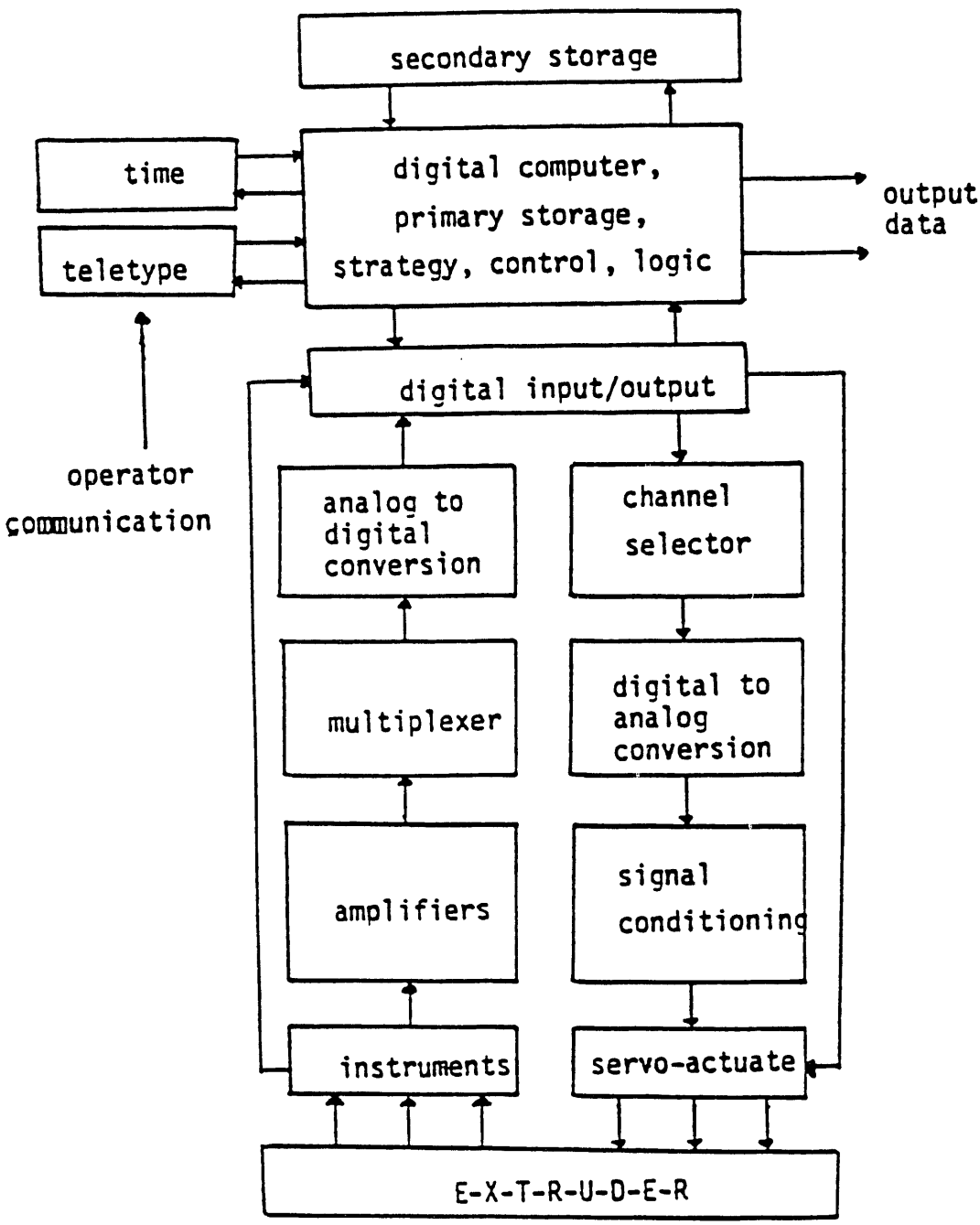

Figure 1.6. Data Acquisition System .

speed. Due to the fact the extruder has a thick barrel wall (to provide a 10,000 psi working pressure) and that the temperature is not uniform along the barrel, it takes considerable time to reach steady state. Obviously, the extruder is a large *"heat sink"* and heat transfer along the barrel length is taking place, even at steady state conditions. A near steady-state condition can be obtained by experience, utilizing a combination of how barrel heaters are set during the two-hour heat-up session (non-operating) and by manipulating the barrel heaters during the first half-hour of actual operations.

1.4.4 Initial Experimental Results

It was visualized from the outset of this project that viscous wood oil vacuum bottoms would be used to convey the wood flour feedstock into a pressure system. However, no heavy vacuum bottoms were available from the Albany plant in 1978. Therefore, it was necessary to use *"model compounds"* of mixtures of polyethylene to provide a range of viscosities. These polyethylene model carrier materials were mixed with various concentrations of wood flour to provide a wide range of feedstocks.

The Prodex single screw extruder had a valve near its outlet, which could be adjusted to different degrees of opening. This provided a back-pressure simulating the pumping of the feedstock into a pressure system. Pressure and temperature data from outlets along the extruder barrel were measured and recorded continuously by a Mini-Computer Data Acquisition System, available in the Department of Chemical Engineering, University of Arizona, for this project as well as many other research projects simultaneously.

This research project started January 1, 1978. Immediately, laboratory data on the viscosities of various wood flour slurries were initiated. The Prodex extruder was placed into operation in June, 1978. The feasibility of the overall project goals were achieved (proved) by the end of August, 1978, wherein finely-ground Albany sawdust in slurry concentrations up to 67 weight percent sawdust was extruded, while developing outlet pressures in the range of 5,000 to 8,500 psi. This compares with existing piston pumps with intermittent check valves that can handle a maximum of only 10 to 15 weight percent sawdust. During the year of 1979, a maximum slurry concentration of 70 weight percent sawdust solids was achieved, with 50-60 weight percent slurries being handled routinely with no problems except the necessity of using forced feeding. Thus, the operability of pumping concentrated wood flour slurries into pressure systems was proven early on, but there was little data available to design a real biomass liquefaction unit.

1.4.5 Extruder-Feeder Parameter Results

The development of the extruder-feeder in the period 1978-1981 involved conducting experimental runs upon both (a) wood flour slurries in mixtures of polyethylenes and (b) wood flour slurries in Albany crude wood oil vacuum bottoms. The major extruder-feeder parameters studied during this period are as follows:

1. Wood flour slurry concentrations, varied from 40 to 65 wt.% wood flour.

2. Extruder-feeder outlet temperatures over the rather narrow range possible, namely, about 320°F to 400°F. The reason this range is narrow is that the wood flour slurries must maintain a high viscosity in order to provide the necessary drag flow to generate 3,000 psi outlet pressure.

3. Extruder-feeder outlet pressure, varied from near zero pressure to a maximum of 5,000 psi (but normally up to 3,000-3,500 psi). This was accomplished by varying the degree of closure of the valve located near the outlet of the extruder-feeder.

4. Extruder-feeder screw speed, varied from 40 rpm to about 120 rpm (normally the upper limit of motor capacity for the existing extruder).

5. Viscosity of the polyethylene carrier fluid, achieved by varying the proportions of a high-viscosity polyethylene with a low-viscosity polyethylene.

Extensive experimental runs were made wherein these extruder-feeder parameters were investigated. By necessity, more work was done upon the polyethylene carrier fluids than upon the Albany crude wood oil vacuum bottoms. This was due to (a) vacuum bottoms not being available until mid-1981, and (b) the quantity provided was small, such that the experiments had to be carefully planned.

1.4.5.1 Experimental Runs with Prodex-Type Extruder-Feeder

The experimental work with the Prodex-type extruder-feeder was done with a variety of materials as previously outlined. Some 22 of the better runs were selected for more detailed analysis and correlations, as shown in Appendix A. Some typical experimental results are presented later in graphical form which enabled us to analyze the extruder-feeder behavior and the effects of various physical and operational parameters of the system. As a general rule, the data are scattered due in part to the characteristics of the system, but much more due to the variation in feedstocks and to the unsteady-state conditions that often prevailed, especially with regard to temperatures and pressures. However, the general performance is quite clear, conclusive and can be quantitatively defined.

The first experiments were conducted with Dow 515 LDPE for two reasons:

1. Data were available for this material, so a basis for comparison is possible.

2. LDPE was a logical choice for the first carrier for the wood flour mixtures.

Similar work was also done with mixtures of LDPE and Allied Chemical AC6-PE, wood oil vacuum bottoms, and asphalt before mixtures of wood flour and these carriers were tested. Our analyses of results for the extruder-feeders were made according to the operational conditions and the feedstocks used.

1.4.5.2 LDPE (Low Density Polyethylene)

Flow rates for polyethylene as a function of the rotational speed of the screw for several different experimental conditions are shown on Figure 1.7. The linear relationship between the flow rate and rotational speed is quite evident, which was expected based on extrusion fundamentals. In general, there is little effect on the flow rate of the extruder-feeder of most of the operational conditions except the rotational speed of the screw, which reflects that high viscosity/drag flow existed. Even the opening of the valve at the die from 20% to 100% open has little effect on the flow rate as shown on Figure 1.8 where the flow rates for two different screws are given as a function of rotational speed and valve opening. However, one can see on Figure 1.8 that there is a significant difference in the flow rates obtained under similar operating conditions for the two different screw types as specified in Table 1.4. Also, pressures of up to 21 MPa (3050 psi) were developed with the HRHT screw at 80 min^{-1} while only 7 MPa (1015 psi) were obtained with the MRLT screw at 100 min^{-1}. A balance between the flow rates and pressures produced would be used to determine the optimum screw design. For evaluating design parameters, an experiment was also made with the die removed, and the flow rates versus rotational speed were obtained as shown in Figure 1.9. From the slope of this line a drag flow coefficient F_d was derived, as will be discussed later.

Unlike the linear relationship between the flow rates and the rotational speed of the screw, the pressure rise as a function of the rotational speed, N, should be correlated on a log-log scale due to the non-Newtonian characteristics of the mixtures (McKelvey, 1962). Thus, based on this theoretical consideration, a typical log-log plot of ΔP versus N is shown on Figure 1.10 as plot (a). The slope of this line gives the flow index, n, for the non-Newtonian material which follows the power law. The slope for polyethylene on Figure 1.10 is approximately 0.55 thus the pseudoplastic nature of polyethylene was evident. The other two lines will be discussed later.

The output pressure is dependent on parameters like rotational speed of the screw, opening of the die valve, type of materials pumped and temperatures of the melt. However, one should emphasize that the effect of temperature on the generated outlet pressure is less compared to the effect of rotational speed in the range of temperature and rotational speeds tested.

1.4.5.3 LDPE and AC6-PE mixtures

AC6-PE, which is a low molecular weight polyethylene, has been mixed with LDPE so as to obtain a lower viscosity carrier for the wood flour. Pure AC6-PE was not tested for

Table 1.4. Specifications of the Prodex and Killion Extruder-Feeders and Screws.

Prodex Extruder-Feeder		
P_w, kW	5.6	
phase	3	
voltage	220	
RPM	5-160	
water-cooled	yes	
heating range, °C	150-250	
venting	optional	
	HRHT Screw	MRLT Screw
L/D	24:1	20:1
D_b, mm	44.45	44.32
e, mm	5.71	6.35
W, mm	38.80	37.85
θ, (°)	17.7	17.7
H_m, mm	2.00	-
H_f, mm	7.75	4.65
H_c, mm	2.00-7.75*	2.28-4.65*
N_f	8	4
N_c	6	16
N_m	10	-

*Changing linearly between these values along the compression section.

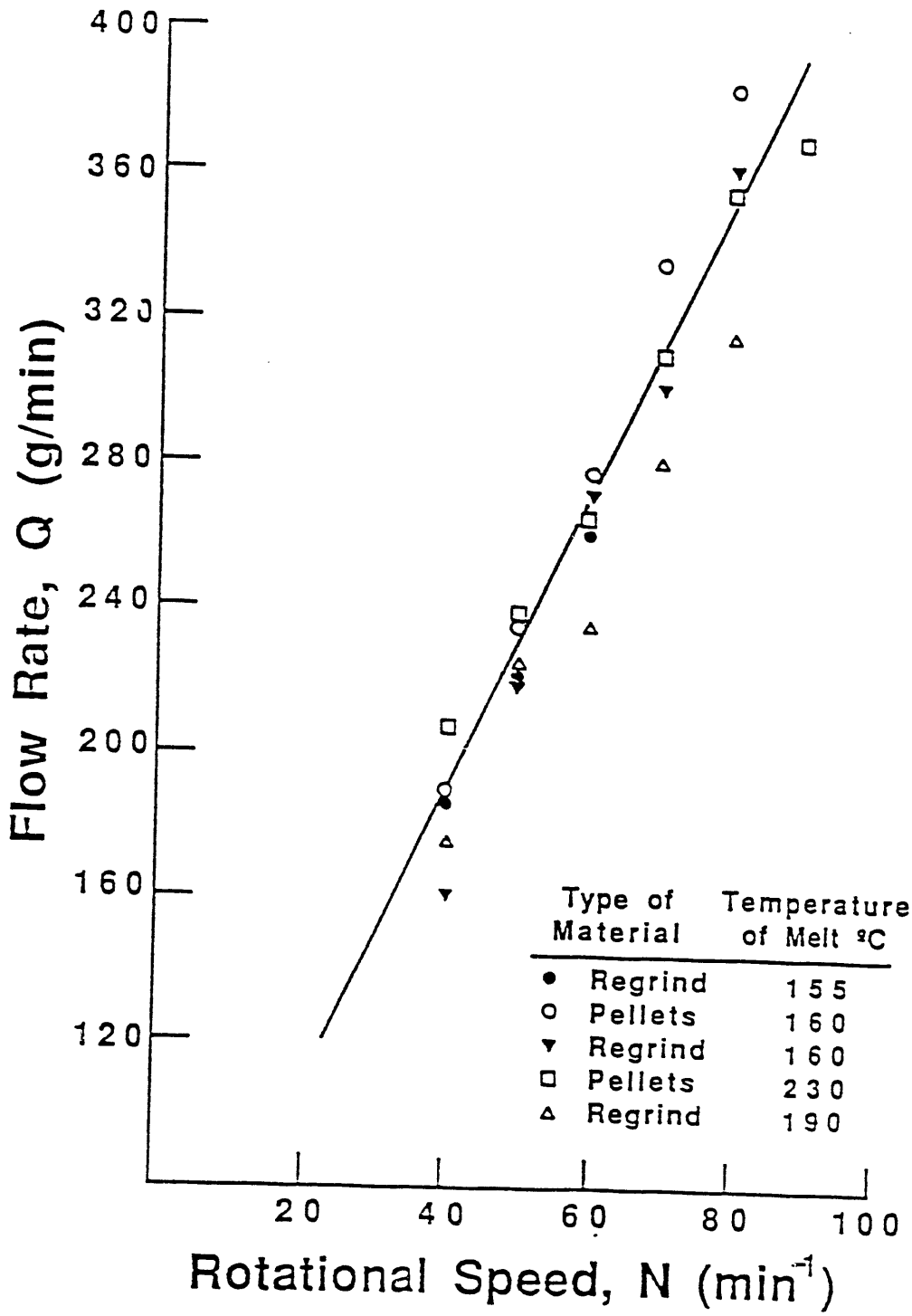

Figure 1.7. Flow Rates as a Function of Rotational Speed of HRHT Screw for the Prodex-type Extruder-feeder with the Die on and for Polyethylene as Feed.

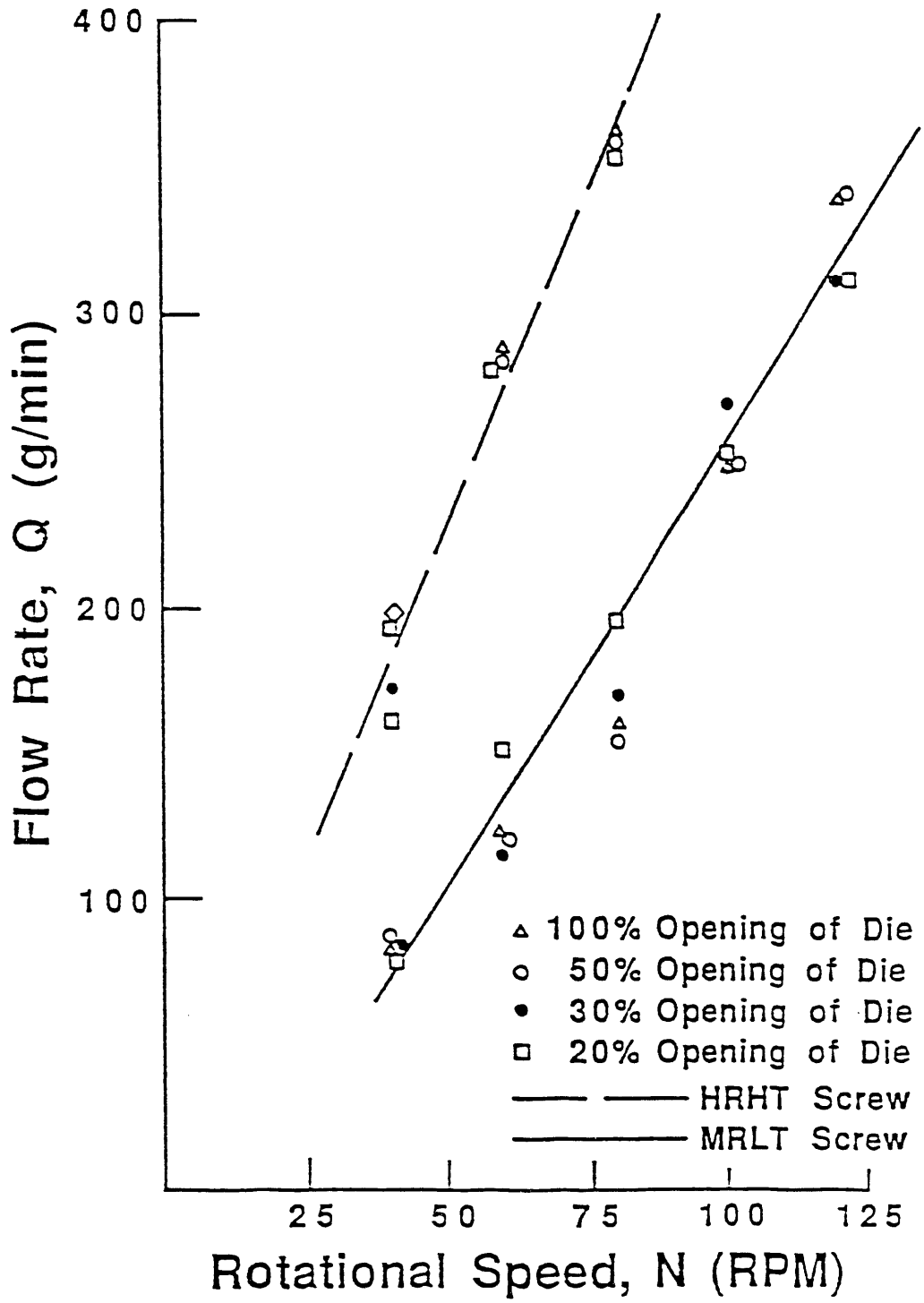

Figure 1.8. Flow Rates as a Function of Rotational Speed of HRHT and MRLT Screws for the Prodex-type Extruder-feeder with the Die on and Polyethylene as Feed.

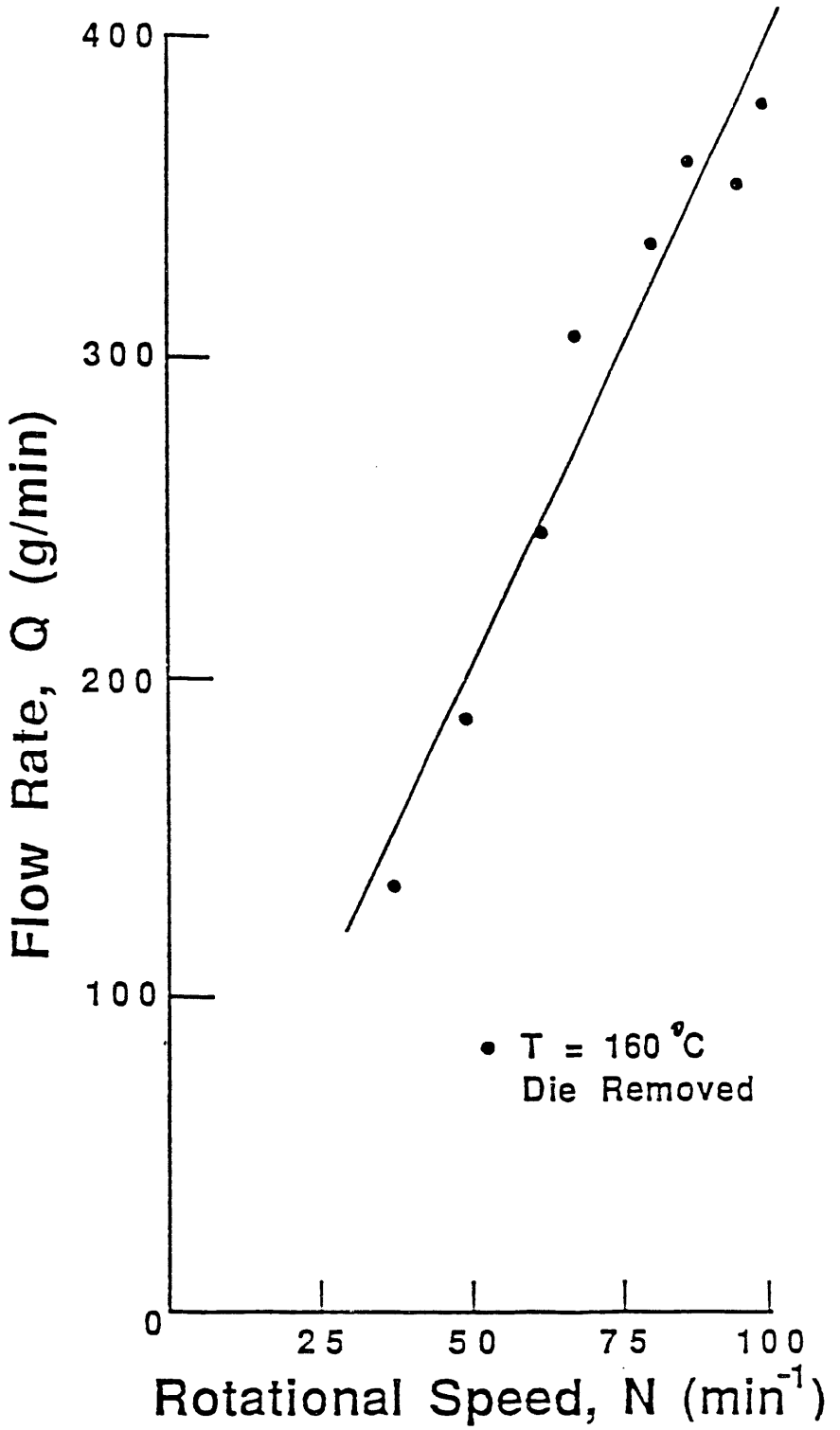

Figure 1.9. Flow Rates as a Function of Rotational Speed of HRHT Screw for Prodex-type Extruder-feeder with Die Removed and Polyethylene as Feed.

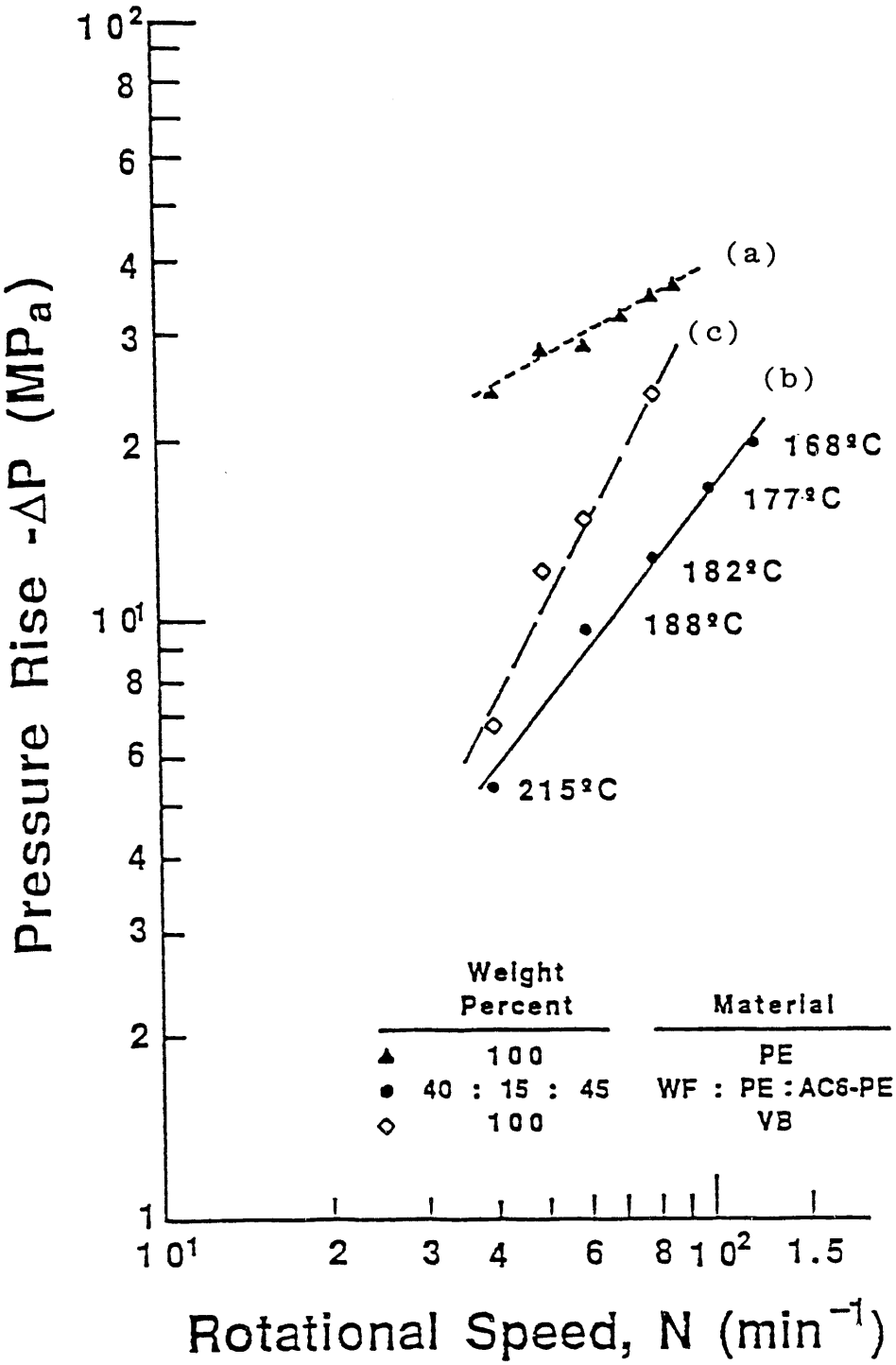

Figure 1.10. Pressure Rise as a Function of Rotational Speed of HRHT Screw for Prodex Type Extruder-feeder with the Die on and for Several Feedstock Material.

pumpability by the extruder-feeder because its melt viscosity is too low to develop proper drag flow. In order to obtain homogeneous mixtures of LDPE and AC6-PE the two components were mixed, passed through the extruder-feeder for homogenization, and then reground before they were used as carriers for the wood flour. The pumpability of this reground material was good, but it depended on the amount of AC6-PE added. Better results were obtained as the ratio of LDPE to AC6-PE was increased. As a general rule, mixtures with an LDPE to AC6-PE ratio of less than one have more of the characteristics of AC6-PE than of LDPE even though they are still pumpable and generate some pressures. These experimental results can be correlated with the pseudo-homogeneous apparent viscosity of the wood flour slurry.

1.4.5.4 Mixtures of Wood Flour, LDPE, and AC6-PE

Before testing mixtures of wood flour, LDPE and AC6-PE, several experimental runs were made with mixtures of wood flour with pure AC6-PE and with pure LDPE. As expected, AC6-PE as a carrier is very poor due to its low viscosity at high temperatures. In fact, AC6-PE acts much like water as a carrier in that it is *"squeezed"* out of the wood flour solids and results in a plug that shuts down the extruder-feeder. Even a weight ratio of 50:50 wt.% wood flour to AC6-PE produced pressures only up to 6 MPa (870 psi). However, mixtures of wood flour and pure LDPE produced relatively high flow rates and also high pressures of more than 20 MPa (2900 psi). The flow rates increased significantly with increase of rotational speed and increase in percentage of wood flour.

Mixtures of 40, 50, and 60 wt.% of wood flour and with various ratios of LDPE to AC6-PE were then tested, and the flow rates versus rotational speed of the screw are shown in Figure 1.11. One can see on this figure that a linear relationship between flow rate and rotational speed prevails. However, for low ratios of AC6-PE to LDPE in the range of up to 1.5, the flow rates increase at a much higher rate than the flow rates for high ratios of AC6-PE to LDPE in the range of 3 and more. This is in agreement with the results obtained for the wood flour mixtures with pure LDPE and with pure AC6-PE which are also shown on Figure 1.7 as the upper and lower lines of the experimental results.

Also on Figure 1.11, one can see the flow rates for a mixture of 40:15:45 wt. ratio of wood flour:LDPE:AC6-PE, once with the die removed and once with the die on and 90% closed. Low pressures of up to 6 MPa (870 psi) were measured with the die removed while high pressures of more than 40 MPa (5800 psi) were obtained with the die in place. The pressures increased significantly with an increase in the rotational speed of the screw. On Figure 1.10, plot (b), one can see the pressure rise for this mixture as a function of rotational speed of the screw on a log-log scale. The increase in the pressure as seen on Figure 1.10 is also due to the effect of the temperature superimposed on the effect of the rotational speed of the screw. The appropriate temperatures for each experimental point on plot (b) of Figure 1.10 are indicated on the plot. From these experiments we concluded that LDPE in a mixture with AC6-PE at the right proportions is a good carrier fluid for the wood flour.

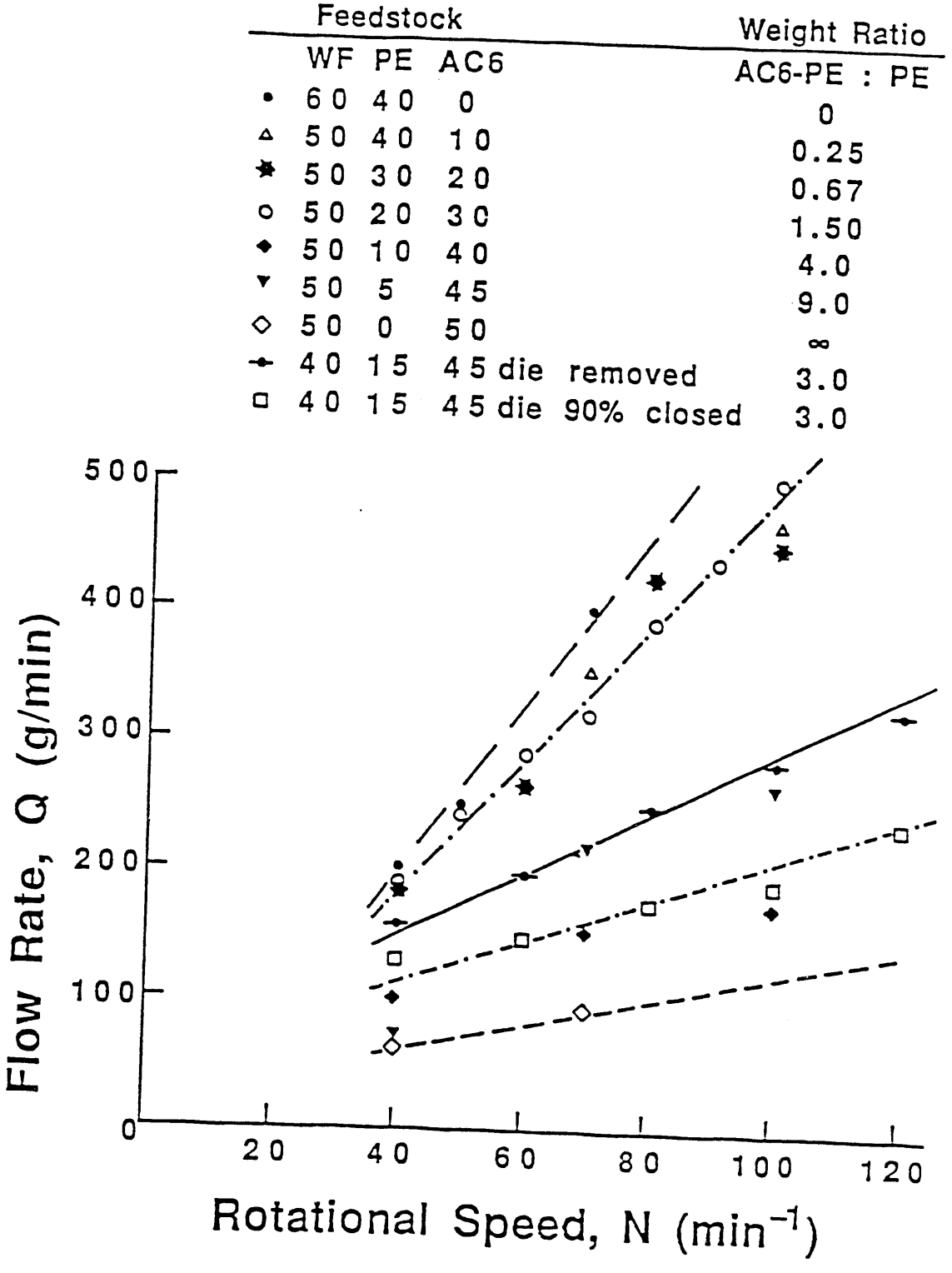

Figure 1.11. Flow Rates as a Function of Rotational Speed of HRHT Screw for Prodex-type Extruder-feeder for Various Mixtures of Wood Flour, Polyethylene and AC6PE.

1.4.5.5 Wood Oil Vacuum Bottoms

Wood oil vacuum bottoms are considered as the real carrier for the wood flour to be pumped into the biomass liquefaction reactor. Therefore, as soon as Albany crude wood oil vacuum bottoms were made available in mid-1981, experiments with vacuum bottoms were conducted in order to confirm its pumpability. Flow rates as a function of rotational speed are shown in Figure 1.12. One can see on the figure that vacuum bottoms are pumpable and that the flow rates and rotational speeds correlate, although the results obtained are very scattered. These data were scattered due to making short runs (due to limited amount of available vacuum bottoms) wherein steady-state extruder conditions were not quite achieved. The flow rates are much higher for the vacuum bottoms at the same rotational speed than for the LDPE. The pressures generated were well in the range of interest and even exceeded it in some cases by rising to 28 MPa (4062 psi) and more. A typical set of experimental data is shown on Figure 1.10, plot (c), from which a value of 2.0 for the flow index n was determined. A comparison can be made from this figure between the properties of LDPE and vacuum bottoms.

1.4.5.6 Mixtures of Wood Flour and Wood Oil Vacuum Bottoms

Typical results for various concentrations of wood flour vacuum bottoms at several operating conditions are shown in Figure 1.13. Almost every experiment showed good pumpability and a linear relationship between the flow rate and the rotational speed. As for the pressures, although high pressures were obtained, the results were scattered and were difficult to correlate.

1.4.5.7 Mixtures of Wood Flour and Asphalt

Petroleum asphalt was tested because it was considered to be a good model material similar to wood oil vacuum bottoms with respect to high viscosities at temperatures just above its softening point. Experiments with asphalt and mixtures of asphalt and wood flour showed that good pumpability and high pressures were obtained (cooling the asphalt until it became brittle was necessary). Figure 1.14 shows the flow rates versus rotational speed for several experiments made with mixtures of wood flour and asphalt. The flow rate increases linearly with the screw speed.

1.4.5.8 Calculation of Drag and Pressure Flow Coefficients, F_d and F_p

The flow rates for biomass feedstock mixtures through the extruder-feeder can be calculated either from the characteristics of the screw including the drag and pressure flow coefficients F_d and F_p, the properties of the feedstock especially viscosity, and the operational condition of the extruder-feeder, or from the output rate through the die and its coefficient of restriction.

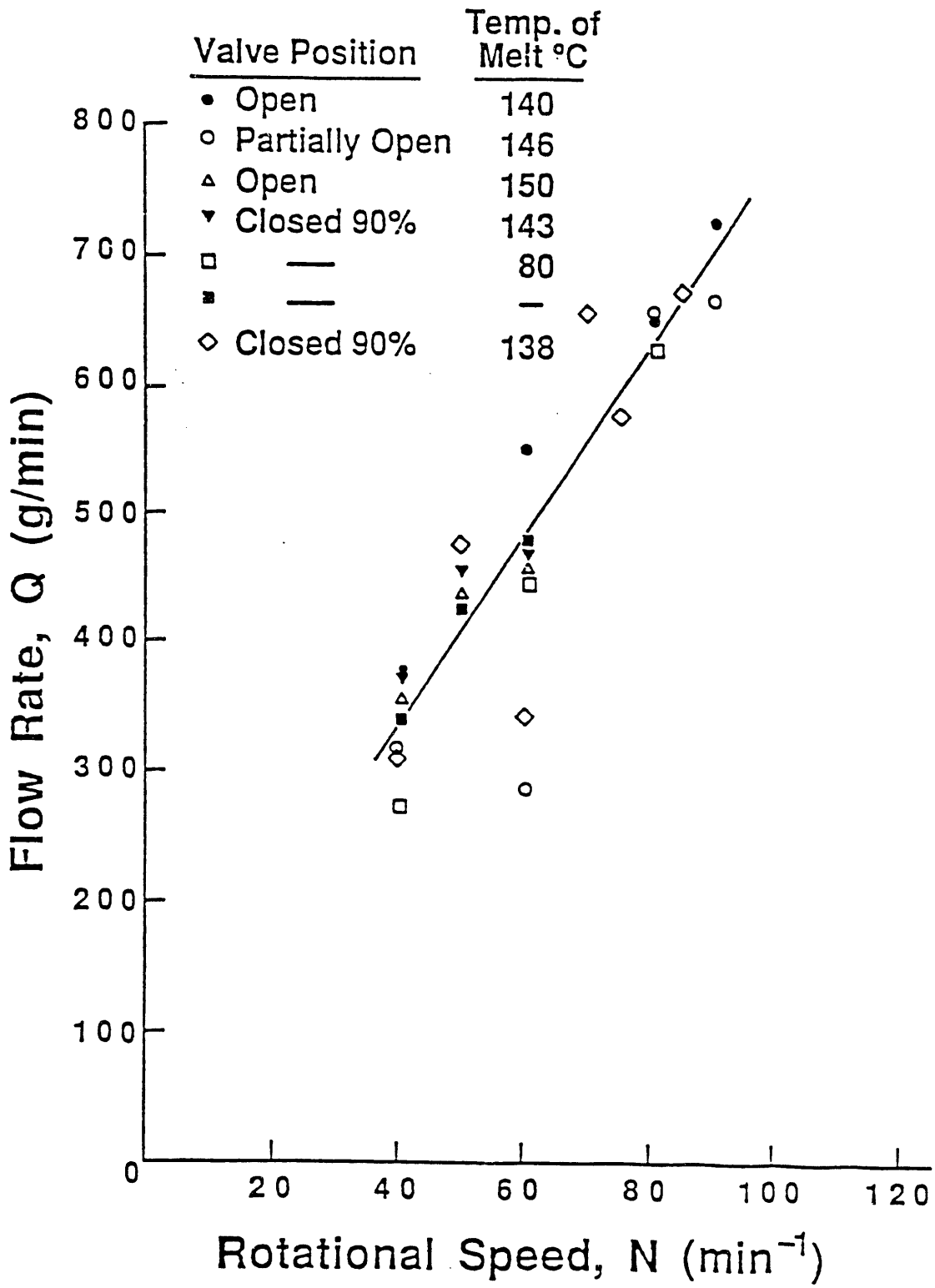

Figure 1.12. Flow Rates as a Function of Rotational Speed of HRHT Screw for Prodex-type Extruder with the Die on and Vacuum Bottoms as Feed.

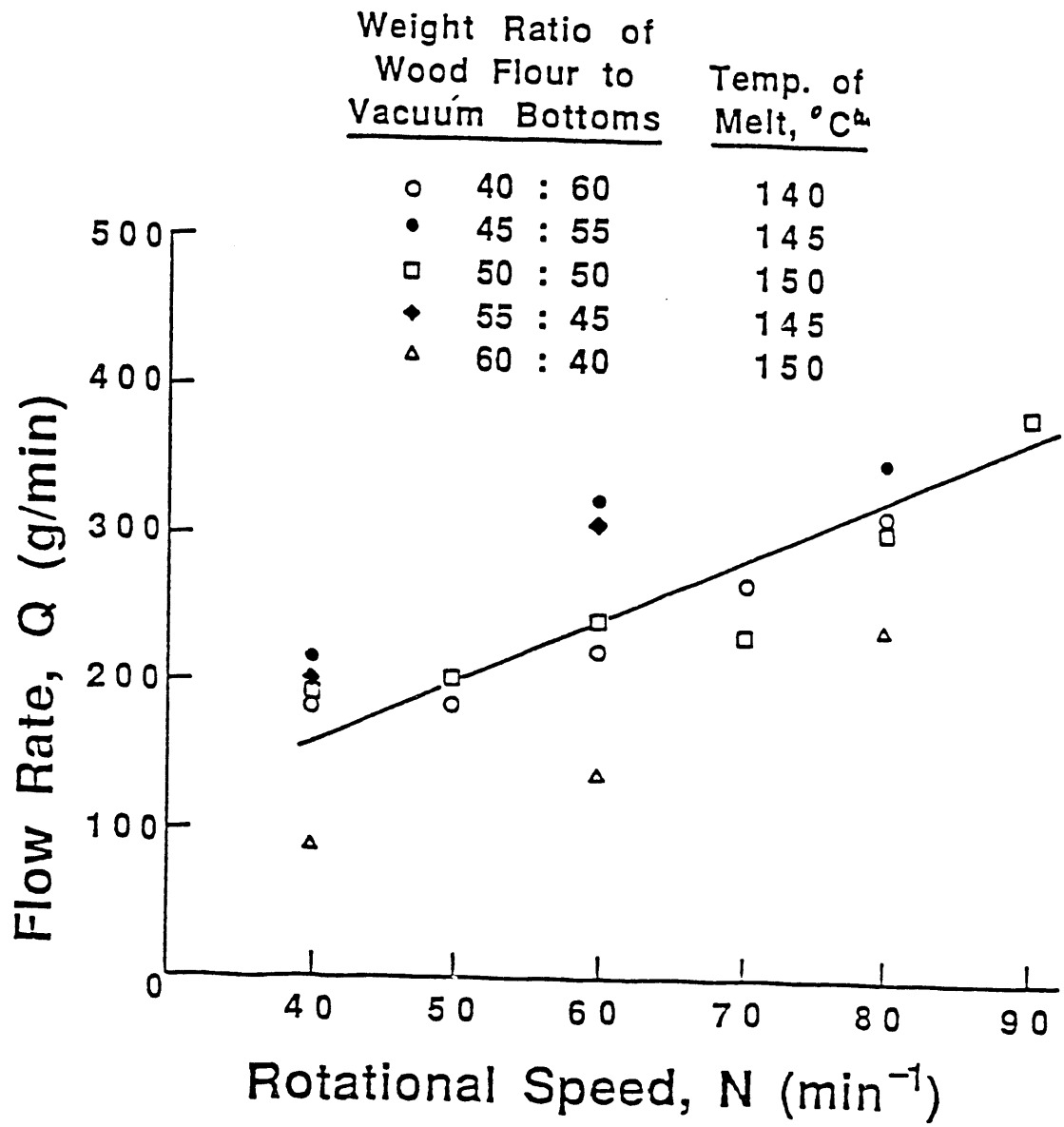

Figure 1.13. Flow Rates as a Function of Rotational Speed of HRHT Screw for Prodex-type Extruder-feeder with the Die on and Mixtures of Wood Flour and Vacuum Bottom as Feed.

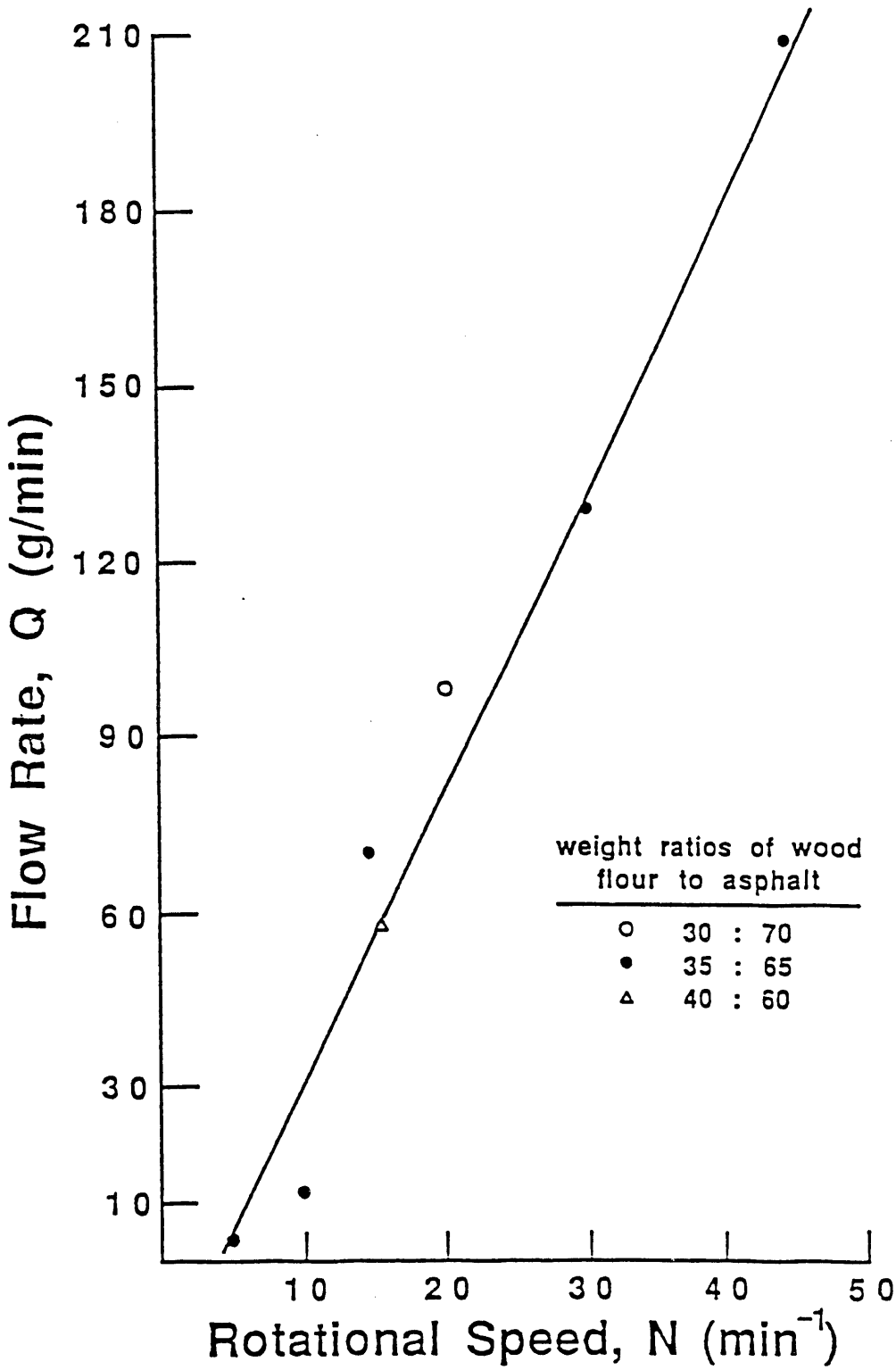

Figure 1.14. Flow Rates as a Function of Rotational Speed of Screw for Killion-type Extruder-feeder with the Die on and Mixtures of Wood Flour and Asphalt as Feed.

The theoretical values of F_d and F_p have been calculated by McKelvey (1962) and obtained as a function of the depth of the screw channel to the width of the channel, H/W. These values of F_d and F_p that are defined as the shape factors of the screw are between 0 and 1. For our most commonly used screw the ratio of H to W is approximately 0.05 and the theoretical values of F_d and F_p for this H to W ratio are both approximately 0.95. Our definition of F_d and F_p as drag and pressure flow coefficients implies that we consider these values as proportionality factors to the theoretical expressions rather than as pure shape factors only.

The first part of Equation (1.5) gives the drag flow Q_d and the second part is the pressure flow Q_p. Experiments were made with and without the die attached. From the output rates with the die removed, only the drag flow coefficient, F_d, is obtained since ΔP is small and the viscosity is high, and thus Q_p is negligible. Calculations of the value of Q_d and Q_p in Equation (1.5) show that the value of Q_p is much less than one percent of the value of Q_d under our operating conditions with the removed die. One should note that the fraction of pressure flow in Equation (1.5) out of the total flow is a function of N, η and ΔP. The fraction of pressure flow decreases as N and η increase, and it increases as ΔP increases.

At our operating conditions of up to 25 MPa (3630 psi) pressure and up to 100 min^{-1} rotational speed and especially with the very high apparent viscosity of feedstock in the range of 1-10 kPa•s, the two parameters N, and η, override the effect of ΔP on the pressure flow even with the die on. Thus, the pressure flow is negligible when the die is removed and is of little significance with the die in place, as will be discussed later.

From the experiments with the die on and with the F_d values known from the experiments without the die, the value of F_p are obtained. Using only the drag flow term in Equation (1.5), values of the drag flow coefficient, F_d, were calculated for the different materials and wood flour mixtures as summarized in Table 1.5. A comparison to the reference data for polyethylene can be made by analyzing Table 1.5. One can see that the values of F_d range between 0.62 and 1.06 for most of the cases except for pure vacuum bottoms which gives the high value of 1.31. The scattering of the data is expected because of the inherently unstable operating conditions of the extruder-feeder. The high value of F_d obtained for the vacuum bottoms may be significant, but additional experiments are necessary in order to verify this results obtained from a single experimental data point. It also appears that the value of F_d decreases slightly with increased rotational speed which may also be significant. The increased rotational speed, although producing some increase in pressure, has very little effect on pressure flow as one can see by calculating the theoretical pressure term in Equation (1.5). In our range of pressure of up to 25 MPa (3630 psi) and high viscosity of material of around 5 kPa•s, the values of Q_p are only 1-2% of the value of Q_d.

Table 1.5. Values of Drag Coefficients F_d for Various Materials and the Appropriate Drag Flows.

	LDPE		25 wt% *LDPE* 75 wt% *AC6-PE*		40 wt% *WF* 15 wt% *LDPE* 45 wt% *AC6-PE*		40 wt% *WF* 60 wt% *VB* Regrind		50 wt% *WF* 50 wt% *VB*		Vacuum Bottoms Fresh	
N (min^{-1})	Q'_d g/min	F_d *	Q'_d g/min	F_d	Q'_d g/min	F_d	Q'_d g/min	F_d	Q'_d g/min	F_d	Q'_d g/min	F_d
40	135	0.73	176	1.03	137	0.80	193	0.87	-	-	347	1.31
50	188	0.88	-	-	-	-	-	-	218	0.78	-	-
60	245	0.95	201	0.78	198	0.76	260	0.78	275	0.82	-	-
65	308	1.04	-	-	-	-	-	-	281	0.77	-	-
73	335	1.06	-	-	-	-	-	-	-	-	-	-
80	362	1.04	223	0.63	248	0.72	305	0.69	335	0.75	-	-
90	380	0.88	-	-	-	-	-	-	380	0.76	-	-
100	-	-	283	0.66	285	0.66	-	-	-	-	-	-
120	-	-	318	0.62	328	0.64	-	-	-	-	-	-
Average		0.94		0.74		0.72		0.78		0.78		

* F_d is dimensionless.

Q_d has units of m^3/min according to nomenclature (and also defining equations).

For the calculation of F_p both terms of Equation (1.5) are used. The results obtained for F_p are scattered and have an average value of 0.91. Values of F_d as obtained from the experiments with the die removed were used for these calculations.

The value of K_d for the valve on the die of the extruder-feeder was calculated using Equation (1.8) and the known data for LDPE. An average value for K_d of 0.00033 cm^3 was obtained for a die valve opening of 90%. The feedstock densities used for the calculations of the volumetric flow rates were 0.77 g/cm^3 for the LDPE mixtures and 1.0 g/cm^3 for the vacuum bottoms mixtures.

1.4.5.9 Calculation of the Drag and Pressure Flow Parameters, A and B

Using the experimental data with the die removed and the plots of Q versus N for several materials, the values of the drag flow parameter A were obtained from Equation (1.5) while neglecting the pressure term. Values of A in the range of 4-5 cm^3 were found for the various mixtures of wood flour and carriers of LDPE and vacuum bottoms.

From the experiments with the die on and the plot of Q versus N for the LDPE case, the value of the pressure flow parameter B was determined from Equation (1.9) and the known values of A and K_d. The value obtained for B was 7.3×10^{-5} cm^3.

Average values of F_d and F_p can be calculated from the values of A and B and the screw geometry data from their definitions as given in Equation (1.5).

1.4.5.10 Discussion and Analysis of Results

The single screw plasticating extruder was found to be adaptable as an extruder-feeder for pumping biomass mixtures such as wood flour and various carriers, such as high viscosity fluids or plasticating solids at appropriate temperatures, to the required high pressure of 25 MPa (3630 psi). The extruder-feeder as a unit operation has great potential and could prove to be the only practical solution in many cases where solids are to be pumped into reactors at very high pressures. A linear relationship was obtained between the flow rate and the rotational speed, and a power law relationship was obtained between the pressure rise and the rotational speed. The effects of several operational conditions, as well as, type of feedstock on the performance of the extruder-feeder were determined.

Experiments with asphalt and mixtures of asphalt and wood flour showed that good pumpability and high pressures were obtained (cooling the asphalt until it became brittle was necessary). Figure 1.14 shows the flow rates versus rotational speed for several experiments made with mixtures of wood flour and asphalt. The flow rate increases linearly with the screw speed.

As a first approximation, the basic design criteria and equations described by various authors (McKelvey, 1962; Tadmor and Klein, 1978; Glanvill, 1971; Bernhardt 1959) for

plasticating extruders also prevail for the extruder-feeder of solid mixtures in the biomass liquefaction process while using proper drag and pressure flow coefficients or drag and pressure flow parameters. However since the experimental data do not always follow exactly the theoretical and idealized equations, experimental runs on specific feedstock for accurate design equations are warranted. The effect of feedstock on flow rates and pressures generated is of special interest.

1.4.6 An Alternative Analysis of Pressure Generation

Referring to the fact that the extruder-feeder is equipped with a die and die valve that changes the openings of the die, there is no restriction to output flow when the die valve is fully open. Ideally, when there is no restriction at the outlet of an extruder the pressure in the metering zone should be small because there is no back pressure. However, this has rarely been the case. Even when the die valve was fully open, some pressures of up to 7 MPa (1,015 psi) were generated. This makes it impossible to separate the drag flow from pressure flow. When there is no pressure generation in the metering zone (i.e., P = 0), the equation we obtain for the flow rate is:

$$Q = 5.45\delta N \tag{1.13}$$

which is by drag flow only.

Equation 1.13 may be used to compare the fit of theory to experiment. It should only be used when ΔP is negligible. However, it can be used when small pressure drop is generated in the metering zone, provided the viscosity is high. To illustrate, Equation 1.2 can be rewritten after several substitutions as following:

$$\frac{Q}{\delta} = 5.45\ N - 1.1 \times 10^4\ \frac{\Delta P}{\mu} \tag{1.14}$$

Suppose N = 40 rpm, ΔP = 1,000 psi, $\mu = 10^6$ cp. Then:

$$\frac{Q}{\delta} = 218 - 11 = 207$$

The error introduced by neglecting the pressure term in Equation 1.14 is only 5 percent, but when $\mu = 10^5$ cp the error is 50 percent. In this case if $\Delta P = 100$ psi, the error would be again 5 percent. Note that Equation 1.14 is applicable only to the specific extruder-feeder utilized in this work.

To illustrate further, data on LDPE will be used here. Figure 1.15 shows the output flow rate of LDPE (measured experimentally) as a function of screw speed at various die valve opening conditions. It is obvious from Figure 1.15 that the net output flow rate decreases as the pressure in the metering zone increases. The difference of flow rate diminishes at lower screw speeds.

Experimental data on LDPE at 325°F (where upper value of pressure is 1,000 psi) are:

N (RPM)	$\dot{\gamma}$ *(sec^{-1})*	μ *(cp)*	δ *(g/cm^3)*	*Q (g/min)*
60	68.7	3.3×10^6	0.77	240
90	103	2.5×10^6	0.77	360

Using Equation 5.10:

	Drag Term	*Pressure Term*	*Total*
At 60 RPM, Q =	252	- 3.3	249
At 90 RPM, Q =	378	- 4.4	374

It is obvious that the pressure term is extremely small for the extruder-feeder. Therefore, neglecting it (at low pressure) introduces small errors indeed. This error is much smaller than the error in the net flow rate, Q.

1.4.6.1 Theoretical to Experimental Fit of Flow Rate

In order to obtain a quantitative measurement of the fit of theory to experiment, the following is proposed. As mentioned earlier, the net flow rate of an extruder consists of drag flow minus pressure flow. To determine the theoretical to experimental fit of the net flow rate, it is important to have a fit for the drag and pressure flow separately. Thus Equation 1.14 can be modified to:

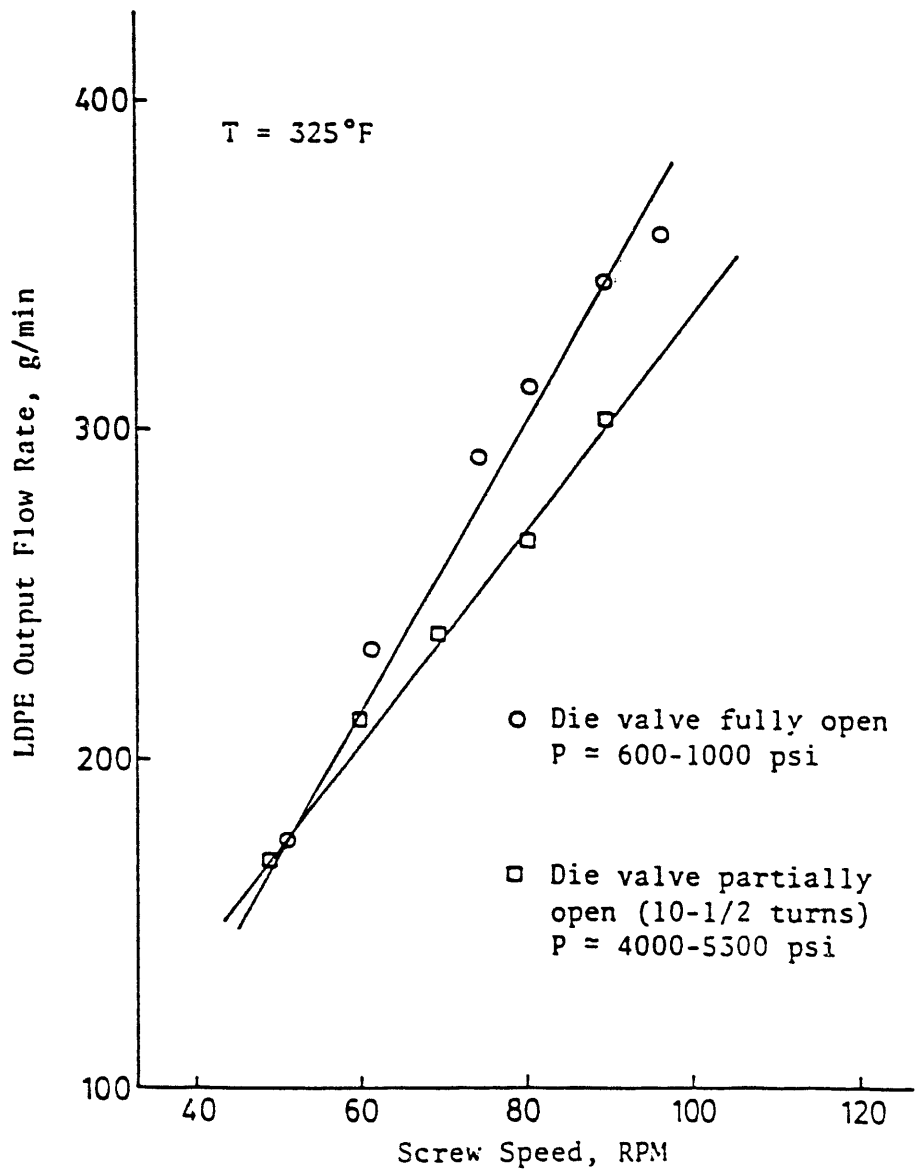

Figure 1.15. Effect of RPM Upon Extruder-feeder Output Flow Rates Under Fully Open and Partially Open Die Valve Conditions.

$$Q = 5.45\ \delta N\ a_d - 1.1 \times 10^4 \delta\ \frac{\Delta P}{\mu}\ a_p \qquad (1.15)$$

where

a_d is the non-Newtonian deviation factor for drag flow
a_p is the non-Newtonian deviation factor for pressure flow.

1.4.6.2 Non-Newtonian Deviation Factor for Drag Flow

For low pressure drop in the metering zone, Equation 1.15 is reduced to:

$$\frac{Q_d}{N} = 5.45\ \delta a_d \qquad (1.16)$$

Thus, the deviation factor a_d can be calculated by reading the slope Q/N of the flow rate versus rpm curve. Density data for wood flour slurries at experimental conditions are not available, but they can be approximated.

The deviation factor a_d will include, in addition to the experimental errors, the deviation from non-Newtonian behavior of slurries to the Newtonian behavior that was assumed in deriving the flow rate equation. Thus, the non-Newtonian effect will be incorporated in the drag flow term as it should be.

Table 1.6 shows the calculated values of a_d's for several carrier fluids and wood flour slurries. Density values that were assumed are included in the table. The densities for LDPE and LDPE/WAX mixture are accurately known.

For LDPE, two values of a_d were calculated. Each value is at different experimental conditions. The first one is equal to 1.0, which means that LDPE flow behavior was perfectly Newtonian. The second value is 0.96, which is very close to 1.0 and is probably due to experimental errors in measurement. These results are in accordance with those found in the literature. After all, polyethylene was used mostly to test the theoretical to experimental fit of the extruder flow rate equation.

For LDPE/AC-6 PE mixtures, the values of a_d were 0.54 and 0.58. This is expected, since the viscosity of AC6-PE is about 600 cp, which lowers the viscosity of the mixture dramatically. In addition, the output flow rate of LDPE/AC6-PE mixtures (especially at low LDPE concentration) is often erratic. The AC6-PE melts at a lower temperature than LDPE, and the extruder output at times contained unmelted LDPE. In addition, there was a separation

Table 1.6. Non.Newtonian Deviation Factor for Drag Flow, a_d.

Feedstock	Density g/cm3	Q/N g	a_d dimensionless
LDPE	0.85	4.62	1.0
	0.77	4.03	0.96
25% LDPE 75% AC-6	0.78 0.77	2.48 2.27	0.58 0.54
40% WF 15% LDPE 45% AC-6	1.0	2.45	0.43
VB	1.31	7.08	0.99
10% WF 90% VB	1.32	6.93	0.96
50% WF 50% VB	1.38	4.44	0.59

of AC6-PE from LDPE due to the difficulty of mixing two polyethylenes having such large differences of viscosity. An observation of the output as it was coming out of the extruder revealed an irregular output at times, when mostly LDPE would come out, followed by mostly AC6-PE and then LDPE again.

For vacuum bottoms, the value of a_d was 0.99. This shows that VB flow behavior did not deviate from that of LDPE. Even though VB mass flow rate was substantially higher than LDPE, the volumetric flow rate was the same. The extruder throughput is on a volume basis.

For wood flour/vacuum bottoms mixtures, the deviation increases as the concentration of wood flour increases. It is obvious that the addition of wood flour to vacuum bottoms changes the flow behavior of VB. For 10 wt.% WF/90 wt.% VB, the value of a_d was 0.96, while for 50 wt.% WF/50 wt.% VB, the value of a_d decreased to 0.59, about 60 wt.% less than predicted by the Newtonian model. Obviously there is a relationship between the non-Newtonian deviation factor and the slurry concentration measured as weight percent of wood flour. An exponential curve fit is used to determine such an effect. The resulting equation for WF/VB slurry is:

$$a_d = 1.025 \exp(-1.087^\circ C) \tag{1.17}$$

with $r^2 = 0.981$ (the closer to 1.0 the better the fit).

where:

a_d is the non-Newtonian deviation factor
c is the slurry concentration.

Substituting the value of a_d into Equation 1.16 yields:

$$Q_d = 5.99\ \delta N \exp(-1.087^\circ C) \tag{1.18}$$

This equation is applicable for the UA extruder-feeder upon wood flour/vacuum bottoms concentrated slurries. It includes the effect of non-Newtonian behavior of slurries upon the drag flow term only.

When a_d is less than one, the actual output flow rate is less than predicted by the Newtonian model. Middleman (1977) showed that when this is the case, the power law flow behavior index is less than one. This is the case of pseudoplastic behavior. Therefore, it can be concluded that WF/VB slurries are pseudoplastics.

1.4.6.3 New-Newtonian Deviation Factor a_p for Pressure Flow

The factor a_p is sensitive to pressure drop in the metering zone. As discussed earlier, the pressure fluctuations in this zone were great. This factor also depends on the viscosity. Since viscosity data for WF/VB concentrated slurries are not available, the evaluation of this factor is futile. Some calculations were made by assuming viscosity values, and the a_p factor ranged between 0.002 and 2.9.

Since the drag flow term is several times larger than the pressure flow term (at high values of viscosities), the importance of the pressure flow is small, and so is a_p.

1.4.7 Importance of Temperature Profile

The coefficient of friction is strongly affected by the temperature, and the extruder output decreases with increasing temperature in the solids conveying zone. Two experiments were made whereby the cooling water to the feed hopper was stopped. The temperature at the beginning of the feed section, T_7, increased sharply in a short time. In the first experiment vacuum bottoms (VB) was used. Figure 1.16 shows the results. At T_7 = 194°F the extruder-feeder output flow rate was 400 g/min. As T_7 increased to about 210°F the flow rate decreased sharply to 100 g/min. Thus an increase of temperature by 8% above 194°F resulted in a 75% decrease of vacuum bottoms output flow rate.

Figure 1.17 shows similar results for a 55% WF/45% VB slurry. At 40 rpm the output flow rate decreased 25% as the temperature increased some 10%. At this instance the screw speed was increased to 60 rpm. The flow rate increases sharply to well above 300 g/min. But it started declining slightly. At this point the screw speed was increased to 80 rpm. The output flow rate increased slightly, only to decline sharply to zero as the temperature reached 275°F.

These experiments show that the barrel temperature effect upon the extruder-feeder output flow rate of VB and WF/VB slurry is more significant than for other polymers (see Figure 1.18). Therefore, proper cooling of not only the feed hopper but also a section of the solids conveying zone may be necessary.

It is important to mention here that the temperature of the screw in the solids conveying zone is unknown for these experiments since there are no thermocouples inside the screw, nor at the screw surface. Since the screw is in contact with fresh feedstocks at room temperature, one might think that its temperature is low--at least in the first few turns. However, this was not always the case. A careful inspection of the screw at the end of these experiments revealed that some of the feedstocks were stuck down the helical channel, thus partially blocking the channel. They were, in effect, rotating with the screw without forward axial movement, i.e., $\phi = 0$. Therefore, as the output flow rate decreases as the temperature increases (Figures 1.16 and 1.17) the effective channel depth in the feed section was decreasing. Fresh feedstocks were contracting the materials already stuck in the channel instead of the smooth surface of the screw

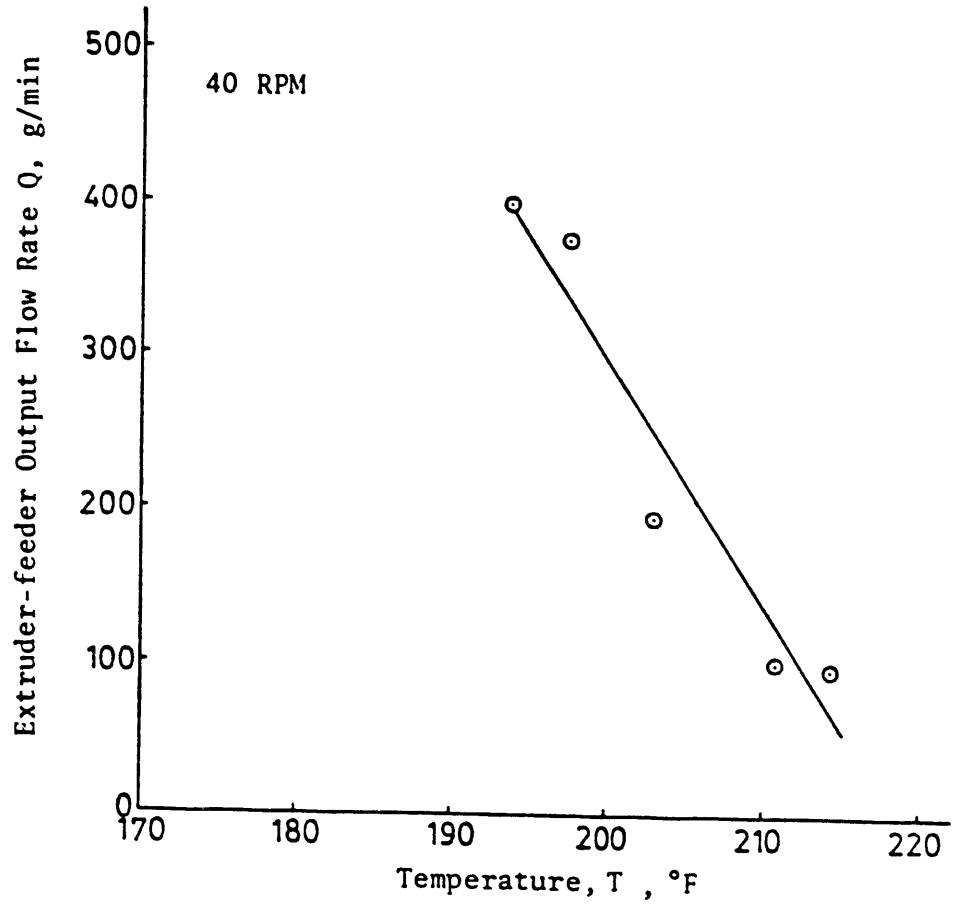

Figure 1.16. Effect of Inner Barrel Temperature in the Feed Section Upon the Output Flow Rate of Vacuum Bottoms.

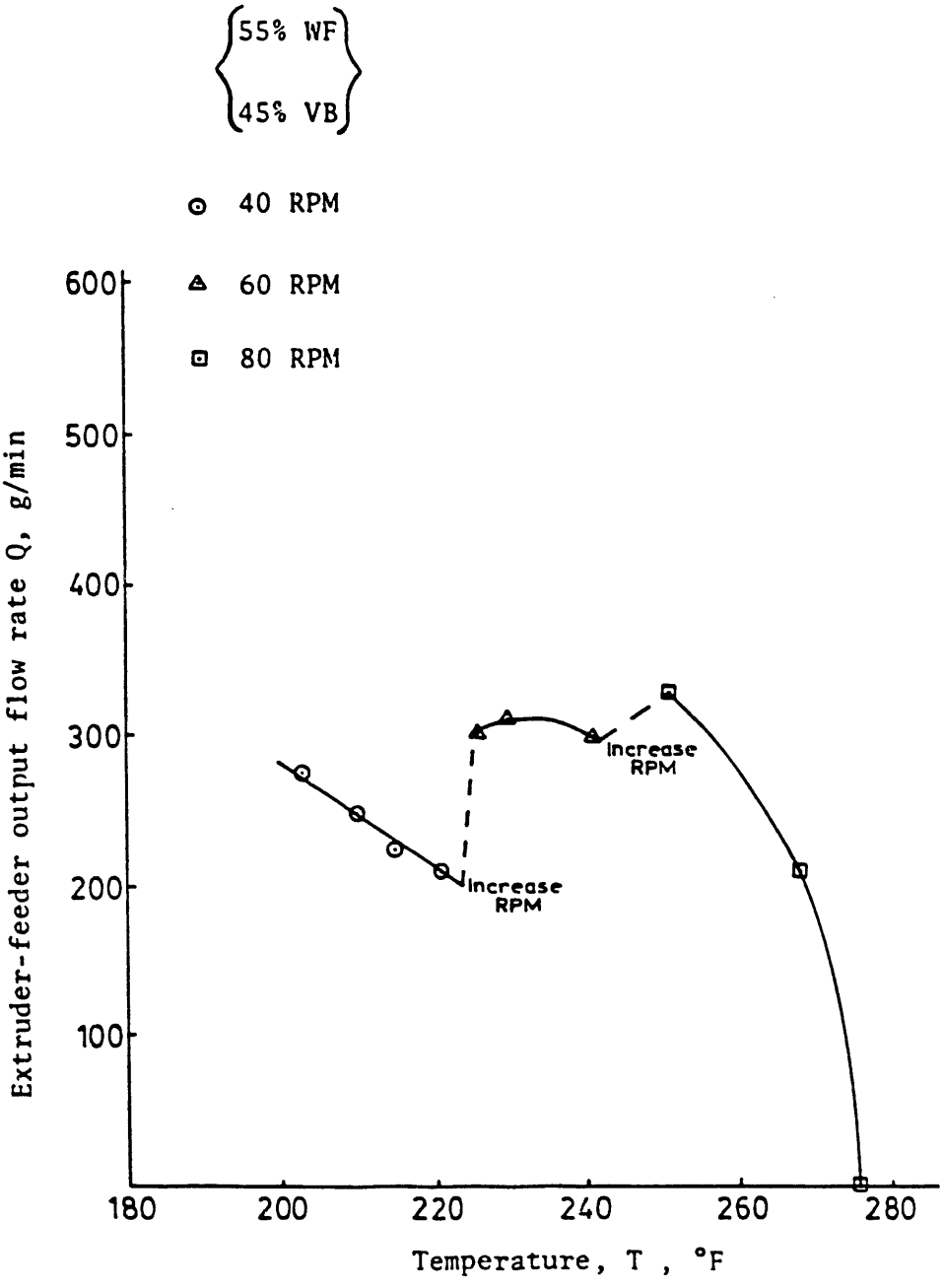

Figure 1.17. Effect of Inner Barrel Temperature in the Feed Section Upon the Output Flow Rate of Wood Flour Slurry at Various RPM.

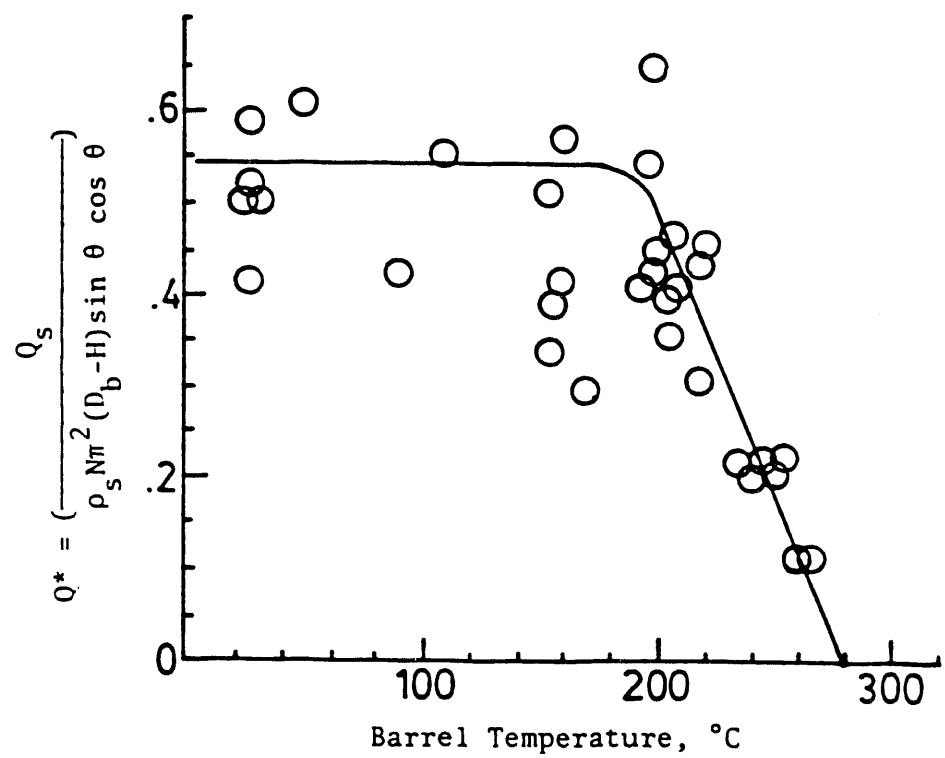

Figure 1.18. Effect of Barrel Temperature Upon Output for Polymethylmethacrylate in Various Screws and at Different Screw Speeds (courtesy of Griffith, 1967).

channel. Therefore, the temperature increase in these conditions is higher than normal and is due to particle-particle friction.

1.4.7.1 Importance of Particle Shape

Large uniform pellets result in higher extruder flow rate as compared to regrind feedstock on irregular shape. The same results were obtained for the extruder-feeder. Figure 1.19 shows the difference in output flow rate when LDPE pellets (fairly uniform particle diameter) and LDPE regrind (various particle sizes and shapes) were used. Figure 1.19 shows that at any screw speed, pellets yield higher output than regrind. The difference in output is 28% at 50 rpm, but it is only 18% at 85 rpm. But as the figure shows, the actual difference in output flow rate is higher at high rpm than at lower rpm. Hence the divergence of these two curves. In addition, regrind feedstock makes uniform control of extruder-feeder output rates difficult to control as seen in Figures 1.20 through 1.23, it was difficult to maintain a steady state operation with regrind feedstock. For LDPE pellets the pressure fluctuations at 40 rpm was as high as 500 psi (about 25% of actual pressure). For LDPE regrind the pressure fluctuations were more than 700 psi for the pressure just before the die, and more than 1,600 psi for the pressure just before the outlet of the melting zone. In the latter case the pressure increased by about 100%. If these values of pressure were to be used to calculate the viscosity of slurries, the error introduced might be as high as 100%, since the flow rate fluctuation is considerably less.

At 80 rpm the pressure and power fluctuations are even more significant than at 40 rpm. Figure 1.22 shows P_1 and P_2 fluctuating some 20% for LDPE pellets. Figure 1.23 shows extreme fluctuations for all pressures and power for LDPE regrind. P_1 ranged from a low of 50 psi to a high of 1,500 psi. P_2 ranged from 1,000 psi to 1,750 psi. Both P_1 and P_2 fluctuated in a wave-like fashion.

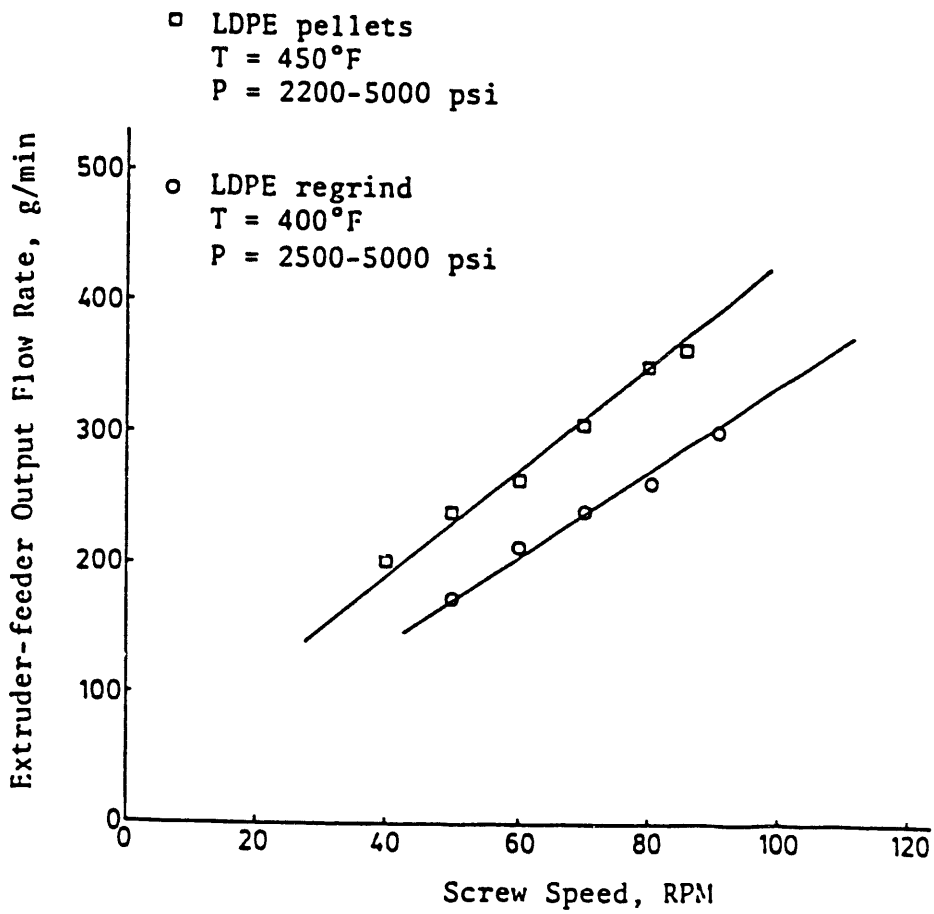

Figure 1.19. Effect of Screw Speed Upon Extruder-feeder Output Flow Rate for LDPE Pellets and LDPE Regrind.

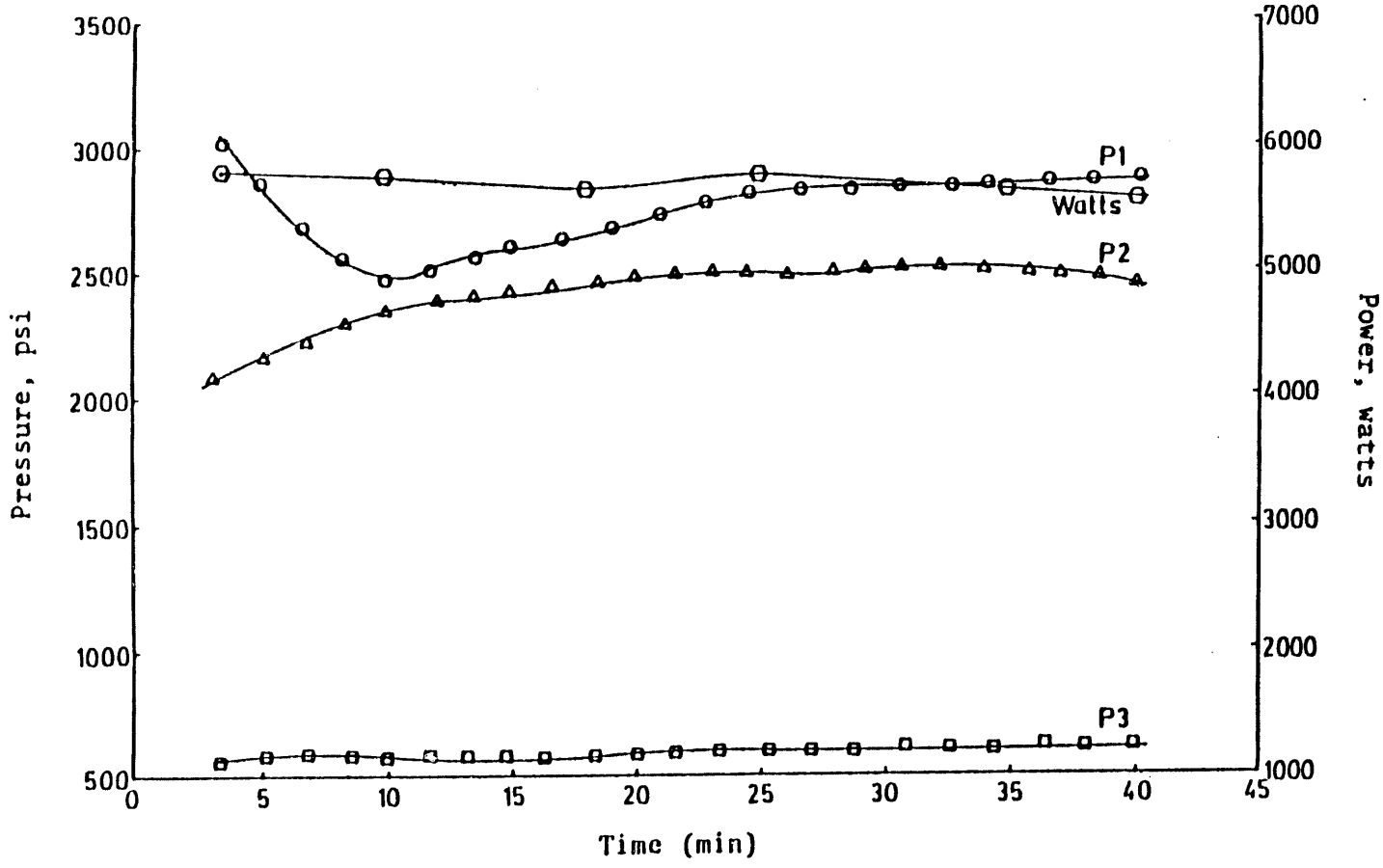

Figure 1.20. Pressure and Power Fluctuations with Time for LDPE Pellets at 40 RPM .

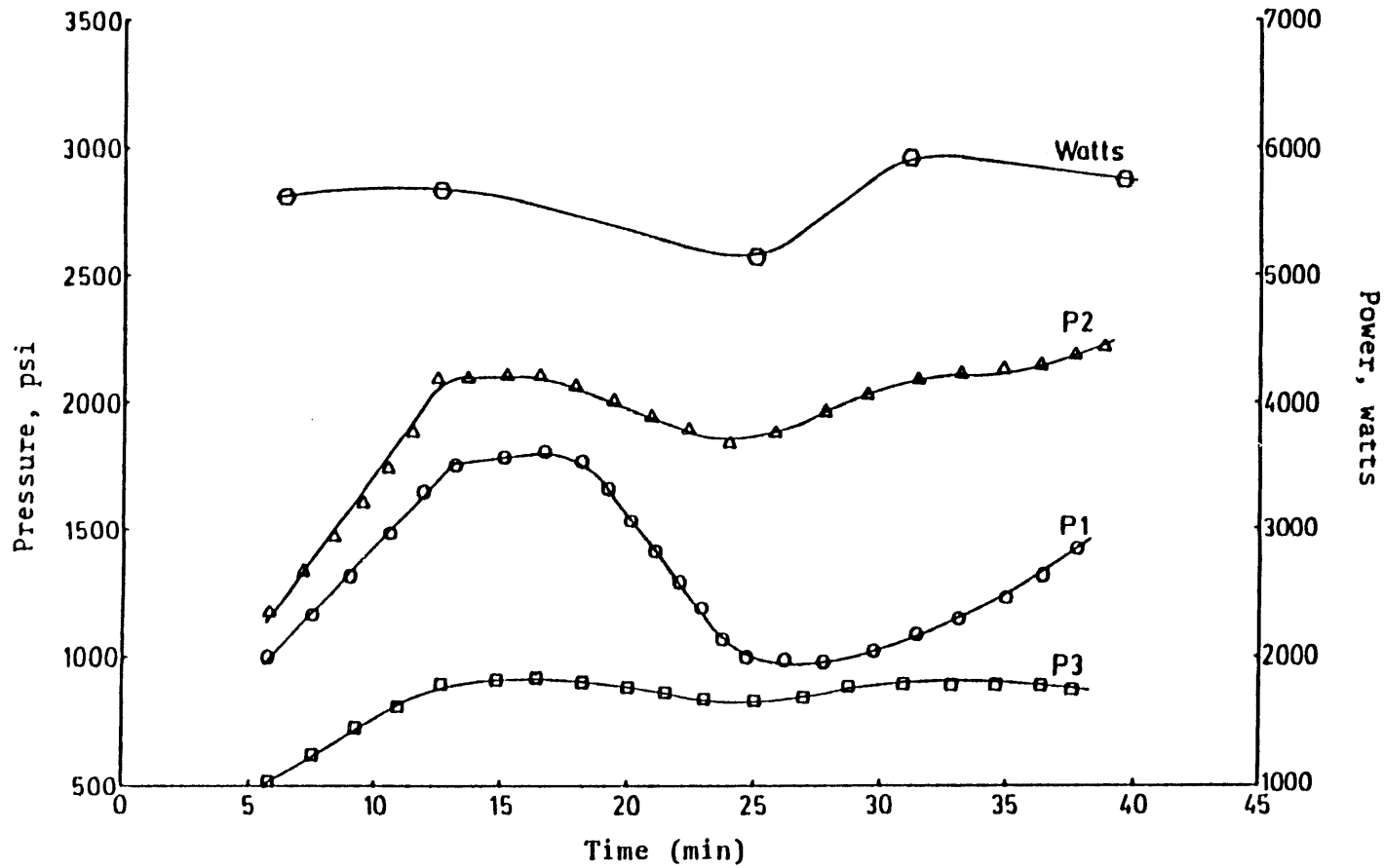

Figure 1.21. Pressure and Power Fluctuations with Time for LDPE Regrind at 40 RPM.

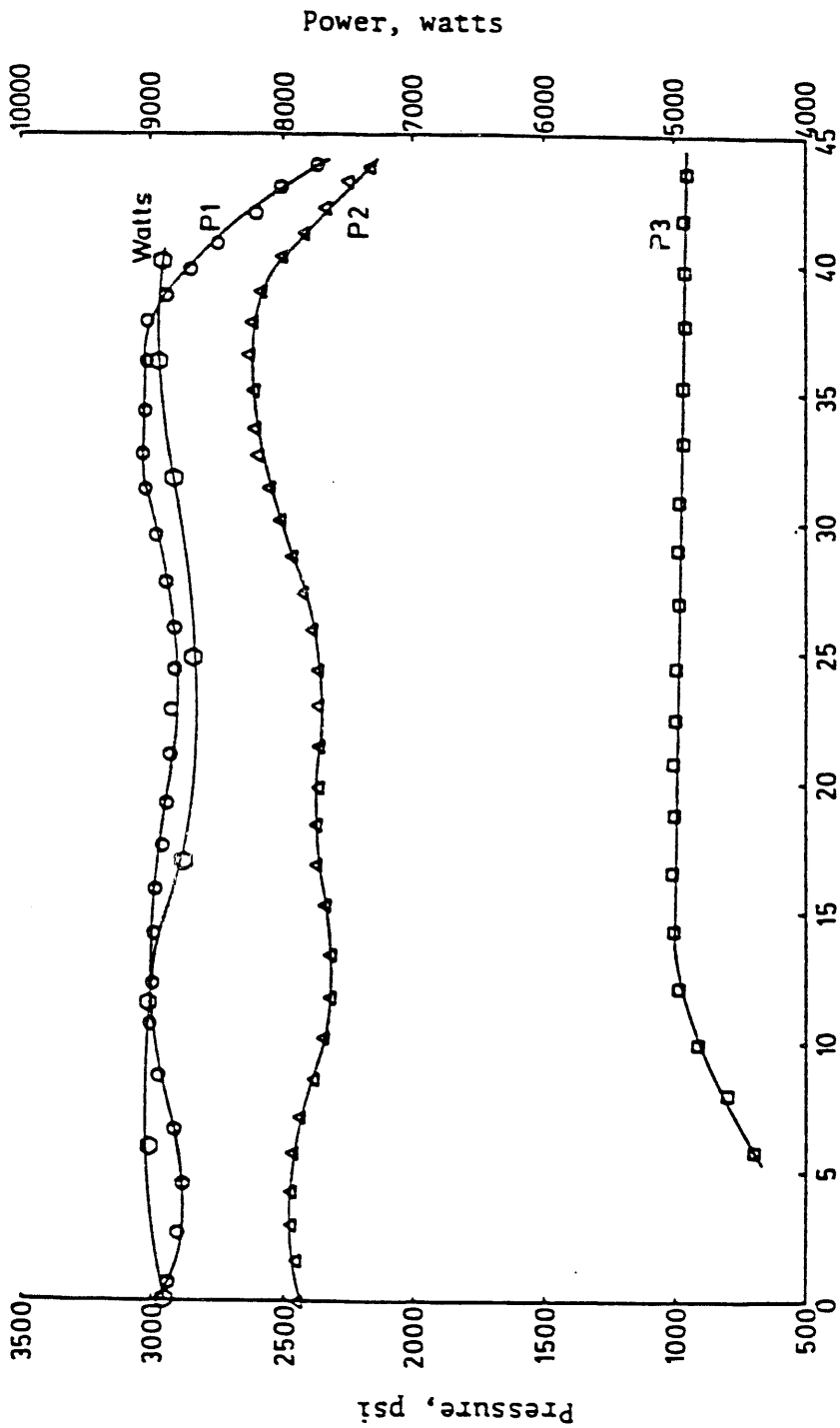

Figure 1.22. Pressure and Power Fluctuations with Time for LDPE Pellets at 80 RPM.

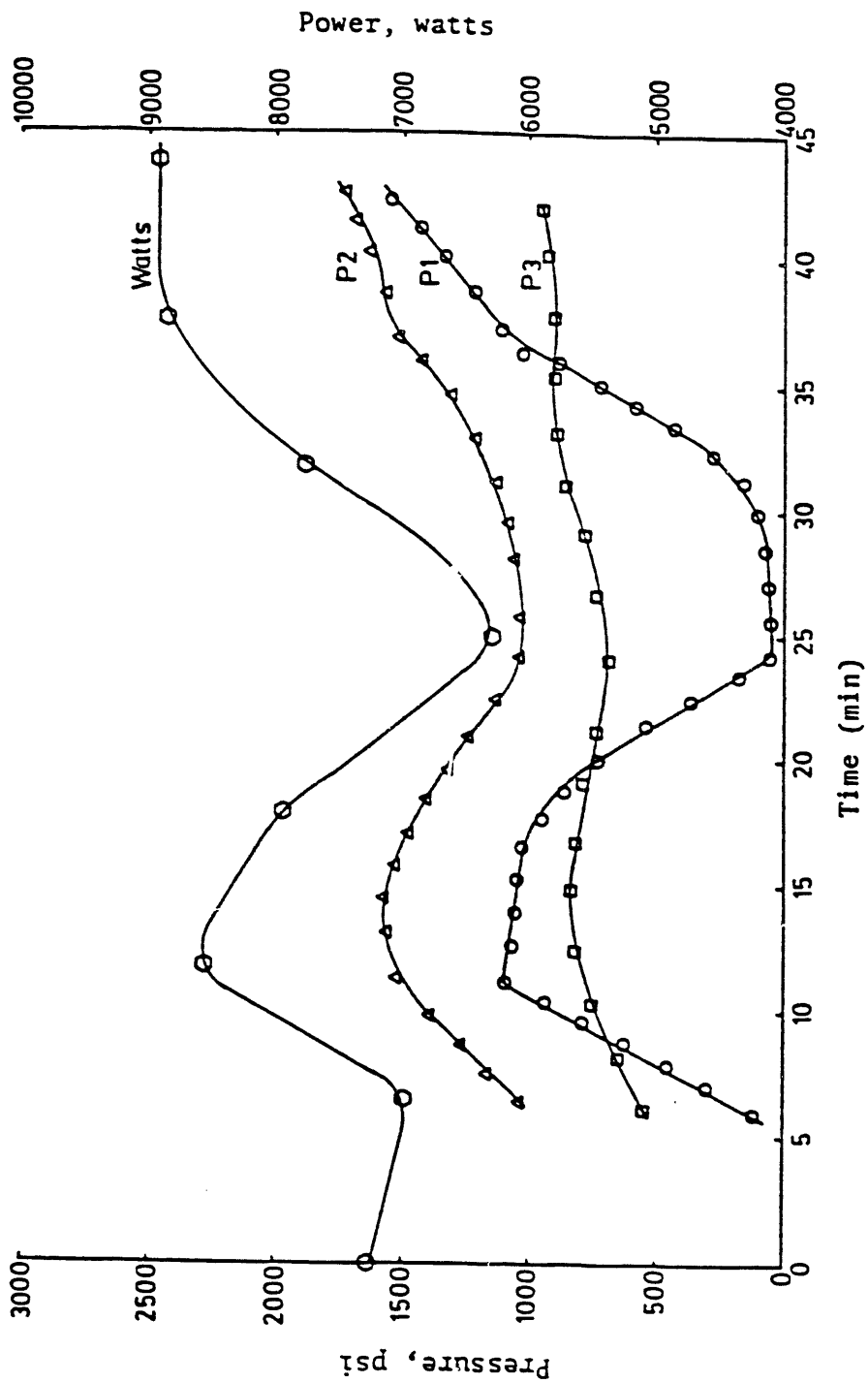

Figure 1.23. Pressure and Power Fluctuations with Time for LDPE Regrind at 80 RPM.

1.5 NOMENCLATURE

A	=	constant for drag flow
a_d	=	deviation factor for drag flow, dimensionless
a_p	=	deviation factor for pressure flow, dimensionless
B	=	constant for pressure flow
C	=	constant for leakage flow, or concentration of slurry, weight percent of solid
D	=	outer diameter of screw, or particle diameter
D_{e1}	=	equivalent diameter of particle to a cube with the same volume
D_{e2}	=	equivalent diameter of particle to a cube with the same volume
D_s	=	diameter of the root of the screw
$E\dot{\gamma}$	=	molar activation energy
e	=	flight width
f_b	=	coefficient of friction at the barrel surface in the axial direction, dimensionless
f_s	=	coefficient of friction at the screw surface
F_d	=	drag flow coefficient
F_p	=	pressure flow coefficient
H	=	depth of channel of screw
K_d	=	restriction coefficient of the die
L	=	total length of screw and length of particle
M	=	constant in Equation 1.7
N	=	rotational speed of screw
P	=	pressure
p	=	number of flights
P_1	=	inlet pressure to metering zone
P_2	=	exit pressure from metering zone
Q	=	total flow rate from extruder-feeder
Q_d	=	drag flow
Q_p	=	pressure flow
Q_l	=	leakage flow
Q_s	=	volumetric flow rate of solids
Q_v	=	flow rate through the die
R	=	gas constant
r	=	radial distance in cylindrical and spherical coordinates
t	=	time
T	=	temperature or thickness of particle
V_b	=	velocity of barrel surface relative to screw
V_{bz}	=	velocity component of V_b in the down channel direction
V_{pl}	=	axial velocity of the solid in the solids conveying zone
V_{pz}	=	velocity of the solid in the down channel direction at the barrel surface
W	=	average channel width or width of particle
Δz	=	length of metering section
$\dot{\gamma}$	=	shear rate, sec^{-1}

$\bar{\theta}$ = average helix angle, degrees
η = kinematic viscosity
μ = viscosity
δ = density
ϕ = angle at which the plug moves relative to the barrel
θ_b = helix angle at the barrel surface.

1.6 REFERENCES FOR PART I

Appell, H.R., et al., *"Converting Organic Wastes to Oil,"* U.S. Bureau of Mines, Reports of Investigations 7560 (1970).

Appell, H.R., et al., *"Converting Organic Wastes to Oil,"* U.S. Bureau of Mines, Reports of Investigations 8013 (1975).

Bernhardt, E.C., *"Processing of Thermoplastic Materials,"* Reinhold Publishing Corp., New York (1959).

Chan, I.C., *"Maximum Pressure Developed by Solid Conveying Force in Screw Extruders,"* Poly. Eng. & Sci, 15, 29-34 (1975).

Chehab, M.N., *"The Rheology of concentrated Cellulosic Slurries,"* MS Thesis, Department of Chemical Engineering, University of Arizona, Tucson, Arizona (1982).

Glanvill, A., *"The Plastics Engineer's Data Book,"* Industrial Press, New York (1971).

Iregbulem, I., *"Data Acquisition System for Single Screw Extruder,"* MS Thesis, University of Arizona, Tucson, Arizona (1982).

Lezzar, A., *"Effect of Void Volume on the Friction and Rheology of Concentrated Slurries,"* MS Thesis, Department of Chemical Engineering, University of Arizona, Tucson, Arizona (1983).

McKelvey, J.M., *"Polymer Processing,"* John Wiley & Sons, Inc., New York (1962).

Middleman, S., Fundamentals of Polymer Processing, McGraw-Hill Book Company, New York (1977).

Schenkel, G., *"Plastics Extrusion Technology and Theory,"* Elsevier Publishing Co., Inc., New York (1966).

Tadmor, Z., and I. Klein, *"Engineering Principles of Plasticating Extrusion,"* Robert E. Krieger Publishing Company, New York (1978).

White, D.H., D. Wolf, et al., *"Modified Extruder for Feeding Fine-Ground Cellulosic Slurries to Pressure Systems,"* Proceedings of the 13th Biomass Thermochemical Conversion Contractor's Meeting, CONF-8110115, October 27-29, 1981, Arlington, Virginia.

Wolf, D., and D.H. White, *"Effect of Flight Clearance on Mixing Characteristics in Plasticating Extruders,"* Society of Plastics Engineers, Annual Technical Conference, 33, pp. 439-442 (1975).

Yang, L.C., *"Rheology of Sawdust Filled Polymer,"* MS Thesis, Department of Plastics Engineering, University of Lowell (1981).

PART 2

Rheology of Wood Flour Slurries

TABLE OF CONTENTS

LIST OF TABLES

LIST OF FIGURES

PART 2

2.0 RHEOLOGY OF WOOD FLOUR SLURRIES

2.1 INTRODUCTION

The term *"shear-dependent materials"* is used in this study to describe shear thinning and shear thickening fluids. A shear thinning fluid is a material whose apparent viscosity decreases as the shear rate is increased. One subclass of shear thinning fluids is Bingham or the ideal plastic material. The Bingham fluid has a yield stress, ψ, and does not flow until the shear stress exceeds ψ. However, after flow begins, this fluid may in many cases flow almost like a Newtonian fluid or it may exhibit shear thinning. If the fluid flows like a Newtonian fluid after the yield stress is exceeded then its rheological equation can be written as in Equation 2.1,

$$\begin{aligned} &\text{if } |\tau_{yx}| < |\Psi| \Rightarrow \frac{dv_x}{dy} = 0 \quad \textit{No Flow} \\ &\text{if } |\tau_{yx}| > |\Psi| \Rightarrow |\tau_{yx} - \Psi| = \mu' \left|\frac{dv_x}{dy}\right| \end{aligned} \tag{2.1}$$

where μ' is called the plastic viscosity. Equation 2.1 can be used to approximate the flow behavior of many important substances such as paints, printing inks, toothpaste, drilling muds and some slurries. The Bingham or ideal plastic material was first introduced by Bingham and Green (1919). During later investigations Bingham noticed that some shear thinning materials did not possess a yield stress. High polymers like polyethylene and high polymer solutions such as rubber in toluene are examples of these shear thinning materials. Williamson (1929) introduced the term psuedoplastic to describe shear thinning materials that do not have a yield stress. There is no simple empirical or semi-empirical correlation that represents the rheology of psuedoplastic substances for the complex range of shear rates. The widely accepted empirical equation for shear thinning and shear thickening materials is the *"Power Law"* of Ostwald and de Waele. This model can be written as:

$$\tau_{yx} = -m\left|\frac{dv_x}{dy}\right|^{n-1}\frac{dv_x}{dy} \tag{2.2}$$

or

$$T_{yx} = -m|\dot{\gamma}|^{n-1}\dot{\gamma}$$

It is a two-parameter model, the two parameters being m and n. When n=1 Equation 2.2 reduces to Newton's law and $m=\mu$. If $n < 1$ the material is psuedoplastic; and if $n > 1$ the material is shear thickening. A subclass of shear thickening materials is dilatational substances which dilate when the shear rate is increased. These two terms should not be used interchangeably.

The *"power law"* fails at very low and very high shear rates. However, a three-parameter model called the Ellis model can be used to represent shear thinning substances at very low shear rates. The Sisko model, which is a three-parameter model also, can be used for the high shear rate range in laminar shear flow. Models with more constants have been suggested. Bird et al. (1977) reviewed some of these models.

2.2 RHEOLOGY OF CONCENTRATED WOOD SLURRIES

The rheology of Albany wood oil (TR12) and its wood flour (WF) slurries was investigated using a Couette type viscometer. TR12 oil was found to be a shear thinning fluid that obeyed the *"power law"* model. It did not possess any yield stress and it did not exhibit any viscoelastic behavior. TR12 oil had a thermal-history dependence but no shear-history dependence (Chehab, 1982).

WF/TR12 slurries were found to be shear thinning. The extent of shear thinning behavior increased with increased wood flour volume fraction, ϕ. The dependence of the apparent viscosity of these slurries on shear rate obeyed the *"power law"* model in the range of shear rates investigated. WF/TR12 slurries did not exhibit any yield stresses even at a wood flour volume fraction of 0.242. These slurries were found to be viscoelastic. The Weissenberg effect was observed during viscometric measurements. The Weissenberg effect was found to increase with increased wood flour volume fraction and shear rate when the particle dimensions were dept constant. A Dow Corning (DC23) silicone oil was used to compare the rheology of WF/TR12 slurries to that of WF/DC23 slurries. DC23 silicone oil is a Newtonian fluid up to a shear rate of about 250 sec^{-1}. The rheology of WF/DC23 slurries was very similar to that of WF/TR12 slurries.

Attempts at correlating the dependence of relative viscosity of these wood flour slurries on wood flour fraction included the use of: (1) Brodnyan's equation; (2) a modified Brodnyan equation; and (3) and exponential equation. Brodnyan's equation predicted relative viscosity values which were orders of magnitude smaller than the measured values. A modified Brodnyan equation gave a better fit than Brodnyan's equation, but the fit was far from exact. An exponential empirical equation gave a slightly better fit than the modified Brodnyan equation; however, the fit was still not exact. The dependence of relative viscosity on shear rate was incorporated into the exponential empirical equation. The resulting empirical equation gave the dependence of relative viscosity of wood flour slurries on wood flour volume fraction and shear rate. The fit provided by this empirical correlation was not exact, but it seemed to improve at higher shear rates.

Apparent and relative viscosities of these wood flour slurries were very high. These high values are thought to be primarily due to the properties of wood fibers which tend to increase particle-particle and fluid-particle interactions.

The experimental testing on the rheological behavior of TR12 oil, WF/TR12 slurries, DC23 silicone oil and WF/DC23 slurries were conducted. All figures that contain plots of apparent viscosity, η, versus shear rate, $\dot{\gamma}$, or time, t, as presented later, were drawn using actual data. All data were reported in terms of *"true"* apparent viscosity, η, and true shear rate, $\dot{\gamma}$. Plots of relative viscosity, η_r, versus shear rate or wood flour volume fraction, ϕ, were drawn based on actual apparent viscosity data except where specifically noted.

2.2.1 Rheology of Albany TR12 Wood Oil

The rheological behavior of TR12 oil was investigated at various temperatures and shear rates. The apparent viscosities of pure TR12 oil were measured at various shear rates at the following temperatures: 22°C, 41°C, 55°C, 65°C, 75°C, 84°C and 93°C. The effect of shear rate, $\dot{\gamma}$, on the apparent viscosity, η, of TR12 oil at various temperatures is shown in Figure 2.1. From this figure it can be seen that TR12 oil is shear thinning. Moreover, the extent of shear thinning increases with increased temperature of the sample. For example, the line representing the data at 22°C is almost flat, indicating a mild shear thinning effect, whereas the line representing the data at 93°C is relatively steep, implying a stronger shear thinning effect. Thus, the shear thinning behavior of TR12 oil is dependent on temperature.

Apparent viscosity data versus shear rate yielded straight lines when plotted on logarithmic scales as in Figure 2.1. Thus, the *"power law"* model was used to correlate apparent viscosity and shear rate data employing a standard non-linear regression program using a calculator. The resulting correlation gave a good fit of the data in the range of shear rates investigated. The particular form of the *"power law"* model used to correlate the data was:

$$\eta = \frac{m_1}{|\dot{\gamma}/\dot{\gamma}_1|^{(1-n)}} \tag{2.3}$$

where

m_1 = a constant, $m_1 = n$ when $\dot{\gamma}_1 = \dot{\gamma} = 1\ sec^{-1}$

$\dot{\gamma}_1$ = a constant, $\dot{\gamma}_1 = 1\ sec^{-1}$

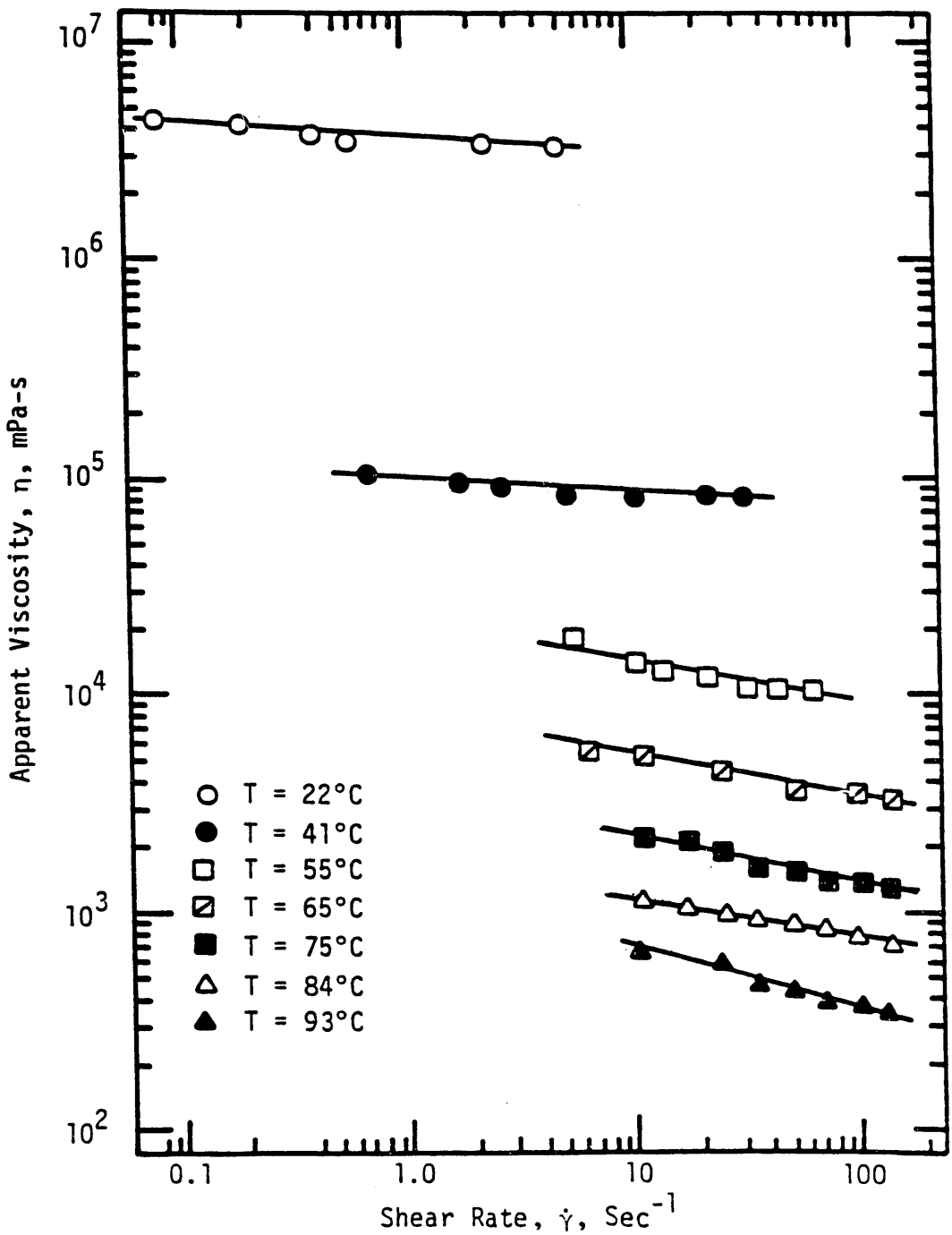

Figure 2.1. Effect of Shear Rate on Apparent Viscosity of TR12 Oil.

Since $\dot{\gamma}_1 = 1\ sec^{-1}$ and the Haake viscometer employs the magnitude of the shear rate, and the shear stress, regardless of their signs, Equation 2.3 becomes:

$$\eta = \frac{m_1}{\dot{\gamma}^{(1-n)}} \tag{2.4}$$

Equation 2.4 has two parameters, namely m and n. These two parameters were calculated using the non-linear least squares regression program. All correlations of $\dot{\gamma}$ versus η are reported using Equation 2.4. *"Power Law"* correlations for TR12 oil are presented in Table 2.1. From this table, it can be seen that the *"power law"* flow index, n, decreased with increased temperature. A decrease in the value of n indicates increased shear thinning. TR12 oil did not possess a yield stress, ψ, in the range of shear rates investigated. TR12 oil did not exhibit the Weissenberg effect at any shear rate used in the experiments. Thus, TR12 oil is not viscoelastic.

2.2.2 Rheology of WF/TR12 Slurries

The rheological behavior of WF/TR12 slurries was investigated at two temperatures, namely 65°C and 93°C. The effect of shear rate, $\dot{\gamma}$, on the apparent viscosity, η, of WF/TR12 slurries at 65°C is shown in Figure 2.2. Similar plots for WF/TR12 slurries at 93°C are presented in Figures 2.3 and 2.4. As can be seen from these three figures, all WF/TR12 slurries are shear thinning. Moreover, the extent of shear thinning behavior increases with increased WF volume fraction, ϕ. Also, all the curves in these figures are straight lines. Thus, the *"power law"* model should fit the apparent viscosity versus shear rate data in the range of shear rates investigated. A standard non-linear least squares regression program was used to correlate the apparent viscosity data versus shear rate. Apparent viscosity correlations for WF/TR12 slurries at 65°C and 93°C are presented in Tables 2.2 and 2.3. As can be seen from these tables, WF/TR12 slurries become more shear thinning as WF volume content increases. Moreover, the *"power law"* flow index, n, decreases with increased ϕ. From the high values of quality of fit, it is evident that the *"power law"* model fits the apparent viscosity data fairly well in the range of shear rates investigated.

WF/TR12 slurry did not show any yield stress in the range of shear rates investigated. The Weissenberg effect was noticed, especially at higher values of ϕ and $\dot{\gamma}$. No measurement of normal stresses were made since the Haake viscometer used is not designed to measure normal stresses. However, it was observed that at a certain wood flour volume fraction, ϕ, if the shear rate was increased the Weissenberg effect, as manifested by the escape of the sample from the viscometer gap, increased. A similar Weissenberg effect was noticed when ϕ was increased. This can be realized best by noting that the range of shear rates, $\dot{\gamma}$, for WF/TR12 slurries at 93°C was limited to very low $\dot{\gamma}$ values at $\phi = 0.1989$ and $\phi = 0.242$ due to the Weissenberg

Table 2.1. "Power Law" Correlations of TR12 Oil.

Temperature (°C)	Shear Rate Range (sec^{-1})	Correlation	Flow Index, n	Quality of Fit
25	0.08 - 5	$\eta = \frac{3{,}636{,}024.091}{\dot{\gamma}^{0.056}}$	0.944	0.91
41	0.7 - 32	$\eta = \frac{98{,}477.002}{\dot{\gamma}^{0.057}}$	0.943	0.93
55	5.6 - 64	$\eta = \frac{25{,}865.243}{\dot{\gamma}^{0.0215}}$	0.785	0.95
65	6.4 - 145	$\eta = \frac{7{,}918.164}{\dot{\gamma}^{0.178}}$	0.820	0.94
75	12.8 - 145	$\eta = \frac{3{,}754.77}{\dot{\gamma}^{0.208}}$	0.792	0.94
84	12.8 - 145	$\eta = \frac{1{,}846{,}756}{\dot{\gamma}^{0.191}}$	0.809	0.94
93	12.8 - 145	$\eta = \frac{1{,}060{,}434}{\dot{\gamma}^{0.277}}$	0.773	0.98

Table 2.2 Apparent Viscosity Correlations of WF/TR12 Slurries at 65°C.

Wood Flour Content, ϕ x 100, (vol%)	Shear Rate Range, (sec^{-1})	Correlation	Flow Index, n	Quality of Fit
0	6.4 - 145	$\eta = \frac{7{,}918.164}{\dot{\gamma}^{0.178}}$	0.822	0.94
3.84	3.2 - 102	$\eta = \frac{21{,}950.095}{\dot{\gamma}^{0.233}}$	0.767	0.97
7.77	0.4 - 72	$\eta = \frac{131{,}473.792}{\dot{\gamma}^{0.411}}$	0.589	0.97
11.81	0.1 - 58	$\eta = \frac{1{,}337{,}075.347}{\dot{\gamma}^{0.756}}$	0.244	1.0
15.94	0.1 - 32	$\eta = \frac{6{,}036{,}148.494}{\dot{\gamma}^{0.812}}$	0.188	1.0

Table 2.3 Apparent Viscosity Correlations of WF/TR12 Slurries at 93°C.

Wood Flour Content ϕ x 100 (vol%)	Shear Rate Range (sec^{-1})	Correlation	Flow Index, n	Quality of Fit
0	12.8 - 145	$\eta = \frac{1,060.434}{\dot{\gamma}^{0.227}}$	0.773	0.98
3.77	12.8 - 145	$\eta = \frac{6,141.404}{\dot{\gamma}^{0.409}}$	0.591	1.0
7.64	12.8 - 145	$\eta = \frac{17,174.092}{\dot{\gamma}^{0.484}}$	0.516	0.97
11.62	2.3 - 102	$\eta = \frac{336,232.351}{\dot{\gamma}^{0.796}}$	0.204	1.0
15.70	1.8 - 79	$\eta = \frac{1,383,413.370}{\dot{\gamma}^{0.744}}$	0.256	1.0
19.89	0.02 - 0.14	$\eta = \frac{7,653,552.446}{\dot{\gamma}^{0.879}}$	0.121	1.0
24.20	0.02 - 0.07	$\eta = \frac{15,504,177.780}{\dot{\gamma}^{0.878}}$	0.122	1.0

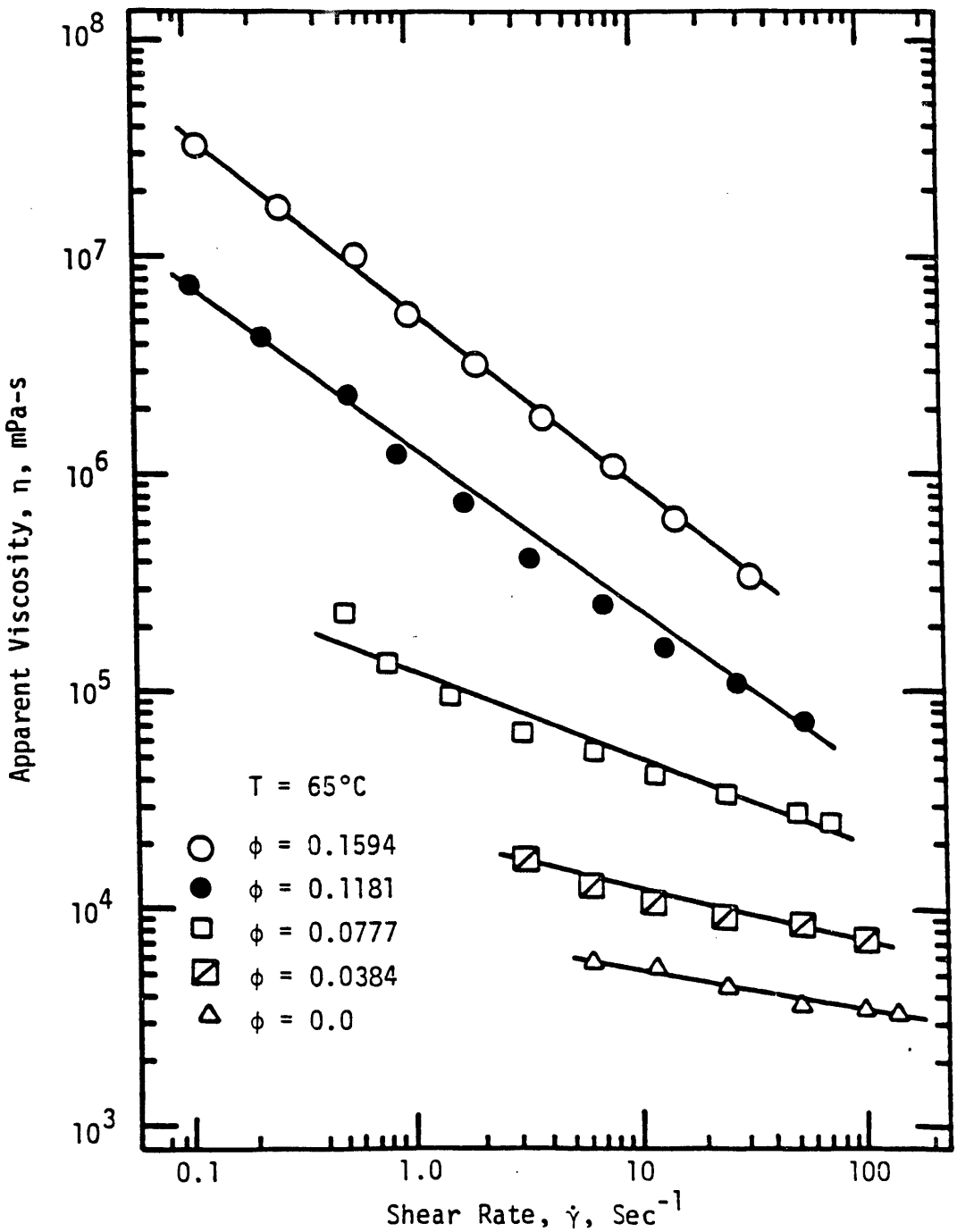

Figure 2.2. Effect of Shear Rate on Apparent Viscosity of TR12 Oil and WF/TR12 Slurries at 65°C.

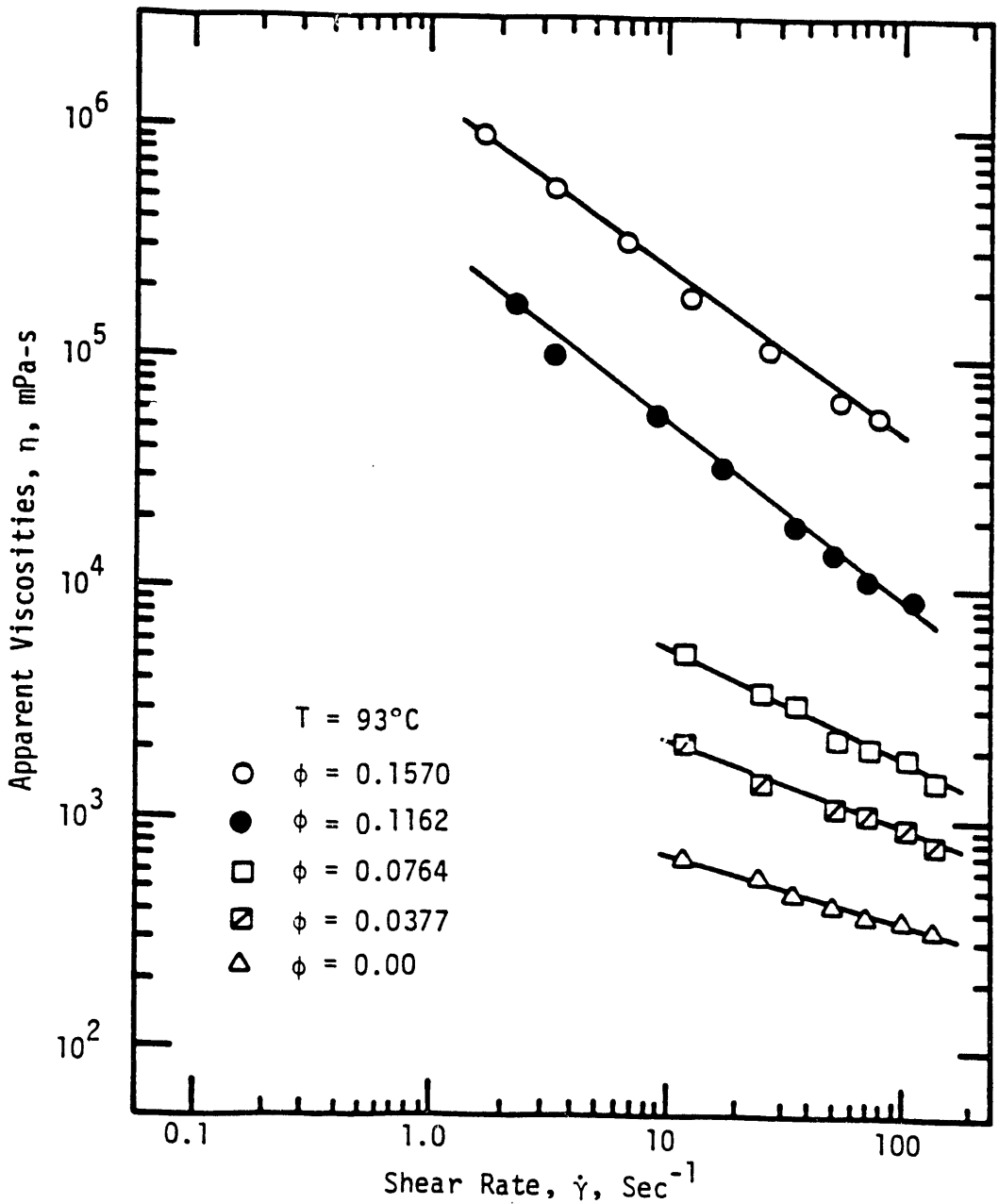

Figure 2.3. Effect of Shear Rate on Apparent Viscosity of TR12 Oil and WF/TR12 Slurries at 93°C.

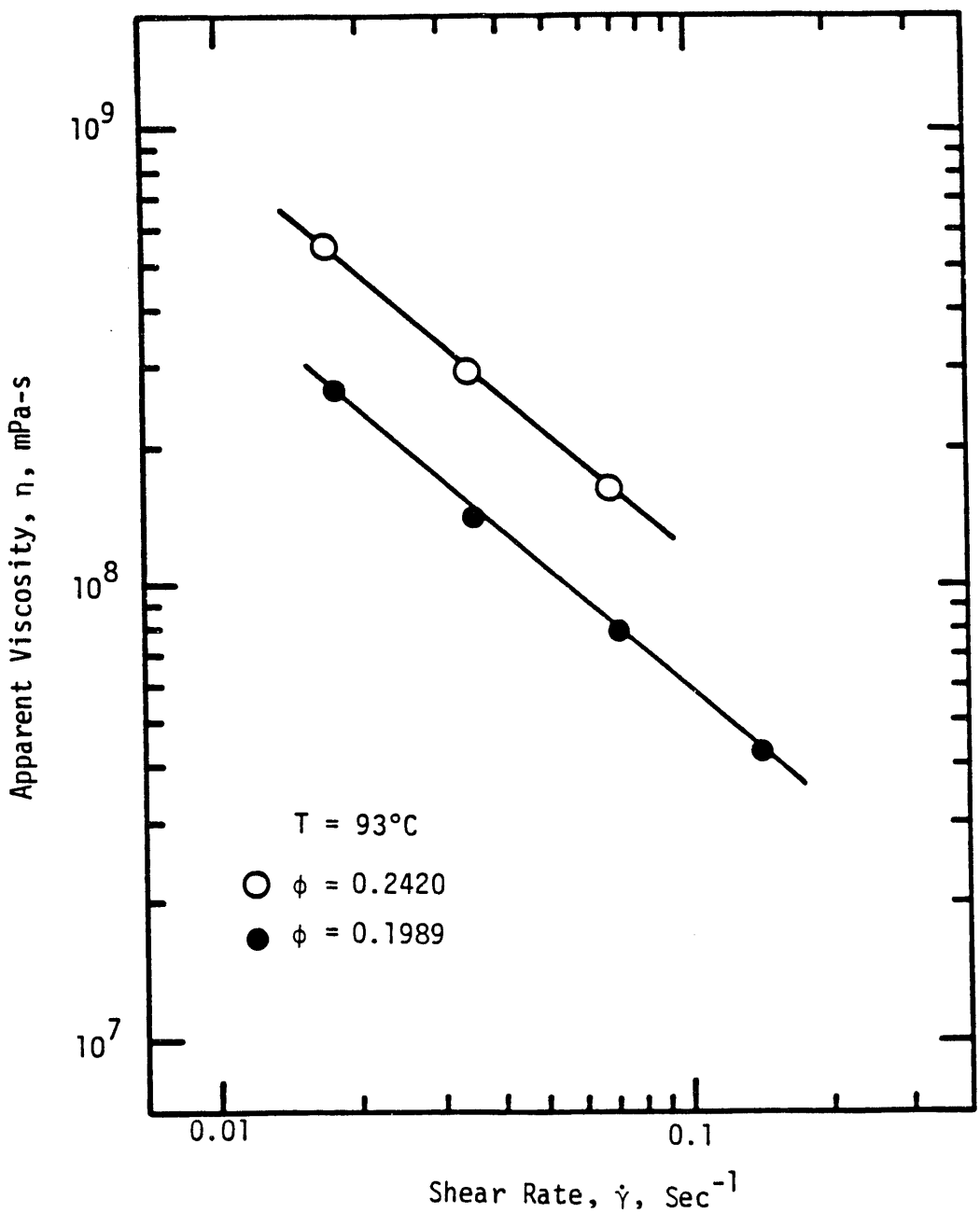

Figure 2.4. Effect of Shear Rate on Apparent Viscosity of WF/TR12 Slurries at 93°C for ϕ = 0.199 and ϕ = 0.242.

effect. An increase in the Weissenberg effect is indicative of increased normal stresses. Thus, although no quantitative measurements of normal stresses were made, qualitative observations confirmed that normal stresses increase with increased solids volume fraction, ϕ, or with increased shear rate. Fortunately, the Weissenberg effect was more pronounced at higher ϕ and $\dot{\gamma}$ and those values were not reported. Consequently, WF/TR12 slurries are viscoelastic. However, no decisive conclusion could be made regarding the cause of normal stresses.

The values of the relative viscosity, η_r, were calculated for the slurries using actual apparent viscosity data. The relative viscosity of a slurry is the ratio of the apparent viscosity of the slurry to that of the pure fluid at the same temperature and shear rate. The effect of shear rate on the relative viscosity, η_r, of WF/TR12 slurries at 65°C and 93°C is shown in Figures 2.5 - 2.7. From these figures it can be seen that the relative viscosity, η_r, of WF/TR12 slurries decreases quickly with increased shear rates, especially at high WF volume fractions. The dotted lines in Figures 2.6 and 2.7 represent η_r values which were not calculated from actual apparent viscosity values. These dotted portions were extrapolated using the *"power law"* correlations obtained earlier. The relative viscosity, η_r, was correlated as a function of the shear rate, γ, for WF/TR12 slurries. The correlations were obtained using a standard non-linear least squares regression program. It was found that an expression like the *"power law"* model can represent the dependence of η_r on $\dot{\gamma}$ very accurately. This result should not be surprising, since η versus $\dot{\gamma}$ data for TR12 oil and WF/TR12 slurries obey the *"power law"* model. From the definition of relative viscosity one can write:

$$\eta_r = \frac{\eta_s}{\eta_f} \tag{2.5}$$

where

η_r = relative viscosity of the slurry
η_s = apparent viscosity of the slurry
η_f = apparent viscosity of the fluid

But from the *"power law"* model η_s and η_f can be written as:

$$\eta_s = \frac{m_1'}{\dot{\gamma}^{(1-n_s)}} \tag{2.6}$$

and

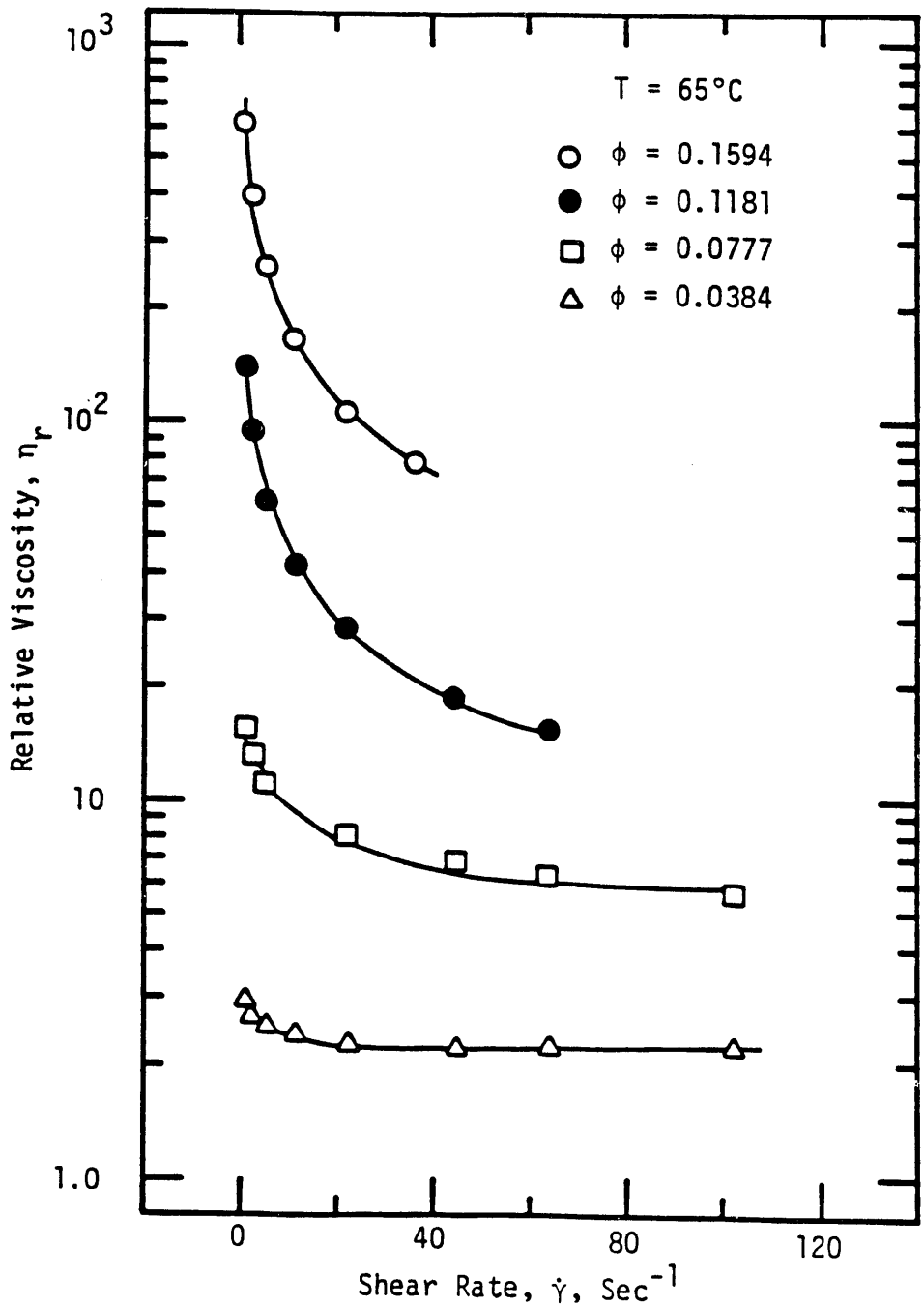

Figure 2.5. Effect of Shear Rate on Relative Viscosity of WF/TR12 Slurries at 65°C.

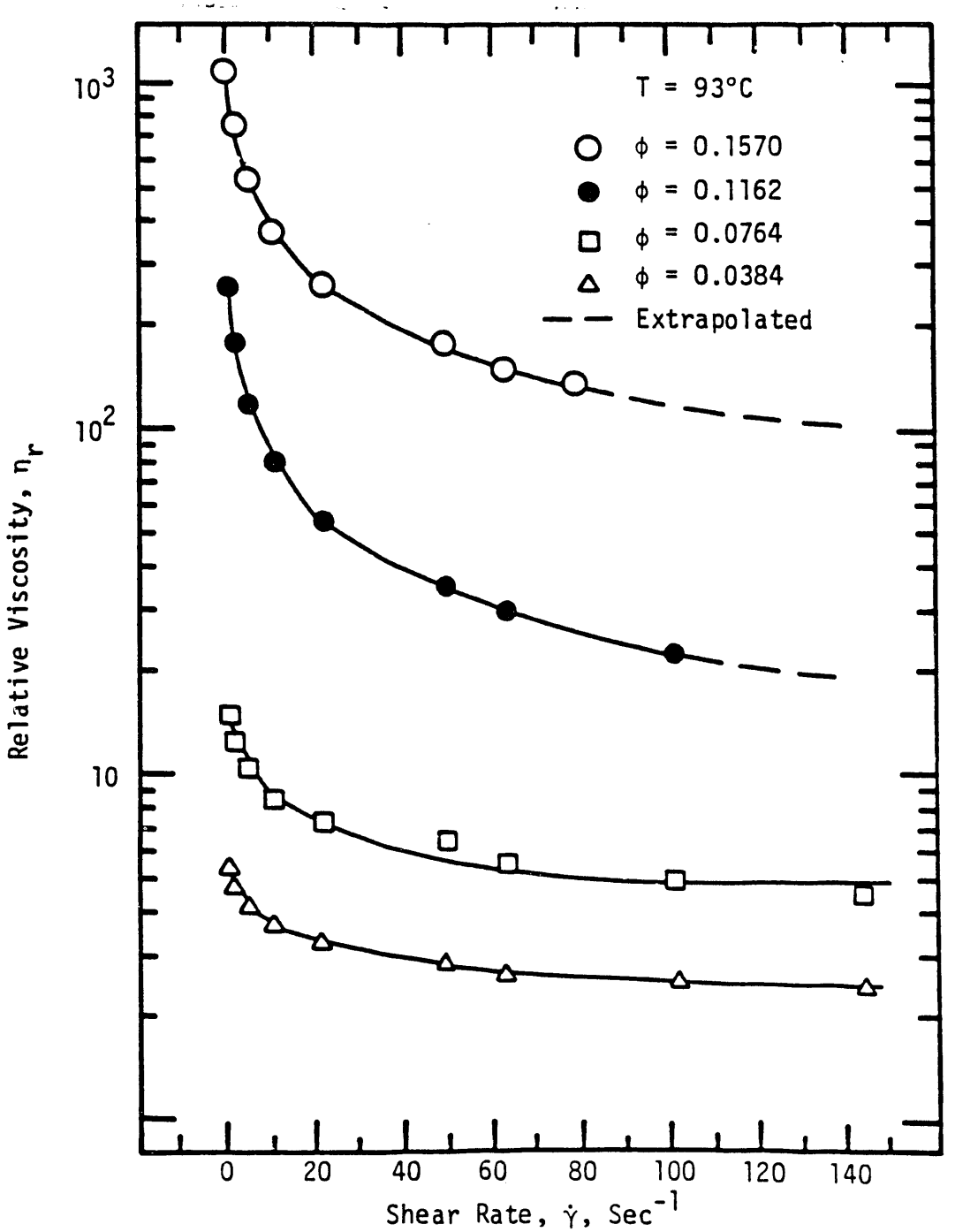

Figure 2.6. Effect of Shear Rate on Relative Viscosity of WF/TR12 Slurries at 93°C.

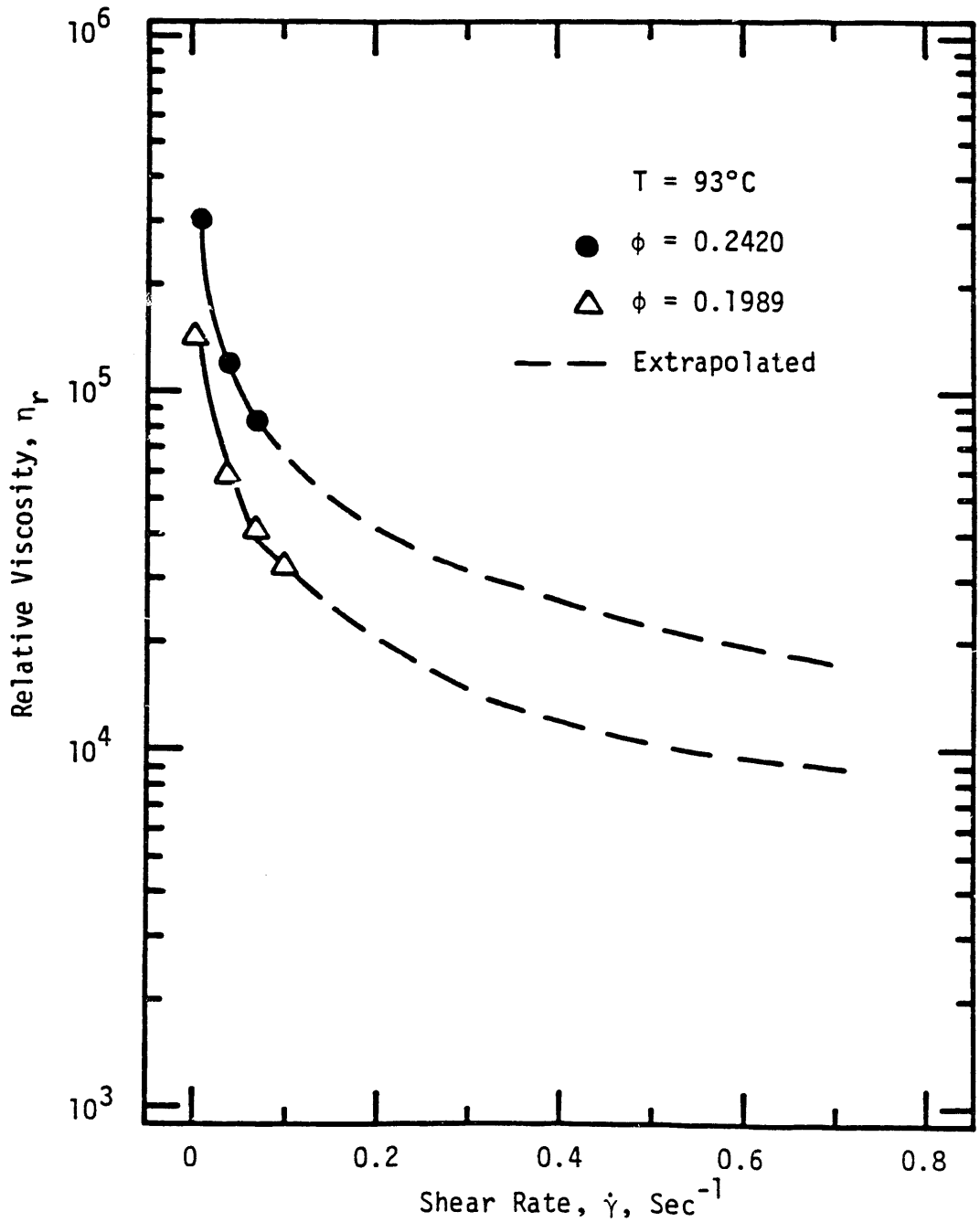

Figure 2.7. Effect of Shear Rate on Relative Viscosity of WF/TR12 Slurries at 93°C for ϕ = 0.199 and ϕ = 0.242.

$$\eta_f = \frac{m''_1}{\dot{\gamma}^{(1-n_f)}} \qquad (2.7)$$

where
n_s = flow index of slurry
n_f = flow index of fluid
m'_1 = a constant for slurry, $m'_1 = n_s$ when $\dot{\gamma} = 1\ sec^{-1}$.
m''_1 = = a constant for fluid, $m''_1 = \eta_f$ when $\dot{\gamma} = 1\ sec^{-1}$

Substitution of Equations 2.6 and 2.7 in Equation 2.5 yields:

$$\eta_r = \frac{m_o}{\dot{\gamma}^{(n_f-n_s)}} \qquad (2.8)$$

where $m_o = m'/m''$ and $m_o = \eta_r$ when $\dot{\gamma} = 1\ sec^{-1}$. Equation 2.8 was the equation used to represent the correlations of η_r versus $\dot{\gamma}$. These correlations are shown in Tables 2.4 - 2.5.

The effect of wood flour volume fraction, ϕ, on the relative viscosity, η_r, of WF/TR12 slurries at 65°C and 93°C is shown in Figures 2.8 - 2.9. From these figures it can be seen that the relative viscosity of these slurries increases considerably with increased WF volume fraction. This increase in η_r with ϕ is strongly dependent on shear rate. However, the nature of the dependence of η_r on ϕ is fairly similar at different shear rates since the curves of η_r versus ϕ at different shear rates have the same general shape. The effect of wood flour (WF) volume fraction and shear rate on the relative viscosity of wood flour slurries will be discussed in more detail later on.

Exploratory experiments were performed to determine any possible effects due to particle size, particle size distribution, particle aspect ratio, q, and particle aspect ratio distribution. To determine the effects of particle size and particle aspect ratio it is usually desirable to use uniform particles with uniform particle size and aspect ratio in each suspension. However, the wood flour used in slurries that are handled in cellulosic liquefaction processes does not have uniform particles with the same particle size or same particle aspect ratio. Actually, the wood flour used in this study is the same wood flour utilized by the cellulosic liquefaction facility in Albany, Oregon as mentioned earlier. Moreover, these experiments were exploratory in nature. They were designed to check if any effect can be detected and whether the magnitude of this effect warranted any future investigations. In these experiments a wood flour fraction between 65 and 100 mesh was used. Particle size and particle aspect ratio analyses of this wood flour fraction are shown in Figures 2.10 - 2.12. A similar analysis for the -200 mesh fraction, which was used in most experiments, is shown in Figures 2.13 - 2.15. As can be seen from Figures

Table 2.4. Relative Viscosity Correlations of WF/TR12 Slurries at 65°C.

Wood Flour Content, ϕ x 100 (vol%)	Shear Rate Range (sec^{-1})	Correlation	Quality of Fit
3.84	3.2 - 109	$\eta_r = \frac{2.867}{\dot{\gamma}^{0.081}}$	0.98
7.77	0.4 - 72	$\eta_r = \frac{16.642}{\dot{\gamma}^{0.233}}$	1.00
11.81	0.1 - 58	$\eta_r = \frac{168.839}{\dot{\gamma}^{0.578}}$	1.00
15.94	0.1 - 32	$\eta_r = \frac{762.149}{\dot{\gamma}^{0.634}}$	1.00

Table 2.5. Relative Viscosity Correlations of WF/TR12 Slurries at 93°C.

Wood Flour Content, ϕ x 100 (vol%)	Shear Rate Range (sec^{-1})	Correlation	Quality of Fit
3.77	12.8 - 145	$\eta_r = \frac{5.736}{\dot{\gamma}^{0.179}}$	1.00
7.64	12.8 - 145	$\eta_r = \frac{16.188}{\dot{\gamma}^{0.254}}$	1.00
11.62	2.3 - 102	$\eta_r = \frac{317.753}{\dot{\gamma}^{0.569}}$	1.00
15.70	1.8 - 79	$\eta_r = \frac{1,304.557}{\dot{\gamma}^{0.518}}$	1.00
19.89	0.02 - 0.2	$\eta_r = \frac{7,218.497}{\dot{\gamma}^{0.651}}$	1.00
24.20	0.02 - 0.1	$\eta_r = \frac{14,649.927}{\dot{\gamma}^{0.650}}$	1.00

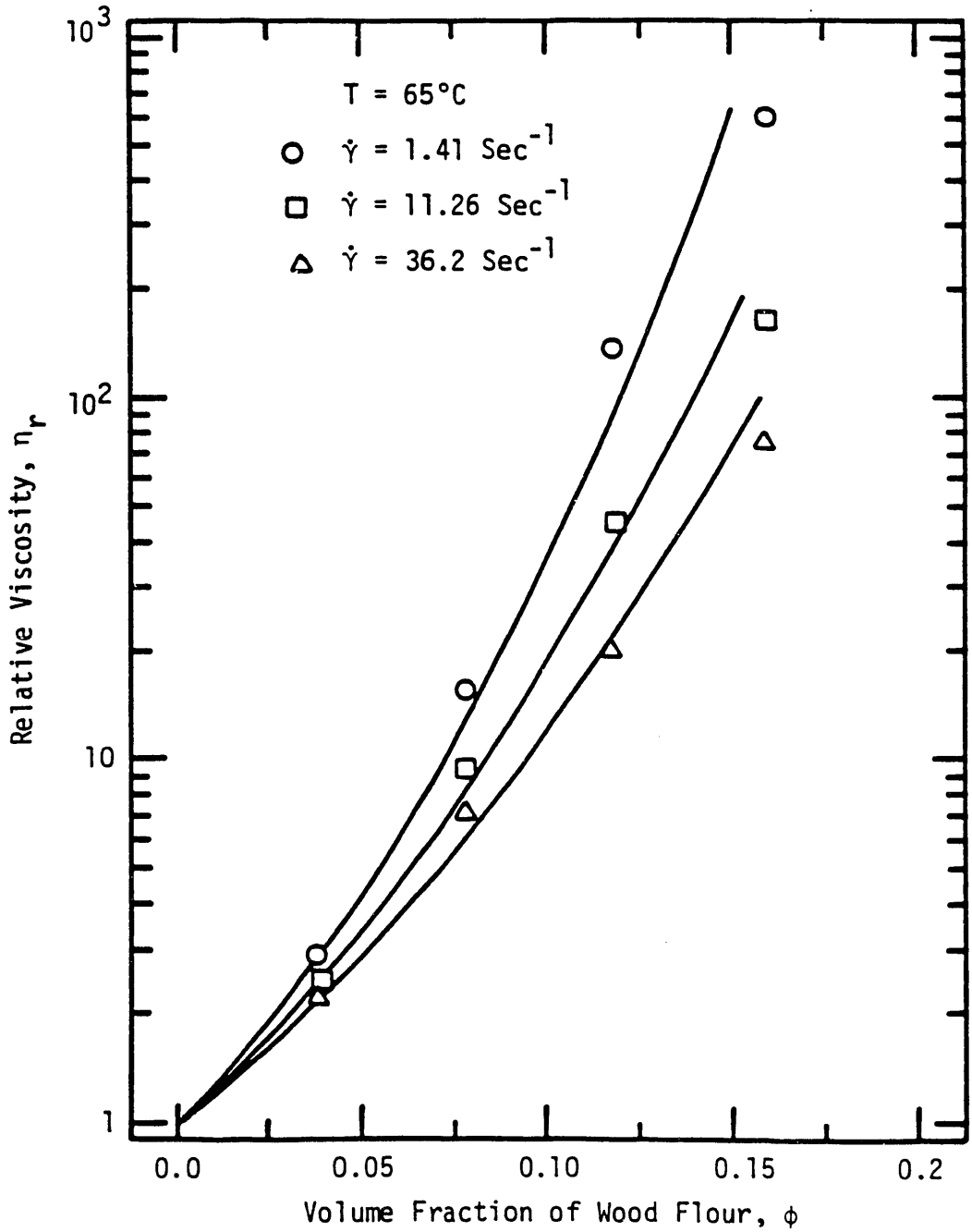

Figure 2.8. Effect of Wood Flour Volume Fraction on Relative Viscosity of WF/TR12 Slurries at 65°C.

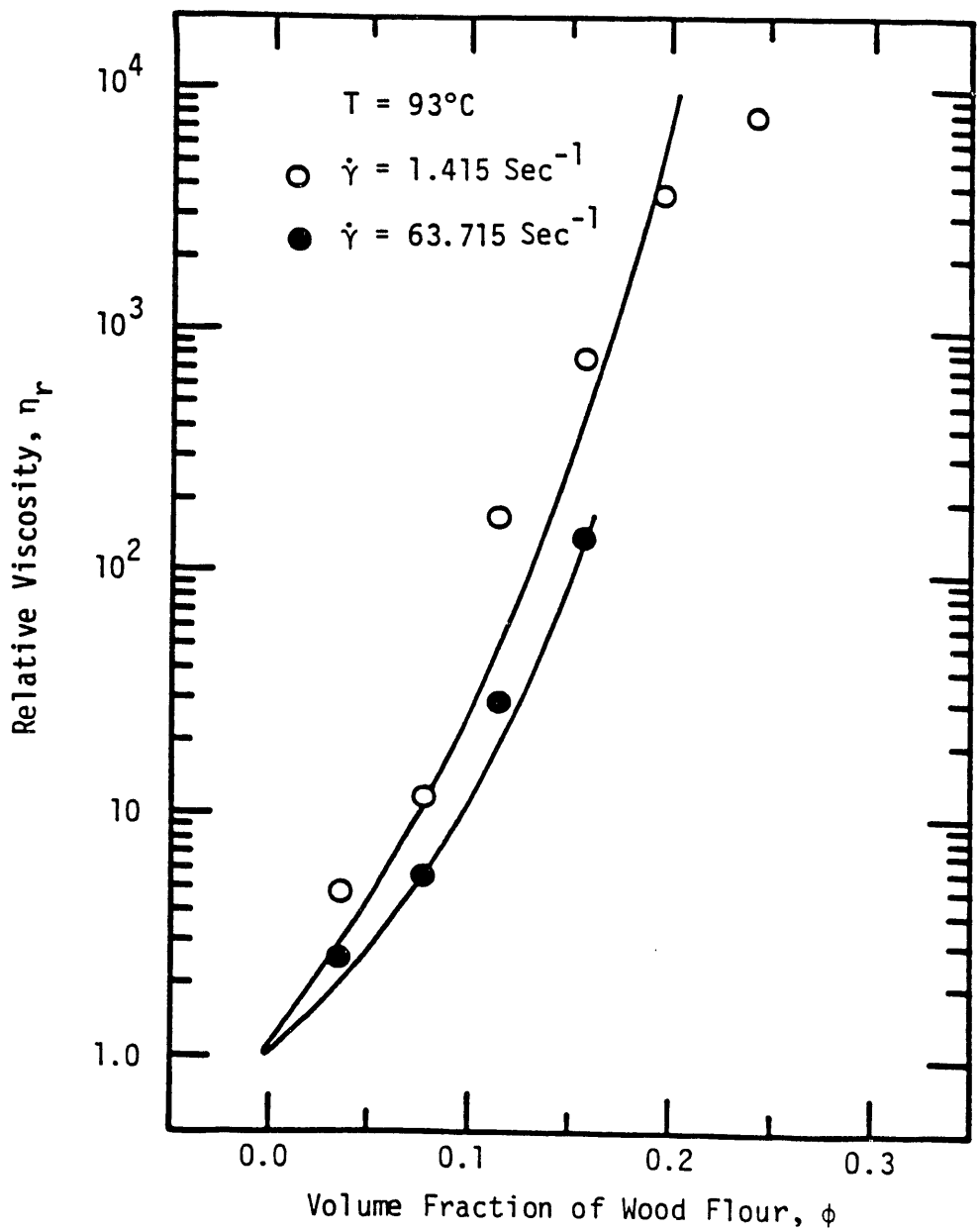

Figure 2.9. Effect of Wood Flour Volume Fraction on Relative Viscosity of WF/TR12 Slurries at 93°C.

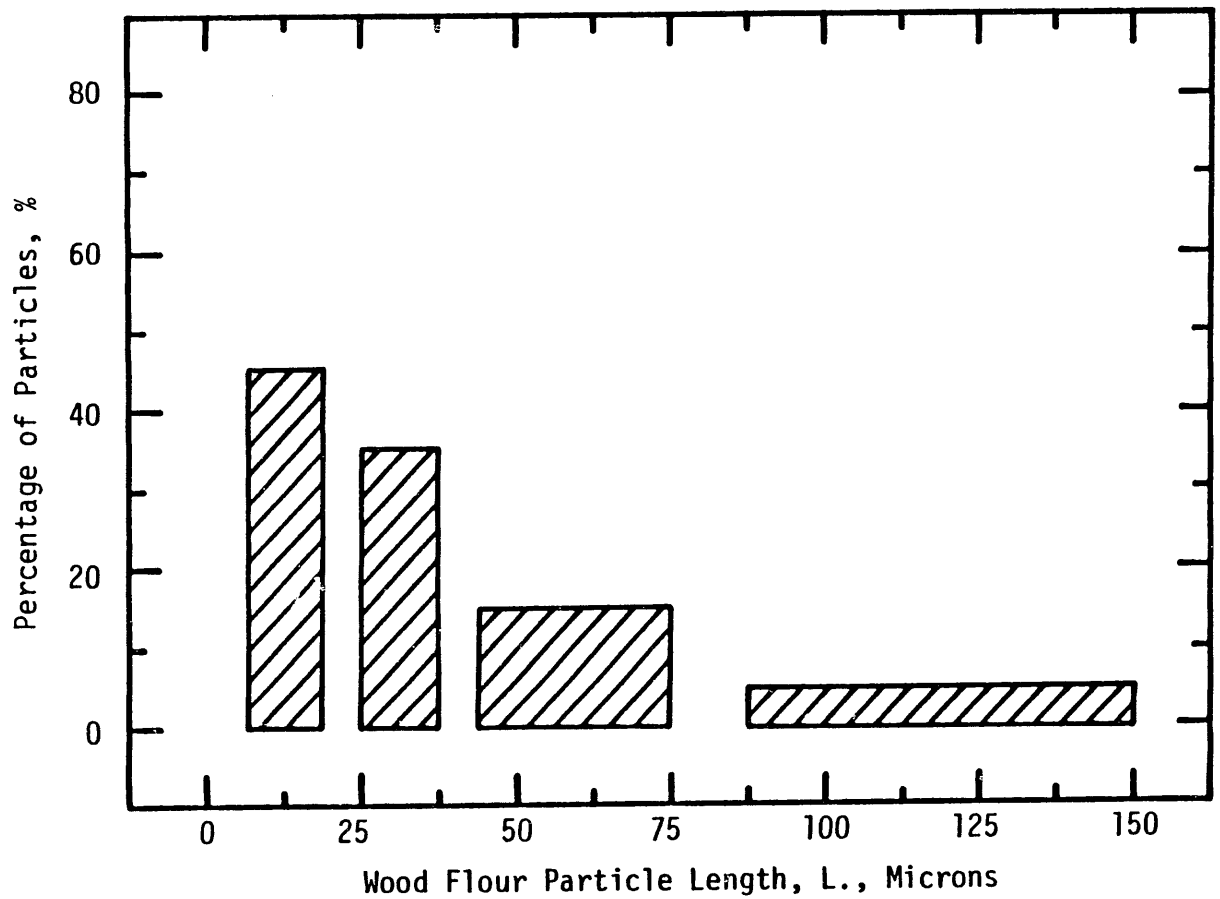

Figure 2.10. Particle Length Distribution for Albany Wood Flour, 65-100 mesh.

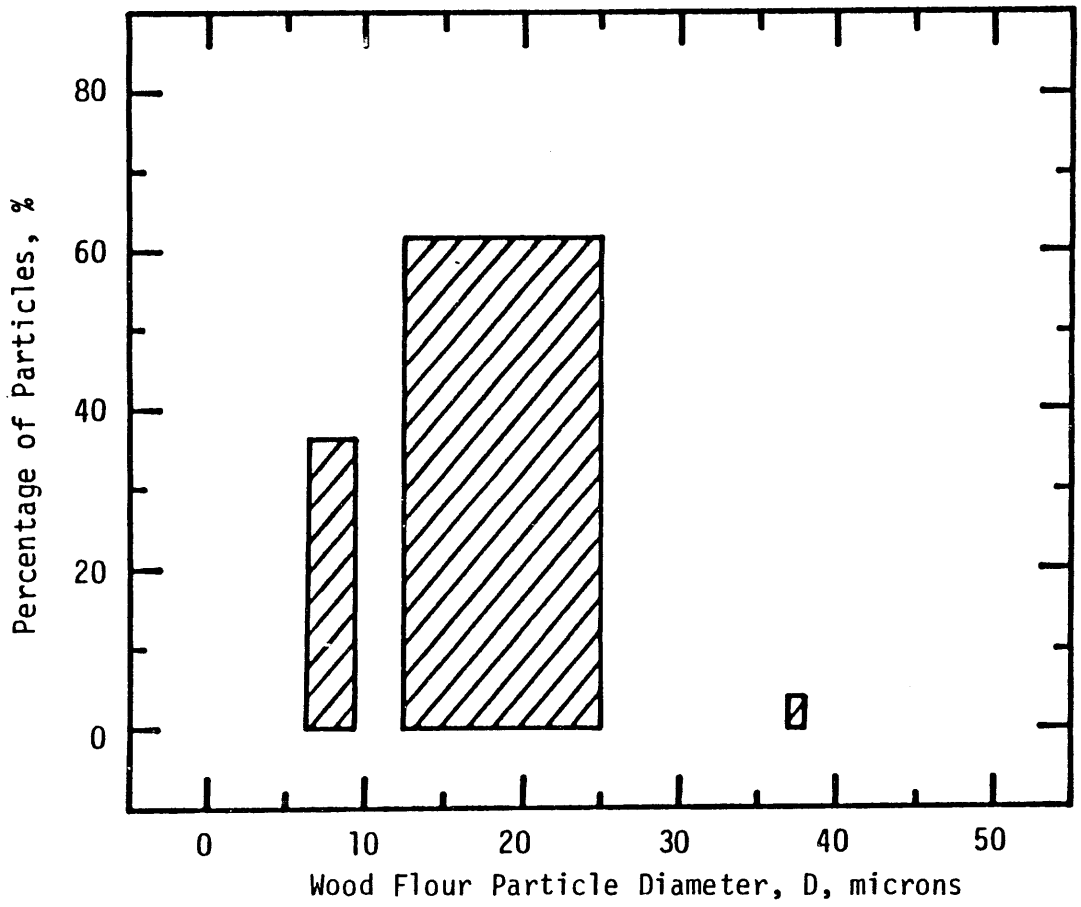

Figure 2.11. Particle Diameter Distribution for Albany Wood Flour, 65-100 mesh.

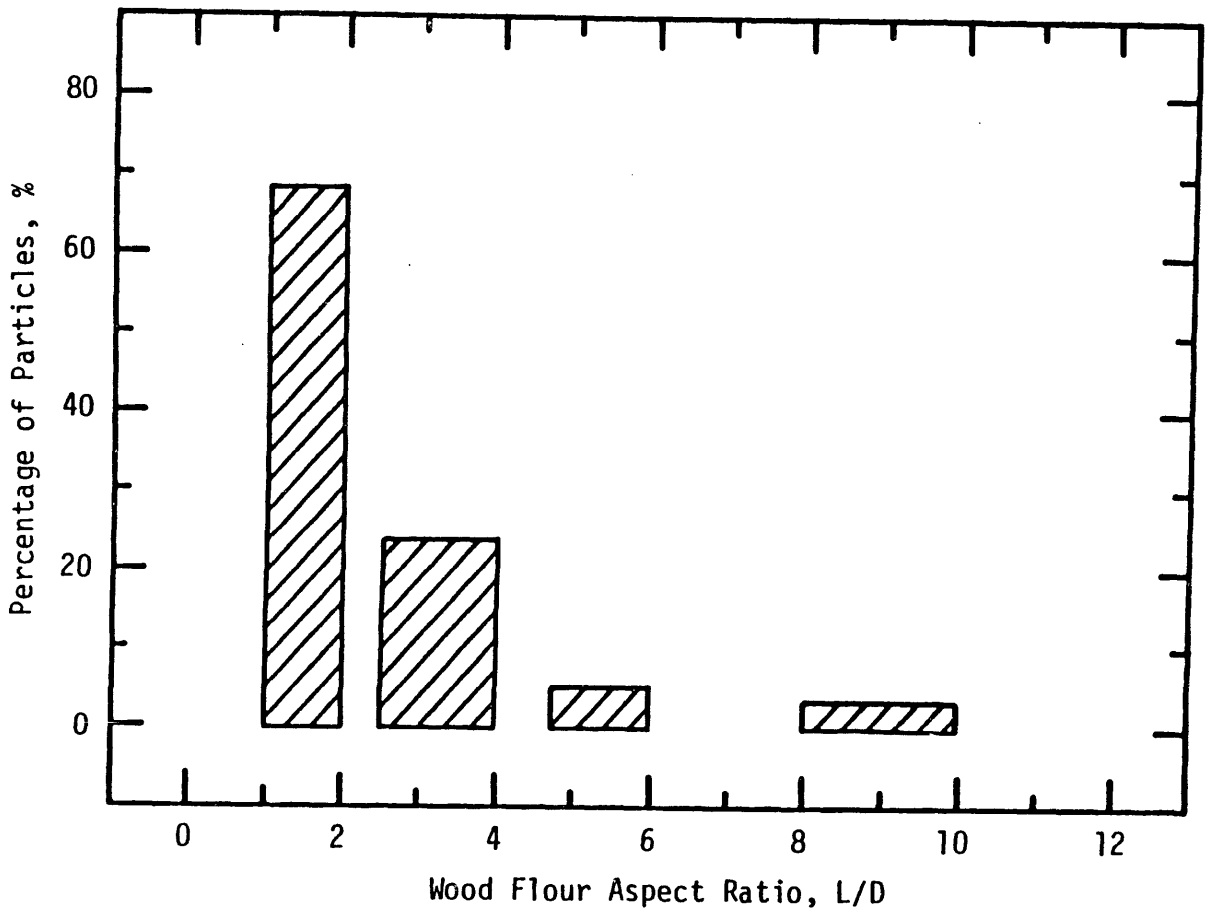

Figure 2.12. Particle Aspect Ratio Distribution for Albany Wood Flour, 65-100 mesh.

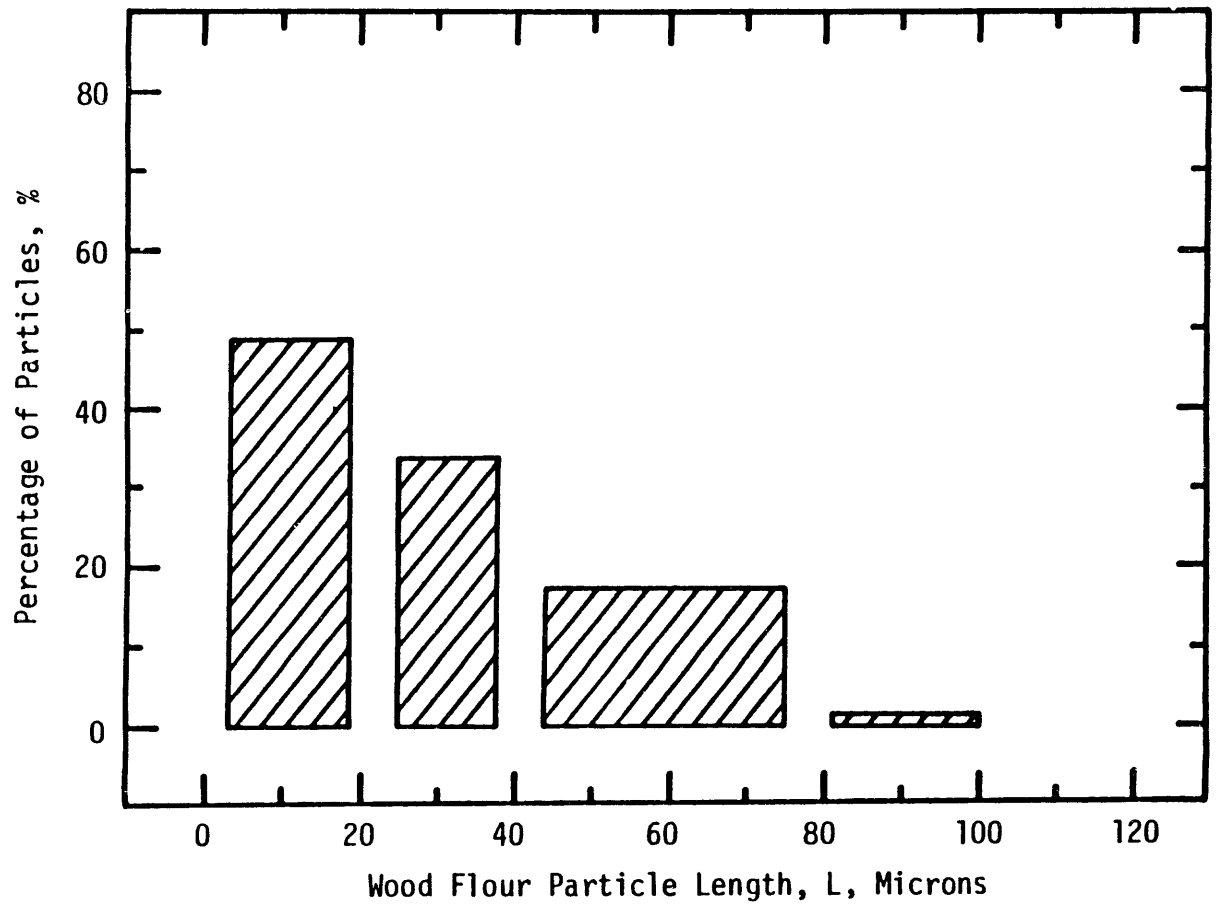

Figure 2.13. Particle Length Distribution for Albany Wood Flour, -200 mesh.

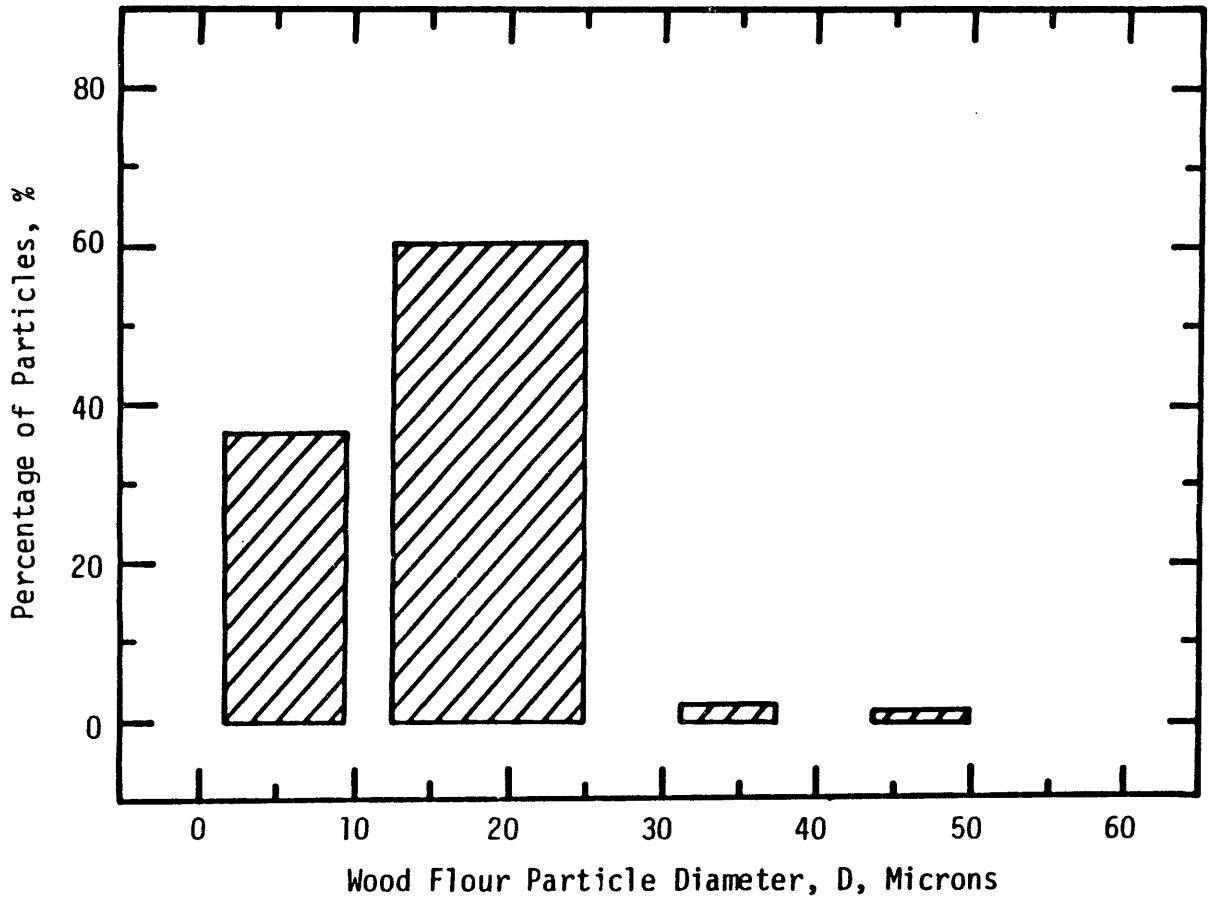

Figure 2.14. Particle Diameter Distribution for Albany Wood Flour, -200 mesh.

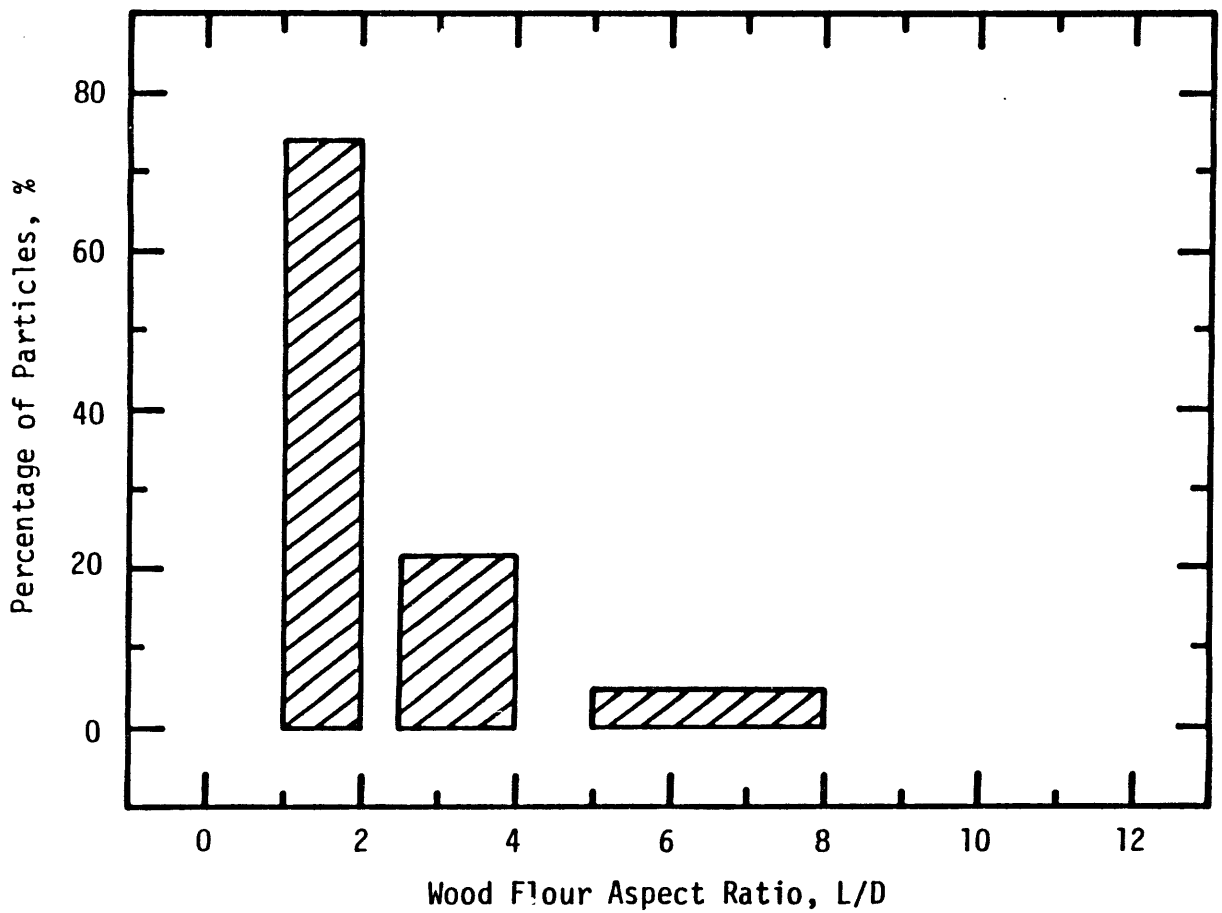

Figure 2.15. Particle Aspect Ratio Distribution for Albany Wood Flour, -200 mesh.

2.15 and 2.12, the distribution of particle aspect ratio for the two fraction is almost the same. The 65 - 100 mesh fraction has a very small percentage of particles with higher aspect ratios, q, more than the -200 mesh. From Figures 2.13 and 2.10 it can be seen that the particle length distribution for both fractions is fairly close, too. However, the -200 mesh fraction has a very small amount of shorter particles more than the 65 - 100 mesh fraction, whereas the latter has a few longer particles more than the -200 mesh fraction. Finally, from Figures 2.14 and 2.11 it can be seen that the -200 mesh fraction has a few particles with smaller diameters than the 65 - 100 mesh fraction. It is obvious that the effects of particle size, particle size distribution, particle aspect ratio and particle aspect ratio distribution cannot be separated. Thus, all these effects will be combined and referred to collectively as the effect of *"particle dimensions."* The effect of particle dimensions on the apparent viscosity of WF/TR12 slurries is shown in Figure 2.16. As can be seen from this figure, the ratio of the apparent viscosity of the 65 - 100 mesh fraction, η_{65}, to that of the -200 mesh fraction, η_{200}, is higher than one. This shows that the apparent viscosity of a WF slurry increases with increased particle dimensions. Moreover, this increase is much more pronounced at higher wood flour volume fractions. Consequently, this effect warrants further investigation.

The thermal-history dependence of one WF/TR12 slurry was investigated. The effect of heating time on the apparent viscosity of 7.77 vol.% WF in TR12 oil is shown in Figure 2.17. The ratio of the apparent viscosity at time t, η_t, to that at time zero, η_o, decreased with time. However, comparison of this figure to Figure 2.18 shows that the decrease in η_t/η_o for this slurry is qualitatively and quantitatively similar to that of pure TR12 oil. Thus, the thermal-history dependence of this WF slurry is mainly due to that of TR12 oil.

2.2.3 Rheology of DC23 Silicone Oil

In order to compare and contrast the rheology of wood flour slurries to slurries of more uniform particles like glass fibers, DC23 silicone oil was chosen as the suspending fluid for the following set of experiments. DC23 silicone oil is very similar to the silicone oils used by Maschmeyer (1974) to study the rheology of glass fibers in silicone oils. Thus, the rheology of WF/DC23 will be compared and contrasted to the rheology of glass fiber suspensions studied by Maschmeyer (1974).

DC23 silicone oil is a Newtonian fluid up to a shear rate of about 250 sec^{-1}. At shear rates higher than 250 sec^{-1} it becomes shear thinning. However, in this study the higher shear rate, $\dot{\gamma}$, used was 144.8 sec^{-1}. Consequently, DC23 silicone oil should be Newtonian in this study. Experimental measurements verified this conclusion. From Figure 2.19 it can be seen that the viscosity of DC23 silicone oil is independent of shear rate in the range of shear rates used in this study. DC23 silicone oil does not have a thermal-history dependence or a shear-history dependence.

2.2.4 Rheology of Wood Flour/DC23 Slurries

The rheology of WF/DC23 slurries was studied at 41°C. The values of the wood flour (WF) volume fraction, ϕ, in these slurries were: 0.0341, 0.0694, 0.1059, 0.1437, 0.1828 and

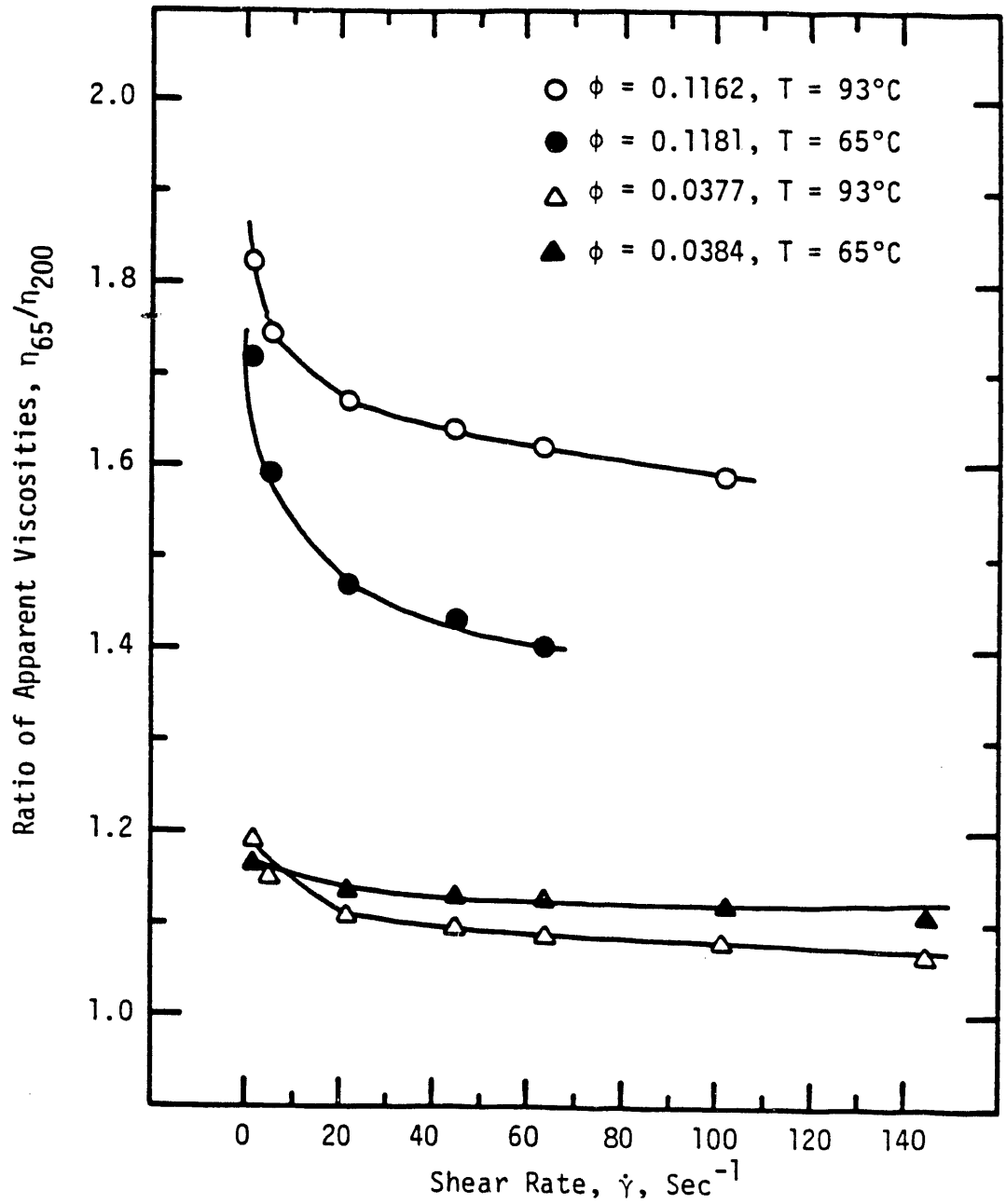

Figure 2.16. Effect of Particle Dimensions on Apparent Viscosity of WF/TR12 Slurries.

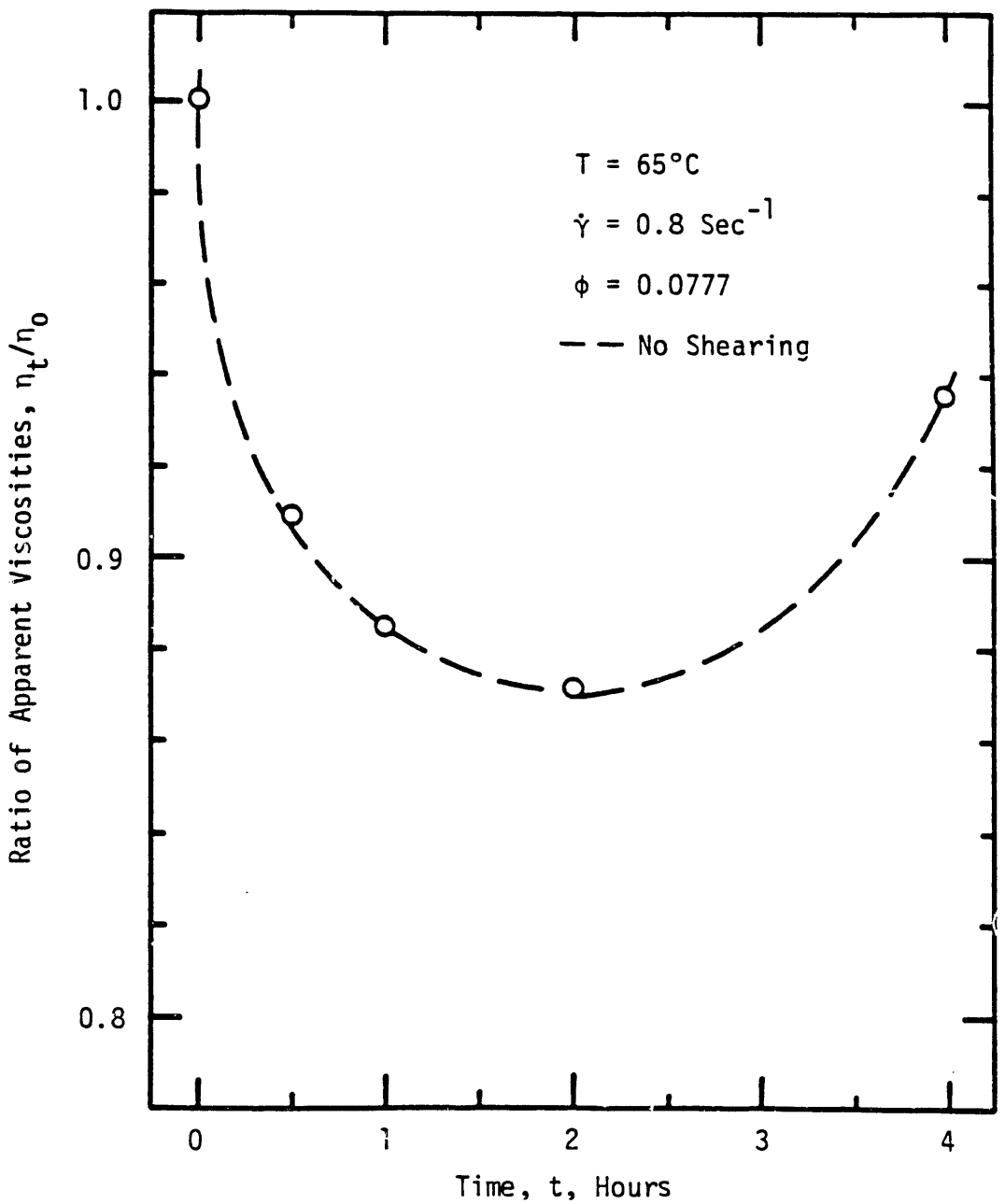

Figure 2.17. Effect of Heating Time on Apparent Viscosity on 7.77 Vol. % WF in TR12 Oil.

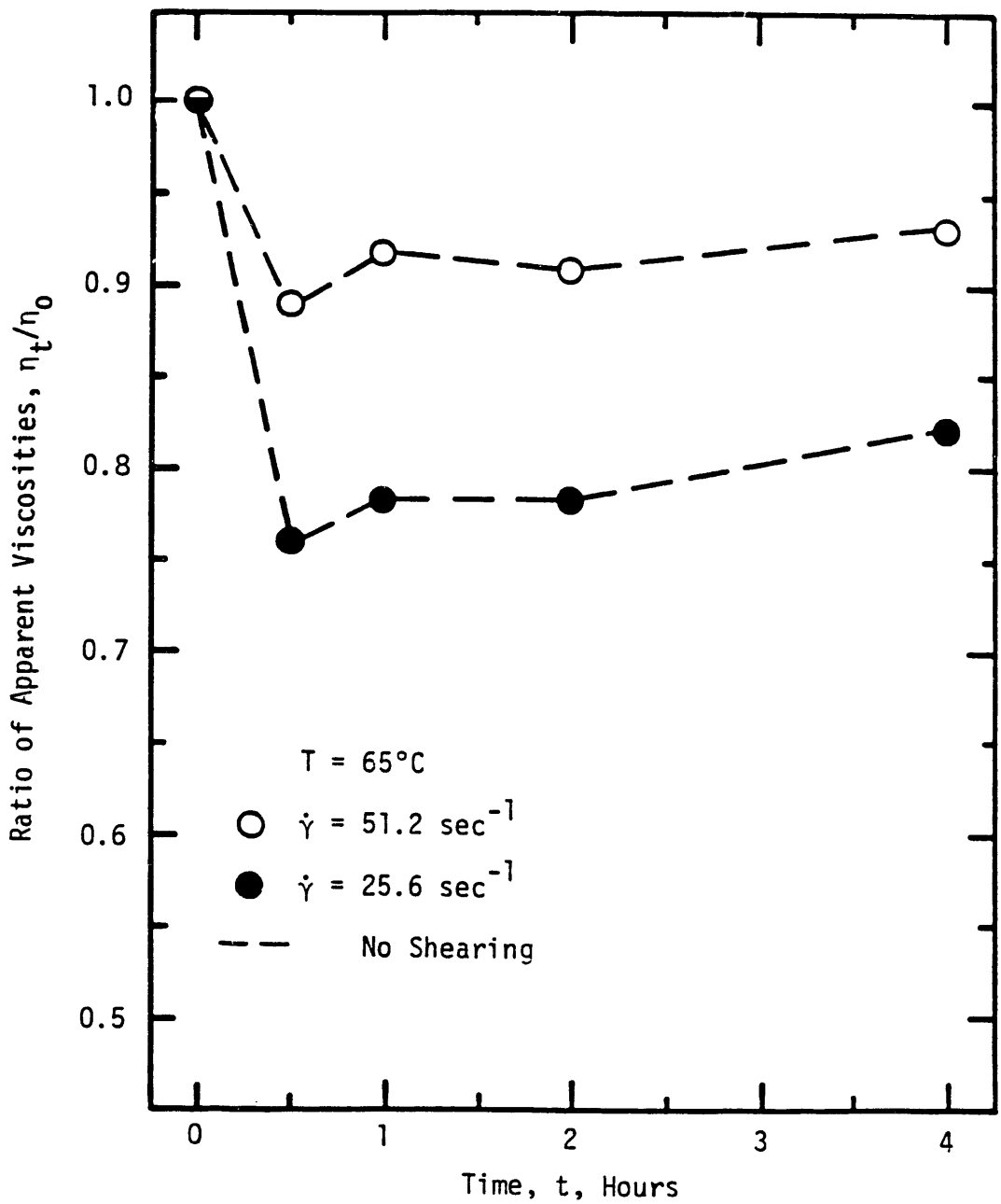

Figure 2.18. Effect of Heating Time on Apparent Viscosity of TR12 Oil.

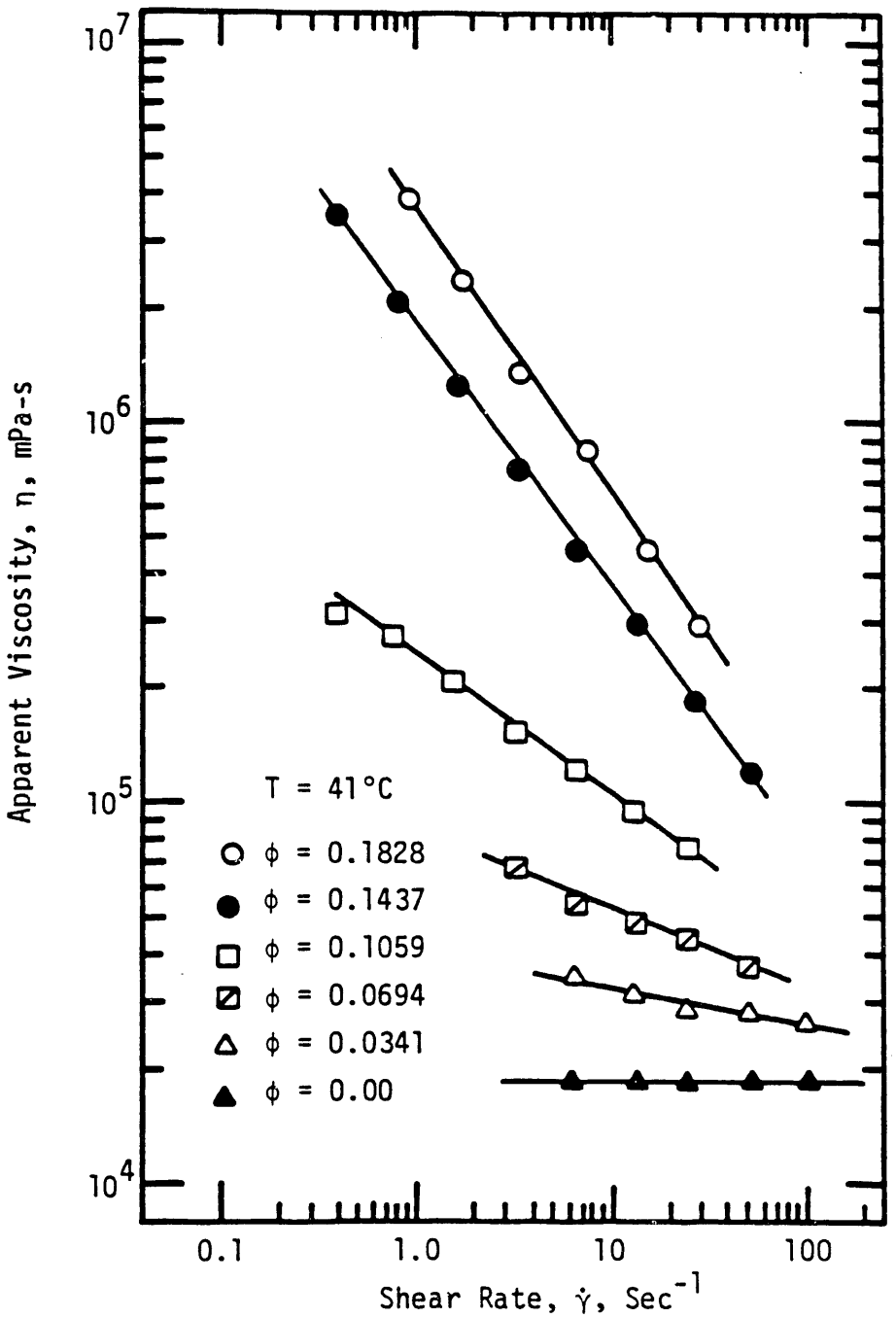

Figure 2.19. Effect of Shear Rate on Viscosity of DC23 Silicone Oil and Apparent Viscosity of WF/DC23 Slurries.

0.2234. The apparent viscosities, η, of these slurries were measured at 41°C and various shear rates. The effect of shear rate on the apparent viscosity of these slurries is shown in Figures 2.19 and 2.20. Although pure DC23 silicone oil is not shear thinning in the range of shear rates investigated, all WF/DC23 were shear thinning. Moreover, the shear thinning behavior increased with increased wood flour volume fraction, ϕ. This behavior is similar to that exhibited by WF/TR12 slurries. As in the case of WF/TR12 slurries, the *"power law"* model was used to correlate the apparent viscosity, η, versus shear rate data of WF/DC23 slurries. A standard non-linear least squares regression method was used to obtain the correlations. Apparent viscosity correlations of WF/DC23 slurries are shown in Table 2.6. As can be seen from this table, all the values of the quality of fit are either 1.0 or very close to 1.0 which indicates that the *"power law"* model fits the data very accurately in the range of shear rates investigated. Also, it can be noticed that the flow index, n, decreases with increased wood flour content in a manner similar to that exhibited by WF/TR12 slurries.

Relative viscosity, η_r, values of WF/DC23 slurries were calculated based on actual apparent viscosity data as was done in the case of WF/TR12 slurries. The effect of shear rate, $\dot{\gamma}$, on the relative viscosity of WF/DC23 slurries is shown in Figures 2.21 and 2.22. From these figures it can be seen that the relative viscosity, η_r, of these slurries increases quickly with increased wood flour volume fraction, ϕ, while it decreases with increased shear rate. This behavior is similar to that of WF/TR12 slurries. Employing the non-linear least squares regression method, Equation 2.8 was used to correlate the relative viscosity and shear rate data of WF/DC23 slurries. Relative viscosity correlations of these slurries are shown in Table 2.7. The effect of wood flour volume fraction, ϕ, on the relative viscosity, η_r, of these slurries is shown in Figure 2.23. As shown in this figure, the relative viscosity of WF/DC23 slurries increases very quickly with increased ϕ. Also, this increase in η_r is strongly dependent on shear rate. However, the shape of the curve of η_r versus ϕ is almost the same at various shear rates.

2.3 CORRELATIONS FOR WOOD FLOUR SLURRIES

2.3.1 Effects of Wood Flour Volume Fraction

The effect of wood flour volume fraction, ϕ, on the rheology of WF/TR12 and WF/DC23 slurries is qualitatively similar. The shape of the curves of relative viscosity, η_r, versus ϕ is almost the same. This can be realized by inspection of Figure 2.24. All the curves in this figure exhibit the strong dependence of the relative viscosity on the wood flour volume fraction. Thus, it can be concluded that, among the variables that were investigated, wood flour volume fraction, ϕ, is the variable that affects the relative viscosity of wood flour (WF) slurries the most. However, at constant shear rate, the dependence of η_r on ϕ seems to be affected by two other variables, namely, the flow index, n, and the viscosity of the pure oil. The contribution of each of these variables cannot be isolated based on the experimental data of this study. From the data reported by White (1979) and which is shown in Figures 2.25 - 2.26, the apparent viscosity, η, of WF/gear oil slurries increased faster than the apparent viscosity of WF/water slurries as the wood flour mass fraction was increased at constant shear rate. Gear oil is a non-Newtonian

Table 2.6. Apparent Viscosity correlations of WF/DC23 Slurries.

Wood Flour Content, ϕ x 100 (vol%)	Shear Rate Range (sec^{-1})	Correlation	Flow Index, n	Quality of Fit
0	$\dot{\gamma} < 250$	μ = 18,430 mPa-s	1.00	-
3.41	6.4 - 102.4	$\eta = \frac{40{,}058.160}{\dot{\gamma}^{0.094}}$	0.906	0.95
6.94	3.2 - 51.2	$\eta = \frac{81{,}720.749}{\dot{\gamma}^{0.201}}$	0.799	0.98
10.59	0.8 - 25.6	$\eta = \frac{238{,}395.486}{\dot{\gamma}^{0.352}}$	0.648	1.00
14.37	0.4 - 52.7	$\eta = \frac{1{,}803{,}013.068}{\dot{\gamma}^{0.696}}$	0.304	1.00
18.28	0.8 - 29.0	$\eta = \frac{3{,}613{,}563.382}{\dot{\gamma}^{0.754}}$	0.246	1.00
22.34	0.02 - 0.2	$\eta = \frac{11{,}874{,}291.70}{\dot{\gamma}^{0.892}}$	0.108	1.00

Table 2.7. Relative Viscosity Correlations of WF/DC23 Slurries.

Wood Flour Content, ϕ x 100 (vol%)	Shear Rate Range (sec^{-1})	Correlation	Quality of Fit
3.41	6.4 - 102.4	$\eta_r = \frac{2.178}{\dot{\gamma}^{0.094}}$	1.00
6.94	3.2 - 51.2	$\eta_r = \frac{4.434}{\dot{\gamma}^{0.201}}$	1.00
10.59	0.8 - 25.6	$\eta_r = \frac{12.942}{\dot{\gamma}^{0.352}}$	1.00
14.37	0.4 - 52.7	$\eta_r = \frac{97.826}{\dot{\gamma}^{0.696}}$	1.00
18.28	0.8 - 29.0	$\eta_r = \frac{196.125}{\gamma\dot{\gamma}^{0.754}}$	1.00
22.34	0.02 - 0.2	$\eta_r = \frac{642.931}{\dot{\gamma}^{0.893}}$	1.00

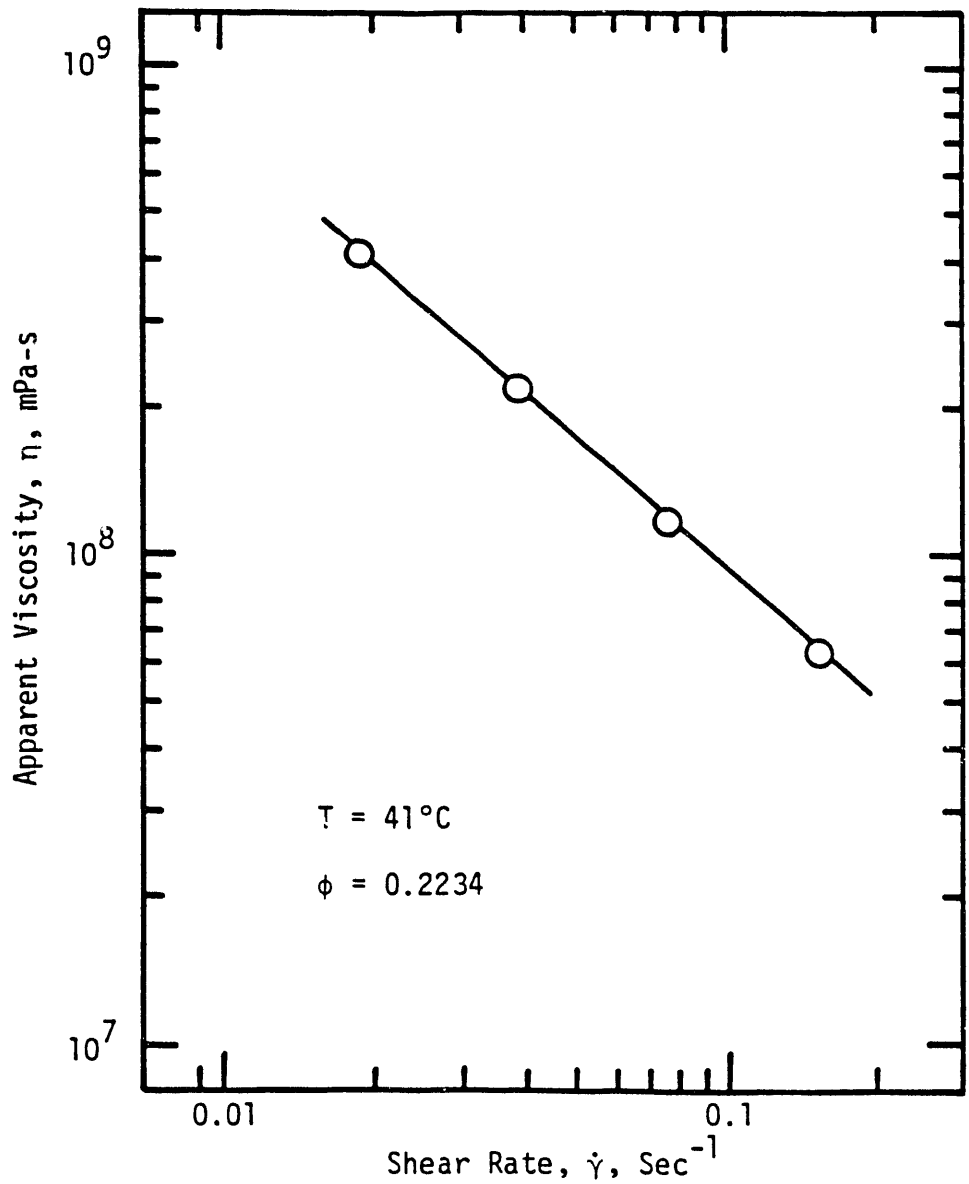

Figure 2.20. Effect of Shear Rate on Apparent Viscosity of 22.34 Vol. % WF in DC23 Silicone Oil.

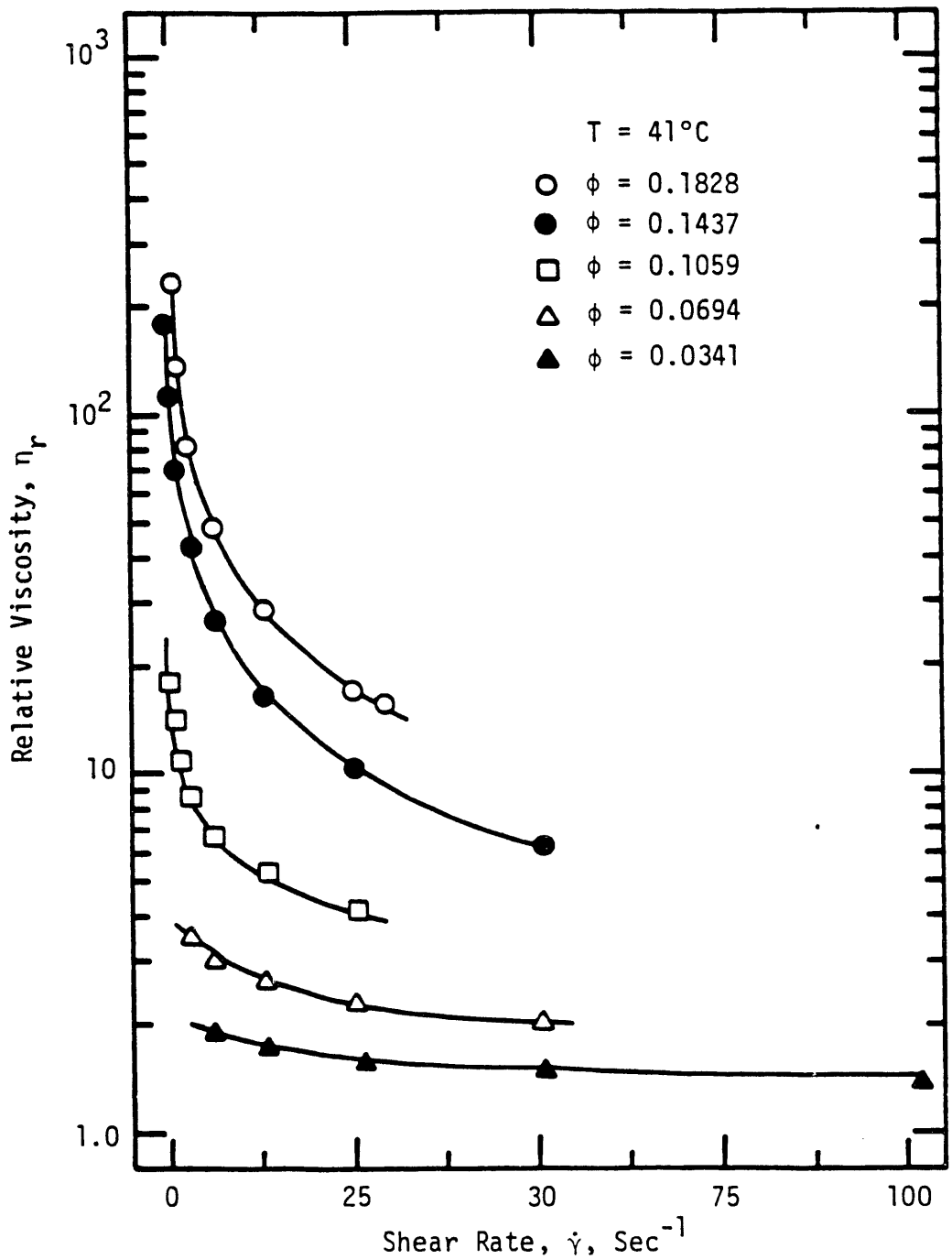

Figure 2.21. Effect of Shear Rate on Relative Viscosity of WF/DC23 Slurries.

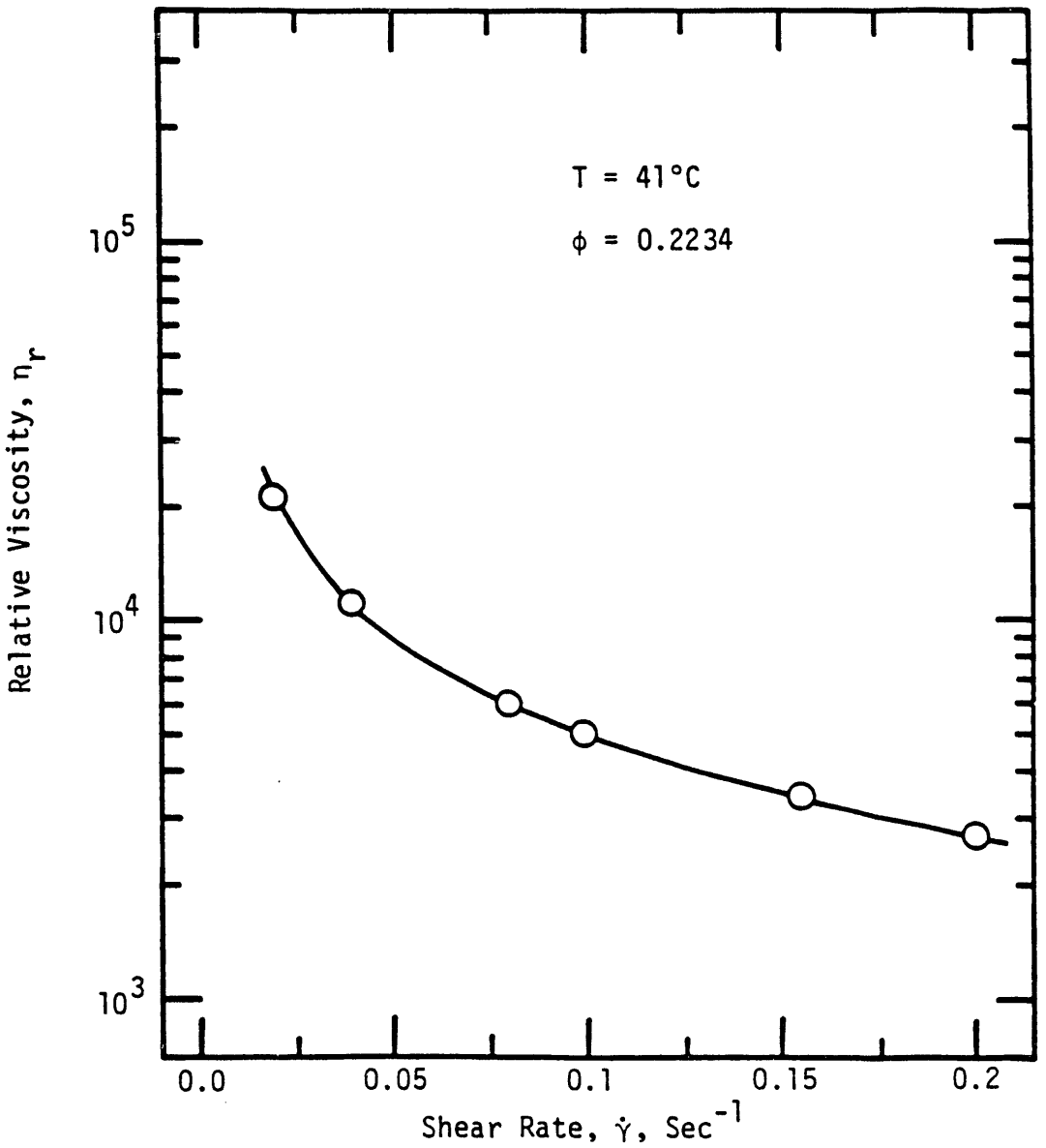

Figure 2.22. Effect of Shear Rate on Relative Viscosity of 22.34 Vol. % WF in DC23 Silicone Oil.

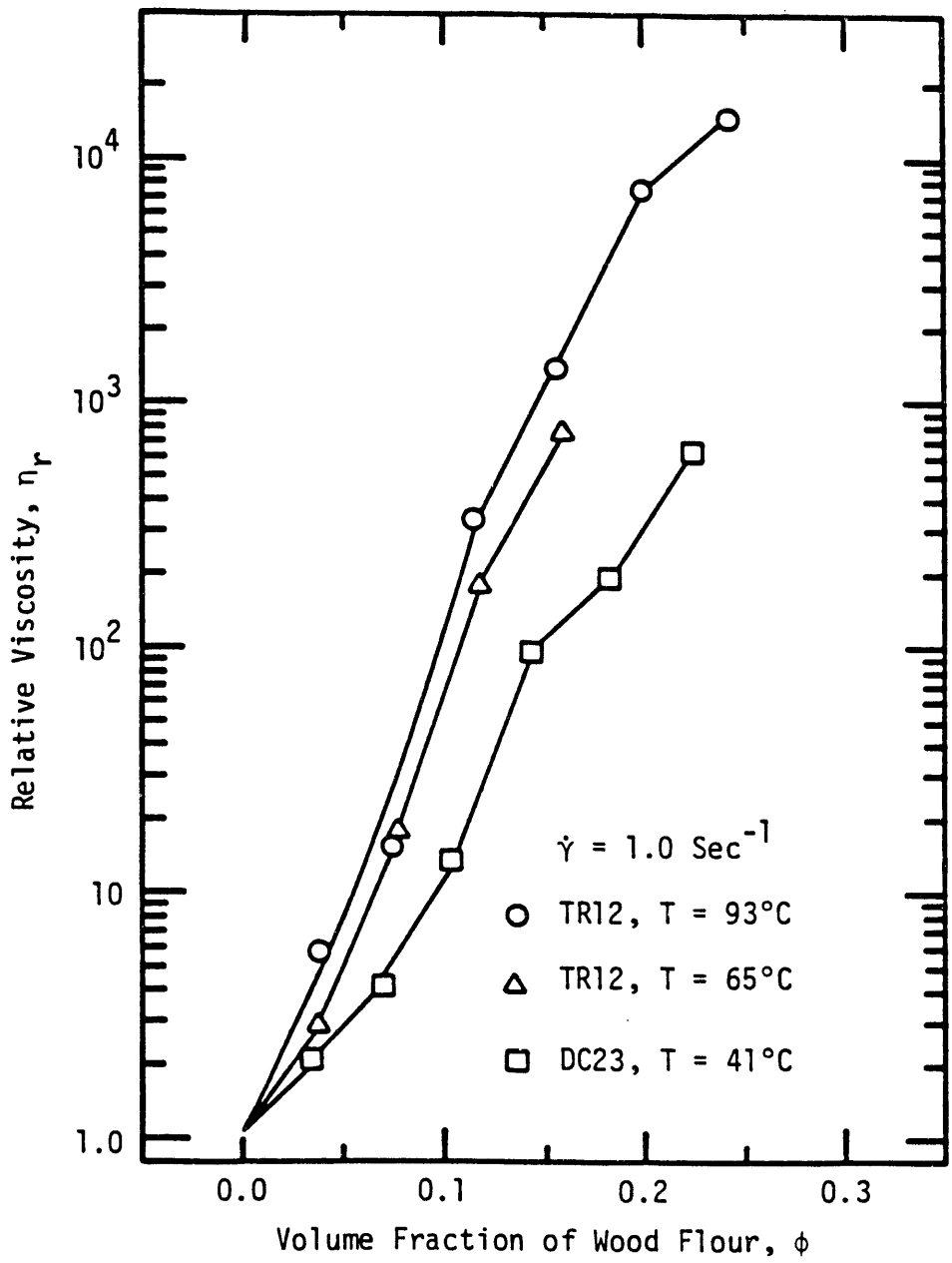

Figure 2.24. Effect of Wood Flour Volume Fraction on Relative Viscosity of Wood Flour Slurries.

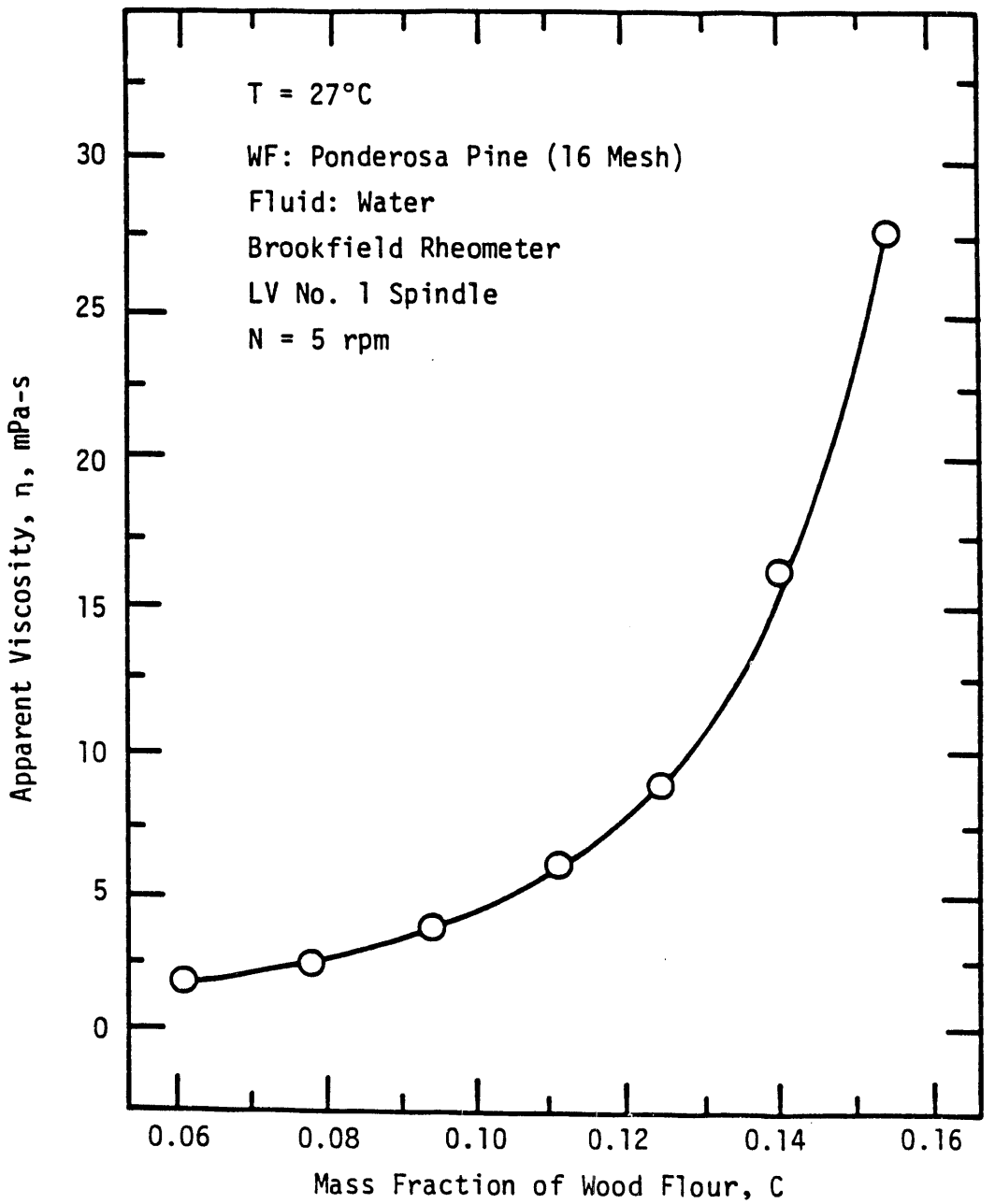

Figure 2.25. The effect of Wood Flour Mass Fraction on Apparent Viscosity of WF/Water Slurries as Reported by White (1979).

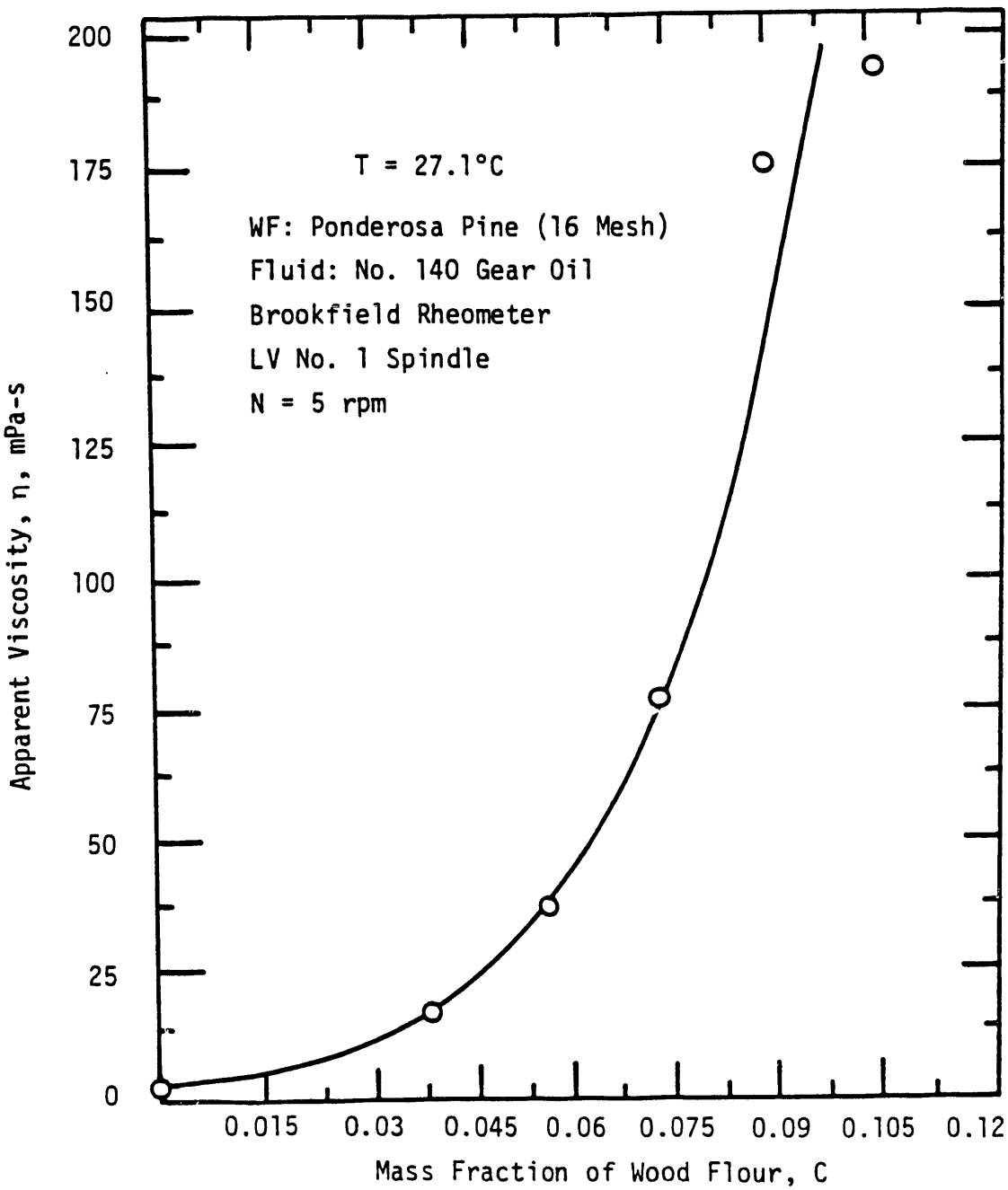

Figure 2.26. The Effect of Wood Flour Mass Fraction on the Apparent Viscosity of WF/Great Oil Slurries as Reported by White (1979).

fluid, while water is a Newtonian fluid. Thus, the apparent viscosity, or equivalently the relative viscosity, of a slurry where the suspending fluid is non-Newtonian increases faster than that of a slurry where the suspending fluid is Newtonian as the solids volume fraction is increased. A similar behavior is exhibited in Figure 2.24. DC23 silicone oil is a Newtonian fluid while TR12 oil is not. The flow index, n, of TR12 oil varies with temperature, at 65°C n = 0.82 and at 93°C n = 0.773. In this figure the relative viscosity of WF/TR12 slurries at 93°C is higher than that of WF/TR12 slurries at 65°C and higher than that of WF/DC23 slurries at constant ϕ and $\dot{\gamma}$. Thus, the relative viscosity of WF slurries increases with decreasing flow index of the suspending fluid at constant ϕ and $\dot{\gamma}$.

In this study, a phenomenon similar to that observed by Blakeney (1966) was noticed. Blakeney demonstrated the dependence of the relative viscosity of nylon fibers slurries on the fiber volume fraction, ϕ, in the range covering the critical volume fraction, ϕ^*. He reported that the relative viscosity increased slowly but linearly at values of ϕ less than ϕ^*. At $\phi = \phi^*$ the relative viscosity increased quickly but non-linearly up to $\phi = 0.005$. At $\phi > 0.005$ the relative viscosity dropped and then it increased more quickly but in a linear manner. This behavior is shown in Figure 2.27 which was reproduced from Blakeney's (1966) work. A similar behavior was exhibited by wood flour slurries as shown in Figure 2.24. Actually, the curves in this figure were not drawn smoothly as other plots of η_r versus ϕ to help the reader notice the following phenomenon. From this figure, it can be seen that the sharpest increase in the relative viscosity of WF/TR12 slurries occurred between $\phi = 0.078$ and $\phi = 0.118$, while for WF/DC23 slurries it occurred at $\phi = 0.106$ to 0.144. After this sharp increase a lower increase occurred for all slurries. For WF/DC23 slurries this slower increase was followed by a sharper increase. Although no actual drop in relative viscosity was observed in this study, this variation of relative viscosity with ϕ is similar to what Blakeney (1966) reported.

The dependence of the relative viscosity of WF slurries on ϕ is roughly exponential. This high increase in η_r with increased ϕ is thought to be strongly dependent on non-hydrodynamic interactions. The dependence of η_r on ϕ is in itself a function of shear rate. Finally, an increase in ϕ causes the Weissenberg effect and thus, normal stresses to increase especially at higher values of ϕ.

2.3.2 Effects of Shear Rate

The shear rate was the next most important variable that affected the apparent viscosity, η, and the relative viscosity, η_r, of wood flour slurries. All the slurries were shear thinning. This shear thinning behavior is thought to be due to the following effects: (1) changes in particle orientation in a manner which reduces energy dissipation; (2) destruction of the particle network; (3) disruption of particle agglomerates; (4) the presence of the particles disturbs the velocity profile and induces higher shear rates in the fluid, causing a decrease in viscosity around the particles. This is turn decreases the energy dissipation and causes the suspension viscosity to be lower.

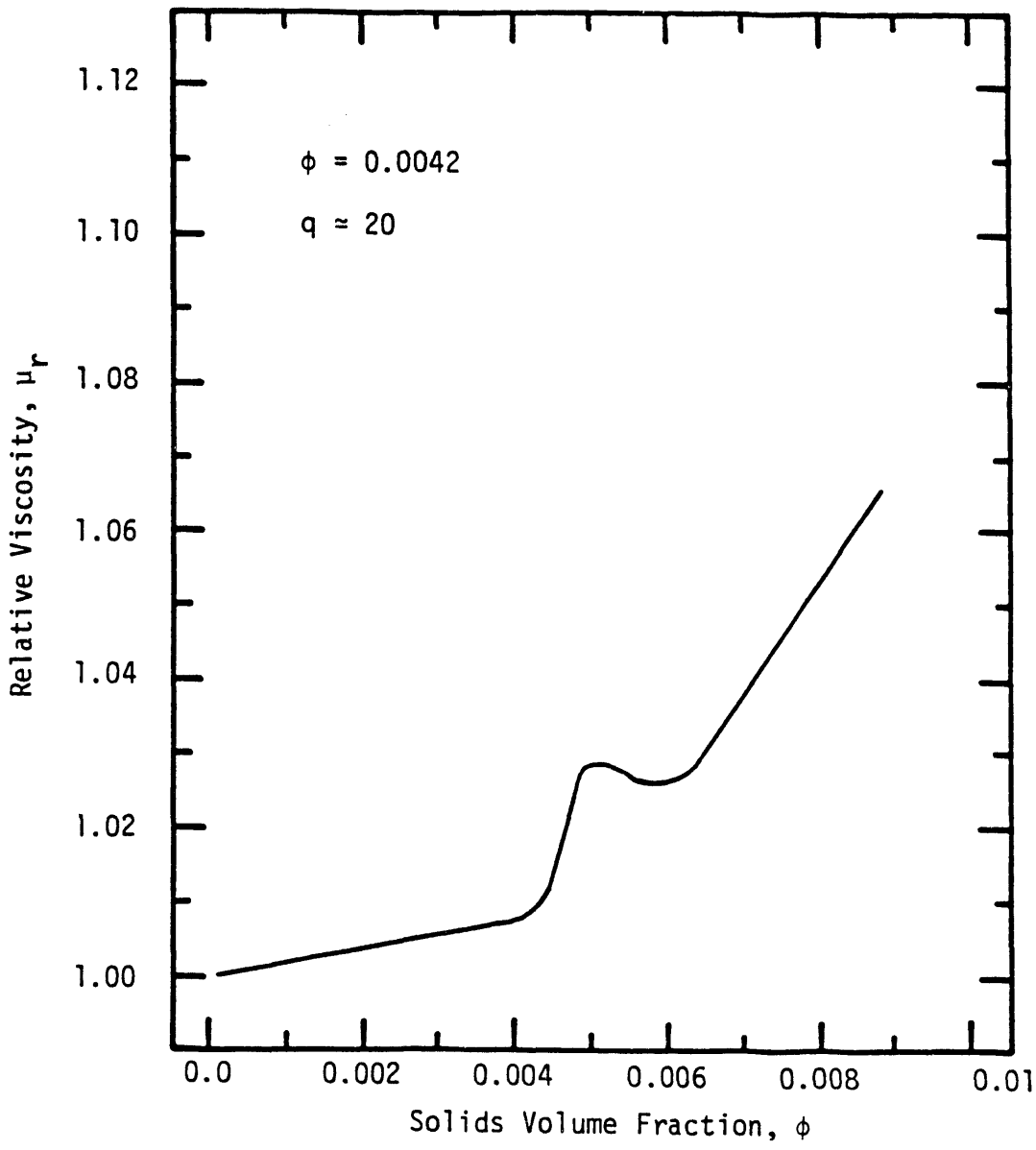

Figure 2.27. Effect of Solids Volume Fraction on Relative Viscosity of Nylon Fibers Slurries Investigated by Blakeney (1966).

2.3.3 Effects of Temperature

The effect of temperature on the apparent viscosity, η, and the relative viscosity, η_r of WF/TR12 slurries was found to rank third when compared to wood flour volume fraction, ϕ, and shear rate, $\dot{\gamma}$. The apparent viscosity decreased with increased temperatures, as expected. However, the dependence of the apparent viscosity on temperature was complicated by the fact that the flow index, n, of TR12 oil decreased with increased temperature. This decrease in the flow index causes TR12 oil to depart more from Newtonian behavior, leading to a higher apparent viscosity value than expected for the slurry. The apparent viscosity of WF/TR12 slurries was not correlated as a function of temperature since only two temperatures were used.

2.3.4 Effects of Particle Dimensions

The term *"particle dimensions"* refers to the combined effect of particle size, particle size distribution, particle aspect ratio and particle aspect ratio distribution. The reason for the use of this term was explained earlier in this chapter. The effect of particle dimensions on the apparent viscosity of wood flour slurries is believed to rank fourth after ϕ, $\dot{\gamma}$ and temperature based on the experimental data. However, the findings in this study are not conclusive because the aspect ratios and the particle size distribution of the two wood flour size fractions used were very close in the exploratory experiments that were conducted. Moreover, the discussion about the critical volume fraction, ϕ^*, shows that these two variables are fairly important. Based on the experimental data, it is evident that the apparent viscosity of wood flour slurries increases with increased particle dimensions. This increase is more pronounced at higher wood flour volume fractions.

2.3.5 Effects of Heating Rate

The effect of heating time on the apparent viscosity of WF/TR12 slurries can be ranked fifth based on the experimental data. The apparent viscosity of 7.77 vol.% WF in TR12 oil initially decreased upon heating then it started increasing with time. However, this/ thermal dependence is mainly due to the dependence of TR12 oil on heating time. Actually, a stronger thermal dependence was expected for WF/TR12 slurries. This is due to the fact that TR12 oil is supposed to dissolve certain components of wood. This interaction, if it occurred during data acquisition, would have caused the apparent viscosity of the slurry to increase considerably with heating time. Obviously, this did not happen and the small increase in the viscosity of the WF/TR12 slurry used was due to TR12 oil. This finding cannot rule out this interaction between TR12 oil and wood flour since it could have taken place when the sample was heated during mixing and while it was being heated in the viscometer itself prior to commencing the experimental measurements. WF/DC23 slurries were not affected by heating time.

2.3.6 Correlation of Data using the Equation of Brodnyan

Inspection of the dependence of the relative viscosity, η_r, on wood flour volume fraction, ϕ, revealed that η_r increased very rapidly with increased ϕ. Plots of η_r versus ϕ

indicated that the dependence of η_r on ϕ was non-linear. It was found that an exponential function in ϕ can give curves that resemble the plots of η_r versus ϕ. Thus, since Brodnyan's (1959) equation is exponential in form and it is supposed to apply for concentrated suspensions of rods, it was chosen for correlating the relative viscosity dependence on the wood flour volume fraction. When the crowding factor, K, is taken to be 1.91, Brodnyan's (1959) equation can be written as:

$$\eta_r = Exp\ [\frac{2.5\phi + 0.399(q-1)^{1}.48\phi}{1 - 1.91\phi}] \qquad \textbf{(2.9)}$$

However, Brodnyan's equation requires a unique value for the aspect ratio, q, of the particles. But the wood flour fibers used in this study do not have a single value of q since they consist of a distribution of particle aspect ratios. The -200 mesh fraction, which was used in most of the experiments, has the following aspect ratio distribution: about 73% of the particles have aspect ratios between 1 and 2, about 22% of the particles have an aspect ratio between 2.5 and 4, while about 5% of the particles have an aspect ratio between 5 and 8. Thus, q can be anywhere between 1 and 8. Instead of substituting values of q from 1 to 8 in Equation 2.9 or using statistical methods that depend on the weighting of different fractions, Mason's (1950) definition of critical volume fraction, ϕ^*, was used. The critical volume fraction, ϕ^*, is defined as the solids volume fraction beyond which the relative viscosity increases more quickly. From Figure 2.22 it can be seen that the sharpest increase in η_r with ϕ for WF/TR12 slurries occurred at ϕ = 0.078 to 0.118, while for WF/DC23 slurries the sharpest increase took place at ϕ = 0.106 to 0.144. Thus, the critical volume fraction, ϕ^*, for WF/TR12 slurries should be ϕ^* = 0.978 - 0.118 whereas for WF/DC23 slurries, ϕ^* = 0.106 - 0.144. These values of ϕ^* are relatively close. Thus, the average of these values was used. Consequently, the critical volume fraction, ϕ^*, became 0.112. Mason (1950) defined ϕ^* mathematically as:

$$\phi^* = \frac{1.5}{(q)^2} \qquad \textbf{(2.10)}$$

Thus, having obtained ϕ^*, q was evaluated using Equation 2.10 and was found to be 3.664. This value of q is in fact between 1 and 8, which is the actual range of the wood flour aspect ratios. This method of evaluating q may not be completely valid, but it was felt that it was the most realistic method since the curves of η_r versus ϕ showed that ϕ^* must be between 0.077 and 0.144. Substitution of the value of q in Equation 2.9 yielded:

$$\eta_r = Exp[\frac{2.5\phi + 0.399(3.664-1)^{1.48}\phi}{1-1.91\phi}] \quad (2.11)$$

or

$$\eta_r = Exp[\frac{4.2012\phi}{1-1.91\phi}]$$

Equation 2.11 can give the dependence of the relative viscosity, η_r, on the wood flour volume fraction, ϕ. However, the dependence of η_r on ϕ is in itself a function of the shear rate, $\dot{\gamma}$. The dependence of η_r on $\dot{\gamma}$ can be represented very accurately by Equation 2.12:

$$\eta_r = \frac{m_o}{\dot{\gamma}(n_f - n_s)} \quad (2.12)$$

where

m_o = a constant, $m_o = \eta_r$ when $\dot{\gamma} = 1$ sec^{-1}
n_f = *"power law"* flow index of the fluid
n_s = *"power law"* flow index of the slurry

The plots of η_r versus ϕ, at various shear rates, for the wood flour slurries used were similar in shape. Thus, plots of m_o versus ϕ should be representative of plots of η_r versus ϕ. Moreover, plots of η_r versus ϕ for WF/TR12 and WF/DC23 were similar in shape. Thus, in the initial search for a correlation to represent the behavior of η_r with ϕ or m_o with ϕ, it is sufficient to use WF/DC23 slurries data. Utilizing data of WF/DC23 slurries, Equation 2.11 was used to calculate m_o for each value of ϕ. The results are shown in Table 2.8. As can be seen from this table, the values of m_o as calculated using Brodnyan's equation are much lower than the measured values of m_o. Even if the aspect ratio, q, was assumed to be 8, which is an unreasonable assumption since very few particles in the -200 mesh fraction have a value of q = 8, Equation 2.11 still gave very low values of m_o. Thus, Brodnyan's equation does not fit the relative viscosity data of the wood flour slurries. This conclusion is not surprising since most of the theoretical correlations neglect non-hydrodynamic interactions between particles and between the fluid and particles. One such interaction which should be prevalent in wood flour slurries is surface interactions.

Having realized that Brodnyan's equation does not fit the relative viscosity, η_r, data of wood flour slurries, it was thought that this equation may be modified to fit the data. Nicodemo and Nicolais (1974) reported that Brodnyan's (1959) equation did not fit their data. However, they fit their data using a modified version of Brodnyan's equation, namely,

Table 2.8. Values of m_o Calculated using Brodnyan's Equation.

Wood Flour Volume Fraction, ϕ	Measured m_o	Calculated m_o
0.0341	2.18	1.17
0.0694	4.43	1.40
0.1059	12.94	1.75
0.1437	97.83	2.30
0.1828	196.13	3.25
0.2234	642.93	5.14

Table 2.9. Values of m_o for WF/DC23 Slurries as Calculated using the Modified Brodnyan Equation.

Wood Flour Volume Fraction, ϕ	Measured m_o	Calculated m_o
0.0341	2.18	2.12
0.0694	4.43	5.06
0.1059	12.94	13.84
0.1437	97.83	45.24
0.1828	196.13	185.54
0.2234	642.93	1,031.97

$$\mu_r = Exp\ (8.52\phi) \tag{2.13}$$

The method used in this study to modify Brodnyan's equation can be described as follows:

1. The value of the particle aspect ratio, q, was kept as 3.664.
2. The value of the crowding factor, K, was allowed to vary since K = 1.91 was supposed to apply for ellipsoids with a very high aspect ratio, while wood flour fibers have small aspect ratios, q.
3. Equation 2.11 was rewritten as:

$$m_o = Exp[\frac{4.2012\phi}{1-K\phi}] \tag{2.14}$$

4. Equation 2.14 was rearranged to be of the form:

$$\frac{1-4.2012\phi}{Lnm_o} = K\phi \tag{2.15}$$

5. The expression [1 - (4.2012ϕ)/Lnm$_o$] was correlated as a function of ϕ using linear regression and the resulting expression was:

$$1-\frac{4.2012\phi}{Lnm_o} = 0.29\phi+0.8 \tag{2.16}$$

6. After simplification and rearrangement of Equation 2.16 the final expression for m$_o$ was:

$$m_o = Exp[\frac{21\phi}{1-1.45\phi}] \tag{2.17}$$

As can be seen from Equation 2.17, the crowding factor, K, was found to be 1.45 using this method. Values of m$_o$ for WF/DC23 slurries were calculated using Equation 2.17. The calculated and measured values of m$_o$ are shown in Table 2.9. From this table, it can be seen that the calculated values of m$_o$ are closer to the measured values but fit is not exact.

Other methods can be used to modify Brodnyan's equation. As an example, terms with ϕ^2 and higher order can be used in the numerator of the exponential term in Equation 2.17. Having established that an equation of the form of Equation 2.17 can represent the dependence of m_o on ϕ for WF/DC23 slurries, Equation 2.18 was used to represent the dependence of m_o on ϕ for WF/TR12 slurries.

$$m_o = Exp[\frac{b\phi}{1 - 1.45\phi} \quad \textbf{(2.18)}$$

where b is a coefficient that should be evaluated from the data of each slurry. The values of b for WF/TR12 slurries at 65°C and at 93°C can be evaluated from the slope of a plot of [(1 - 1.45ϕ)Lnm_o] versus ϕ, or by trial and error. The method of trial and error was used in this study. Thus, for WF/TR12 slurries at 65°C the final expression for m_o was Equation 2.19, whereas for WF/TR12 slurries at 93°C the final expression for m_o was Equation 2.20.

$$m_o = Exp[\frac{32\phi}{1 - 1.45\phi}] \quad \textbf{(2.19)}$$

and

$$m_o = Exp[\frac{35\phi}{1 - 1.45\phi}] \quad \textbf{(2.20)}$$

The values of m_o for WF/TR12 slurries at 65°C were calculated using Equation 2.19 and the results are shown in Table 2.10. Similarly, values of m_o for WF/TR12 slurries at 93°C were evaluated using Equation 2.20 and the results are shown in Table 2.11. From these tables it is evident that the modified version of Brodnyan's equation does not give an exact fit of the data, but at least this fit is better than what could be obtained using Brodnyan's equation.

So far, no attempt has been made to incorporate the shear rate into expressions of η_r versus ϕ. Such an attempt is presented here and a new endeavor to correlate m_o and ϕ is made.

Table 2.10. Values of m_o for WF/TR12 Slurries at 65°C as calculated using the Modified Brodnyan Equation.

Wood Flour Volume Fraction, ϕ	Measured m_o	Calculated m_o
0.0384	2.87	3.67
0.0777	16.64	16.48
0.1181	168.84	95.60
0.1594	762.15	760.63

Table 2.11. Values of m_o for WF/TR12 Slurries at 93°C as Calculated using the Modified Brodnyan Equation.

Wood Flour Volume Fraction, ϕ	Measured m_o	Calculated m_o
0.0377	5.74	4.04
0.0764	16.19	20.23
0.1162	317.75	133.1
0.1570	1,304.56	1,223.0
0.1989	7,218.50	17,728.9
0.2420	14,649.9	465,000

2.4 CONCLUSIONS AND RECOMMENDATIONS

2.4.1 Conclusions

TR12 oil was found to be a shear thinning fluid. This shear thinning behavior increased with temperature. The *"power law"* model fit the apparent viscosity data of TR12 oil very accurately in the range of shear rates investigated. TR12 oil did not exhibit any viscoelastic behavior. This fluid was found to possess a thermal-history dependence, while no shear-history dependence was observed. TR12 oil did not exhibit any yield stress.

WF/TR12 and WF/DC23 slurries were found to be shear thinning. This shear thinning behavior increased with increased wood flour volume fraction, ϕ. The apparent viscosity data of these slurries fit the *"power law"* model very accurately in the range of shear rates investigated. These slurries did not exhibit any yield stress in the range of shear rates, $\dot{\gamma}$, and wood flour volume fractions studied. The Weissenberg effect was noticed during experimental measurements involving these slurries. Thus, wood flour slurries are viscoelastic. The Weissenberg effect increased with increased ϕ and $\dot{\gamma}$ when the particle dimensions were held constant. The dependence of relative viscosity, η_r, on shear rate, $\dot{\gamma}$, for these slurries obeyed a correlation similar to the *"power law"* model very accurately. The dependence of the shear rate power index, (n_f-n_s), on wood flour volume fraction, ϕ, was found to be roughly linear. Brodnyan's (1959) equation gave relative viscosity values which were orders of magnitude lower than the measured values. The modified Brodnyan equation yielded relative viscosity values which were of the same order of magnitude as the measured values. However, the fit provided by this equation was far from exact. An exponential equation was used to correlate the relative viscosity dependence on wood flour volume fraction, ϕ, and on shear rate, $\dot{\gamma}$. The fit provided by this equation was slightly better than that obtained by the modified Brodnyan equation, but the fit was still not exact. However, this fit seemed to improve at higher shear rates. This equation should not be extrapolated beyond the range of experimental data. This is especially true for extrapolations at higher ϕ values. WF/TR12 slurries possess a thermal-history dependence which is mainly due to the thermal-history dependence of TR12 oil. WF/DC23 slurries do not possess a thermal-history dependence. The apparent viscosity of wood flour slurries increased with increased particle dimensions. This increase was more pronounced at higher wood flour volume fractions. The apparent viscosity, η, and relative viscosity, η_r, of wood flour slurries are considerably higher than η and η_r values predicted based on theoretical correlations. Also, η and η_r values of wood flour slurries are much higher than glass fiber suspensions. These high values of apparent and relative viscosities of wood flour slurries are believed to be mainly due to the particle properties of wood flour. These properties are not taken into account in theoretical correlations and they are negligible for glass fiber/silicone oil suspensions.

2.4.2 Recommendations

An investigation of the rheological behavior of complex slurries like wood flour slurries, as was done in this study, can only be considered as one step forward toward the understanding of the rheology of wood flour slurries. Although a considerable amount of data were reported and a few interesting phenomena were noticed, much work is needed in the future to elucidate the rheological behavior of these slurries. The bulk of this future work must be accomplished experimentally. This is due to the fact that the theory of dilute suspensions and previous investigations using other fiber suspensions can only provide clarifying insight and general guidelines for the understanding of the rheology of concentrated wood flour slurries.

Some of the areas that require more study are:

1. The effect of particle dimensions on the rheological behavior of wood flour slurries.

2. The presence of normal stresses and their variation with wood flour volume fraction, shear rate (or shear stress) and particle aspect ratio.

3. The interactions between wood flour particles and their effect on the rheology of wood flour slurries.

4. The interactions between wood flour fibers and suspending fluids and their effect on the rheology of wood flour slurries.

Obviously, investigation of the effect of each of the variables mentioned above on the rheological behavior of wood flour slurries will not be easy. It will involve the use of very difficult experimental techniques and a great amount of research efforts. But often this is how scientific knowledge is acquired.

2.5 CORRELATION OF DATA USING AN EXPONENTIAL EQUATION

As was mentioned earlier, the relative viscosity, η_r, dependence on shear rate, γ, can be accurately represented by:

$$\eta_r = \frac{m_o}{\dot{\gamma}(n_f - n_s)} \tag{2.21}$$

where

m_o = a constant, $m_o = \eta_r$ at $\dot{\gamma} = 1\ sec^{-1}$
n_f = *"power law"* flow index of the fluid
n_s = *"power law"* flow index of the slurry

Since Equation 2.21 gives the dependence of η_r on $\dot{\gamma}$ accurately, it is a good equation to use to develop an expression for the dependence of η_r on ϕ and on $\dot{\gamma}$. Thus, it is necessary to incorporate the dependence of η_r on ϕ in Equation 2.21. From the data, it was noticed that both m_o and $(n_f - n_s)$ varied with ϕ. Consequently, two correlations are needed. The first correlation should give the dependence of m_o on ϕ, while the second should give the dependence of $(n_f - n_s)$ on ϕ.

The dependence of m_o on ϕ was discussed before. It was shown that Brodnyan's (1959) equation gave values of m_o which were too low, whereas the modified Brodnyan equation gave values of m_o which were closer to the measured values but the fit was far from exact. Another attempt was made to correlate m_o and ϕ. This endeavor led to an expression which gave a slightly better fit of the data than the modified Brodnyan equation. Nevertheless, the fit was still not exact. This attempt was based on the correlation of $[(m_o - 1)/\phi]$ versus ϕ using the non-linear least squares regression method. The form of the resulting expression was:

$$m_o = B\phi \; Exp \; (B'\phi) + 1 \qquad (2.22)$$

Equation 2.22 is still an expression with an exponential term in ϕ. Thus, it is similar to Brodnyan's equation. Based on the data for each slurry the final equations were:

for WF/DC23 at 41°C

$$m_o = 11.657\phi \text{ Exp } (24.908\phi) + 1 \qquad (2.23)$$

for WF/TR12 at 65°C

$$m_o = 11.0\phi \text{ Exp } (38.942\phi) + 1 \qquad (2.24)$$

for WF/TR12 at 93°C

$$m_o = 33.34\phi \text{ Exp } (33.241\phi) + 1 \qquad (2.25)$$

Using Equations 2.23 - 2.25 values of m_o were calculated for each slurry. Calculated values of m_o for WF/DC23, WF/TR12 (at 65°C) and WF/TR12 (at 93°C) slurries are shown in Tables 2.12 - 2.14, respectively. As can be seen from these tables, calculated values of m_o are often not very close to the measured values; however, the quality of the fit of the data is slightly improved over that obtained using the modified Brodnyan equation.

Having obtained expressions for the dependence of m_o on ϕ the next task was to determine the dependence of $(n_f - n_s)$ on ϕ. The shear rate power index, $(n_f - n_s)$, was correlated as a function of ϕ using linear regression. The calculated and experimental values of $(n_f - n_s)$ of WF/DC23, WF/TR12 at 65°C and WF/TR12 at 93°C slurries are given in Tables 2.15 - 2.17, respectively.

Table 2.12. Values of m_o for WF/DC23 Slurries.

Wood Flour Volume Fraction, ϕ	Measured m_o	Calculated m_o
0.0341	2.18	1.93
0.0694	4.43	5.56
0.1059	12.94	18.26
0.1437	97.83	61.05
0.1828	196.13	203.30
0.2234	642.93	680.64

Table 2.13. Values of m_o for WF/TR12 Slurries at 65°C.

Wood Flour Volume Fraction, ϕ	Measured m_o	Calculated m_o
0.0384	2.87	2.88
0.0777	16.64	18.62
0.1181	168.84	130.12
0.1594	762.15	871.36

Table 2.14. Values of m_o for WF/TR12 Slurries at 93°C.

Wood Flour Volume Fraction, ϕ	Measured m_o	Calculated m_o
0.0377	5.7	5.4
0.0764	16.2	33.3
0.1162	317.8	185.4
0.1570	1,304.6	967.9
0.1989	7,218.5	4,932.7
0.2420	14,649.9	25,000

Table 2.15. Calculated and Experimental Values of Shear Rate Power Index of WF/DC23 Slurries.

Wood Flour Volume Fraction, ϕ	Experimental (n_f-n_s)	Calculated (n_f-n_s)
0.0341	0.094	0.079
0.0694	0.201	0.241
0.1059	0.352	0.410
0.1437	0.696	0.584
0.1828	0.792	0.764
0.2234	0.893	0.951

Table 2.16. Calculated and Experimental Values of Shear Rate Power Index of WF/TR12 Slurries at 65°C.

Wood Flour Volume Fraction, ϕ	Experimental (n_f-n_s)	Calculated (n_f-n_s)
0.0384	0.055	0.066
0.0777	0.233	0.268
0.1181	0.578	0.477
0.1594	0.634	0.689

Table 2.17. Calculated and Experimental Values of Shear Rate Power Index of WF/TR12 Slurries at 93°C.

Wood Flour Volume Fraction, ϕ	Experimental (n_f-n_s)	Calculated (n_f-n_s)
0.0377	0.179	0.226
0.0764	0.254	0.320
0.1162	0.569	0.417
0.1570	0.518	0.516
0.1989	0.651	0.618
0.2420	0.650	0.723

The dependence of $(n_f - n_s)$ on ϕ was roughly linear. Thus, the expression used to correlate this dependence was:

$$(n_f - n_s) = b'\phi + b'' \tag{2.26}$$

where b′ is the slope of the straight line and b" is the intercept. The calculated values of $(n_f - n_s)$ for each slurry were obtained using Equations 2.27 - 2.29

For WF/DC23 at 41°C

$$(n_f - n_s) = 4.6068\phi - 0.0783 \tag{2.27}$$

for WF/TR12 at 65°C

$$(n_f - n_s) = 5.1536\phi - 0.1321 \tag{2.28}$$

and for WF/TR12 at 93°C

$$m_o = 33.34\phi \; Exp\; (33.241\phi) + 1 \tag{2.29}$$

Based on Equations 2.21, 2.22 and 2.26 the final expression for the dependence of the relative viscosity, η_r, on wood flour volume fraction, ϕ, and shear rate, γ, can be written as:

Equation 2.30 is similar to Brodnyan's (1959) equation in that it uses the exponential expression in ϕ. However, it accounts for the dependence of η_r on $\dot{\gamma}$ while Brodnyan's equation does not. Also, the dependence of η_r on particle aspect ratio, q, is included implicitly in Equation 2.30. If several sets of particles with uniform but varied aspect ratios were available, the effect of q can be incorporated into Equation 2.30 in any or some of the coefficients B, B′, b′ and b″. For example, if B′ were to be a function of q, then Equation 2.30 could be written,

Equation 2.31 is even more similar to Brodnyan's equation. Similarly, the effect of other variables like temperature, T, can be incorporated into Equation 2.30. This equation is not

$$\eta_r = \frac{B\phi Exp[2.5\phi + f(q)\phi] + 1}{\dot{\gamma}^{(b'\phi + b'')}} \qquad (2.31)$$

completely consistent mathematically since when $\phi = 0$ the numerator becomes unity while the denominator does not. This should not pose any problems. On the other hand, it is consistent mathematically when both the fluid and slurry are Newtonian, since $n_f = 1$ and $n_s = 1$, giving $(n_f - n_s) = 0$ and the dependence of η_r on $\dot{\gamma}$ is eliminated. However, this equation may lack the theoretical consistency that Brodnyan's equation possesses. Also, Equation 2.30 does not have the possible predictive power of theoretical correlations, since it is completely based on fitting of the data. This means that the data must be obtained first and then the empirical correlation can be attained. Thus, there is no convenient substitute for rigorous theoretical correlations. Yet, theoretical correlations are usually derived based on many simplifying assumptions that often make their predictive power almost useless. This will illustrated before, where an attempt was made to fit the data of WF/DC23 slurries using Brodnyan's equation. Consequently, if the rheological behavior of a certain slurry is required, the best and most accurate approach would be to conduct experiments to determine the rheology of the slurry in question. Meanwhile, theoretical correlations and previous research efforts can often provide some clarifying insight and general guidelines about the possible rheological behavior of the slurry. Finally, although empirical correlations like Equation 2.30 are of limited utility, they may prove convenient in process design calculations involving the use of computers. This is due to the fact that it is often easier to use equations in computer programs rather than inserting various values of data obtained from charts or figures.

Having discussed the advantages and disadvantages of empirical correlations like Equation 2.30, the specific equation for each slurry can be rewritten as:

<u>for WF/DC23 at 41°C</u>

$$\eta_r = \frac{11.657\phi Exp(24.908\phi) +}{\dot{\gamma}(5.1536\phi - 0.1321)} \qquad (2.32)$$

<u>for WF/TR12 at 65°C</u>

$$\eta_r = \frac{11.0\phi Exp(38.942\phi) + 1}{\dot{\gamma}(5.1536\phi - 0.1321)} \qquad (2.33)$$

for WF/TR12 at 93°C

$$\eta_r = \frac{33.34\phi\, Exp(33.241\phi) + 1}{\dot{\gamma}2.43\phi + 0.1348} \qquad (2.34)$$

Using Equation 2.32 the values of η_r for WF/DC23 slurries were calculated at various ϕ and $\dot{\gamma}$. The calculated values of η_r for these slurries are presented in Table 2.18, whereas the measured values of η_r are shown in Table 2.19. Similarly, Equation 2.33 was used to calculate η_r for WF/TR12 slurries at 65°C, while Equation 2.34 was used to calculate η_r for WF/TR12 slurries at 93°C. Calculated and measure values of η_r for WF/TR12 slurries at 65°C are presented in Tables 2.20 and 2.21, respectively, while calculated and measured values of η_r for WF/TR12 slurries at 93°C are shown in Tables 2.22 and 2.23, respectively. As can be seen from Tables 2.18 - 2.23, the measured and calculated values of the relative viscosity η_r are not that close. This is due to the fact that correlations of m_o and ϕ are not exact and thus they introduced some error. Similarly, correlations of $(n_f - n_s)$ and ϕ were not exact and they also introduced some error. These errors might cancel each other at times and at others the error may be compounded. Values followed by an asterisk in Tables 2.20 - 2.23 were obtained by extrapolation, and thus do not represent actual data.

2.6 INSTRON RHEOMETRY DATA ON MODEL COMPOUND SLURRIES

The viscosities of concentrated wood flour slurries at medium to high shear rates cannot be obtained on the Haake Rotary Viscometer; instead, one must use the Instron capillary Rheometer in order to apply sufficient pressure upon the slurries to obtain high shear rates. The University of Arizona did not have an Instron Capillary Rheometer, so that this required data was subcontracted to the University of Lowell. The University of Arizona provided the wood flour (obtained from the Albany DOE plant) and the various polyethylene model fluid carriers.

The Instron Capillary Rheometer is a unit that is attached to a conventional Instron Tensile/Compression machine. Pellets of resins are melted in a pressure chamber, after which a piston plunger forces the viscous melt through precise-dimensional capillaries. The true shear stress and shear rate at the wall can be calculated, and adjusted by known theory for the entrance and exit losses of pressure differential. The results are usually correlated by the power law equation:

$$\sigma = k\dot{\gamma}^n \qquad (2.35)$$

where
σ = shear stress
$\dot{\gamma}$ = Apparent shear rate.

Table 2.18. Calculated Values of Relative Viscosity of WF/DC23 Slurries.

Shear Rate, $\dot{\gamma}$ (sec^{-1})	Relative Viscosity, η_r					
	ϕ=0.0341	ϕ=0.0694	ϕ=0.1059	ϕ=0.1437	ϕ=0.1828	ϕ=0.2234
0.02	-	-	-	-	-	2.81×10^4
0.08	-	-	-	-	-	7,520
0.2	-	-	-	-	-	3,150
1.0	1.93	5.56	18.3	61.1	203	681*
3.2	1.76	4.20	11.4	31.0	83.5	225*
12.8	1.58	3.00	6.44	13.8	29.0	60.3*
25.6	1.49	2.54	4.85	9.21	17.1	31.2*
51.2	1.42	2.15	3.65*	6.14	10.0*	16.14*

* Extrapolated value

Table 2.19. Measured Values of Relative Viscosity of WF/DC23 Slurries.

Shear Rate, $\dot{\gamma}$ (sec^{-1})	Relative Viscosity, η_r					
	ϕ= 0.0341	ϕ= 0.0694	ϕ= 0.1059	ϕ= 0.1437	ϕ= 0.1828	ϕ= 0.2234
0.02	-	-	-	-	-	2.12×10^4
0.08	-	-	-	-	-	6,140
0.2	-	-	-	-	-	2,710
1.0	2.18	4.43	12.9	97.8	196	643*
3.2	1.95	3.51	8.60	43.5	81.4	228*
12.8	1.71	2.66	5.27	16.6	28.7	66.2*
25.6	1.61	2.31	4.13	10.2	17.0	35.7*
51.6	1.50	2.01	3.23*	6.32	10.1*	19.2*

* Extrapolated value

Table 2.20. Calculated Values of Relative Viscosity of WF/TR12 Slurries at 65°C.

Shear Rate, $\dot{\gamma}$ (sec^{-1})	Relative Viscosity, η_r			
	ϕ=0.0384	ϕ=0.0777	ϕ=0.1181	ϕ=0.1594
1.0	2.88	18.6	130	871
2.82	2.69	14.1	79.3	426
5.63	2.57	11.7	57.1	265
11.26	2.46	9.71	41.0	164
45.06	2.24	6.70	21.2	63.1
63.71	2.19	6.10	18.0	49.7*

* Extrapolated value

Table 2.21. Measured Values of Relative Viscosity of WF/TR12 Slurries at 65°C.

Shear Rate, $\dot{\gamma}$ (sec^{-1})	Relative Viscosity, η_r			
	ϕ=0.0384	ϕ=0.0777	ϕ=0.1181	ϕ=0.1594
1.0	2.87	16.6	169	762
2.82	2.60	13.1	92.8	395
5.63	2.50	11.2	62.3	254
11.26	2.40	9.5	41.6	164
45.06	2.25	6.85	18.7	68.2
63.71	2.21	6.30	15.3	54.7*

* Extrapolated value

Table 2.22. Calculated Values of Relative Viscosity of WF/TR12 Slurries at 93°C.

Shear Rate, $\dot{\gamma}$ (sec^{-1})	Relative Viscosity, η_r					
	ϕ=0.0377	ϕ=0.0764	ϕ=0.1162	ϕ=0.1570	ϕ=0.1989	ϕ=0.2420
0.02	-	-	-	-	5.5×10^4	4.2×10^5
0.04	-	-	-	-	3.6×10^4	2.6×10^5
0.07	-	-	-	-	2.6×10^4	1.7×10^5
0.2	-	-	-	-	1.3×10^4	80,000*
1.0	5.4	33.3	185	968	4,930*	25,000*
5.63	3.65	19.1	90.0	397	1,690*	7,170*
22.53	2.67	12.3	50.5	194	719*	2,630*
63.71	2.11	8.8	32.7	113	378*	1,240*

* Extrapolated value

Table 2.23. Measured Values of Relative Viscosity of WF/TR12 Slurries at 93°C.

Shear Rate, $\dot{\gamma}$ (sec^{-1})	Relative Viscosity, η_r					
	ϕ=0.0377	ϕ=0.0764	ϕ=0.1162	ϕ=0.1570	ϕ=0.1989	ϕ=0.2420
0.02	-	-	-	-	9.3×10^4	1.9×10^5
0.04	-	-	-	-	5.9×10^4	1.2×10^5
0.07	-	-	-	-	4.1×10^4	8.2×10^4
0.2	-	-	-	-	2.1×10^4	42,000*
1.0	5.7	16.2	318	1,305	7,220*	14,700*
5.63	4.2	10.4	119	534	2,350*	4,750*
22.53	3.3	7.3	54.0	261	947*	1,924*
63.71	2.7	5.6	30.0	152	482*	981*

* Extrapolated values

The constants K and n can be determined over short ranges of shear rates of interest.

As described earlier in Part 2, blends of a high molecular weight LDPE (Dow Grade 515) and a very low molecular weight polyethylene (Allied Chemical AC6 PE) were made to provide a range of viscosities for these fluid carriers of wood flour in concentrated slurries. Typical properties of these polyethylenes are given in Table 2.24.

The experimental data obtained for these blends, using the Instron Capillary Rheometer, are shown in Table 2.25. Various shear rates at the corresponding shear stresses for these model fluid carriers for wood flour are shown in Figure 2.28. The n values of the power law equation were calculated and summarized in Table 2.26.

2.7 ADDITIONAL RHEOLOGY STUDIES

The importance of the rheology of concentrated wood flour slurries cannot be over-emphasized. Thus, additional work was conducted as funds and time were made available. Some important early work was conducted at the University of Lowell by Yang (1981). Some additional rheological concepts for concentrated slurries were studied by Lezzar (1983).

Table 2.24. Typical Properties of Allied Chemical AC6 PE and Dow LDPE 515		
	AC6 PE	*LDPE 515*
Appearance	Fine White Powder	White Pellet
Softening Point	222°F (106°C) (ASTM E-28)	208°F (97°C) (ASTM D-1525)
Density (g/cc)	0.92 (ASTM D-5)	0.919 (ASTM D-792)
Viscosity	200 cps at 140°C (Brookfield)	2130 poise at 190°C (shear rate 1,000 second^{-1})

Table 2.25. Instron Capillary Rheometer Data on Model Fluid Carriers					
Cross-Head Speed (cm/min)	Shear Rate $\dot{\gamma}$ (sec^{-1})	Plunger Force (Kg)	Shear Stress τ (g/cm^2)	Log τ	Log $\dot{\gamma}$
(a) Data for 100% LDPE at 210°C					
0.06	3.5	12	105	2.02	0.54
0.2	11.6	24	21	2.32	1.06
0.6	34.8	47	413	2.62	1.54
2.0	116.0	89	782	2.89	2.06
6.0	348.0	156	1370	3.14	2.54
(b) Data for 75 wt. % LDPE/25 wt. % AC6 PE at 150°C					
0.06	3.5	8.0	70.0	1.85	0.54
0.2	11.6	18.0	158.0	2.20	1.06
0.6	34.8	34.5	303.0	2.48	1.54
2.0	116.0	67.5	593.0	2.77	2.06
6.0	348.0	122.0	1070.0	3.03	2.54
(c) Data for 50 wt. % LDPE/50 wt. % AC6 PE at 150°C					
0.2	11.6	3.6	31.6	1.50	1.06
0.6	34.8	8.6	75.5	1.88	1.54
2.0	116.0	17.0	149.0	2.17	2.06
6.0	348.0	46.0	404.0	2.61	2.54
(d) Data for 25 wt. % LDPE/75 wt. % AC6 PE at 143°C					
0.2	11.6	0.4	3.5	0.55	1.06
0.6	34.8	0.6	5.3	0.72	1.54
2.0	116.0	2.2	19.3	1.29	2.06
6.0	348.0	5.4	47.4	1.68	2.54
20.0	1160.0	16.4	144.1	2.16	3.06

Table 2.26 Summary of Calculated n Values of All Formulations				
Ingredients of Resin Blends	Concentration of Resin Blends			
	30%	40%	50%	100%
75% wax 25% LDPE	**	0.43	0.45	*0.86
50% wax 50% LDPE	0.36	0.42	0.44	*0.70
25% wax 75% LDPE	0.36	0.37	0.40	*0.59
100% LDPE	0.24	0.25	0.39	*0.57
* Data obtained on Instron rheometer.				
** Material does not flow like a continuum.				

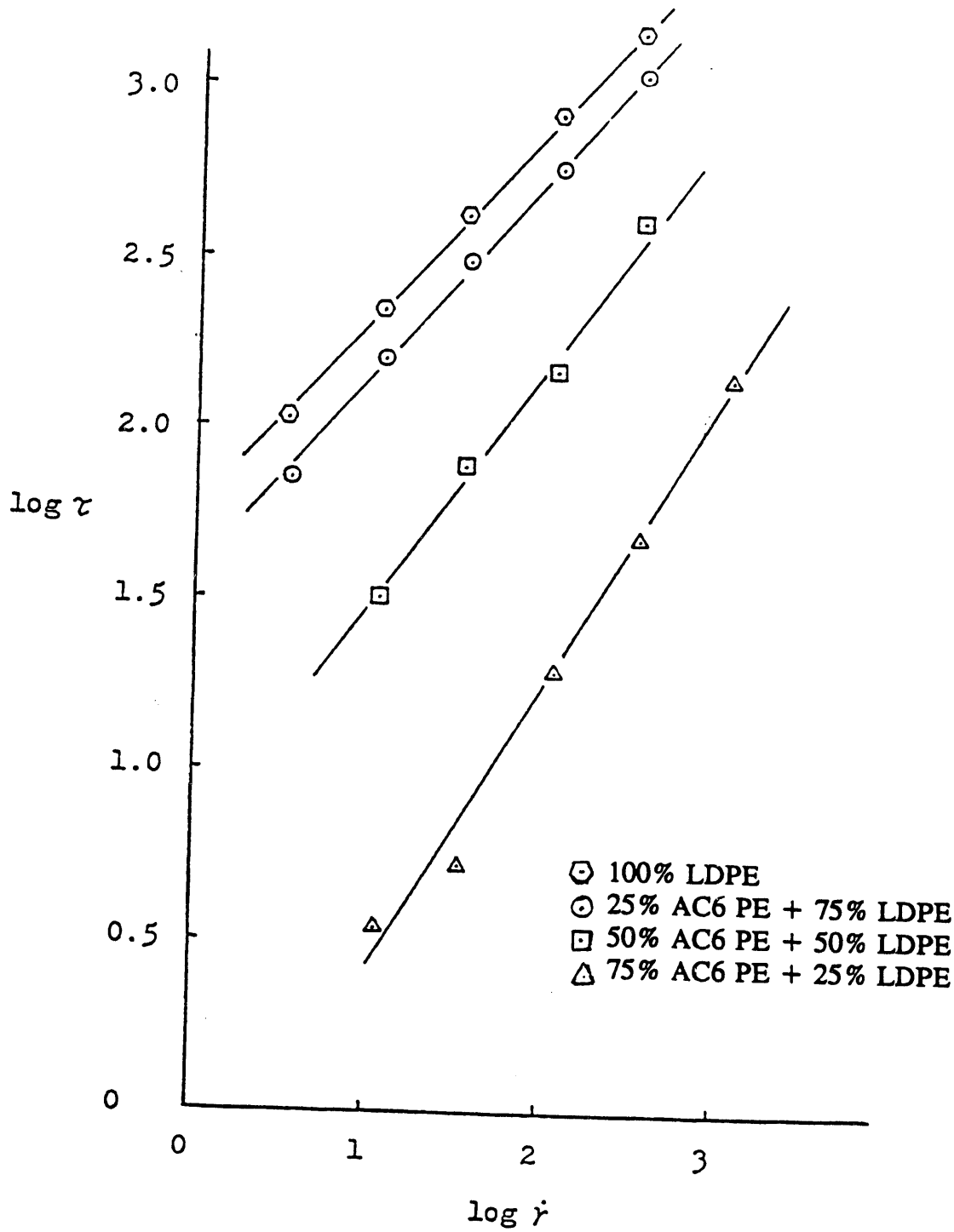

Figure 2.28. Apparent Shear Rates as Function of Shear Stress for Model Fluid Carriers for Wood Flour.

2.8 NOMENCLATURE

B	=	Parameter in Equation 2.22.
B'	=	Parameter in Equation 2.22.
b	=	Coefficient in Equation 2.18.
b'	=	Slope in Equation 2.26.
b"	=	Intercept in Equation 2.26.
c	=	Solid mass frction.
K	=	Interaction coefficient or crowding factor.
L	=	Particle length
m	=	"Power law" constant.
m_1	=	"Power law" constant.
m_o	=	Coefficient in relative viscosity equation
n	=	"Power law" flow behavior index
n_f	=	"Power law" flow behavior index for fluid
n_s	=	"Power law" flow behavior index for slurry or suspension
q	=	Axis ratio or particle aspect ratio, L/D
t	=	Time
m′	=	a constant for the slurry in Equation 2.6.
m″	=	a constant for the fluid in Equation 2.7.
v_x	=	x-Component of velocity.
$\dot{\gamma}$	=	Rate of deformation or shear rate.
δ	=	Shear stress.
η	=	Apparent viscosity, used for non-Newtonian materials.
η_f	=	Apparent viscosity of fluid.
η_s	=	Apparent viscosity of slurry or suspension.
η_r	=	Relative viscosity, used for non-Newtonian materials.
μ	=	Viscosity, used for Newtonian materials.
μ_f	=	Viscosity of fluid.
μ_s	=	Viscosity of suspension.
μ_r	=	Relative viscosity, used for Newtonian materials.
τ	=	Shear stress tensor.
ϕ	=	Solids volume fraction.
μ'	=	plastic viscosity
η_1	=	Apparent viscosity at time t.
η_o	=	Apparent viscosity at time o.
ϕ^*	=	Critical solids volume fraction or concentration.
ψ	=	Yield stress.

2.9 REFERENCES FOR PART 2

Bingham, E.C. and H. Green, *"Paint, a Plastic Material and Not a Viscous Liuqid; the Measurement of its Mobility and Yield Value,"* Proceedings of the American Society for Testing and Materials, 19, pp.640-675 (1919).

Bird, R.B., R.C. Armstrong and O. Hassager, Dynamics of Polymeric Liquids: Volume 1, Fluid Mechanics. John Wiley and Sons, New York (1977).

Blakeney, W.R., *"The Viscosity of Suspensions of Straight, Rigid rods,"* Journal of Colloid and Interface Science, 22, pp.324-330 (1966).

Brodnyan, J.C., *"The Concentrtion Dependence of the newtonian Viscosity of Prolate Ellipsoids,"* Transactions of the Society of Rheology, 3, pp.61-68 (1959).

Chehab, M., *"The Rheology of Concentrated Cellulosics Slurries,"* M.S. Thesis in Chemical Engineering, University of Arizona, Tucson, Arizona (1982).

Lezzar, A., *"Effect of Void Volume on the Friction and Rheology of Concentrated Slurries,"* M.S. Thesis in Chemical Engineering, University of Arizona, Tucson, Arizona (1983).

Maschmeyer, R.O., *"Rheology of Concentrated Suspensions of Fibers,"* Doctor of Science Dissertation, Washington University, St. Louis, Missouri, June (1974).

Mason, S.G., *"The motion of Fibers in Flowing Liquids,"* Pulp and Paper Magazine of Canada, 51, pp.93-100 (1950).

Nicodemo, L., and L. Nicolais, *"Viscosity of Concentrated Fiber Suspensions,"* The Chemical Engineering Journal, 8, pp.155-156 (1974).

Williamson, F.V., *"The Flow of Pseudoplastic Materials,"* Industrial and Engineering Chemistry, 21, pp.1108-1111 (1929).

Yang, L.C., *"Rheology of Sawdust Filled Polymer,"* M.S. Thesis, Department of Plastics Engineering, University of Lowell, Lowell, Massachusetts (1981).

PART 3

SCALE-UP OF THE EXTRUDER-FEEDER AND PRELIMINARY ECONOMIC EVALUATION

TABLE OF CONTENTS

LIST OF TABLES

LIST OF FIGURES

PART 3

SCALE-UP OF THE EXTRUDER-FEEDER AND PRELIMINARY ECONOMIC EVALUATION

3.1 INTRODUCTION

The feasibility and operability of the extruder-feeder was proven during the period 1978-1980, and its operating characteristics were determined as reported in Parts 1 and 2 of this final report. In order to determine its merits as the pumping and preheating stage for a biomass direct liquefaction process, scale-up calculations and a preliminary economic evaluation was performed during 1981, as reported in this Part 3 section.

This work formed the basis for then designing a continuous bench-scale extruder-feeder biomass liquefaction unit. This work showed that the extruder-feeder is a promising unit operation in biomass liquefaction.

Some remarks regarding operability and performance are as follows:

1. The vacuum bottoms from the Albany fractionator can be utilized as the fluid carrier for the wood flour feedstock.

2. The viscous dissipation of the vacuum bottoms (internal friction) has been shown to be some 20- to 30-fold less than viscous plastics, and hence require less than half of the horsepower (Hp) needed for low-density polyethylene. In fact, only about one-fourth as much Hp is needed for pumping the wood flour slurry into a 3,000 psi pressure reactor and the other one-fourth is used to preheat the slurry from 80°F to 300°F.

3. Due to the viscous dissipation of 50 and 60 wt. % WF/vacuum bottom slurries being so much less than plastics, the extruder-feeder can be operated at a much higher screw rpm. This means that a given extruder-feeder can have a much higher capacity for a given capital investment. Only a small fraction of this potential has been scaled into the projected commercial units evaluated in this Part 3 section.

4. The extruder-feeder-preheater system is the only known system which has the potential of circulating hot reactor effluent back to the feedstock without reducing pressure, because it does not need a low-viscosity oil to dilute the wood flour slurry for proper pumping.

5. The extruder-feeder has proven to have much flexibility, both in design factors and operating factors. Design factors include extruder size (sizes available up to 24-inch diameter), screw compression, screw pitch, channel depth and screw speed. Operating factors include screw speed, temperature profile, slurry concentration and carrier oil

viscosity. In other words, a choice can be made of several different combinations of these factors.

6. The extruder-feeder-preheater system is the only known system that can recycle the heavy ends of liquefaction products in such high-concentrations and thus offer the potential of converting these ends to a lighter, less-viscous, more-useful product. Exxon has recently discovered that this is advantageous in coal liquefaction, resulting in higher overall yields of light oils.

7. The operability of the extruder-feeder has proven to be very reliable. No plugging was experienced in the preliminary runs (from even concentrated slurries), and outlet pressures and temperatures were closely controlled. Thus, this system appeared to be well-adapted for a continuous process, especially where temperature and residence time should be closely controlled.

3.2 EXPERIMENTAL DATA FOR SCALE-UP PURPOSES

The experimental data generated in Parts 1 and 2 were used for this scale-up work. Additional experimental data was generated directly related to scale-up, and these data are summarized later in this section.

3.2.1 Energy Balance for Extruder-Feeder

If an energy balance is made around a typical extruder-feeder, the major energy inputs are the extruder-feeder screw drive and the barrel heaters. The energy outputs are the heat loss from the barrel to the cooling system, a negligible loss from the gear reducer and thrust bearing system, the hydraulic energy necessary to pump the plastic material against the die pressure, and the heat content of the material leaving the extruder-feeder.

A modern extruder-feeder operates nearly adiabatically. The thermal energy introduced by barrel heating is equivalent to the thermal energy lost by the barrel cooling plus other cooling losses. The energy necessary to pump against the die pressure is equal to about 5 to 10 percent of the total energy requirement. This analysis shows that almost all of the applied horsepower is used to heat the thermoplastic material from inlet to outlet temperature. This generalization invokes an encouraging potential for the extruder-feeder to act as low cost pump on highly concentrated finely ground cellulosic slurries to improve the economics of direct liquefaction of wood to yield synthetic fuels, especially when the remaining 80 percent of the input energy can be furnished mainly by steam injection which itself takes part in the thermochemical catalytic process as a reactant. The theoretical horsepower can be determined simply by knowing the throughput of the extruder-feeder, the heat capacity of the feed material and the temperature rise from the inlet to the outlet of the extruder-feeder.

A number of formulas have been developed for determining the drive power requirements for extruders (Glanvil 1971, McKelvey 1962, Middleman 1977, Tadmor and Klein 1970). One

method of calculating power requirements is by an energy balance of the extruder-feeder, that is as follows:

$$P_w + q = C_p Q \Delta T + \frac{Q \Delta P}{\rho} + H_L \qquad (3.1)$$

where:

P_w	=	mechanical power to screw
q	=	electric power to heaters
$C_p \Delta T$	=	enthalpy of the particular material
P	=	pressure rise in extruder-feeder
H_L	=	heat loss from radiation and conduction
ρ	=	melt density

A series of careful experimental runs were made on the Prodex extruder-feeder for energy balances. The total electrical power, the enthalpies of feedstocks and products from mass flows and temperatures, heat losses from a well-insulated barrel and heat losses to cooling water at the feed throat were all measured as carefully as possible. A computer program and data acquisition system assured lined-out extrusion conditions.

A total of 15 experimental runs for fresh LDPE, LDPE regrind and 50 wt.% wood flour/50 wt.% vacuum bottoms are summarized in Tables 3.1-3.3 and Figures 3.1-3.3. The major sources of errors were probably as follows:

1. The assumption of a ten percent loss in electrical motor power due to gearbox and varidrive motor.

2. A power factor of 0.65 was assumed at 40 rpm. In general, the power factor is a function of the load and varies from as low as 0.65 at 40 rpm to as high as 0.75. The value may be as high as unity at 80 rpm. This is equivalent to an error of approximately 1,800 Btu/hr in this case.

3. Errors due to calibration. Depending on the frequency of use and type of resin, the transducer calibrations tended to deviate with time. However, these deviations were minimal.

3.2.2 Power Requirement

The data above for energy balances were used to calculate power requirements for the extruder-feeder. In addition, the power consumption for various experimental runs with an insulated barrel were recorded, for example, as shown in Figures 3.4-3.6. As one might expect, the power is mainly a function of the output rate, as correlated here as a function of screw speed. The major causes for the scattering of data were different outlet temperatures, outlet pressures and feedstock viscosities.

Table 3.1. Steady State Energy Balances for Fresh LDPE.

Scres Speed rpm	Predicted Output Rate lb/hr	Measured Output Rate lb/hr	Flow Energy Btu/hr	Enthalpy Change Btu/hr	Cooling Water Loss Btu/hr	Gear Loss Btu/hr	Varidrive Loss Btu/hr	Barrel Heat Loss Btu/hr	Total Energy in Btu/hr	Total Energy Out Btu/hr	Percent Error
40.0	24.7	23.2	150.0	5,393	2,900	587.0	587.0	1,877	11,747	11,494	2.0
50.0	27.0	28.7	95.0	6,396	1,450	701.0	701.0	6,517	14,017	15,859	-13.0
60.0	31.1	31.1	91.0	7,169	4,350	730.0	730.0	2,216	14,608	15,287	-5.0
70.0	37.0	35.7	130.0	8,572	5,800	840.0	840.0	-774	16,795	15,408	8.0
80.0	39.3	41.7	73.0	9,666	4,350	931.0	931.0	1,379	18,611	17,330	7.0

Table 3.2. Steady State Energy Balance for LDPE Regrind.

Screw Speed rpm	Predicted Output Rate lb/hr	Measured Output Rate lb/hr	Flow Energy Btu/hr	Enthalpy Change Btu/hr	Cooling Water Loss Btu/hr	Gear Loss Btu/hr	Varidrive Loss Btu/hr	Barrel Heat Loss Btu/hr	Total Energy In Btu/hr	Total Energy Out Btu/hr	Percent Error
40.0	21.3	21.2	-33	4,236	2,400	752	752	6,826	15,040	14,933	1.0
50.0	27.3	29.1	-73	5,982	2,400	803	803	8,534	16,061	18,449	-15.0
60.0	36.3	35.7	-210	7,361	2,400	963	963	5,354	19,249	16,830	13.0
70.0	41.1	39.7	-205	8,364	3,600	1,045	1,045	9,866	20,904	23,716	-13.0
80.0	44.7	47.6	-152	10,181	3,600	1,173	1,173	5,899	23,461	21,874	7.0

Table 3.3. Steady State Energy Balance for 50 wt. % Wood Flour/50 wt. % Vacuum Bottoms.

Screw Speed rpm	Measured Output Rate lb/hr	Flow Energy Btu/hr	Enthalpy Change Btu/hr	Cooling Water Loss Btu/hr	Gear Loss Btu/hr	Varidrive Loss Btu/hr	Barrel Heat Loss Btu/hr	Total Energy In Btu/hr	Total Energy Out Btu/hr	Percent Error
40.0	31.1	244.0	4,213	1,547	602	602	7,554	12,048	14,762	-23.0
50.0	33.1	4.0	4,037	2,011	579	579	3,584	11,577	10,794	7.0
60.0	37.7	37.0	4,971	464	722	722	5,565	14,433	12,480	14.0
70.0	38.8	-31.0	5,203	2,011	684	684	4,099	13,676	12,650	8.0
80.0	44.3	-25.0	6,060	1,083	770	770	8,907	15,399	17,565	-14.0

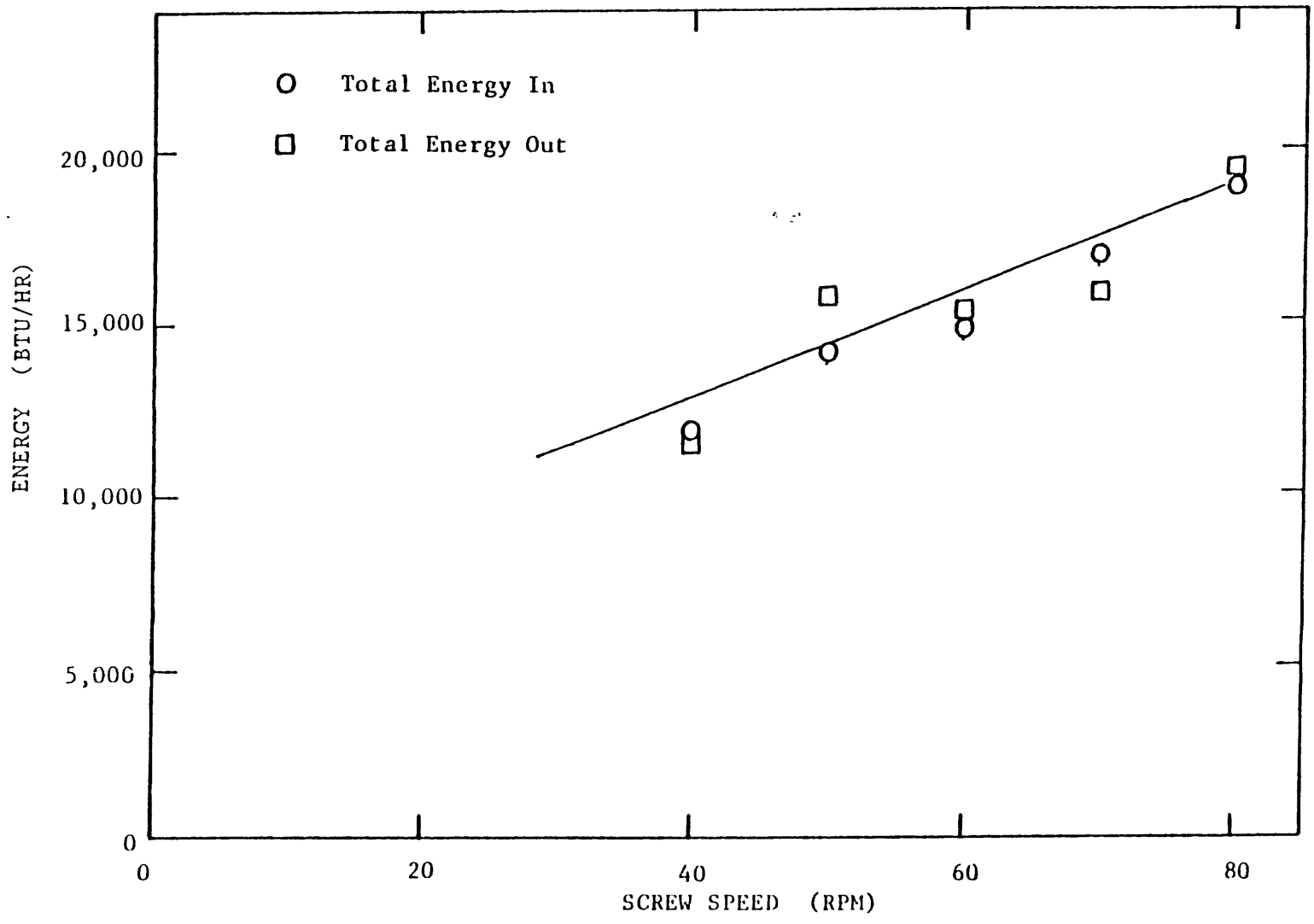

Figure 3.1. Summary of Energy Balances for Fresh LDPE.

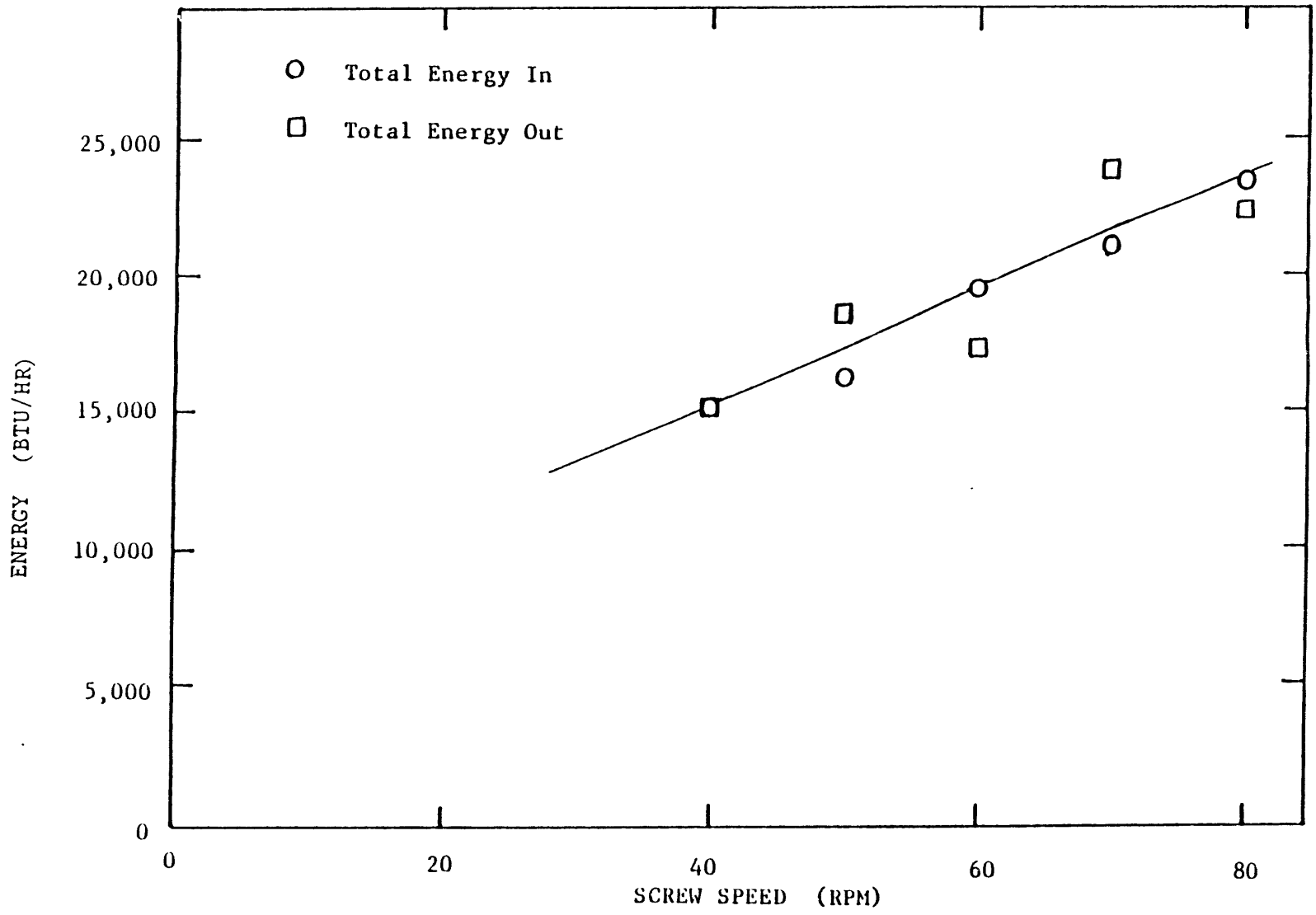

Figure 3.2. Summary of Energy Balances for LDPE Regrind.

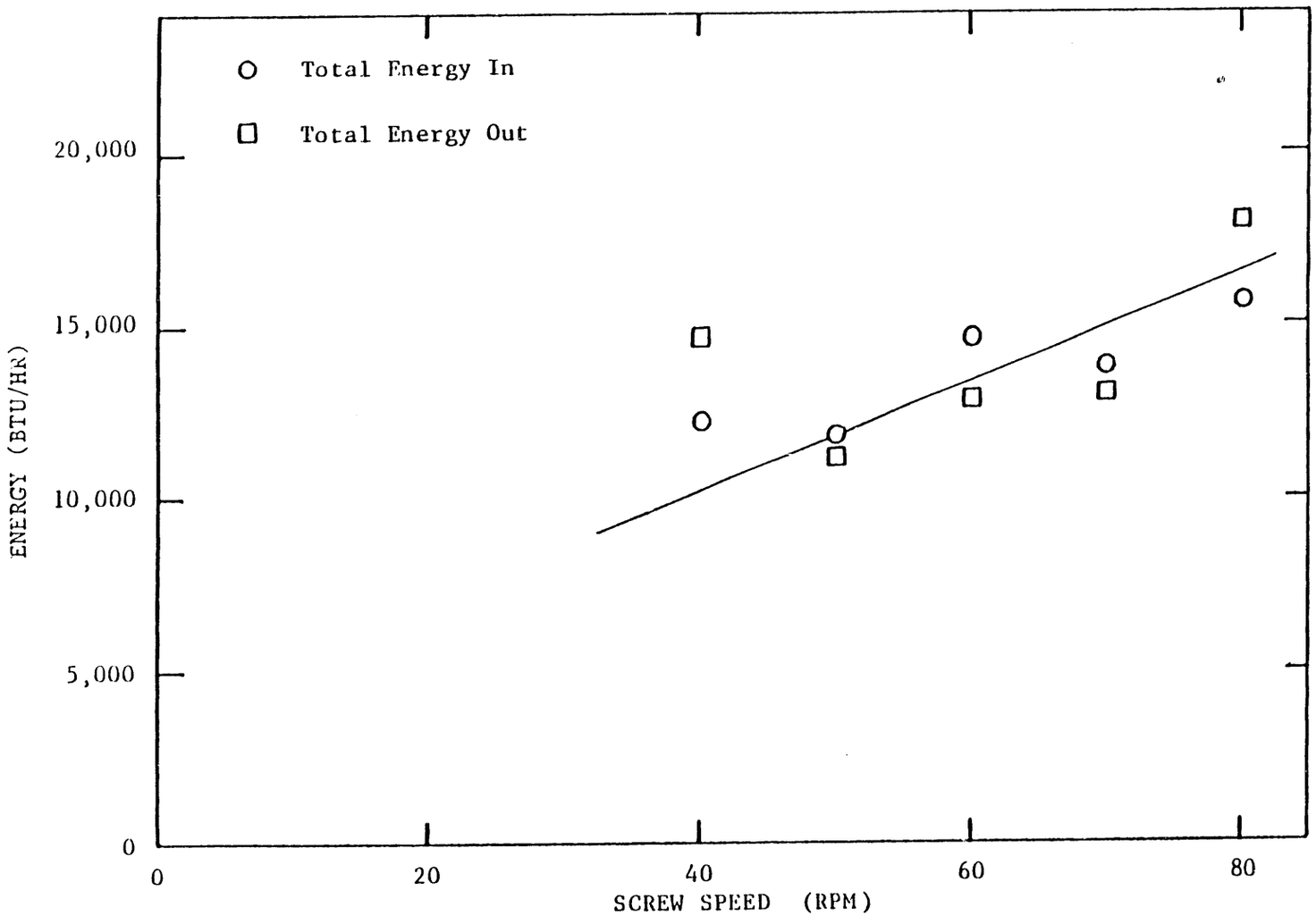

Figure 3.3. Summary of Energy Balances for 50 wt. % Sawdust/50 wt. % Vacuum Bottoms Regrind.

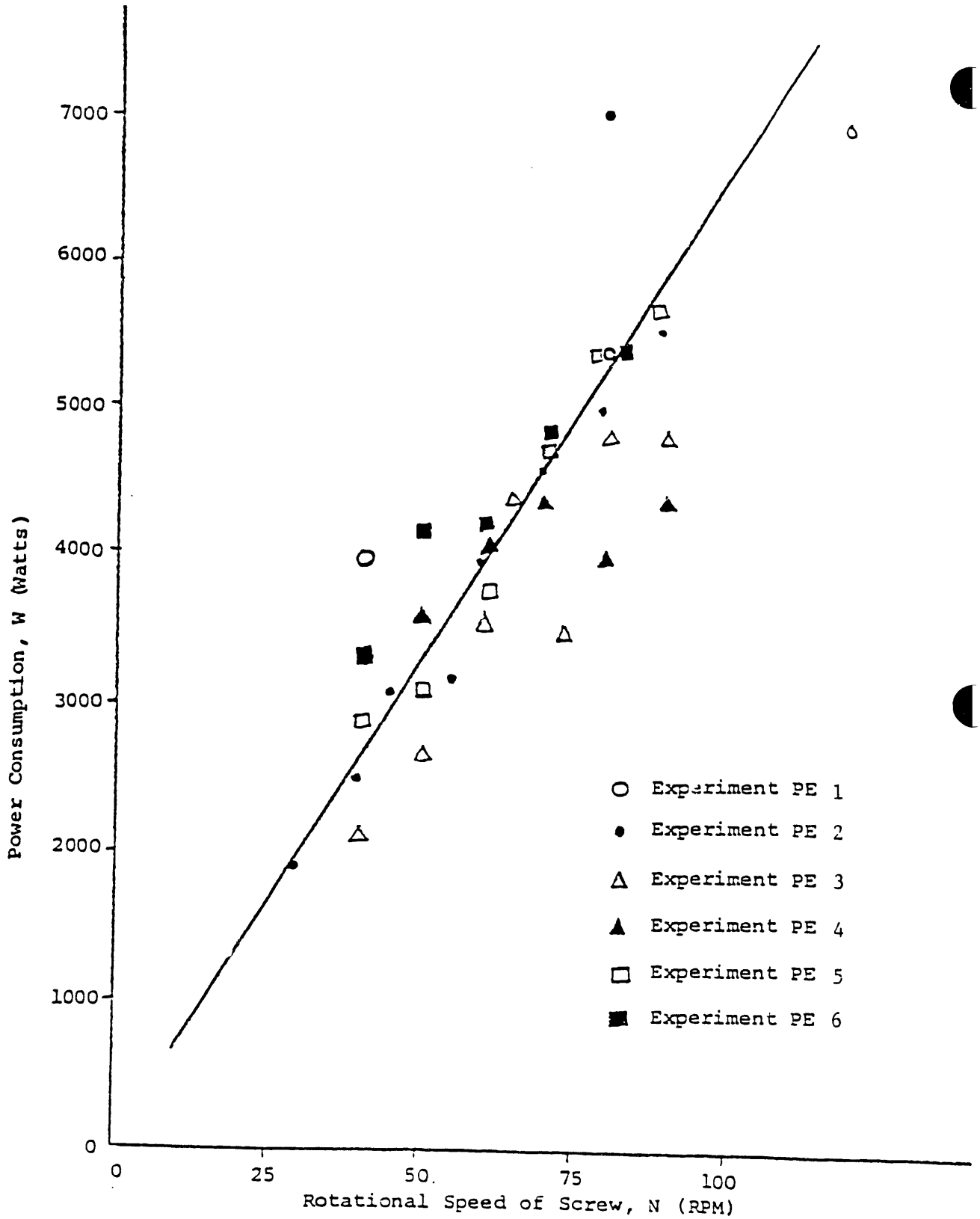

Figure 3.4. Power Input as a Function of Screw Rotational Speed for Polyethylene and Prodex-Type Extruder-Feeder.

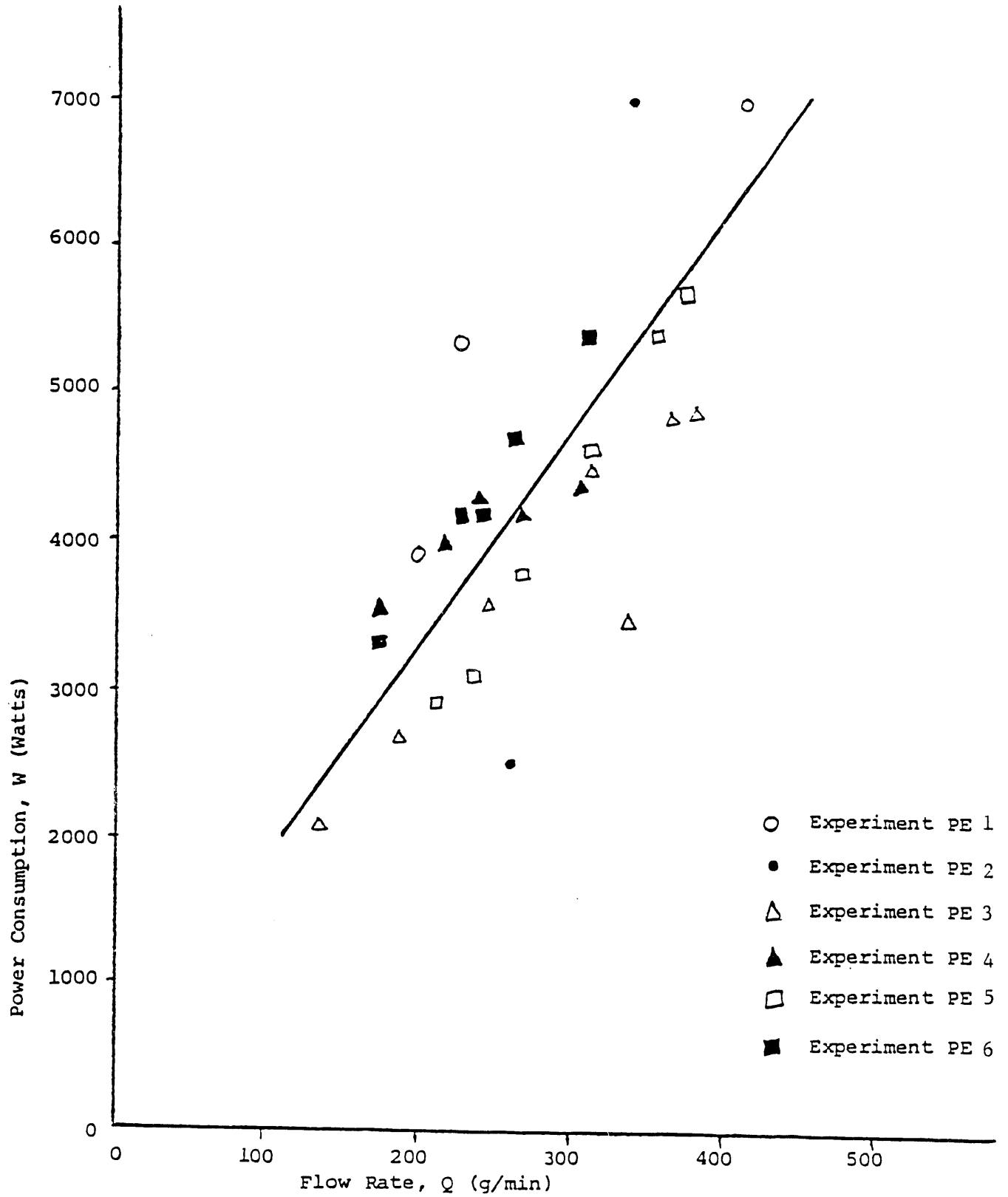

Figure 3.5. Power Input as a Function of Flow Rate for Polyethylene and Prodex-Type Extruder-Feeder.

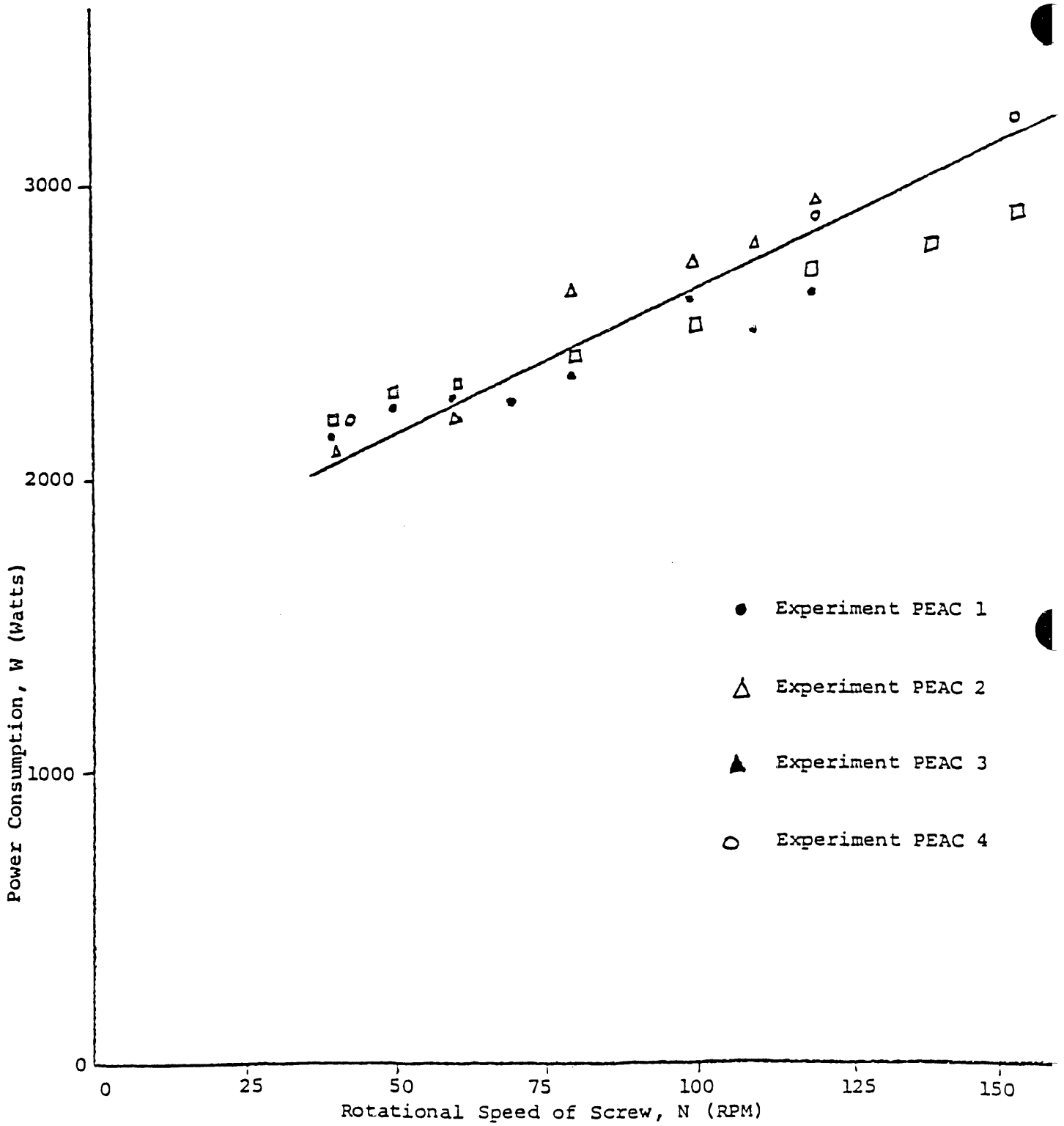

Figure 3.6. Power Input as a Function of Screw Rotational Speed for PE/AC6-Wax and for Prodex-Type Extruder-Feeder.

The feedstock viscosities have a major effect upon viscous dissipation, wherein a viscous mix generates heat by friction in the extruder-feeder. Fundamental data for this affect upon power requirements were determined at the University of Lowell by (Schott 1981, Yang 1981). A Brabender Plasti-Corder PL-V 150 with a torque mixing head was used for the experimental work.

The feedstocks were prepared by fluxing mixtures of LDPE and PE-AC6 into the desired polyblends, using a two-roll mill to assure a uniform blend:

LDPE, wt. %	*PE-AC6, wt. %*
100	0
75	25
50	50
25	75
0	100

The material from the two-roll mill was then ground on the Wiley Mill, and then used for the power test runs as such, or mixed with wood flour for 50, 60, and 70 wt. % wood flour slurries for making power tests.

Torque rheometer readings were made continuously at different mixer speeds with the heat transfer liquid in the mixer jacket held at 13°C. A given material was always fluxed for 18 minutes after the fusion point. The sample was placed in the mixer by using the quick loading chute, and holding it in the mixer for three minutes heat-up time. The mixer was then started and the rotor was set at 120 rpm. Skill is needed to take data under isothermal conditions due to viscous heat dissipation. The technique used was to first set the jacket temperature at some higher temperature, then stop the mixer to let the mix fall 5-10°C below the jacket temperature. The mixer was started and as the sample heated, the torque was noted at the time the sample reaches the jacket temperature. The torque is recorded continuously on a strip chart recorder as a function of time. Since torque (m•kg) is work, then the integrated area under the torque trace is determined. This is used in Equation 3.2 as the T(t)dt term, as given later.

The total work consumed in mixing 40-70 weight percent Albany plant wood flour in PE-AC-6 from a total of two minutes to a total of 20 minutes is given in Figure 3.7. The horsepower, expressed as joules per minute x 10^{-4}, can be obtained by taking the slope over the 12-20 minute range, giving the following results:

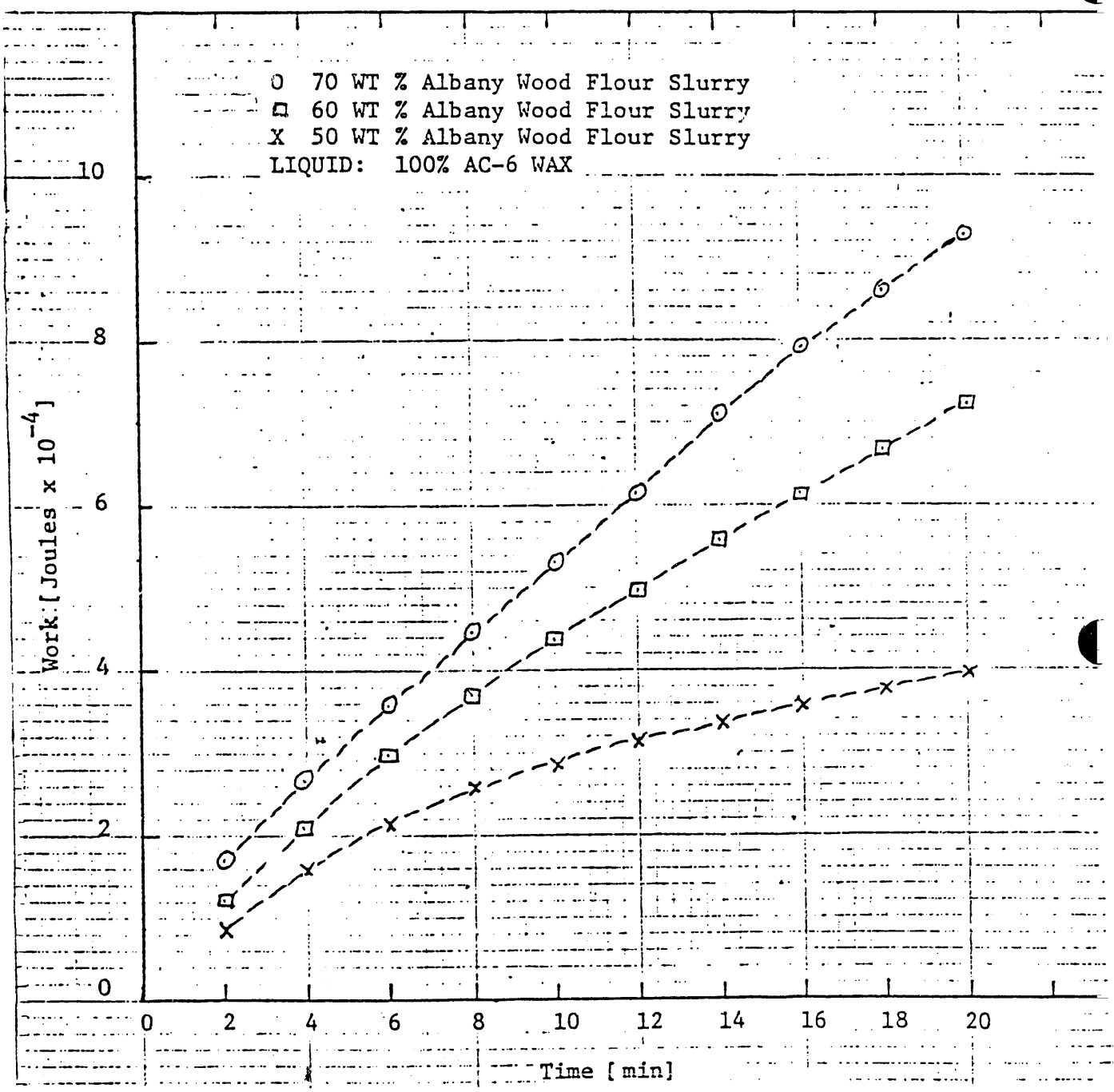

Figure 3.7. Mixing Work for Albany Wood Flour/AC6 Slurries.

Slurry Composition	Joules/Min/54 g • x 10^{-4}
70 wt. % Wood Flour	0.40
60 wt. % Wood Flour	0.28
50 wt. % Wood Flour	0.03

For wood flour slurries in 50 LDPE/50 AC-6 liquid, the total work is shown in Figure 3.8. The corresponding horsepower requirements are given below.

Slurry Composition	Joules/Min/54 g • x 10^{-4}
70 wt. % Wood Flour	0.80
60 wt. % Wood Flour	0.65
50 wt. % Wood Flour	0.58

For wood flour slurries in 75 LDPE/25 AC-6 liquid, the total work is shown in Figure 3.9. The corresponding horsepower requirements are given below.

Slurry Composition	Joules/Min/54 g • x 10^{-4}
70 wt. % Wood Flour	1.05
60 wt. % Wood Flour	0.75

The power consumption in this particular unit was calculated from the calibrated equation:

$$W = 2\pi S_R(9.8) \int_{t_1}^{t_2} T(t)\, dt \qquad (3.2)$$

where:

W = total work, joule
S_R = Rotor rpm, 1/min.
T(t) = Torque, m•kg
t = Time, min.

The work required over a wide range of carrier fluid viscosities for wood flour concentrates from 50 to 70 wt. % wood flour was determined experimentally, and is recorded in Table 3.4.

Table 3.4. Power Consumption of Wood Flour Slurries			
time (min.)	(a) Resin Only--No Wood Flour		
	Cumulative Power Consumption (Joules/Kg), x 10^{-6}		
	75% AC6 PE 25% LDPE	50% AC6 PE 50% LDPE	25% AC6 PE 75% LDPE
2	0.51	1.17	3.11
4	0.74	2.26	5.65
6	0.91	3.25	7.96
8	1.04	4.20	1.02
10	1.16	5.10	1.23
12	1.27	5.95	1.44
14	1.37	6.67	1.64
16	--	7.57	1.84
18	--	8.34	2.04
20	--	9.10	2.24
(b) Resin Carrier Fluid: 100% LDPE			
Time	**Cumulative Power Consumption (Joules/Kg), x 10^{-6}**		
	70 wt. % W.F.	60 wt. % W.F.	50 wt. % W.F.
2	0.74	0.90	0.99
4	1.86	2.35	2.37
8	2.36	3.03	3.00
10	2.84	3.66	3.60
12	3.29	4.30	4.20
14	3.74	4.90	4.80
16	4.17	5.46	5.30
17	-.-	5.75	-.-
18	4.59	-.-	5.90
20	-.-	-.-	3.82

Table 3.4 (Continued)

(c) Resin Carrier Fluid: 75 wt. % LDPE/25 wt. % AC6 PE

Time	Cumulative Power Consumption (Joules/Kg), x 10^{-6}		
	70 wt. % WF	60 wt. % WF	50 wt. % WF
2	0.59	0.67	0.61
4	1.15	1.17	1.09
6	1.63	1.60	1.50
8	2.06	2.00	1.87
10	2.46	2.37	2.22
12	2.85	2.73	2.56
14	3.22	-.-	2.88
16	-.-	0.0	3.20
18	-.-	0.0	3.50
20	-.-	-.-	3.82

(d) Resin Carrier Fluid: 50 wt. % LDPE/50 wt. % AC6 PE

Time	**Cumulative Power Consumption (Joules/Kg), x 10^{-6}**		
	70 wt. % WF	60 wt. % WF	50 wt. % WF
2	0.46	0.49	0.39
4	0.89	0.86	0.69
6	1.27	1.18	0.95
8	1.66	1.46	1.20
10	2.01	1.72	1.44
12	2.33	1.97	1.66
14	2.63	2.21	1.88
15	-.-	-.-	1.98
16	2.91	2.44	-.-
18	3.18	-.-	-.-

Table 3.4 (Continued)

(e) Resin Carrier Fluid: 25 wt. % LDPE/75 wt. % AC6 PE

Time	Cumulative Power Consumption (Joules/Kg), x 10^{-6}		
	70 wt. % WF	60 wt. % WF	50 wt. % WF
2	0.43	0.49	0.24
4	0.74	0.83	0.40
6	0.99	1.08	0.54
8	1.24	1.28	0.66
10	1.47	1.46	0.76
12	1.69	1.63	0.86
14	1.92	1.79	0.96
16	2.13	1.94	1.05
18	2.34	2.09	1.14

(f) Resin Carrier Fluid: 100 wt. % AC6 PE

Time	Cumulative Power Consumption (Joules/Kg), x 10^{-6}		
	70 wt. % WF	60 wt. % WF	40 wt. % WF
2	0.30	0.21	0.15
4	0.49	0.38	0.29
6	0.65	0.54	0.39
8	0.82	0.68	0.47
10	0.97	0.80	0.53
12	1.13	0.92	0.58
14	1.31	1.03	0.62
16	1.46	1.13	0.66
18	1.59	1.24	0.70
20	1.71	1.34	0.73

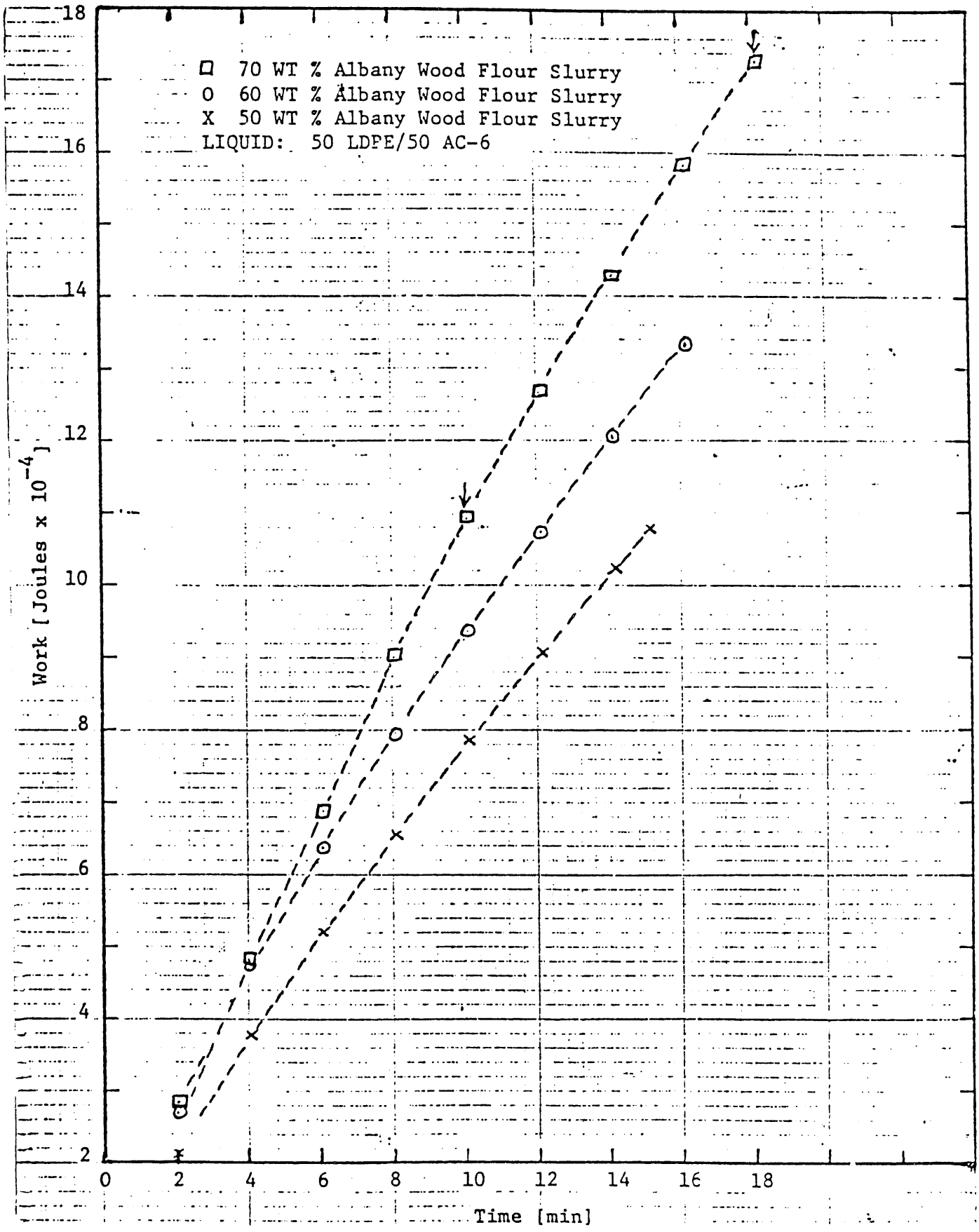

Figure 3.8. Mixing Work for Albany Wood Flour in 50 wt. % LDPE/50 wt. % AC6 Liquid.

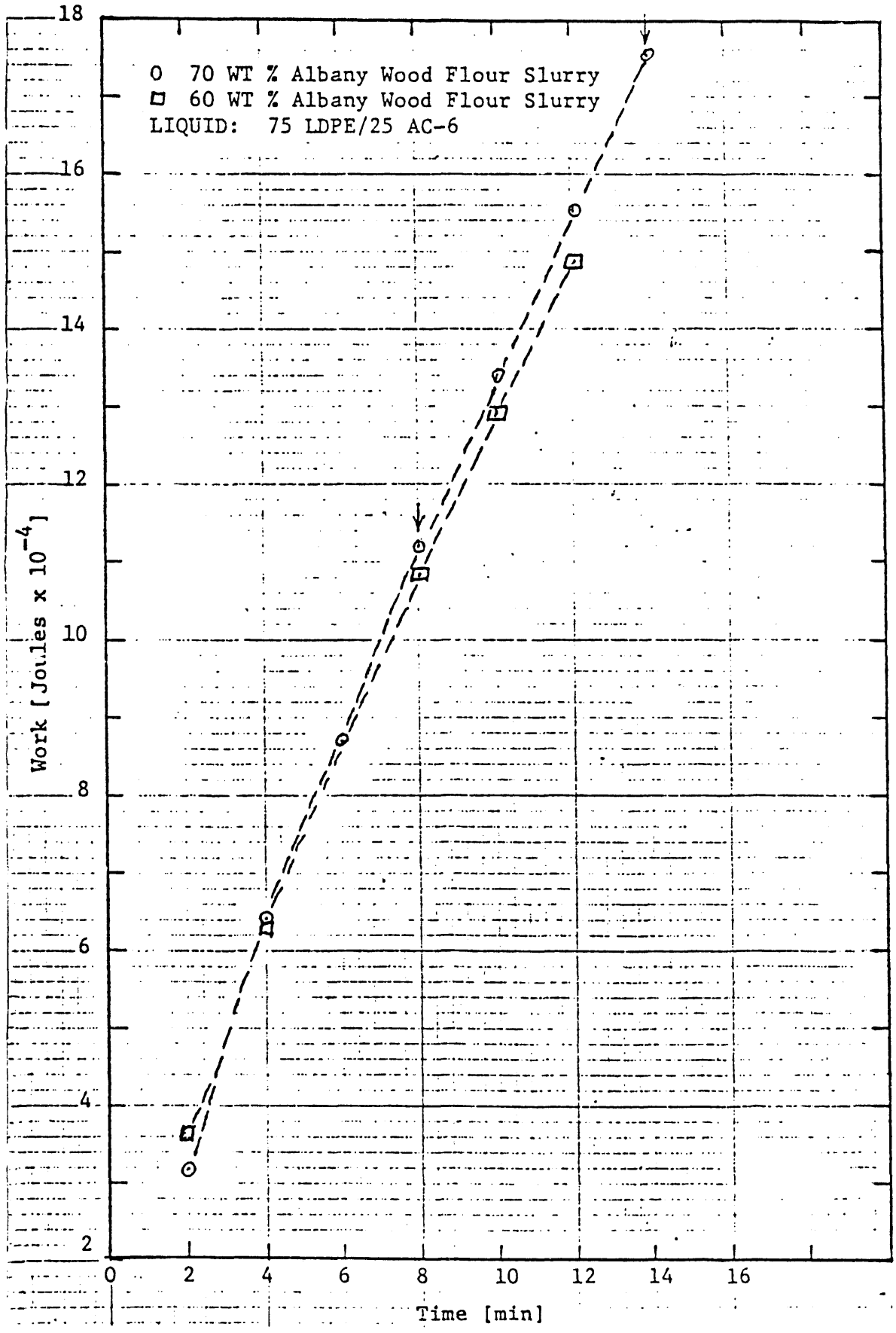

Figure 3.9. Mixing Work for Albany Wood Flour in 75 wt. % LDPE/25 wt. % AC6 Liquid.

3.2.3 Viscous Dissipation in the Extruder-Feeder

The conduction-convection equation has the following vector form:

$$\rho\ C_p U \cdot \nabla\ T = k\ \nabla^2 T + \vec{\phi}_v \tag{3.3}$$

where:

k	=	Thermal conductivity of the melt
ρ	=	Density of the melt
C_p	=	Heat capacity
T	=	Temperature
U	=	Velocity vector
$\vec{\phi}_v$	=	Volumetric rate of conversion of mechanical energy into heat

For an incompressible, Newtonian fluid, the viscous source is given by Bird, Stewart and Lightfoot (1960) as:

$$\vec{\phi}_v = -Txz\ \frac{dv_z}{dx} = \mu\ \frac{dv_z^2}{dx} \tag{3.4}$$

For flow between concentric cylinders, there will be a linear velocity profile in the slit:

$$v_z = \left[\frac{x}{d}\right] V \tag{3.5}$$

where:

d	=	Width of gap
x	=	Coordinate in gap
V	=	Maximum velocity of outer cylinder (inner cylinder is stationary)

A solution for the temperature profile in the slit is given as:

$$\frac{T-T_o}{T_d-T_o} = \left[\frac{x}{d}\right] + \frac{1}{2}\ Br \left[\frac{x}{d}\right]\left[1 - \frac{x}{d}\right] \tag{3.6}$$

Here $Br = \dfrac{\mu V^2}{k(T_d-T_o)}$ = *Brinkman Number*

The Brinkman Number is a measure of the extent to which viscous heating is important relative to an impressed temperature difference (T_d - T_o). For this simple case, it is found that if Br > 2, then there is a maximum in the temperature profile at an intermediate position

between the two walls. For non-Newtonian fluids the viscous heating problem is further complicated. Middleman (1977) reports the solution for viscous heating in an extruder with a power law fluid in which a modified Brinkman Number is generated as follows:

$$\beta = b\, T_b\, Br = \frac{bK_b U_z^{n+1}}{k\, B^{n-1}} \tag{3.7}$$

where:

β	=	Modified Brinkman Number
b	=	Temperature dependence of viscosity
K_b	=	Viscosity at temperature, T_b
T_b	=	Temperature
U_z	=	Velocity
B	=	Channel depth
n	=	Flow index of power law fluid
k	=	Thermal conductivity of the fluid

Two case studies are presented which compare the relative viscous dissipation effects in LDPE and in a 40% wood flour/60% (25% LDPE, 75% AC6 PE). The numerical calculation for these two cases are given in Appendix B. The values of the modified Brinkman Number were 0.453 and 0.031 for the LDPE and the WF and mixtures of LDPE and AC6 PE, respectively.

It is to be noted that the modified Brinkman Number is 10 times larger for the polyethylene but that both are less than 1.0. Middleman (1977) shows that β has a very strong effect on the maximum pressure that may be developed in the extruder-feeder. Small values of β give the highest pressure. Also, at a fixed pressure, the heat generation has a tendency to increase output at a low pressure but to decrease it at a high pressure (see Figures 3.10 and 3.11).

In the Figures of Middleman's book the following nomenclature is used:

$$\pi'_Q = \pi_Q \cos\theta = \frac{Q}{U_z^{BW}} \cos\theta = \textit{dimensionless output}$$

$$\pi'_p = \pi_p (\cos\theta)^n = \frac{\Delta P_B^2}{\mu U_z Z} (\cos\theta)^n = \textit{dimensionless pressure drop}$$

between the two walls. For non-Newtonian fluids the viscous heating problem is further complicated. Middleman (1977) reports the solution for viscous heating in an extruder with a power law fluid in which a modified Brinkman Number is generated as follows:

$$\beta = b\, T_b\, Br = \frac{bK_b U_z^{n+1}}{k\, B^{n-1}} \tag{3.7}$$

where:

β	=	Modified Brinkman Number
b	=	Temperature dependence of viscosity
K_b	=	Viscosity at temperature, T_b
T_b	=	Temperature
U_z	=	Velocity
B	=	Channel depth
n	=	Flow index of power law fluid
k	=	Thermal conductivity of the fluid

Two case studies are presented which compare the relative viscous dissipation effects in LDPE and in a 40% wood flour/60% (25% LDPE, 75% AC6 PE). The numerical calculation for these two cases are given in Appendix B. The values of the modified Brinkman Number were 0.453 and 0.031 for the LDPE and the WF and mixtures of LDPE and AC6 PE, respectively.

It is to be noted that the modified Brinkman Number is 10 times larger for the polyethylene but that both are less than 1.0. Middleman (1977) shows that β has a very strong effect on the maximum pressure that may be developed in the extruder-feeder. Small values of β give the highest pressure. Also, at a fixed pressure, the heat generation has a tendency to increase output at a low pressure but to decrease it at a high pressure (see Figures 3.10 and 3.11).

In the Figures of Middleman's book the following nomenclature is used:

$$\pi'_Q = \pi_Q \cos\theta = \frac{Q}{U_z^{BW}} \cos\theta = \textit{dimensionless output}$$

$$\pi'_p = \pi_p (\cos\theta)^n = \frac{\Delta P_B^2}{\mu U_z Z} (\cos\theta)^n = \textit{dimensionless pressure drop}$$

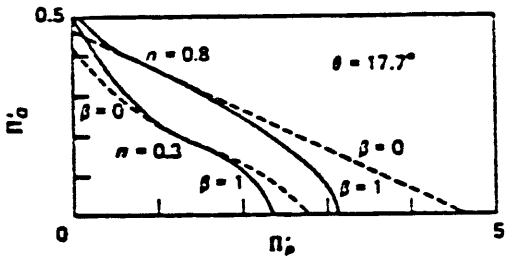

Figure 3.10. Nonisothermal-nonadiabatic Screw Characteristics for Power Law fluids for the Case $\beta = 1$ (Middleman 1977)

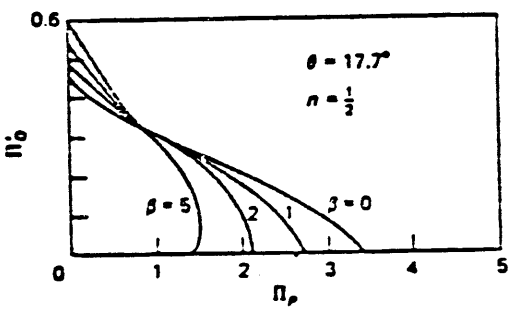

Figure 3.11. Effect of β on Screw Characteristics for n = 1/2 (Middelman 1977)

The data reported by White et al. (1981) showed viscous dissipation of both polyethylene and the 40 wt. % wood flour 60 wt. %/(25 wt. % LDPE/75 wt. % AC6 PE) mixture. Figures 3.12 and 3.13 show these data again. It is noted that the LDPE gave a significantly higher rate of viscous dissipation as predicted by the Brinkman Numbers. This give experimental proof that the Brinkman Number predictions are correct.

Corresponding to the data of Figures 3.12 and 3.13 one can also show the work expended by the mixer motor as the viscous dissipation occurs. The work is highest for the 75 wt. % LDPE/25 wt. % AC6 and decreases as the AC6 PE content goes up. No value for the pure LDPE was measured. Dissipation of the wood flour slurry in which a 25 wt. % LDPE 75 wt. % AC Wax has been used as the modeling fluid. The values are an order of magnitude lower than the 75 wt. % LDPE/25 wt. % AC6 Wax mixture. The Brinkman Numbers were also an order of magnitude apart and predicted this.

The latest data carried out at the University of Lowell (Schott 1981) show the same measurements for wood flour/vacuum bottoms slurries. Since power is defined as work/time one can see that the derivative (slope) of the graphs gives the power consumption. The power consumption calculated from these slopes is shown in Table 3.5.

The above slopes were evaluated in the steady state region. This is the region that would be encountered in the metering section of the screw. Instead, the non-linear region models the feed and transition section. It should be noted that the values for the 50 wt. % wood flour, 50 wt. % (25 wt. % LDPE, 75 wt % AC6 PE) is close to the 40 wt. % and 50 wt. % wood flour/vacuum bottom slurries. This indicates that the LDPE/AC6 PE combination was a good choice as a modeling fluid.

3.2.4. Surface Friction of Cellulosics by Screw Simulator

As discussed in detail under the fundamentals of the extruder-feeder in Part 1, the surface friction on the screw and the barrel are critical factors (Mount and Chung 1978, Chung 1977). The characteristics of the feedstock and temperature differentials between the barrel surface and the screw surface are the main factors that can be controlled.

Arrangements were made with Dr. C.I. Chung (1982), Materials Engineering Department, Rensselaer Polytechnic Institute, Troy, New York, to determine the surface friction characteristics of two stiff cellulosic slurries in his laboratory. He has developed a unique *"screw simulation"* under National Science Foundation funding for use in evaluating solids conveying in a plasticating extruder, and is believed to have the only unit available. His research has contributed to an understanding of extruders in the polymers field, and his technique was utilized to contribute to an understanding of concentrated cellulosic slurries.

A schematic of Dr. Chung's *"Screw Simulator"* is shown in Figure 3.14. He has now completed work upon two cellulosic slurries of quite different composition and physical properties, as follows:

Table 3.5. Power Consumption for Resin Carrier Fluids and Wood Flour Slurries		
Material Composition, wt. %	*Slope (Joule/Kg/g-min)*	*Power (H.P./Kg)*
25% LDPE/75% AC6	5.67×10^4	1.27
50% LDPE/50% AC6	4.08×10^5	9.12
75% LDPE/25% AC6	1.02×10^6	22.80
50% WF/50% (25% LDPE/75% AC6)	4.80×10^4	1.07
60% WF/40% (25% LDPE/75% AC6)	8.20×10^4	1.83
70% WF/30% (25% LDPE/75% AC6)	11.05×10^4	2.46
60% WF/40% Fresh Vacuum Bottoms	1.14×10^5	2.55
50% WF/50% Fresh Vacuum Bottoms	7.44×10^4	1.66
40% WF/60% Fresh Vacuum Bottoms	7.05×10^4	1.56

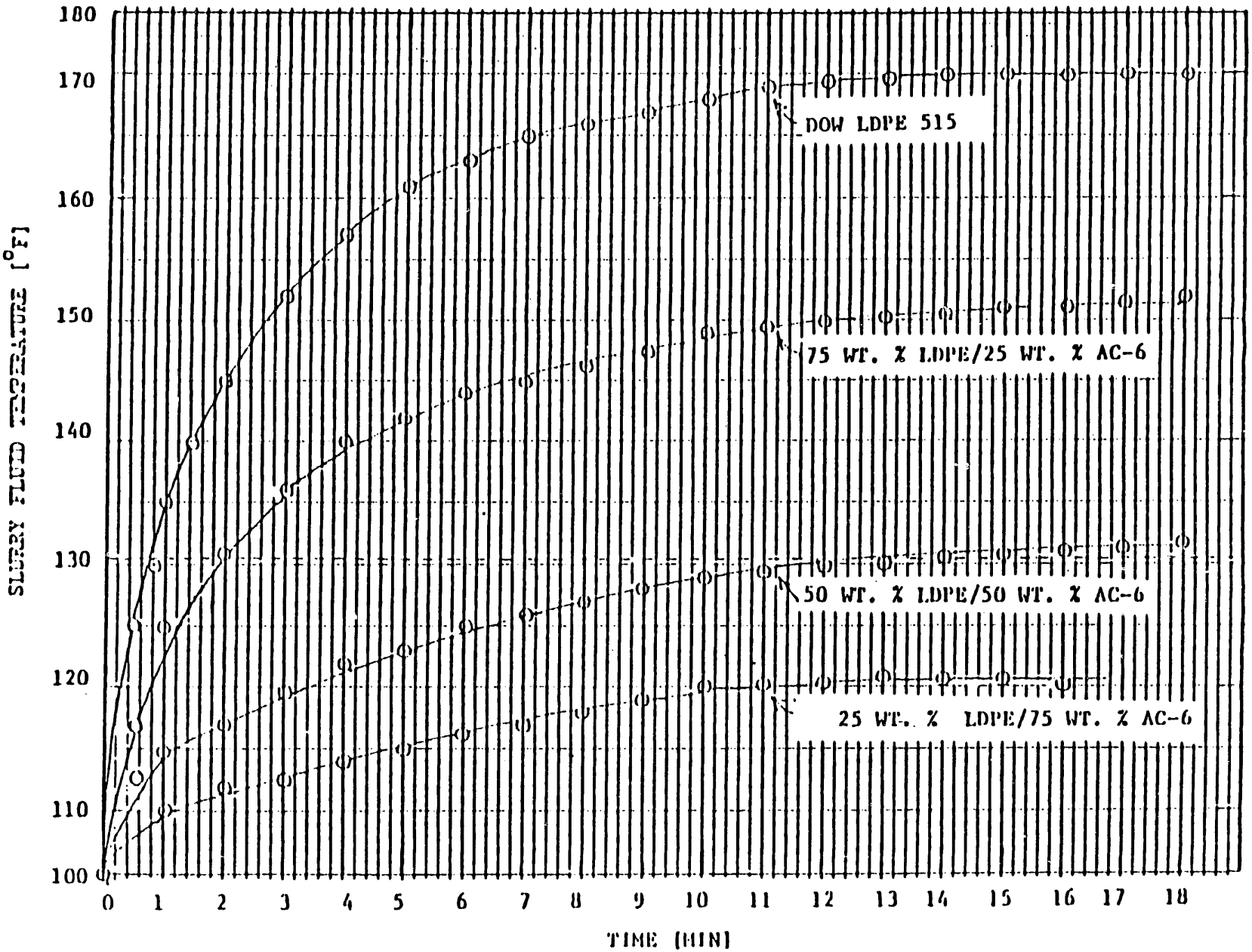

Figure 3.12. Viscous Dissipation of Slurry Fluids in Brabender Plati-Corder Mixer.

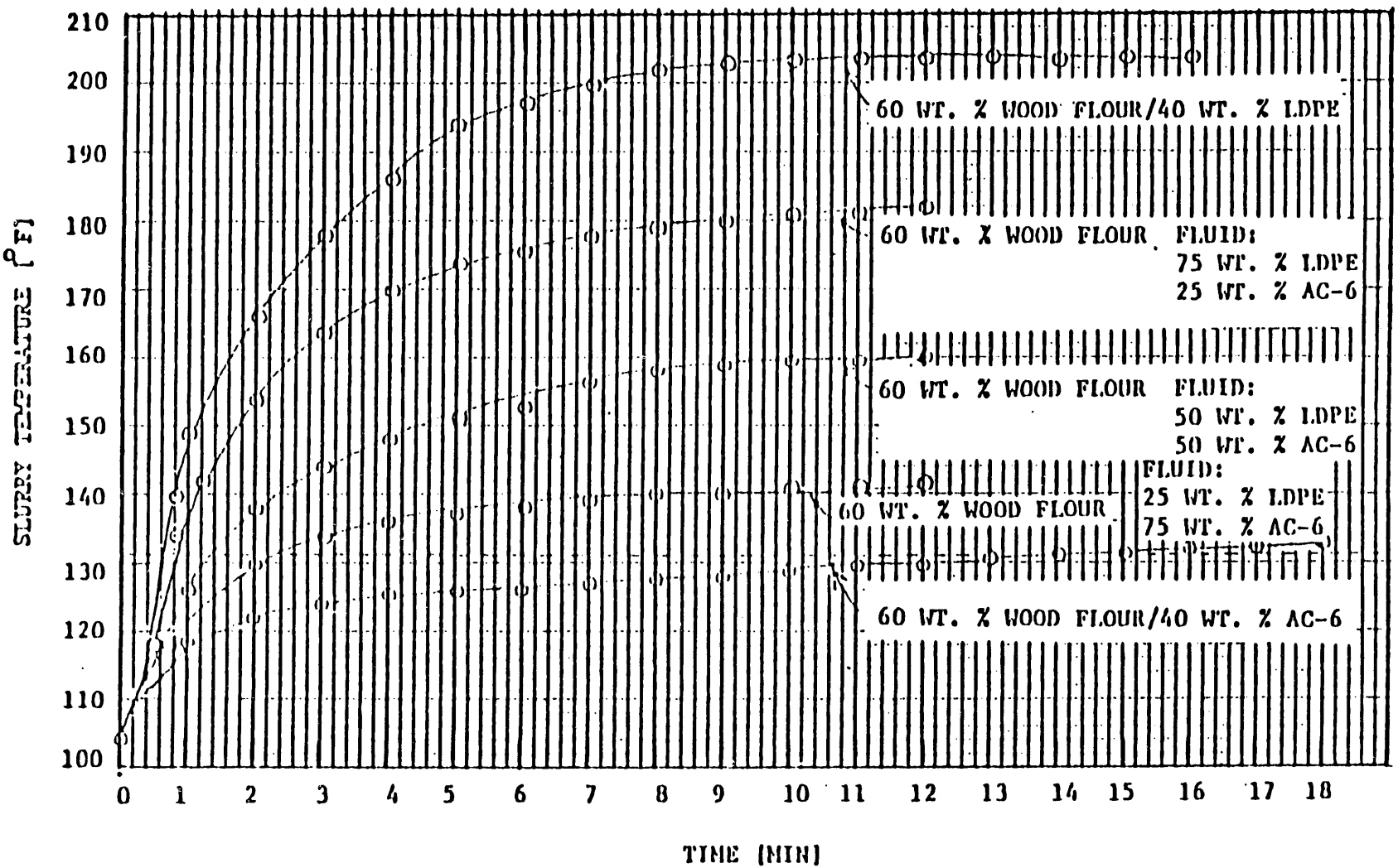

Figure 3.13. Viscous Dissipation of Wood Flour Slurries in Brabender Plasti-Corder Mixer.

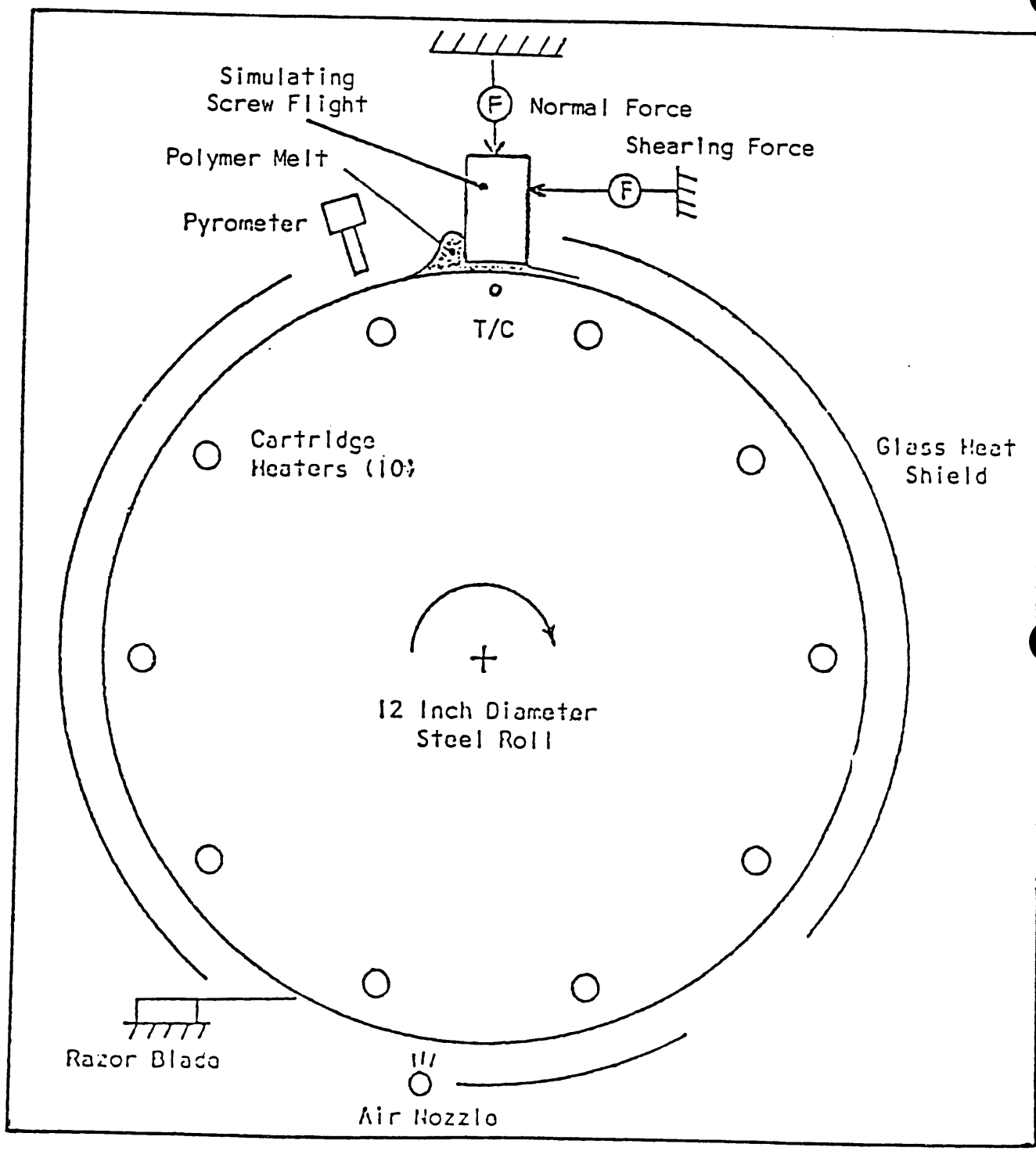

Figure 3.14. Schematic of the Chung Screw Simulator.

1. Pellet -- Consisting of 80 weight percent sawdust with 20 weight percent Allied Chemical AC6 PE powder, blended as discrete solids and pelletized in a California Pellet Mill.

2. Chip -- Consisting of 50 weight percent Albany sawdust, 25 weight percent AC6 PE and 25 weight percent low-density polyethylene, masterbatched in an extruder and made into a *"chip"* by grinding in a plastics regrind machine.

Some significant preliminary conclusions can be drawn from the data on these test samples. The friction of coefficient can be lowered by a factor of three by heating the *"screw roll"* to 200°F, compared with operating at room temperature, as shown in Figure 3.15. This is significant for the performance of an extruder-feeder, whereby the frictional forces on either/both the barrel and screw can be decreased/increased by appropriate heating or cooling. This provides considerable flexibility in the operation of a given extruder-feeder, and also in the design of units intended for cellulosic slurries. It is also encouraging that pressure does not affect significantly the friction coefficient of a given sawdust slurry, as shown in Figure 3.16.

3.3 SCALE-UP CALCULATIONS FOR EXTRUDER-FEEDER

The correlations of extruder-feeder operating data in Part 1 was directed toward (a) understanding the variables of the operating conditions of a given extruder-feeder, and (b) how to design and scale up to a larger unit. Sufficient operating experience was achieved so that meaningful correlations and modeling of the above objectives could be started in mid-1981.

3.3.1. Scale-up Models for Extruder-Feeder

There are subtle but important factors that require a modified extruder-feeder model for cellulosic slurries, different from those used in the plastics field. First, the conveying of slurry solids is more analogous to the *"feed"* and *"metering"* sections of a plasticating extruder, than that in the *"melting section"* of such an extruder. Second, the apparent viscosity term is different due to the friction and interference among the slurry solid particles. Third, the screw design and speed of rotation can be different due to a different mechanism and quantity of internal heat dissipation (Squires, 1962). Fourth, a wider range of extruder operating conditions may be possible based on heating the screw and cooling the barrel wall and on the large effect of temperature upon friction coefficients. Fifth, a shorter extruder-feeder running at higher speeds for higher throughputs appears feasible. Sixth, it may be necessary to introduce a friction term into the model, independent of the apparent viscosity term, in order to handle so-called internal friction between slurry particles (Pearson, 1966, Harmann and Harper, 1974 and 1975).

Despite these subtle differences between plasticating and biomass slurry feeding extruders, it would be unreasonable not to utilize as much as possible the wide experience of extruder modeling that exists in the plastics field. Therefore, work using plasticating extruder models was begun in June, 1980, and a brief summary of the more important approaches is given below.

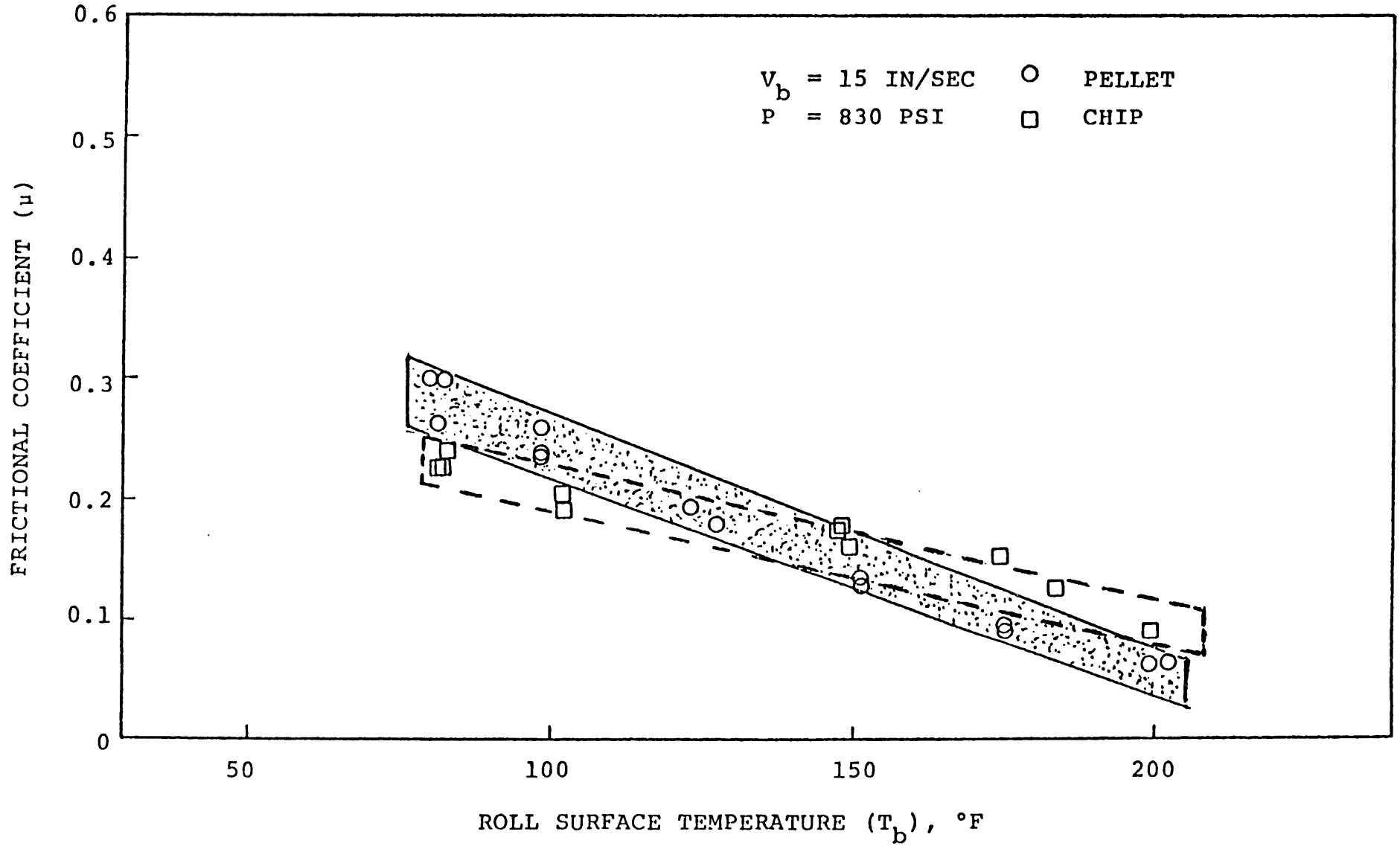

Figure 3.15. Effect of Screw Roll Temperature upon Albany Sawdust Slurry Coefficient of Friction.

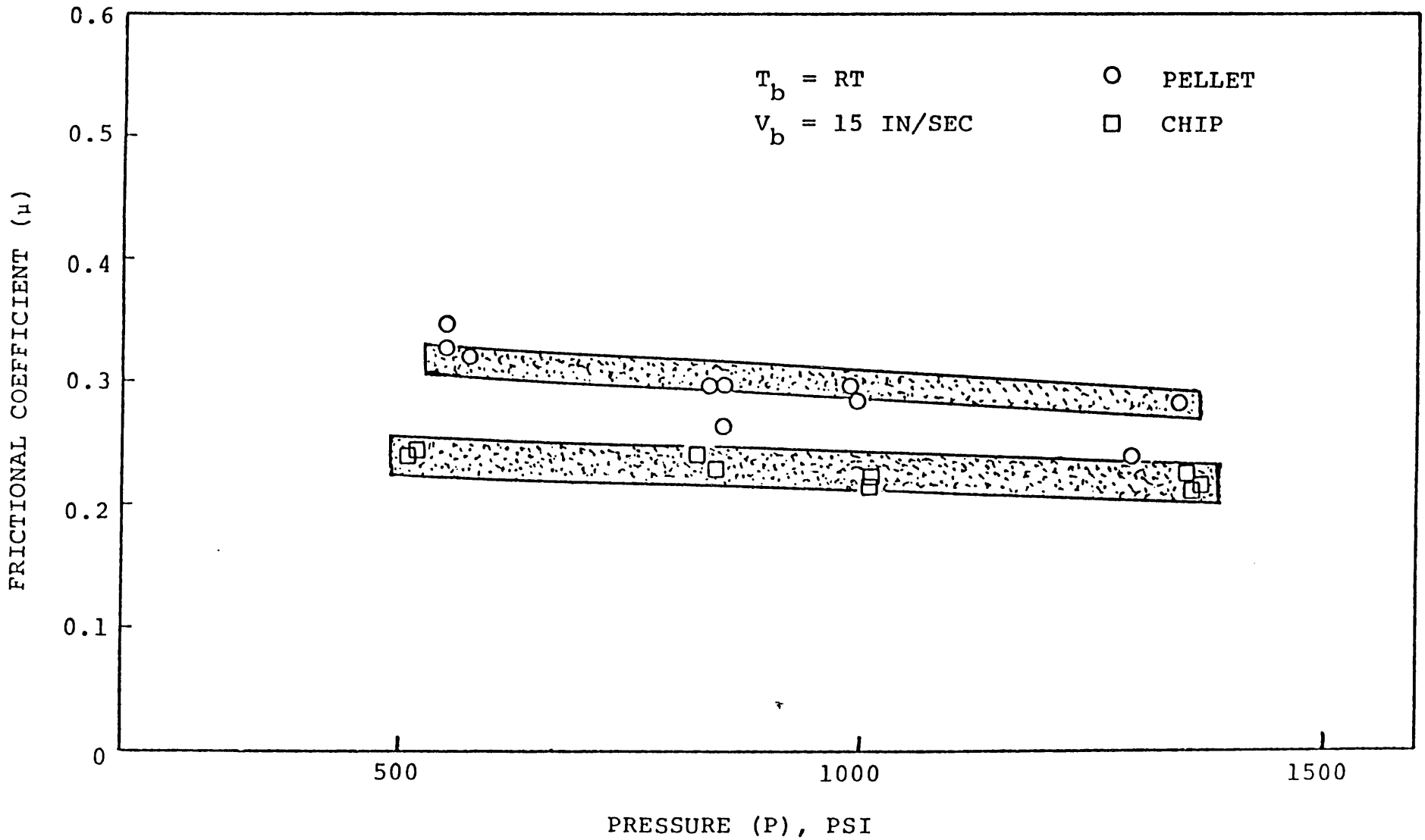

Figure 3.16. Effect of Pressure upon Albany Sawdust Slurry Coefficient of Friction.

1. Tadmor & Klein Model (1970)

$$Q = \alpha_{EX} N F_d \left[1 - \frac{\delta_f}{H}\right] + \frac{\beta_{EX}}{\mu} F_p \left(P_1 - P_2 L\right)(1 + f_L) \tag{3.8}$$

Where:

N = Frequency of screw rotation, revolution/sec.
δ_f = Flight clearance, cm.
H = Channel depth, cm.
μ = viscosity, dyne x sec/cm^2
P_1-P_2 = Pressure drop, dyne/cm^2
L = Screw lead, cm.

and the values of α_{EX}, β_{EX}, F_d, F_p and f_L are as follows:

$$\alpha_{EX} = \frac{\pi^2}{2} D_b^2 H \left[\frac{Cos\ \bar{\theta}}{Cos\ \bar{\theta}_b} - \frac{ep}{\pi D_b sin\,\theta_b}\right] sin\ \theta_b\ cos\,\theta_b$$

$$\beta_{EX} = \frac{\pi}{12} D_b H^3 \left[\frac{cos\ \bar{\theta}}{cos\ \theta_b} - \frac{e\,p}{\pi D_b sin\,\theta_b}\right] sin\,\theta_b\ sin\,\bar{\theta}$$

$$F_d = \frac{16\ W}{\pi^3\ H} \sum_{i=1,3,5}^{\infty} \frac{1}{i^3}\ tan\ h \left[\frac{i\pi H}{2W}\right]$$

$$F_p = 1 - \frac{192 H}{\pi^5 W} \sum_{i=1,3,5}^{\infty}$$

$$f_L = \left[\frac{\delta_f}{H}\right]^3 \cdot \frac{e}{W} \cdot \frac{\mu}{\mu_f} + \frac{(1 + \frac{e}{w})[\frac{6\mu\ V_{bz}(H - \delta_f)}{H^3 (dp/dZ)} + \frac{1 + e/w}{tan^2 e}]}{1 + \mu_f/\mu\,(H/\delta_f)^3 \cdot e/W}$$

Where:

D_b = Inside barrel diameter, cm
θ = Helix angle, radians

$\bar{\theta}$ = Average helix angle
θ_b = helix angle at the barrel surface
e = Width of screw flights, perpendicular to the flights, cm
p = Number of flights in parallel
W = Width of screw channel
h = Heat transfer coefficient, cal/cm^2 °C sec
μ = Viscosity
μ_f - Viscosity in the flight clearance, dyne sec/cm^2
V_{bz} = Velocity component of V_b in the down channel direction, cm/sec
Z = Rectangular coordinate (down channel direction), cm

2. Schenkel Model (1966)

Output flow rate:

$$Q = Q_D - Q_p - Q_L \tag{3.9}$$

where:

Q_D = Drag Flow = $\dfrac{\pi d(\pi d \tan\theta - e)\, Hn \cos^2\theta}{2}$

Q_p = Pressure Flow = $\dfrac{(\pi d \tan\theta - e)\, H^3 \sin\theta \cos\theta}{12\eta} \dfrac{P_2 - P_1}{L}$

Q_L = Leakage Flow = $\dfrac{\pi^2 d^2 \delta^3 \tan\theta}{12\eta' e} \dfrac{P_2 - P_1}{L_2}$

where:

d = barrel diameter
δ = Radial clearance
H = Channel depth
θ = Helix angle, radians
n = Speed
$\dfrac{P_2 - P_1}{L}$ = Pressure drop in the metering section (assumed constant)
η = Bulk viscosity
η' = Viscosity in the clearance
e = Land width

3. Simplified Model

$$Q = \frac{1}{2}\pi D_b \cos\theta \, WHF_D N - \frac{WH^3 \Delta P}{12\mu Z} F_p \qquad (3.10)$$

where:

D_b	=	Inside barrel diameter
θ	=	helix angle, radians
W	=	Width of screw channel
H	=	Channel depth, cm
N	=	Frequency of screw rotation, rpm
μ	=	Viscosity
ΔP	=	Pressure drop, dyne/cm^2
Z	=	Rectangular coordinate (down channel direction)
F_D	=	Drag flow shape factor
F_p	=	Pressure flow shape factor

in short notation: $Q = AN - C\frac{\Delta P}{\mu}$

Two extreme conditions provide useful measures of extruder performance.

1. If there is no die resistance $\Delta P = 0$, and

$$Q_{MAX} = AN \qquad (3.11)$$

2. At the other extreme, if the die resistance is very large, extruder develops it maximum pressure but produces no output. Thus

$$\Delta P_{max} = \frac{\mu A}{C} N \qquad (3.12)$$

A & C can be determined experimentally for a given extruder.

4. Initial Scale-Up Model

The power requirement of an extruder can be predicted from the performance of a geometrically similar model extruding the same slurry at the same frequency of rotation.

In this case, we let the screws of the model and the large extruder differ in size by the factor X

where:

$$X = \frac{e'}{e} = \frac{D'}{D} = \frac{H'}{H} = \frac{L'}{L} = etc. \qquad (3.13)$$

e	=	Width of flight
D	=	Diameter of screw
H	=	Channel depth
L	=	Length of screw
C	=	Clearance between screw flgiht and barrel
θ	=	Helix angle

and the letters with the prime represent the large extruder and the letters without the prime represent the model extruder. It should be noted that the operating conditions and fluid properties are the same.

McKelvey (1962) showed that the power of the large extruder is equal to that of the model times X^3.

Thus:

$$(POWER)_{large} = X^3 \ (POWER)_{small} \qquad (3.14)$$

LARGE		SMALL
ΔP	=	ΔP
Q	=	X^3 Q
POWER	=	X^3 (POWER)

The above equations apply to Newtonian fluids and non-Newtonian fluids following the power-law model.

A rule of thumb proposed by Schenkel (1966) is:

$$(POWER)_{large} = (POWER)_{model} \ X^{3-0.5\psi} \qquad (3.15)$$

Where:

$$\psi = \frac{T_1 - To}{T_2 - To}$$

To = Feed temperature
T_1 = Intermediate temperature in Zone L_1
T_2 = Output temperature

Obviously, if T_1 = To, then:

$$(POWER)_{large} = (POWER)_{model} X^3 \quad (3.16)$$

3.3.2. Calculation of Typical Extruder-Feeder Output Rate

some correlations of extruder-feeder output rates as a function of screw speed, feedstock viscosities and feedstock concentrations were reported in Part 1. Numerous other calculations were made that have been reported in various quarterly and Interim Reports to the DOE, but are too voluminous to report here. In summary, one weighted correlation of screw speed, flow rate, and drag flow coefficient for using the Albany vacuum bottoms in a 50 wt.% wood flour slurry was as given in Table 3.6.

Range of Extruder-Feeder Shear Rate Requirements

It is important to note that the desired extruder-feeder output pressure of about 3,000 psi can be generated at very low shear rates, due to the very high viscosities exhibited by concentrated wood flour slurries. The screw design used for this successful development of the extruder-feeder has shear rates as shown in Figure 3.17. These shear rates for a range of 40-140 screw rpm are about 50 to 160 sec^{-1}, compared with conventional plastics extrusion shear rates of around 1000 sec^{-1}. This means that much lower power consumption will be experienced for pumping concentrate slurries into pressure systems, in comparison to plastics on an output and/or pressure generation basis.

3.3.3 Calculation of Activation Energy for Flow Consistency and Power Consumption

Considerable data was obtained for the rheology of concentrated wood flour slurries as reported in Part 2, including data that allowed the calculation of activation energy for flow characteristics. The activation energy as calculated from the Arrhenius equation for flow consistency is a sensitive measurement of viscosity-temperature dependence.

If the shear rate, $\dot{\gamma}$, is known, we can calculate the activation energy, $E_{\dot{\gamma}}$, from the equation:

$$\dot{\gamma} = 2.025 x 10^7 (e^{-1.669\, E_\eta}) \quad (3.17)$$

Table 3.6. Typical Flow Characteristics for Wood Flour/Albany Vacuum Bottoms		
Screw Speed RPM	Flow Rate Q* g/m	Drag Flow Coefficient F_d
50	223	0.80
70	261	0.67
80	335	0.75
90	380	0.76
* These flow rates are the average of several experimental runs.		

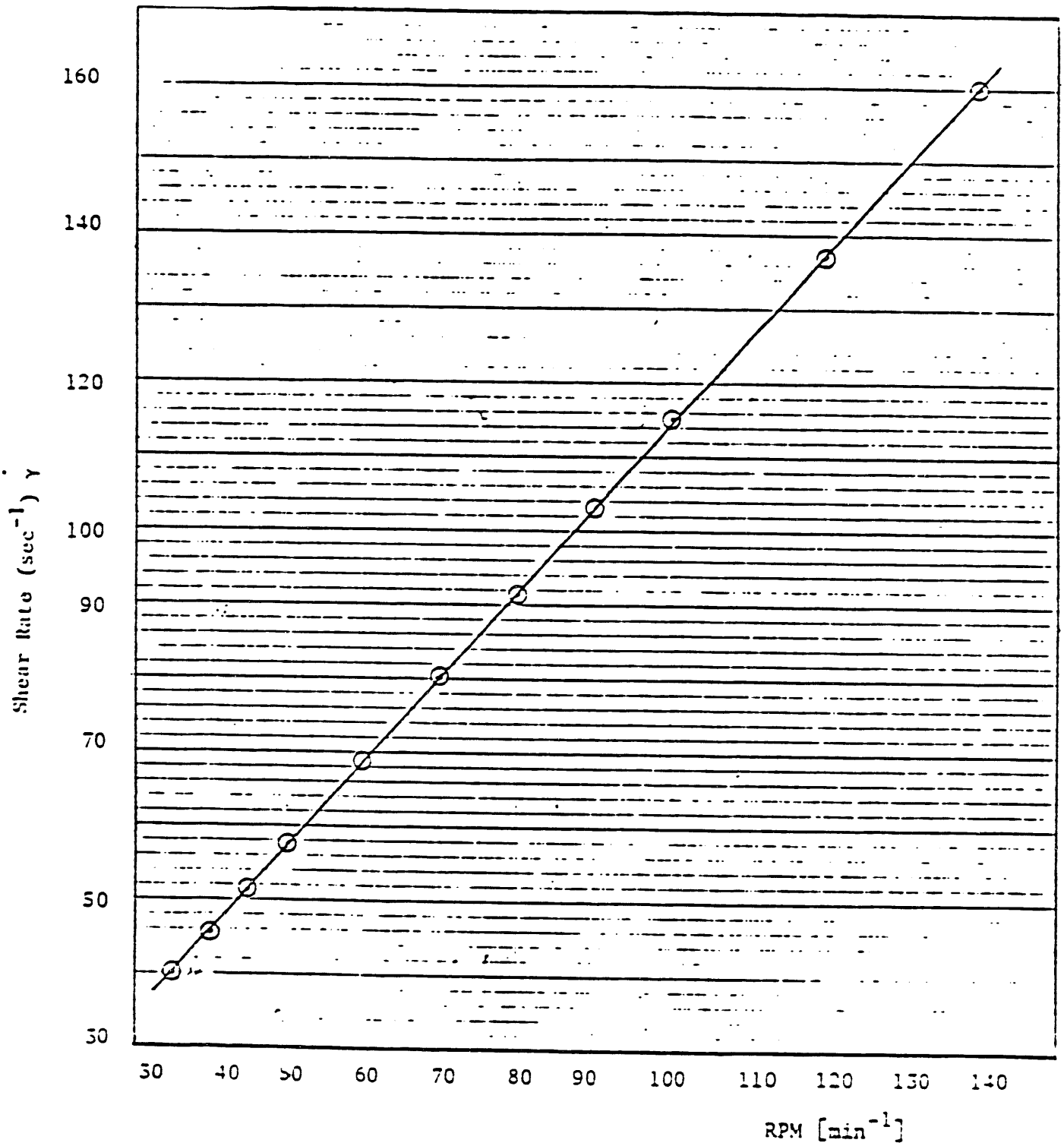

Figure 3.17. Shear Rate as a Function of RPM in the Prodex Extruder-Feeder.

Equation 3.17 was obtained using the data of McKelvey (1962) (his Table 2.7) for polyethylene in the temperature range of 108-230°C and is reproduced here in the form of a semi-log plot as shown on Figure 3.18.

Knowing $E_{\dot{\gamma}}$ and T, the viscosity is obtained from the equation:

$$\mu = A \exp E_{\dot{\gamma}}/RT \qquad (3.18)$$

The values of A in the Equation 3.18 were obtained from experimental data obtained by Yang of the University of Lowell (1981). For 100% LDPE, viscosities were obtained at three different temperatures and three different shear rates as shown on figure 3.19. From this figure at a constant shear rate (7.5 sec^{-1}) we obtained viscosities vs. temperature at this shear rate as shown on Figure 3.20 and the equation representing this graph was obtained as follows:

$$\mu = 548.85 \exp (8{,}453/RT) \qquad (3.19)$$

where:

μ	=	C_p
R	=	1.987 cal/g mol °K
T	=	°K
$E_{\dot{\gamma}}$	=	8,453 cal/g mole
A	=	548.85

A check for $\dot{\gamma} = 1.5\ s^{-1}$ shows that the value of 8.453 is close indeed to the value of 9.87 obtained from Equation 3.17.

3.3.4 Scale-up of the Extruder-Feeder Using the Model Polymer Resin LDPE

Throughout the development period of 1978-1981 for the extruder-feeder model, plastic resins were utilized in addition to Albany vacuum bottoms, so that any serious errors in correlations or scale-up calculations could be detected and corrected. The scale-up of LDPE in our experimental extruder-feeder is shown below and example calculations are given in Appendix C.

The correlations for obtaining F_p after inserting the numerical values of the parameter of the extruder-feeder as derived in Appendix C is:

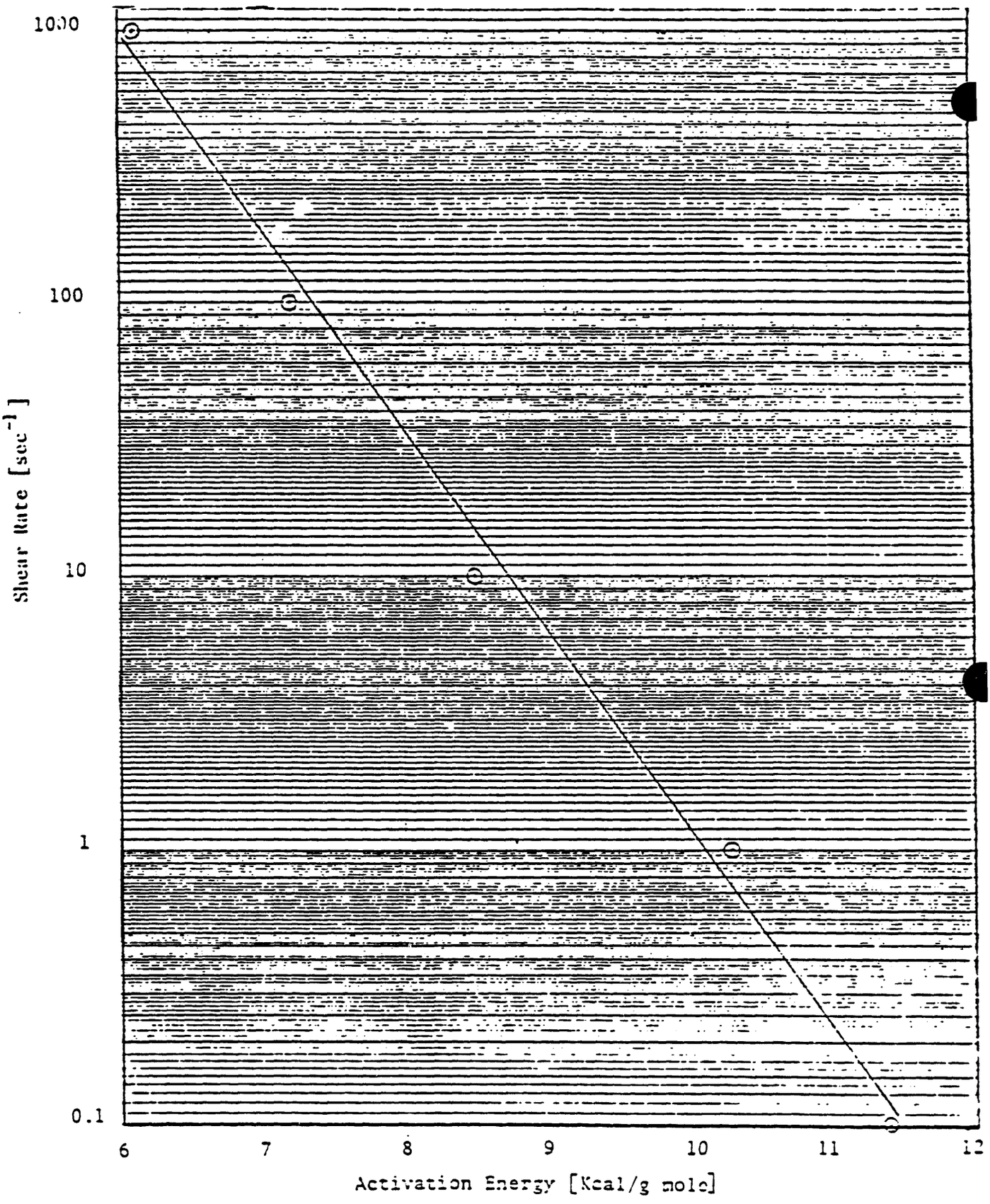

Figure 3.18. Shear Rate as a Function of Activation Energy for LDPE

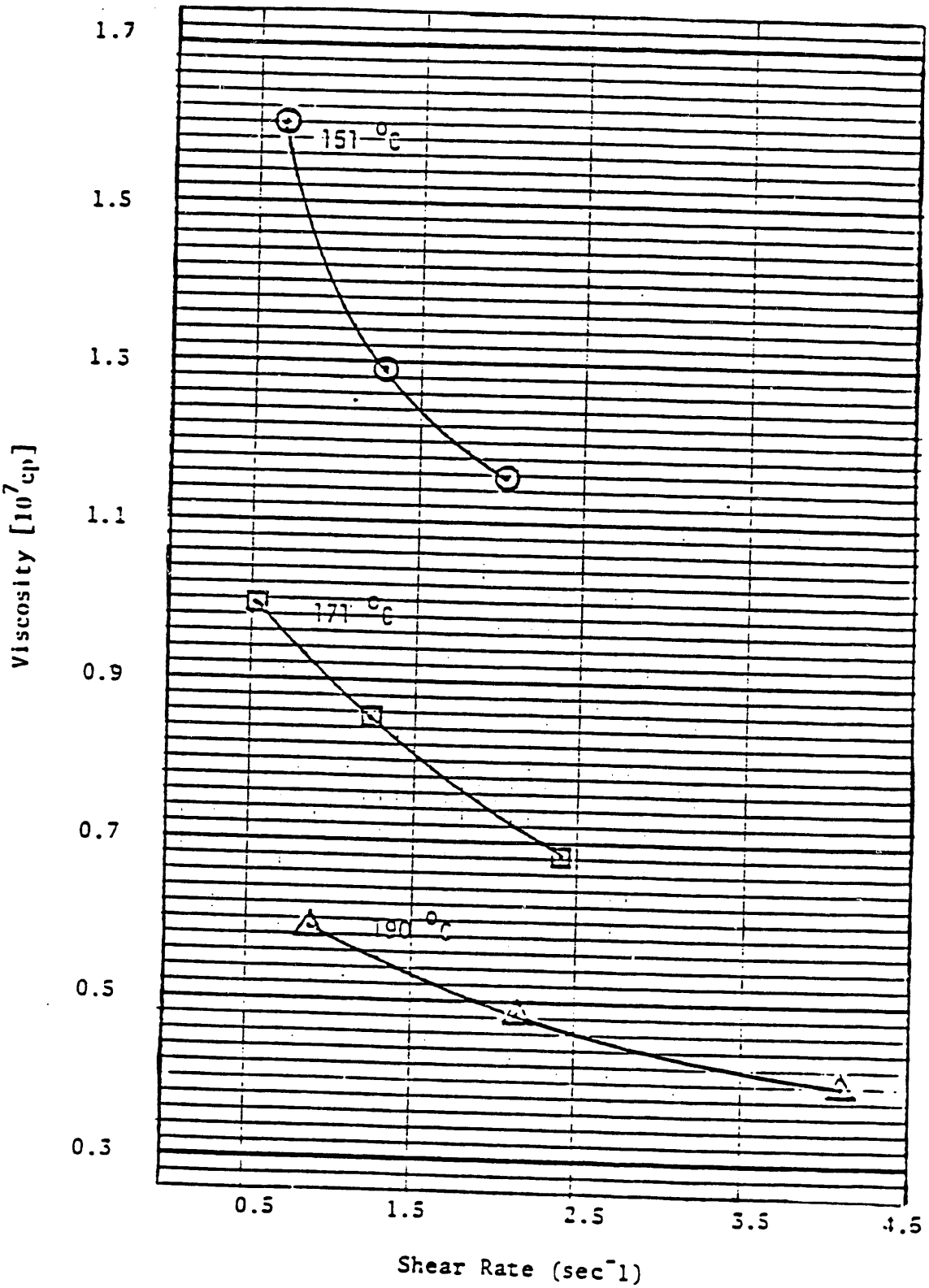

Figure 3.19. Viscosity as a Function of Shear Rate for LDPE.

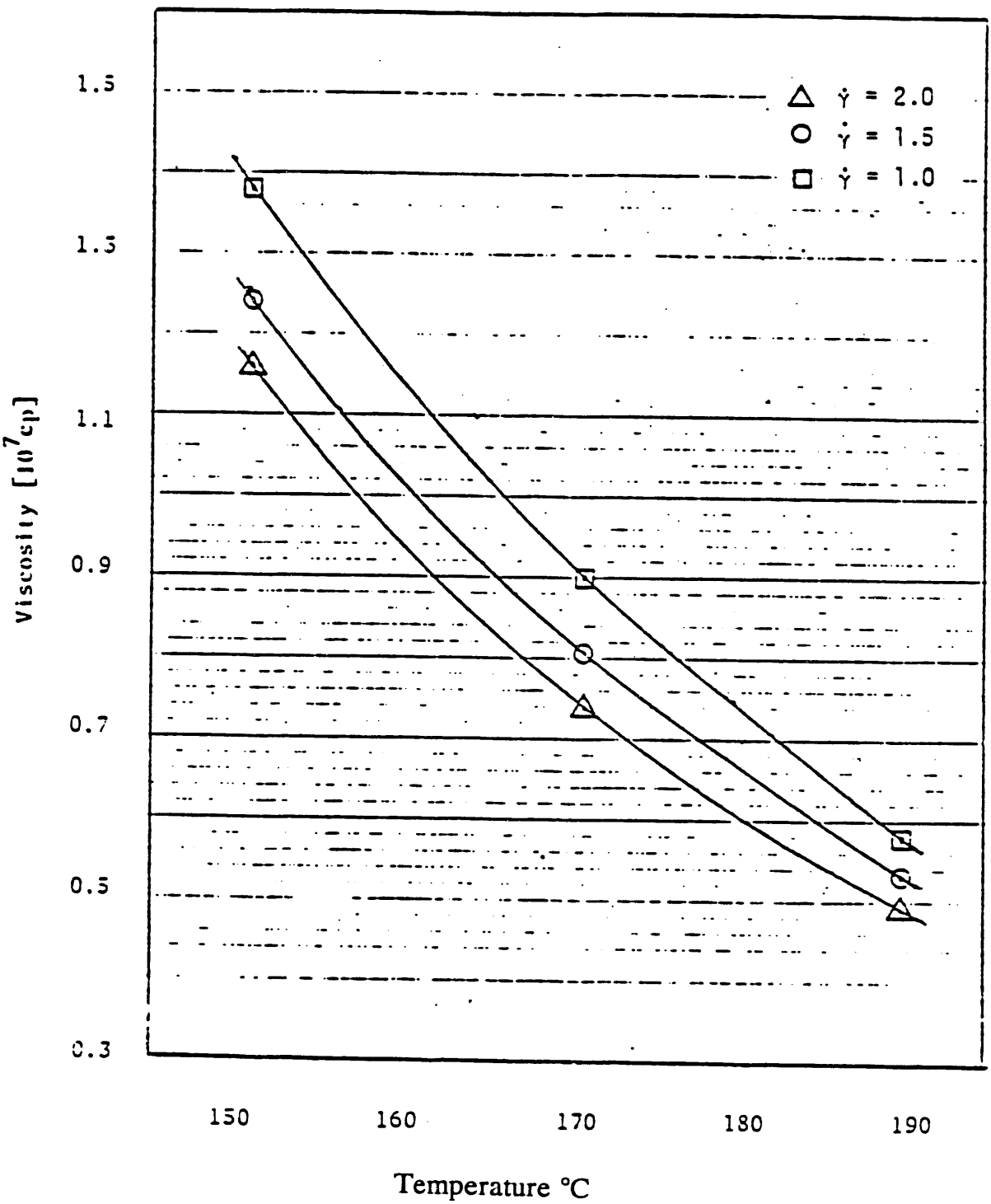

Figure 3.20. Viscosity as a Function of Temperature for Different Shear Rates.

$$F_p = (7.64x10^{-7}Q - 2.95\cdot10^{-6}N) \; x \; 3.271 \; x \; 10^8 \; \frac{\mu}{\Delta P} \qquad (3.20)$$

where:

Q	=	flow rate (g/min)
N	=	Rotational speed of screw (rpm)
μ	=	Viscosity of feedstock ($lb_f \cdot s/ft^2$)
ΔP	=	Pressure drop at the screw (lb_f/ft^2).

The calculations were made for several operating conditions and the results are summarized in Table 3.7.

3.3.5. Calculation of Viscosity Values for Slurries of Wood Flour and Vacuum Bottoms

Viscosities can also be calculated from the flow rates and the die constant. Thus:

$$\mu = \frac{K_d \Delta P}{Q} \qquad (3.21)$$

where:

K_d	=	Die and valve characteristics
ΔP	=	Pressure drop over the die
Q	=	Flow rate through the die

K_d was found to be 0.00033 cm^3 for the LDPE regrind experiment with the die valve close to 10.5 turns. We will use the above K_d value for the following experiment: LDPE Fresh, AC6 PE, wood flour mixtures of LDPE, AC6 PE and vacuum bottoms. All experiments were made with the valve die. The data for several experiments and the calculated values of μ are summarized in Table 3.10.

Calculation of A, B, F_d, F_p and K_d

From the experiments with open die we obtained values of A from which we obtained values of F_d. From experiments with the closed die the values of B and F_p were obtained using the values of A obtained above. Using the above values, K_d were also obtained. Similarly, the other necessary calculations were made, and are summarized before in Tables 3.8 and 3.9 for other viscosities and wood flour concentrations in both model resin carriers and Albany vacuum bottoms.

Table 3.7 Summary of the Experimental Results for LDPE Regrind with 10.5 Turns and F_p as a Function of Screw Speed.

N RPM	$\dot{\gamma}$ (sec^{-1})	$E_{\dot{\gamma}}$ KCal/gmole)	T °K	μ $\frac{lb_f \cdot s}{ft^2}$	ΔP PSI	Q g/min	F_p
40	45.8	8.45	457	61.6	1450	175	1.53
50	57.3	7.65	458	51.3	1340	210	1.14
60	68.7	7.55	455	48.5	650	235	0.47
70	80.2	7.45	457	41.9	700	270	0.007
80	91.6	7.38	460	36.8	350	315	1.19

Table 3.8 Fresh LDPE and 10.5 Turns, Experimental Data and K_d Calculated at Several RPM's.

RPM min^{-1}	P_1 psi	μ $lb_f s/ft^2$	Q g/min	K_d cm^3
40	5020	61.6	175	0.000323
50	4850	51.3	210	0.000334
60	5170	48.5	235	0.000332
70	5000	41.9	270	0.000340
80	5400	36.8	315	0.000323

Table 3.9 Summary of Flow Constants for Various Wood Flour Slurries

	A cm^3	F_d
LDPE	0.000178	0.90
25 wt.% LDPE 75 wt.% AC6	0.00013	0.66
60 wt.% of above mixture 40 wt.% S.D.	0.000156	0.79
40 wt.% S.D. 60 wt.% V.B.	0.000132	0.67

Table 3.10. Calculated Viscosities for Wood Flour/Albany Vacuum Bottom Slurries.

N RPM	Q g/min	P_1 psi	ρ g/cc	μ cp	Material
40	365	1101	1.2	1,030,000	Vacuum Bottoms
40	325	690	1.2	347000	"
50	435	1606	1.2	604000	"
50	440	1663	1.2	619000	"
60	470	1995	1.2	695000	"
60	465	2309	1.2	813000	"
60	460	2478	1.2	735000	"
60	497	2168	1.2	794000	"
40	150	372	0.77	261000	40% Sawdust and 60% (25% LDPE/75% AC6 PE)
60	150	1225	0.77	858000	"
80	160	1475	0.77	969000	"
80	165	1935	0.77	1,232,000	"
80	190	2262	0.77	1,250,000	"
100	165	2000	0.77	1,274,000	"
100	170	2784	0.77	1,727,000	"
100	172	2453	0.77	1,500,000	"
120	188	3319	0.77	1,855,000	"
120	183	4218	0.77	2,422,000	"
120	360	2122	0.77	619,000	"

Calculation of Q_p/Q_d Ratio

$$\frac{Q_p}{Q_d} = \frac{1}{6\mu} \cdot \frac{\Delta P}{\Delta z} \cdot \frac{H^2}{V_{bz}} \tag{3.22}$$

where:

μ = $0.8 \frac{lb_f \cdot s}{in^2}$

ΔP = 1060 psi
Δz = 14 in.
H = 0.078 in.
N = 40 rpm
D_b = 1.75 in.

The substitution of these values would show that Q_p is much smaller than Q_d. This may be generally true. $Q_p = Q_d$ only when Q = 0 or the die valve is closed.

3.3.6. Calculation of Maximum Output Pressure

The maximum output pressure, ΔP_{max}, that can be generated is obtained when Q = 0, namely the die valve closed.

$$\Delta P_{max} = \frac{6\pi \cos\theta_b N D_b \mu 1}{H^2 \sin\theta} = \frac{6 V_{bz} \mu 1}{H^2 \sin\theta} \tag{3.23}$$

By differentiating $\frac{\partial P}{\partial z}$ with regard to H, one obtains the channel depth giving maximum pressure rise for a certain flow rate. The value of H is:

$$H_{p-p_{max}} = \frac{3Q}{W \cdot V_{bz}} \tag{3.24}$$

or the flow rate can be expressed as:

$$Q = \frac{2}{3} Q_d \tag{3.25}$$

The value of ΔP_{max} is very important since this gives us the maximum pressure we can develop for a certain system and by a certain extruder-feeder. In our case, we need some 3,000 psi in order to pump the wood flour slurry into the liquefaction reactor. A numerical calculation is shown in Appendix C.

If we assume that we want $\Delta P = \frac{1}{3} \Delta P_{max}$, we can achieve our 3,000 psi goal by either increasing the rpm three-fold to 180 or consider the viscosity to be much higher than 100,000 C_p, which is a very low and conservative viscosity for our system. To consider the value of μ in the range of 300,000 to 1,000,000 C_p for our system is quite appropriate.

3.3.7 Calculation of Viscous Dissipation and Power Required for Viscous Dissipation

The viscous dissipation was calculated in the metering section for polyethylene based on the Newtonian adiabatic analysis given in the book by Middleman (1977). A sample calculation for the temperature rise due to viscous dissipation is given in Appendix C. The power for viscous dissipation was calculated using the following equation:

$$P_{wvs} = Q\, C_p\, \Delta T \tag{3.26}$$

where:

Q	=	Flow rate
C_p	=	Heat capacity of the feedstock
ΔT	=	Temperature rise due to viscous dissipation.

A numerical calculation of the power for viscous dissipation is also given in Appendix C.

3.3.8. Calculation of Energy Balance for the Extruder-Feeder

The energy balance for the extruder may be written as:

$$Z + q = CQ\Delta T + Q\Delta P + H \tag{3.27}$$

where:

Z	=	Mechanical power to screw
q	=	Electric power to heaters
C	=	Mean volume specific heat to plastic
Q	=	Volumetric extrusion rate
ΔT	=	Temperature rise in plastic
ΔP	=	Pressure rise in extruder-feeder
H	=	Heat loss in extruder-feeder from radiation and conduction

Equation 3.27 is simplified for the experimental runs on the 1.75-inch diameter extruder-feeder at the University of Arizona since the unit was run without electrical barrel heating. Equation 3.27 may thus be written:

$$Z = CQ\Delta T + Q\Delta P + H \tag{3.28}$$

Further, direct readings were taken on the drive power of the motor and recorded on the computer. This drive power should be reduced by a factor of 10 to 20% since the electric motor has about a 90% efficiency and the gear train is also about 85-90% efficient. Hence, $Z_{corr} = (0.9)(0.9)Z = 0.8Z$.

The term $Q\Delta P$ is rather insignificant and will account for less than 5% of the total power consumed. Hence, as a first approximation, the energy balance will be:

$$Z = CQ\Delta T + H \tag{3.29}$$

in which the losses, H, will include those of the electric motor and the gear train. The smoothed data of power consumption were used to make the energy balance. The results are summarized in Tables 3.11 through 3.14. In each Table, the two far right columns show the percent of the power that goes into raising the enthalpy and the percentage of the power that is used to do pressure work, i.e., the pumping efficiency defined by:

$$E = \frac{Q\Delta P}{Z}(100) \tag{3.30}$$

The maximum value of E occurs for a helix angle of 0° and is 33%. For a helix angle between 10 and 20° the theoretical efficiency is about 25%. This value will decrease significantly because of leakage flow. It is seen that for an open die, the efficiency is less than 1 percent and for a closed die, the efficiency is less than 5 percent. In the case of an open die approximately 60 to 70 percent of the power is used for viscous dissipation while for a closed die the value is about 40 percent.

Similar power calculations were also made for the wood flour/vacuum bottom slurries and pure vacuum bottoms. The results are shown in Tables 3.15 through 3.18. As expected, they also show a viscous dissipation of 40 to 50 percent for a closed die. The pumping efficiency is close to zero for an open die when ΔP is close to zero and increases with the product $Q\Delta P$. The maximum efficiency is about 5% for pressures greater than 2,000 psi.

Based on all the extrusion data considered previously one can summarize the behavior of the various compositions. The data show that LDPE is the most power intensive on a Hp/unit mass basis while the fresh pure vacuum bottoms require the least power. The wood flour-vacuum bottoms slurries require slightly less energy than the pure LDPE. The LDPE has the highest viscous dissipation on a mass basis while the pure vacuum bottoms show the least. The wood flour-vacuum bottom slurries have about 25% less viscous dissipation than the pure LDPE. The viscous dissipation measured for the 40 wt. % wood flour/60 wt. % (25 wt. % LDPE/75 wt. % AC6 PE) falls approximately on the same line as the wood flour/vacuum bottom slurry and justifies the use of the 25 wt. % LDPE/75 wt. % AC6 PE mixture as a modeling fluid for use instead of vacuum bottoms.

Table 3.11. Energy Balance for Extrusion of 40 wt. % Wood Flour/60 wt. % (25 wt. % LDPE/75 wt. % AC6PE). Die Open.

Q g/min	ΔT_1 °F	CQΔT HP	Z HP	ΔP psi	QΔP HP	H HP	(CQΔT/Z)100 %	(QΔP/Z)100 %
150	355	1.37	2.34	70	2.19×10^{-3}	0.97	58.5	0.09
200	343	1.75	2.95	70	2.92×10^{-3}	1.20	59.3	0.10
250	339	2.15	3.55	60	3.14×10^{-3}	1.40	60.6	0.09
300	337	2.56	4.15	60	3.76×10^{-3}	1.59	61.7	0.09
350	330	2.90	4.76	50	3.66×10^{-3}	1.86	60.9	0.08

Assume $\bar{\rho}$ = 46 lb/ft^3 $T_{ambient}$ = 80°F

$\bar{C}_p$ = 0.63 Btu/lb-°F

Table 3.12. Energy Balance for Extrusion of 100% Fresh LDPE. Die Closed.

Q g/min	ΔT_1 °F	CQΔT HP	Z HP	ΔP psi	QΔP HP	H HP	(CQΔT/Z)100 %	(QΔP/Z)100 %
150	370	1.44	3.82	4936	0.155	2.23	37.7	4.1
200	368	1.91	4.96	5150	0.215	2.84	38.5	4.3
250	390	2.57	6.07	4769	0.249	3.25	42.3	4.1
300	380	2.99	7.19	5068	0.318	3.88	41.6	4.4

Assume $\bar{C}_p$ = 0.70 Btu/lb-°F $T_{ambient}$ = 80°F

$\bar{\rho}$ = 46 lb/ft^3

Table 3.13. Energy Balance for Extrusion of 40 wt. % Wood Flour/60 wt. % (25 wt. % LDPE/75 wt. % AC6PE). Die Closed.

Q g/min	ΔT_1 °F	CQΔT HP	Z HP	ΔP psi	QΔP HP	H HP	(CQΔT/Z)100 %	(QΔP/Z)100 %
100	385	1.01	2.64	230	4.8×10^{-3}	1.63	38	.2
125	385	1.27	3.08	230	6.0×10^{-3}	1.81	41	0.2
150	380	1.49	3.51	372	1.2×10^{-2}	2.01	42.5	0.3
175	357	1.61	3.94	2262	8.3×10^{-2}	2.25	40.8	2.1
200	340	1.73	4.35	4218	1.76×10^{-1}	2.44	39.8	4.0

Estimated $\bar{\rho}$ = 46 lb/ft^3 $T_{ambient}$ = 80°F

$\bar{C}_p$ = 0.64 Btu/lb-°F

Table 3.14. Energy Balance for Extrusion of 25 wt. % LDPE/75 wt. % AC6PE Regrind. Die Open.

Q g/min	ΔT_1 °F	CQΔT HP	Z HP	ΔP psi	QΔP HP	H HP	(CQΔT/Z)100 %	(QΔP/Z)100 %
150	400	1.59	2.14	29	9.1×10^{-4}	0.54	74.	0.04
200	395	2.09	2.68	37	1.55×10^{-3}	0.58	78.	0.06
250	360	2.32	3.24	37	1.93×10^{-3}	0.90	72.	0.06
300	340	2.59	3.79	40	2.51×10^{-3}	1.18	68.	.07

Assume $\bar{C}_p$ = 0.70 Btu/lb-°F $T_{ambient}$ = 80°F

$\bar{\rho}$ = 46 lb/ft^3

Table 3.15. Energy Balance for Extrusion of 50 wt. % Wood Flour/50 wt. % Vacuum Bottoms. Die Closed 9 Turns.

Q g/min	ΔT_1 °F	CQΔT HP	Z HP	ΔP psi	QΔP HP	H HP	(CQΔT/Z)100 %	(QΔP/Z)100 %
260	364	1.81	5.23	2116	0.11	3.31	34.6	2.1
240	370	1.71	4.38	1874	0.09	2.58	39.0	2.1
250	378	1.84	4.70	1929	0.10	2.76	39.1	2.1
275	381	2.03	4.93	1759	0.10	2.80	41.1	2.0
295	384	2.13	5.13	1798	0.10	2.90	41.5	1.9
327	389	2.49	6.31	1596	0.11	3.71	39.5	1.7
303	394	2.34	6.45	1662	0.11	4.0	36.3	1.7
305	396	2.37	6.34	1559	0.10	3.87	37.4	1.6
450	397	3.51	7.66	1612	0.15	4.0	45.8	2.0

$\bar{C}_p$ = 0.475 Btu/lb-°F $\quad T_{ambient}$ - 80°F

$\bar{\rho}$ = 46 lb/ft^3

Table 3.16. Energy Balance for Extrusion of 50 wt. % Wood Flour/50 wt. % Vacuum Bottoms Reground 2X. Die Closed 9-1/2 Turns.

Q g/min	ΔT_1 °F	CQΔT HP	Z HP	ΔP psi	QΔP HP	H HP	(CQΔT/Z)100 %	(QΔP/Z)100 %
340	419	2.84	6.27	438	3.11×10^{-2}	3.40	45.	0.5
335	390	2.55	6.03	1859	0.13	3.35	42.	2.1
320	432	2.77	5.55	1690	0.11	2.67	50.	2.0
300	411	2.44	5.88	2053	0.13	3.31	41.	2.2
280	410	2.27	5.56	1716	0.10	3.19	41.	1.8

$\bar{C}_p = (0.50)(.55) + (0.50)(0.40) - 0.475 \frac{\text{Btu}}{\text{lb-°F}}$

$T_{ambient}$ = 80°F $\quad \bar{\rho}$ = 46 lb/ft^3

Table 3.17. Energy Balance for Extrusion of 50 wt. % Wood Flour/50 wt. % VB-2, Regrind 2-3 Heaters Off. Die Closed 9 Turns.

Q g/min	ΔT °F	CQΔT HP	Z HP	ΔP psi	QΔP HP	H HP	(CQΔT/Z)100 %	(QΔP/Z)100 %
366	383	2.68	6.08	1131	0.085	3.32	44.1	1.4
350	389	2.66	5.90	1315	0.096	3.14	45.1	1.6
340	396	2.64	5.39	1179	0.084	2.67	49.0	1.6
390	410	3.08	6.01	1051	0.083	2.85	51.2	1.4
370	412	3.02	6.06	1208	0.093	2.95	49.8	1.5
375	414	3.08	5.74	1057	0.083	2.58	53.7	1.4

$\bar{C}_p$ = (0.50)(.55) + (0.50)(.40) = 0.475 Btu/lb-°F $T_{ambient}$ = 80°F

$\bar{\rho}_{slurry}$ = 46 lb/ft^3

Table 3.18. Energy Balance for Extrusion of Fresh Pure Vacuum Bottoms, VB-2, Crushed and Screened, Using Size > Mesh 12.

Q g/min	ΔT_1 °F	CQΔT HP	Z HP	ΔP psi	QΔP HP	H HP	(CQΔT/Z)100 %	(QΔP/Z)100 %
350	312	2.0	3.22	28	$2x10^{-3}$	1.22	62.1	.06
345	307	1.93	3.12	29	$2x10^{-3}$	1.19	61.9	.06
367	290	1.90	3.68	1101	$8x10^{-2}$	1.70	51.6	2.2
325	313	1.86	3.02	690	$5x10^{-2}$	1.11	61.6	1.7
400	284	2.00	3.56	576	$5x10^{-2}$	1.51	56.2	1.4
385	286	1.95	3.88	1351	0.11	1.82	50.3	2.8
378	285	1.91	3.87	1385	0.11	1.85	49.4	2.8
435	284	2.18	4.44	1606	0.15	2.11	49.1	3.4
472	284	2.37	4.20	1606	0.16	1.67	56.4	3.8
440	285	2.22	4.45	1663	0.15	2.08	49.9	3.4
470	283	2.35	4.59	1995	0.20	2.04	51.2	4.4
462	283	2.31	4.59	2309	0.22	2.05	50.3	4.8
460	283	2.30	4.54	2478	0.24	2.00	50.7	5.3
447	284	2.24	4.27	2168	0.20	1.83	52.5	4.7

In summary, it can be seen that the model fluids closely predicted the behavior of the slurries using vacuum bottoms. The viscous dissipation of the wood flour slurries is about 80% or less than that of LDPE in an extrusion operation, but, the LDPE has the potential to be as high as 10 times that of the slurry. Viscous dissipation is higher for open discharge, probably due to the higher viscosity at lower shear rates. The power consumption for pressure generation will be about 5% of the total extruder-feeder power for pressures around 3,000 psi. All the data confirm the assumptions that were made in the scale-up calculations.

3.4 SUMMARY OF SOME IMPORTANT SCALE-UP AND DESIGN FACTORS

3.4.1 Properties of Albany Vacuum Bottoms

Prior to November, 1980 vacuum fractionator bottoms from Albany were not available, except in laboratory quantities. At that time, a 100 pound sample was received from Albany, and when continued funding became available to the University of Arizona on February 2, 1981, emphasis was placed upon using them as the liquid carrier for Albany wood flour in the extruder-feeder development.

It was predicted at the beginning of this project in 1978 that the heavy ends made in the process would be the logical recycle material to convey the finely-ground cellulosics into the pressure reactor system. It was predicted that such fractions would have sufficient viscosity to assist the wood flour in providing the necessary drag flow in the single screw extruder-feeder.

The Albany vacuum bottoms are brittle solids at room temperature, soften at about 103-110°C and become liquid at about 120-125°C. The one to two-inch *"lump vacuum bottoms"* were easily crushed in a conventional jaw crusher and ground to a finer mesh by means of a twin-roller crusher. Since the vacuum bottoms were very brittle and the sample was only 100 pounds total. It was not feasible to screen out the fines in order to use the optimum mesh size, therefore, an *"as is"* mesh size of minus 40 mesh with a large amount of fines (A Ro-tap screen analysis was not run upon this small sample) were used for the extruder-feeder runs. About 60 wt. % of the ground vacuum bottoms were in the 45-80 mesh range.

Vacuum bottoms alone can be extruded at very high rates, exceeding conventional Low-Density Polyethylene (LDPE) about two-fold under the given conditions as shown in Figure 3.21. Equally important, the power requirements for the extruder-feeder operating on vacuum bottoms are only half the power for LDPE, as shown in Figure 3.22. Data on Albany Wood Flour/Vacuum Bottoms slurries are shown in Figure 3.23 where the output rates as a function of screw rpm are shown. These data for 40 and 60 wt. % slurries bracket is believed to be the most desirable operating range. Data correlating one aspect of power requirements are shown on Figure 3.24, from which the power per unit of output can be calculated for this size of extruder-feeder (1.75-inch I.D.).

A project highlight was achieved on Friday, February 20, 1981. Not only was a 60 weight percent Albany wood flour concentration in Albany vacuum bottoms successfully extruded, but also a die pressure of about 8,100 psi was developed (see Figure 3.25). This proved one of the basic concepts of this project, that one mode of operation would utilize a heavy ends recycle stream. The extruder-feeder operating conditions required to generate this 8,100 psi output pressure are important vacuum bottom properties and design factors.

3.4.2 Prediction of Physical Properties of Components in Albany Vacuum Bottom Slurries

Prior to 1981, extruder-feeder operational data were easy to analyze and interpret, because model polymer liquids with well-established physical properties, were used. In 1981, with

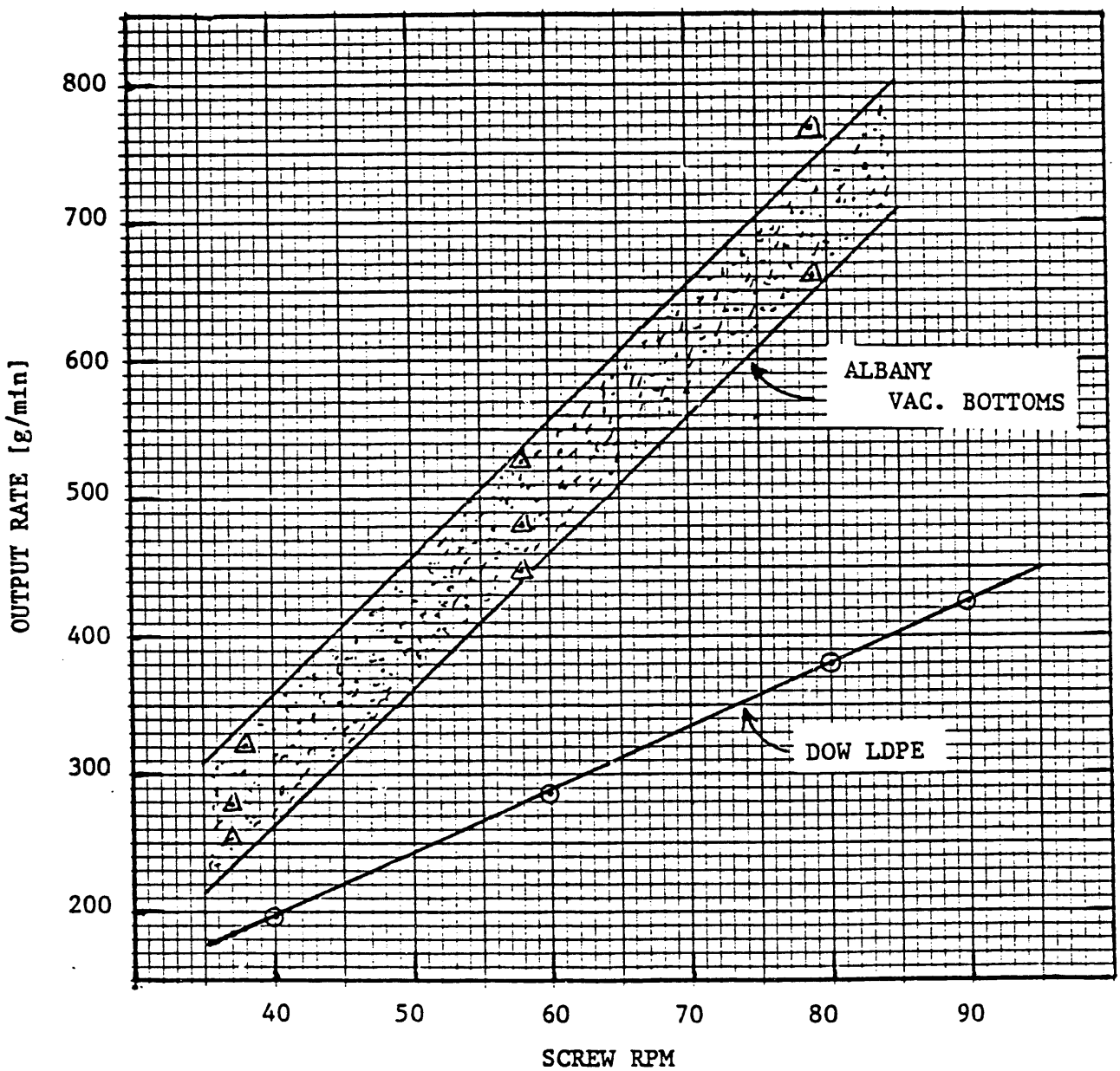

Figure 3.21. Effect of Screw Speed Upon Output Rate for LDPE and Vacuum Bottoms.

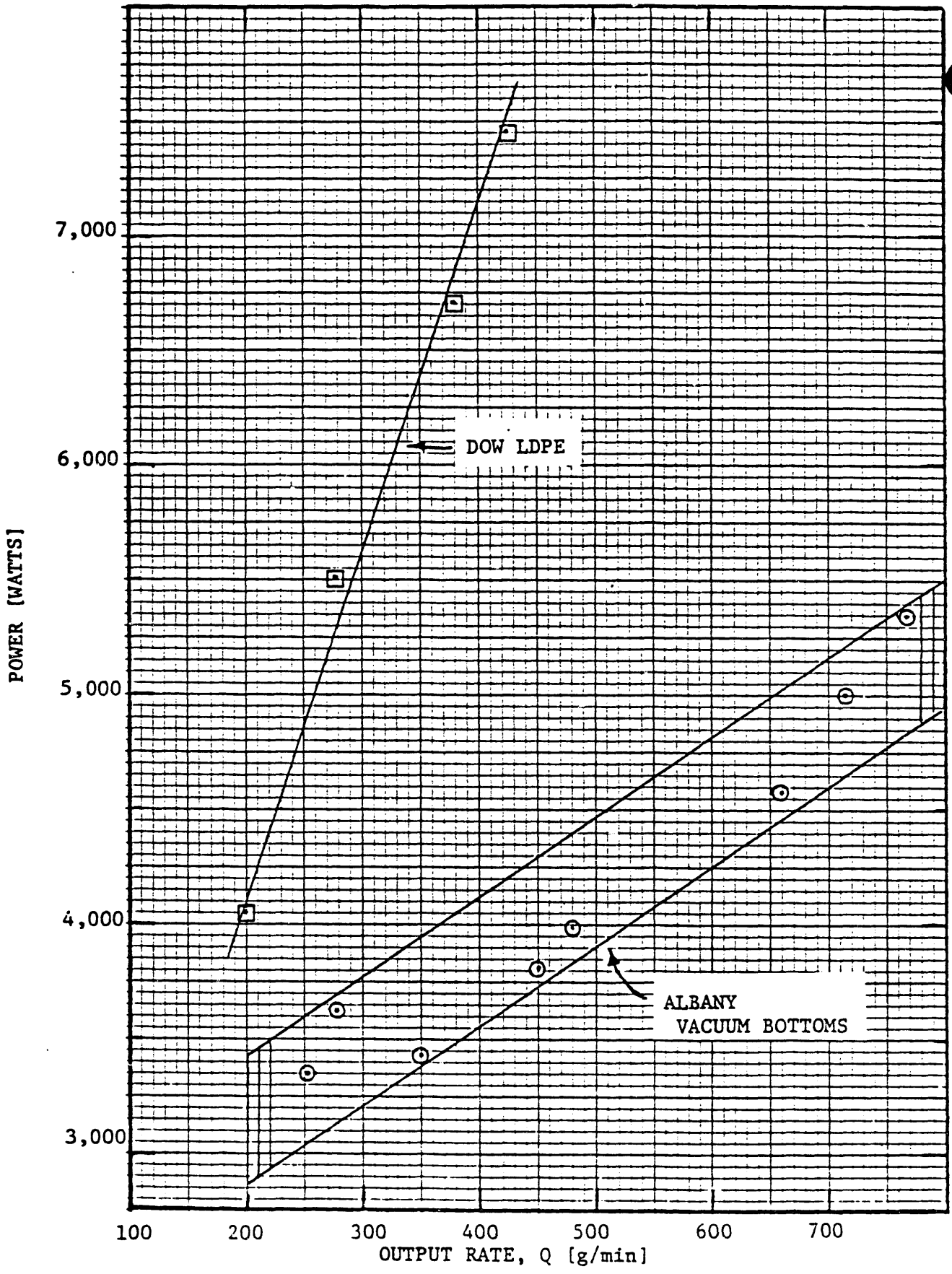

Figure 3.22. Power Requirement for Extrusion of LDPE and Vacuum Bottoms.

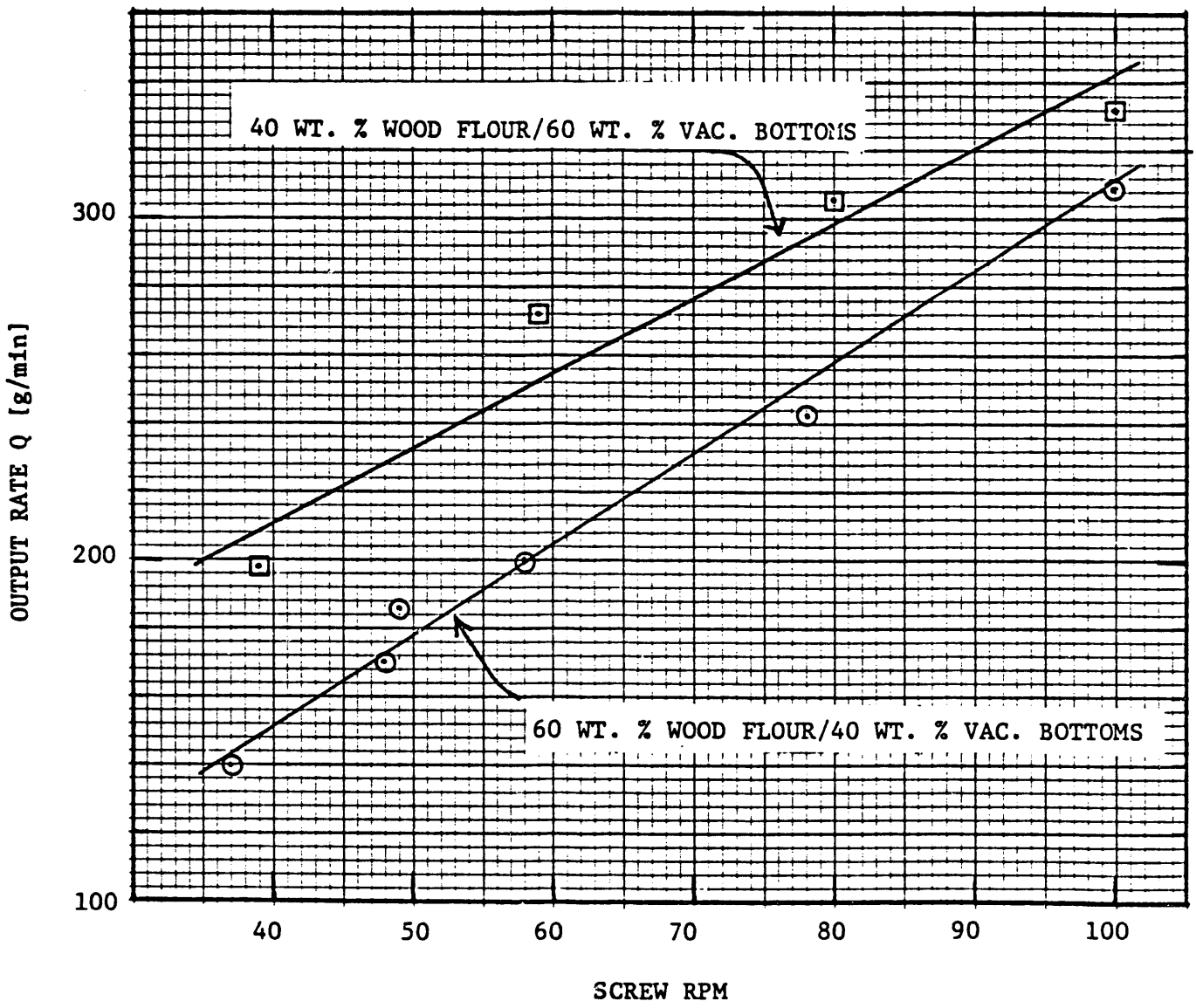

Figure 3.23. Effect of Screw Speed and Slurry Concentration Upon Output Rate.

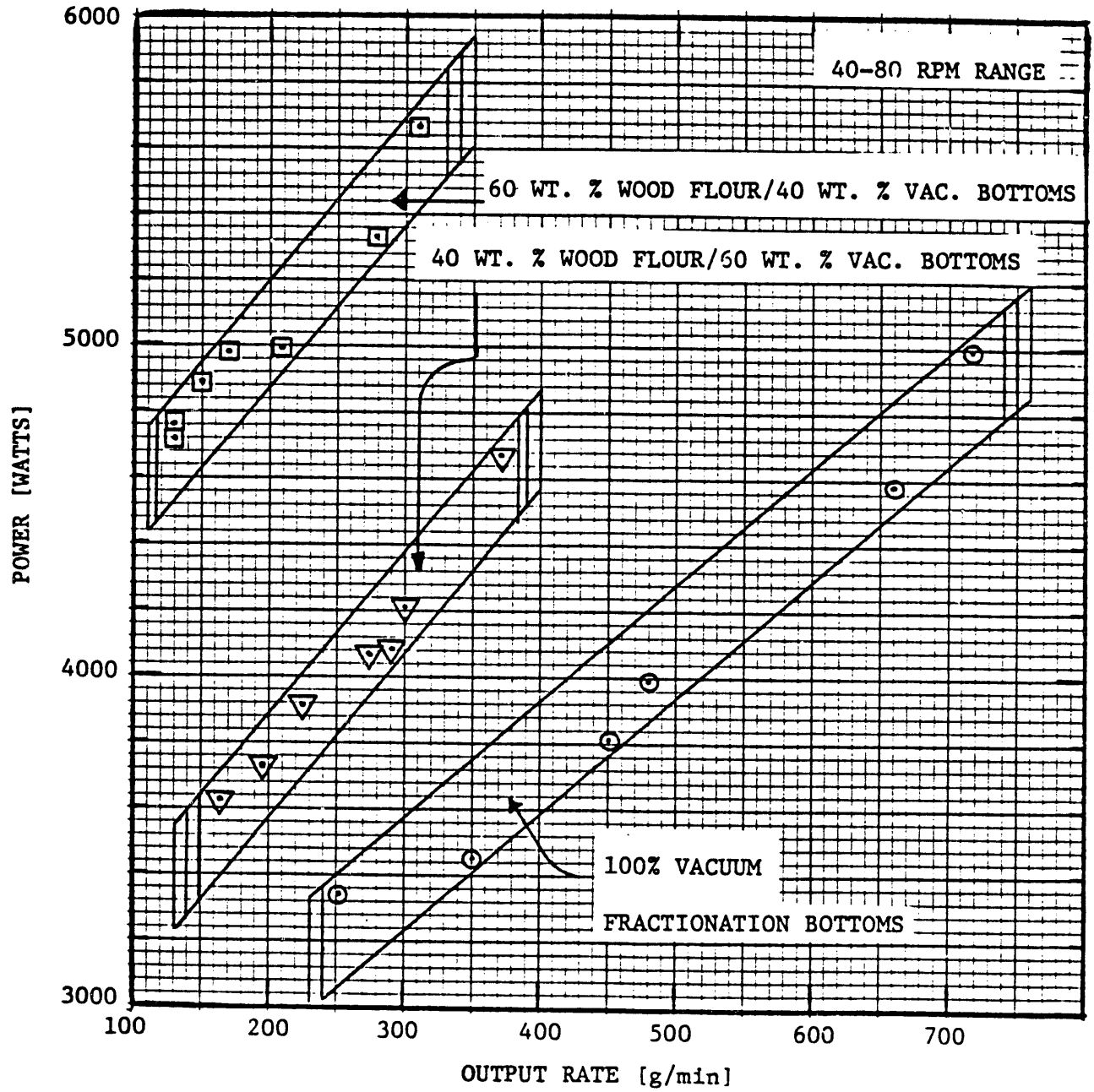

Figure 3.24. Power Requirement for Extrusion of Wood Flour/Vacuum Bottoms Slurries.

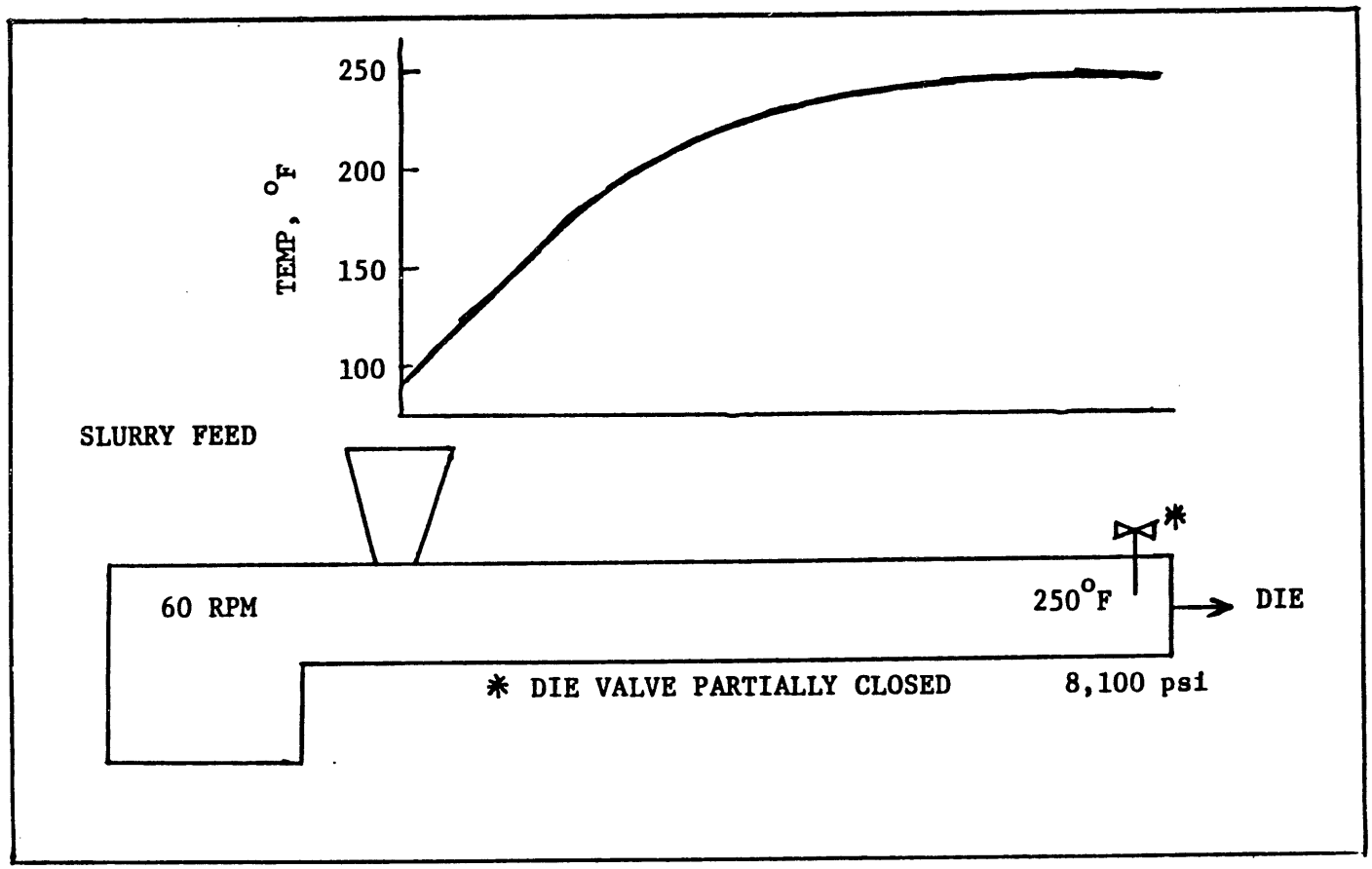

Figure 3.25. Operating Conditions for High Outlet Pressure Feeding 60 wt. % Wood Flour/40 wt. % Vacuum Bottoms Slurry.

vacuum bottoms, it was not that easy. Most of its physical properties were unknown. It was necessary to predict (a) values for the specific heat and thermal conductivity of Douglas Fir (see Figure 3.26 and 3.27), and (b) the specific heat of vacuum bottoms (Figure 3.28). It was evident from this work that there was an urgent need to determine many of the physical, chemical and thermal properties of (a) vacuum bottoms per se, and (b) vacuum bottoms not cut as deeply as the present sample lot. The determination of such properties were accumulated to some extent over the period 1981-1988.

3.5 SCALE-UP AND SPECIFICATIONS FOR A COMMERCIAL EXTRUDER-FEEDER

3.5.1 Extrusion Theory for Scale-Up

The analysis of the extrusion process is based on a momentum balance and hydrodynamic analysis of the melt flow in the metering section. The solids flow in the feed section and the melting process in the transition section are not as well understood and hence design is based on the metering section. This reliance on the metering section is adequate since the rates of pumping in the other two sections if acting by themselves would each be greater than the metering section.

The formulation of the design problem starts with the momentum balance in which the velocity component (axial direction) contributes to the output of the extruder. This has been discussed in the literature and given in a detailed derivation by McKelvey (1962). Equation (3.31) is the starting equation for the momentum balance for a steady state, isothermal, incompressible Newtonian fluid where the acceleration (inertial) terms can be neglected and the channel depth is assumed constant.

$$\frac{1}{\mu}\left[\frac{\partial P}{\partial z}\right] = \left[\frac{\partial^2 v_z}{\partial X^2} + \frac{\partial^2 V_z}{\partial Y^2}\right] \qquad (3.31)$$

After suitable boundary conditions are selected a series solution for the velocity distribution is found. The solution is a case of drag flow and pressure flow added algebraically to produce the net flow. Integration of the velocity distribution gives an expression for the volumetric flow rate as given before in Equation 1.2 of Part 1. It should be noted that F_D and F_p are correction factors that are only a function of extruder geometry. They depend only on the ratio H/W of the screw and are close to 1.0 for small values of H/W, i.e. for shallow screws. Similar analytical solutions can be calculated for a power law fluid and for the case of a variable channel depth. Beyond the removal of these restrictions one has to go to computer methods.

Scale-up assumes that the model and the large extruder-feeder are geometrically similar and differ in size by the factor X. Hence the ratios apply as given above in Equation 3.13. Based on torque limitation and adequate mixing, it has been found that a 20:1 to 30:1 L/D ratio is used on screws with 24:1 being the most common. A compression ratio, which is defined as

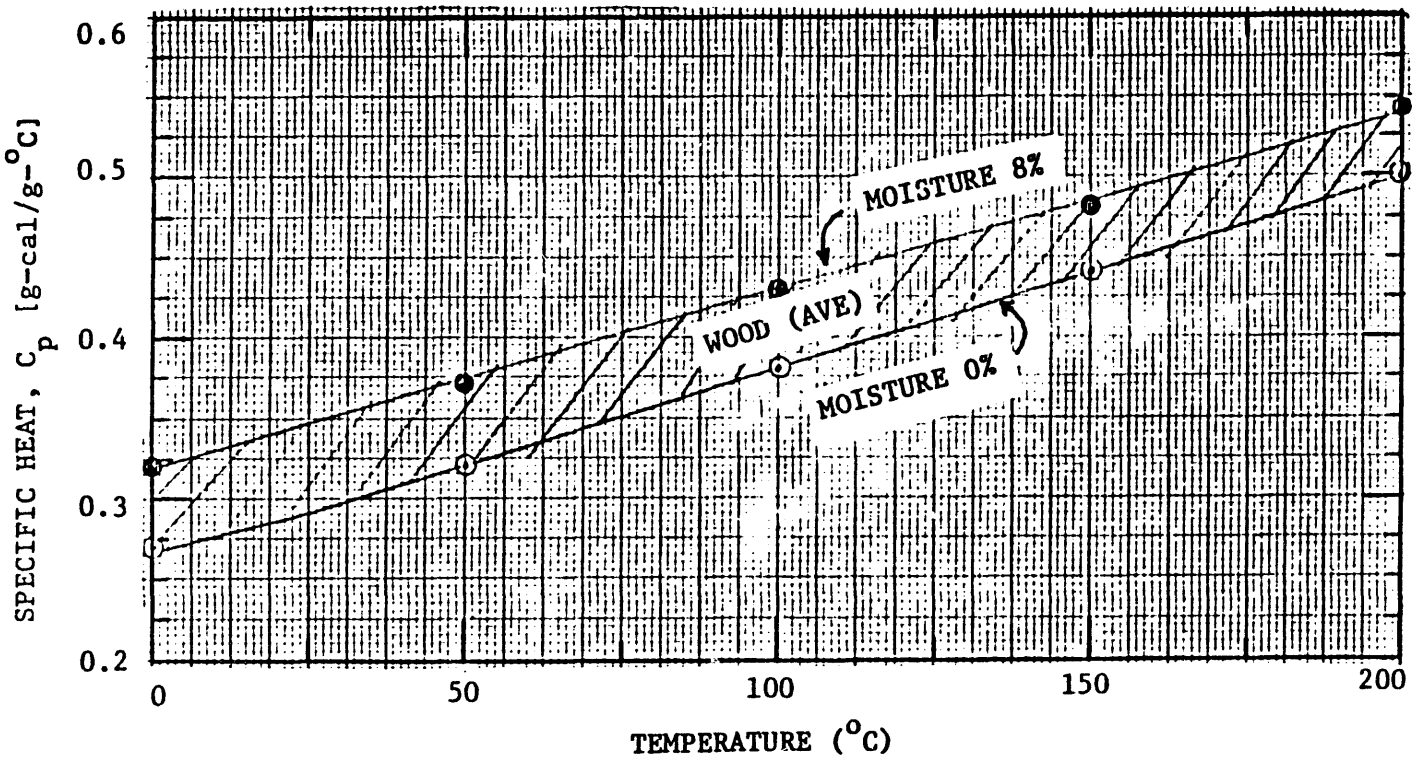

Figure 3.26. Prediction of Specific Heat of Douglas Fir Wood.

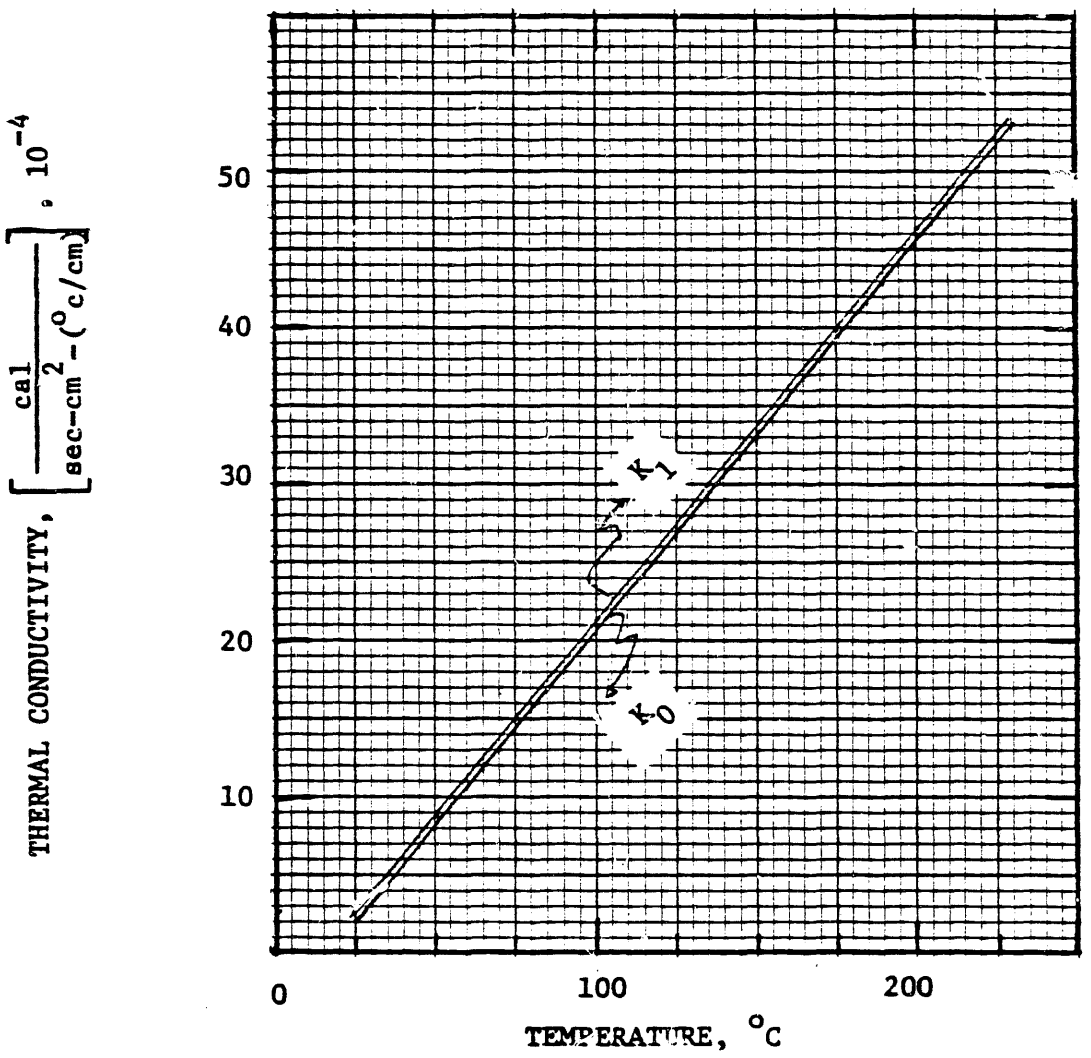

Figure 3.27. Prediction of Thermal Conducting of Douglas Fir Wood.

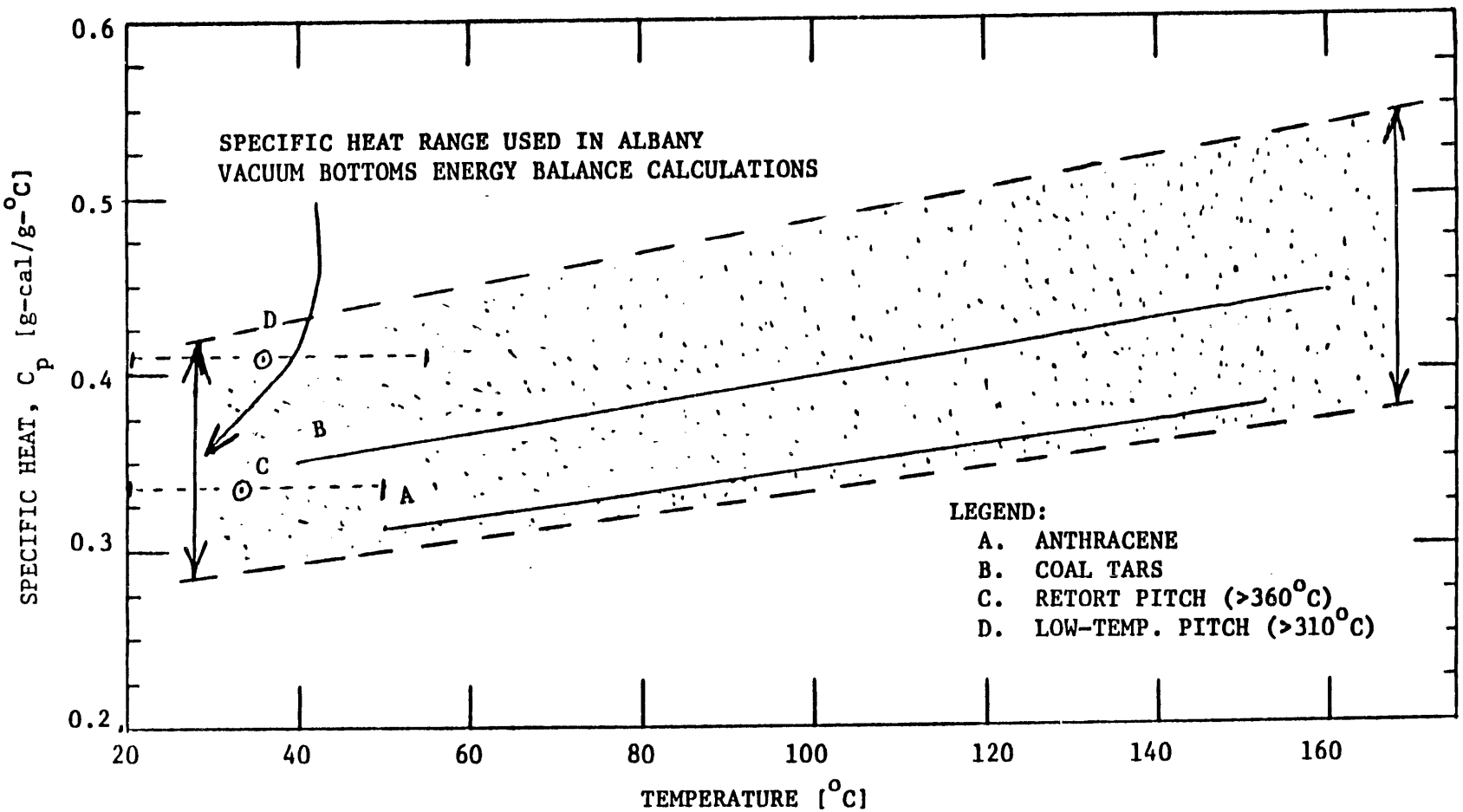

Figure 3.28. Prediction of Specific Heat of Albany Vacuum Bottoms.

the depth of the feed channel divided by the depth of the metering channel is 2:1 to 5:1 with a 3.5:1 being very common for polyolefins. Also, the helix angle, θ, is most commonly 17.7°. This angle gives good output and easy fabrication of the screw. This angle gives a *"square pitch"* where one turn of the screw advances the flight by one diameter. The flow in a die is given by Equation 3.21 above, where K is a die constant that depends only on geometry. Since the linear dimensions of the die are increased by the same scale factor as the screw dimensions, the following relationship exists between the scaled die constants:

$$K' = X^3 K \tag{3.32}$$

Also, the operating conditions and the fluid properties are the same in both extruder-feeders. Hence, the following ratios apply:

$$\frac{b'}{b} = \frac{C'}{C} = \frac{T_i'}{T_i} = \frac{N'}{N} = 1 \tag{3.33}$$

where:

b = Exponent for temperature dependence of the viscosity defined by $\mu = Ae^{-bT}$.
C = Heat capacity of fluid
T_i = Inlet melt temperature into metering section
N = Screw speed

Equation 1.2 of Part 1 may be rewritten in terms of the screw diameter if one makes use of the following relationships:

$$V_z = V\cos\theta = \pi DN \cos\theta \tag{3.34}$$

$$W = \frac{E\cos\theta}{m} - e = \frac{\pi(D-2c)\sin\theta}{m} - e \tag{3.35}$$

where:

W = channel width
E = pitch = π(D-2c) tan θ
m = no. of parallel channels = 1 for the case at hand

one obtains:

$$Q = \alpha N - \frac{\beta}{\mu}\left[\frac{\partial P}{\partial z}\right] \tag{3.36}$$

where

$$\alpha = \frac{\pi^2 D^2 H Sin\theta\, Cos\theta}{2}\left[1 - \frac{2c}{D} - \frac{em}{\pi D Sin\theta}\right] - \left[\frac{C}{H}\right]^2 F_D \tag{3.37}$$

and

$$\beta = \frac{\pi D H^3 Sin\theta}{12}\left[1 - \frac{2c}{D} - \frac{em}{\pi D Sin\theta}\right]\left[1 + \left[\frac{C}{H}\right]^3\left[\frac{W}{e}\right]\left[\frac{1}{Sin\theta\, Cos\theta}\right]\right] F_p$$

α and β are generally functions of the position coordinate (since H may vary) but Q is independent of z. Hence, one can write Equation 3.36 as:

$$\int_{P_o}^{P_z} dP = \mu N \int_o^2 \left[\frac{\alpha}{\beta}\right] dz - \mu Q \int_o^z \frac{1}{\beta}\, dz \tag{3.38}$$

After integration one obtains:

$$Q = A\,N - B\,\frac{\Delta P}{\mu} \tag{3.39}$$

where:

$$A = \frac{\int_o^z \left[\frac{\alpha}{\beta}\right] dz}{\int_o^z \left[\frac{1}{\beta}\right] dz} \quad ; \quad B = \frac{1}{\int_o^z \left[\frac{1}{\beta}\right] dz} \tag{3.40}$$

Examination of Equation 3.36 shows that the following scale relationship holds for the screw constants:

$$\begin{aligned} \epsilon' &= X^2\epsilon \quad (a) \\ \alpha' &= X^3\alpha \quad (b) \\ \beta' &= X^4\beta \quad (c) \end{aligned} \tag{3.41}$$

In Equation 3.41a ϵ is the error associated with modeling an annular drag flow by a parallel plate representation; where ϵ = 1 - Qcc/Qpp. McKelvey (1962) defines the following dimensionless groups:

$$N_1 = \frac{\beta}{KZ} \text{ and } N_2 = \frac{\alpha C}{NZ\mu_i b\epsilon} \tag{3.42}$$

and shows that in an adiabatic case the values of N_1 and N_2 are constant. From this it follows that:

$$Q' = X^3Q \quad ; \quad \Delta P' = \Delta P \quad ; \quad \text{and } \Delta T' = \Delta T \tag{3.43}$$

The total power required is (CQΔT + QΔP), so that

$$p' = X^3p \tag{3.44}$$

Equations 3.43 and 3.44 are thus the final equations for scale-up based on the assumptions set forth at the beginning. The adiabatic operation is most common since the area for heat transfer increases with the square of the diameter while the volumetric flow rate increases with the cube of the diameter. Hence, in large extruder-feeders one usually operates in an adiabatic mode since the heat generated by viscous dissipation cannot escape.

3.5.2 Extruder Scale-Up

Based on the scale-up theory previously presented and the viscous energy dissipation, energy balance, and power requirements data of 50 wt. % wood flour/50 wt. % vacuum bottom slurry, a scale-up was calculated which reflected a higher output rate at a screw speed of 100 rpm. The data are extrapolated to a higher screw speed from the laboratory extruder-feeder. Table 3.19 lists the design, operating and material variables for the extrusion of the 50 wt. % wood flour slurry in a 1.75-inch diameter extruder-feeder and a projected 16-inch diameter extruder-feeder.

3.5.2.1 Scaling for Increased RPM

The data for the 50 wt.% wood flour slurry showed that the output rate, Q, varied linearly with screw speed. The equation is: $Q = A\,N + B$, where $A = 9.5$. The 1.75-inch diameter extruder-feeder operated up to 60 RPM. If one extrapolates to 100 RPM then $Q_{100} = 830$ g/min. The output of a 16-inch extruder-feeder would be:

$$Q = \left(\frac{16}{1.75}\right)^3 \left(\frac{830g}{\min}\right) \left|\frac{60\min}{hr}\right| \left|\frac{1\,lb}{454g}\right| = 83{,}840\ \frac{lb}{hr} = 42\ tons/hr \qquad (3.45)$$

Since this is a 50/50 wt. % mixture, the rate of wood flour is:

$$Q_{WF} = (0.5)\ (42)\frac{tons}{hr} = 21\,tons/hr \qquad (3.46)$$

The number of extruder-feeders required for a 1,000 ton/day plant running with a 90% on stream factor is:

$$\frac{1{,}000\,tons}{day} \left| \frac{1 extruder\text{-}hr}{21 ton} \right| \frac{1 day}{24 hr} \left| \frac{1}{0.90} \right. = 2.2\ extruder\text{-}feeders \qquad (3.47)$$

Thus, with a safety factor of about 33%, thus 3 extruders would be sufficient.

3.5.2.2 Scale-Up of Drive Hp

The extrapolation of the 1.75-inch diameter extruder-feeder gives a drive horsepower of 6.2 Hp at 100 RPM. The drive motor required for the 16-inch diameter unit is thus:

Table 3.19. Operating and Design Variables for Scaling Up to a 16-Inch Diameter Extruder-Feeder.

Variable	Model (1.75-in. Dia.)	Scales Extruder (16-in. Dia.)
L/D	24:1	20:1
X	1.0	9.14
D (inches)	1.75	16
L	18.4	168
$\theta(^{o})$	17.7	17.7
H (inches)	0.0775	0.708
W (inches)	1.45	13.3
e (inches)	0.22	2.01
C.R.	3.8	3.8
c	0.001	0.091
$K(in^3)$	*	*
μ (poise)	15,000	15,000
b ($^{o}K^{-1}$)	*	*
T_1 (^{o}F)	364	364
N (rpm)	40	100
Q (lb/hr)	34.4	83,800
ΔP (psi)	2116	>3000
p (Hp)	5.23	4700 Hp

$$P' = \left[\frac{16}{1.75}\right]^3 6.2 = 4{,}700\ Hp \qquad (3.48)$$

Extruder manufacturers have quoted drives up to 6,000 Hp (two 3,000 Hp units). This indicates that the above scale-up is commercially feasible and is state-of-the-art.

3.6 PRELIMINARY ECONOMIC EVALUATION OF A COMMERCIAL EXTRUDER-FEEDER

3.6.1 Costs of Commercial Extruder-Feeders

A number of commercial companies were contacted in 1981 to estimate the cost of a large plasticating single screw extruder (> 10 inches diameter) together with any other information they could furnish concerning the required drive horsepower of the motor and the expected output rate. Manufacturers were to base their design and cost estimates on the extrusion of low-density polyethylene unit. The capacity/cost relationships were then converted in this economic analysis to capacity/cost figures for 50 and 60 wt. % WF/vacuum bottoms slurries. Additional cost data were also taken from the literature to determine a cost vs. size relationship. Table 3.20 summarizes the cost/size information.

In order to make a comparison it is convenient to take the cost and capacity ratios for each unit. The ratios are based on the values of the 1.5-inch diameter extruder-feeder which is about the smallest scale commercial machine that gives reliable scale-up data.

The cost of the extruder vs. the screw diameter is shown in Figure 3.29. It is seen that a straight line relationship is obtained on a log-log plot up to about 15-inch diameter. For larger diameters the slope of the plot increases. This indicates that in scale-up, the equipment becomes more expensive at a faster rate than the scale-up factor for the diameter. The deviation of the large diameter extruders from the straight line relationship indicates that the cost factor increases further because companies do not have the extensive engineering experience in building and engineering these large units.

A capacity ratio has been plotted vs. a cost ratio in Figure 3.30. The ratios are formed by using the values of the 1.5-inch extruder as a reference base. It is noted that again a straight line relationship is obtained. The slope in this case is 1.42. The data are more scattered since the output (capacity) is estimated from a number of sources and depends on the actual extruder application. In this case an optimistic output has been assumed, one which is not choked back by a severe die restriction. Since the slope is greater than 1.0, the relationship predicts that a larger unit is more economical on a capital investment basis. It also shows that for the very large units (D > 12 inches) this cost advantage declines due to a lack of engineering and construction experience.

Table 3.20. Cost/Capacity Data for Single Screw Extruder.

Extruder Diameter (inches)	Drive Motor HP	Estimated Output 16/hr	Cost of Extruder $	Cost Ratio	Capacity Ratio	Source of Data
1½	15*	130*	15,000	1	1	Davis Standard
2	20*	220*	21,600**	1.44	1.7	Welex
2½	50*	430*	25,000	1.67	3.3	Davis Standard
3½	153*	850*	56,000**	3.73	6.54	Plastics Technology, p 37 (Dec. 1972)
6	300*	2,500*	157,000**	1.05	1.92	Plastics Technology, p 27 (Feb. 1971)
10	700	10,000+	240,000	16	80+	Midland Ross Co.
10	600	10,000+	286,000	19.1	80+	HPM Corp.
12	---	20-25,000	400,000	26.7	192	Welex
20	---	30-40,000	1,200,000	80	308	Farrel Corp. phone conversation
23.6	6000	66,000	2,179,000	146	508	Berstoff
24	2,500	---	1,600,000	107	508†	Farrel Corp.

* Typical values for Midland Ross literature

--- No value given in quote

** Cost scaled to 1981 prices via CE plant cost index

\+ Estimated from capacity ratio vs cost ratio curve

† Assume output is the same as Berstoff Extruder

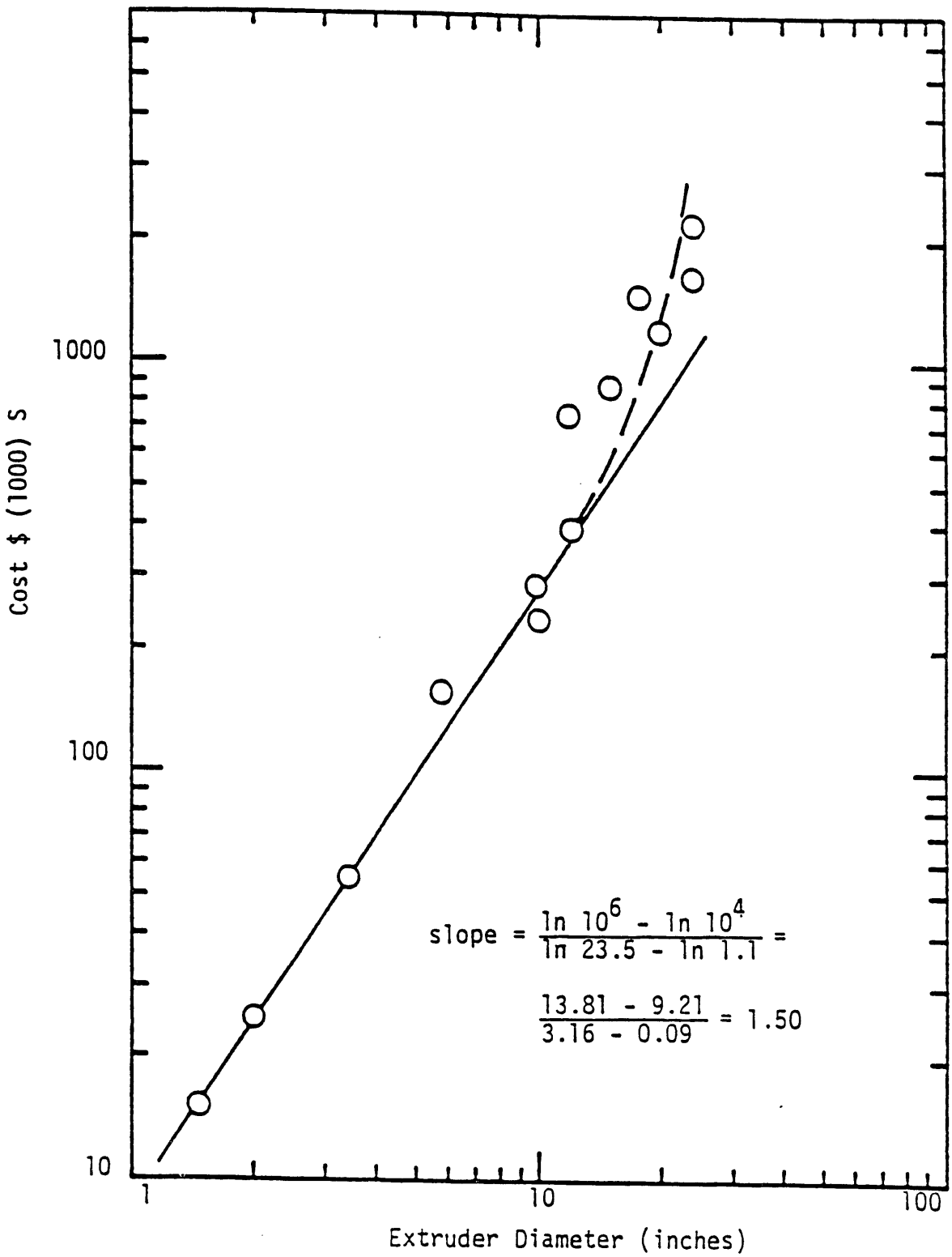

Figure 3.29. Extruder Cost versus Diameter of Screw.

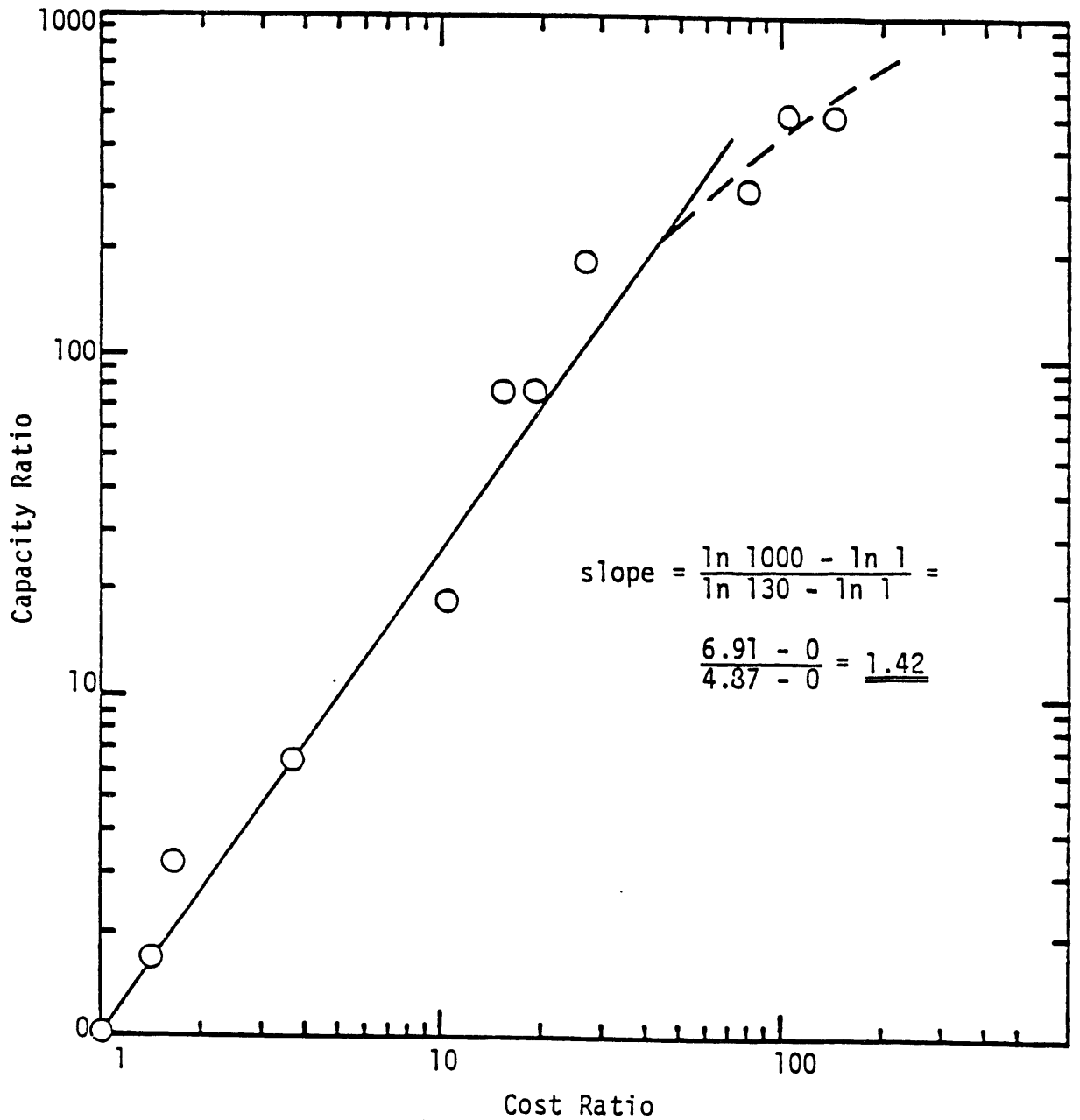

Figure 3.30 Capacity Ratio versus Cost Ratio for Single Screw Plasticating Extruders.

3.6.2 Material and Energy Balances for Commercial Extruder-Feeder

The economics of the extruder-feeder depends not only upon its value for pumping concentrated slurries, but also upon its energy savings by decreased recycle streams. This can be shown by making the appropriate energy balances for comparison to the original PERC process.

1. PERC Feeder-Preheater System:

   Case I -- Pumping 12 wt. % Wood Flour in oil.

2. Extruder-Feeder Preheater System:

   a. Case I -- Pumping 50 wt. % Wood Flour in Vacuum Bottoms.
   b. Case II -- Pumping 60 wt. % Wood Flour in Vacuum Bottoms.

The PERC system is used as the base case, using the longest (and last) run by Rust Engineering (1981) at Albany making TR12 oil. A yield of 52.4 pounds of crude oil (dry basis) per 100 pounds of dry wood flour feedstock was assumed. The extruder-feeder systems were calculated so that they can be compared with this system (Ecoenergy Associates 1980). This was done by calculating material balances to yield 52.4 pounds of crude oil product per unit of time. These mass balances result in the following materials feedstock comparison:

Reactor-Feeder Preheater-System	*Wood Flour Feedstock, lbs.*	*Wood Oil Product, lbs.*
PERC -- Case I	100.0	52.4
Extruder-Feeder -- Case I	91.3	52.4
Extruder-Feeder -- Case II	91.3	52.4

Equally important, the energy requirements of all of these systems have been calculated and found to differ greatly. On the basis of producing 52.4 pounds of crude wood oil (dry basis) it was found that the heating loads were as follows:

Feeder-Preheater-Reactor System	*Total Heating Load, Btu per 52.4 lb. Product*
PERC -- Case I	200,000
Extruder System -- Case I	91,000
Extruder System -- Case II	65,000

PERC - Case I (12 wt. % WF in Oil)

This case, as well as all other cases, assumes a reaction temperature of 670°F. This allows a comparison of heating loads, as summarized above. A product yield of 52.4 pounds of crude wood oil per 100 pounds of wood flour (dry basis) is assumed. Conversion per pass is taken as 95 wt. %. Catalyst used is 5 pounds Na_2CO_3 per 100 pounds fresh wood flour (WF) feedstock, on a dry basis. A minimum of 87 pounds of water is assumed for dissolving the sodium carbonate or being present as water is the reactor, per 100 pounds WF feed. Syngas is held at 64 pounds (2.88 pounds hydrogen plus 61.12 pounds carbon monoxide) per 100 pounds WF feed.

It is believable that the PERC feeder-preheater system is presented herein in its best possible mode by recycling a hot oil from the reactor let-down flash drum for slurrying with fresh wood flour. This conserves the heating of the recycle oil. It must be let-down in pressure to flash off the water, thus (a) providing a dry crude wood oil for product distillation, and (b) a dry oil for recycle. Thus, no indirect heat exchange area is required for cooling the reactor products to this extent. The penalty in terms of recycle oil heating load is that its temperature has been reduced from 670°F to about 540°F during this adiabatic flash. For simplicity, all heat losses and heats of reaction are ignored, since these enthalpies would be approximately the same in all cases presented here. The heating load for the preheater in this case is about 200,000 Btu per 100 WF feedstock.

Extruder-Feeder-Preheater System

Case I -- 50 wt. % WF/50 wt. % Vacuum Bottoms. This system has the inherent advantage of recycling the heavy ends of the crude wood oil product, which can be broken down into the more useful lighter oils. Exxon and others have now proved that this theoretical additional yield is a reality in coal liquefaction. The additional yield per pass for biomass liquefaction has not been proven as yet, but it is assumed to be five wt. % of the vacuum bottoms per pass. Thus, for this case of 100 pounds of vacuum bottoms per 100 pounds fresh wood flour, the yield of crude wood oil (dry basis) would be 52.4 pounds plus 0.05 (100) pounds WF feedstock. This inherently assumes that five pounds of the 52.4 pounds of crude wood oil are *"vacuum bottoms"* capable of being upgraded into a lighter oil.

This Case I of 50 wt. % WF slurry is the lower end of the proven operating range. The heating load of the preheater for extruder-feeder Case I is about 91,000 Btu per 52.4 pounds of crude wood oil product. The system requires about 91.3 pounds of wood flour feedstock for this amount of product compared with 100 lb WF feedstock for the PERC System and 152 lb WF feedstock for the LBL system. The lower requirement for wood flour feedstock (and hence higher product yield) is due to the inherent advantage of the system being theoretically capable of processing a portion of the vacuum bottoms into the more desirable lighter crude wood oil product. The extremely lower preheater load is due mainly to (a) the inherent ability of the extruder-feeder system to recycle a hot reactor effluent stream for dilution of wood flour feedstock while still under pressure (only system capable of pumping wood flour into pressure system prior to dilution), and d(b) the inherent ability of the extruder-feeder system of feeding

sodium carbonate catalyst into the system without water, and hence maintaining proper water concentration in the reactor by other means without heating water from ambient temperature to 670°F under pressure. The specific heat of water at 670°F (reasonably close to its critical temperature) and under pressure of 3,000 psi is abnormally high, and thus causes high preheater energy requirements.

Extruder-Feeder-Preheater-Reactor System

Case II - 60 wt. % WF/40 wt. % Vacuum Bottom. This case has assumed the same premises of the above extruder-feeder Case I, but is close to the upper limit of wood flour concentration that can be pumped into a 3,000 psi pressure system while still maintaining good operability. The heating load for the preheater of extruder-feeder Case II is about 65,000 Btu per 52.4 pounds of crude wood oil product. This is a further savings in process energy over all other cases. Furthermore, the total horsepower for pumping these 60 wt.% slurries into a 3,000 psi pressure system for a 3,000 bbl/day crude wood oil plant is reduced for 10,000 Hp to 8,000 Hp. However, the pumping of a 60 wt. % wood flour system may be beyond the optimum economic concentration. The viscous dissipation (and hence horsepower) appears to be increasing exponentially in this range. Secondly, this concentration results in a slurry so *"stiff"* that at times the die valve or the metering section of the screw is plugged. Thus, the operability of a 60 wt. % wood flour slurry for a commercial plant is questionable, and not yet proven. Probably, a slurry concentration of about 55 wt. % wood flour will prove to be optimum.

3.6.3 Capital Costs and Energy Savings for a 3,000 Barrel Per Day Crude Wood Oil Commercial Plant

It became evident early in the study that it is necessary to consider the entire extruder-feeder-preheater-reactor system in order to see the full potentials of the extruder-feeder. It is called a system rather than a process, because it is only part of a process. In addition to detailed information on the extruder-feeder-preheater-reactor system, a direct comparison with the corresponding PERC system has been made.

In summary, it has been shown that the extruder-feeder-preheater-reactor system has the following technical and economic advantages:

1. It reduces the heating load on the liquefaction preheater and rector to 65,000 to 91,000 Btu per unit of 52.4 pounds crude wood oil product, compared with 160,000 to 200,000 for the PERC system and 350,000 Btu per 52.4 pounds product for the LBL system. This means that only a small fraction of the fuel value energy of the feedstock wood flour is needed for this critical heating load.

2. The estimated capital investment for the extruder-feeder-preheater-reactor system for a 3,000 barrel per day crude wood oil commercial plant is about $12,000,000 compared with $14,000,000 for the PERC system and $21,840,000 for the LBL system. There is a slightly higher capital cost for the extruder-feeders, but this is more than compensated for by a much lower capital investment for the necessary gas-fired preheater furnaces.

Also, in summary, the technical feasibility and operability of the extruder-feeder has now been proven as follows:

1. The vacuum bottoms from the Albany fractionator have been shown to be an excellent carrier for the wood flour feedstock.

2. The viscous dissipation of the vacuum bottoms (internal friction) has been shown to be some 20- to 30-fold less than viscous plastics, and hence requires less than half of the horsepower (Hp) needed for low-density polyethylene. In fact, only about one-fourth as much Hp is needed for pumping the wood flour slurry into a 3,000 psi pressure reactor and the other one-fourth is used to preheat the slurry from 80°F to 300°F.

3. Due to the viscous dissipation of 50 and 60 wt. % WF/vacuum bottom slurries being so much less than plastics, the extruder-feeder can be operated at a much higher screw rpm. This means that a given extruder-feeder can have a much higher capacity for a given capital investment. Only a small fraction of this potential has been scaled into the commercial units specified in this report.

4. The extruder-feeder-preheater-reactor system is the only known system which has the potential to circulate hot reactor effluent back to the feedstock without reducing pressure, because it does not need a low-viscosity oil to dilute the wood flour slurry for proper pumping.

5. The extruder-feeder has proven to have much flexibility, both in design factors and operating factors. Design factors include extruder-feeder size (sizes available up to 24-inch diameter), screw compression, screw speed, temperature profile, slurry concentration and carrier oil viscosity. In other words, a choice can be made of several different combinations of these factors.

6. The extruder-feeder-preheater-reactor system is the only known system that can recycle the heavy ends of biomass liquefaction products, and thus offer the potential of converting these ends to a lighter, less-viscous, more-useful product. Exxon has recently discovered that this is advantageous in coal liquefaction, resulting in higher overall yields of light oils.

7. The operability of the extruder-feeder has proven to be very reliable. There is no plugging from even concentrated slurries under lined-out operations, and outlet pressures and temperatures can be closely controlled. Thus, this system appears to be well-adapted for a continuous process, especially where temperature and residence time should be closely controlled.

It was decided that the best way to evaluate the extruder-feeder system, and to compare it directly with the corresponding PERC system would be to (a) calculate material and energy balances for both systems, and (b) project these to a commercial size plant capable of producing 3,000 barrels per day of crude wood oil products.

A proposed commercial plant for 3,000 bbl/day crude wood oil was selected, because it is an economic size for a regional, wooded-area, requiring about a 1,000 tons per day of dry wood for liquefaction. This also allowed the use of the capital cost data for a 1,000 TPD dry wood facility reported by Econergy Associates, *"A Technical and Economic Assessment of PERC and LBL Wood-to-Oil Conversion Processes,"* March, (1980). The wood flour requirements for such a plant were specified as outlined in the report by SRI International, *"Assessment of the Biomass Liquefaction Facility in Albany, Oregon, and Related Programs,"* June, 1980, as follows:

> "Needed about 75 percent wood for liquefaction and 25 percent for (a) gasification for syngas, and (b) fuel in the plant. Thus, need 1025 T/D wood (dry basis) for liquefaction at 57.4% yield (extruder-feeder system) to give 587.2 T/D crude wood oil, which at 5.1 T/bbl, gives 3,000 bbl/day. Need 327 T/D for gasification and fuel. Total wood needed: 1,350 tons/day (dry basis)."

Rust Engineering in TR12 run at Albany, Oregon (reported as Test Run Number 12, *"An Investigation of Liquefaction of Douglas Fir by a Process Development at the Pittsburgh Energy Research Center as Modified by the Rust Engineering Company,"* The Rust Engineering Company, July 1981) successfully produced considerable wood oil of 1.12 specific gravity and 14,840 heating value.

Thus, the total heating value of the 5878.2 T/D of crude wood oil is 17,428 x 10^6 Btu per day. This number must be kept in mind so that any given wood liquefaction process to fuels does not become so complicated that it uses an excessive amount of this energy in its own operations. It should be noted that the wood feedstock to the plant would be 1,350 T/D with a heating value of about 8,900 Btu per pound, or a total energy content of about 24,030 x 10^6 Btu per day.

These critical preheater loads can be expressed in another fashion, namely, in terms of a percentage of the heating of the crude wood oil being made. For a 3,000 bbl/day wood oil plant, generating a product having 17,428 x 10^6 But/day, we find the following:

System	Dry Wood for Liquefaction, T/D	Preheater Btu/Day x 10^6	Load Percentage Wood Oil Energy
PERC-12 wt. % slurry	1120	4,092	23.5
Extruder-Feeder, 50 wt. % S1	1023	1,862	10.7
Extruder-Feeder, 60 wt. % S1	1023	1,330	7.6

It should be noted that the extruder-feeder also serves as part of the preheater. Experimental data show that a practical amount of preheating in the extruder would be from 80°F to 300°F. On this basis, the extruder-feeder would handle about 20 percent of the overall preheater load, and reduce the above preheater load as shown below.

Extruder System	Mode of Operation	
	50 wt. % Slurry	60 wt. % Slurry
Total Preheater Load, Btu/Dx10^6	1,862	1,330
Extruder Preheating, Btu/Dx10^6	327	266
Net Preheater Load, Btu/Dx10^6	1,535	1,064
Percentage of Wood Oil Energy	8.8%	6.1%

The next most important factor would be a comparison of capital investments for the various feeder-preheater-reactor systems. There appears to be a slight capital cost savings for the extruder-feeder, as follows:

Feeder-Preheater-Reactor System	Estimated Capital Investment, Installed*
PERC-12 wt. % Slurry	$15,540,000
Extruder-50 wt. % Slurry	12,090,000
Extruder-60 wt. % Slurry	11,490,000
*July 1981 Dollars	

However, it should be quickly pointed out that this is a rough, preliminary cost estimate, based in turn on a preliminary process design, and must be checked by a more thorough engineering analysis.

As predicted from the earlier work on model liquid carriers for the wood flour slurries, the viscous dissipation for wood flour/vacuum bottoms slurries is an order of magnitude lower than for conventional plastics, such as low-density polyethylene (LDPE). The viscous dissipation (represented by the Hp per Kg of slurry, measured on a Brabender Torque Rheometer Mixing Head), even for LDPE diluted with 25 weight percent wax, is still 22.8 Hp per Kg, compared with 2.55 Hp/Kg for 60 wt. % wood flour/40 wt. % vacuum bottoms.

The significance of these results are two-fold, namely, (a) the pumping horsepower is much less, and, equally important, (b) the extruder-feeder can be run at a much higher rpm without wasting power by excessive frictional heat energy.

Another critical aspect of this economic analysis of the extruder-feeder was obtaining realistic, current data on commercial extruders. This was done by contacting all extruder manufacturers in the United States that market extruders larger than 10-inches in diameter (12 manufacturers in all), and they were all very cooperative.

The scale-up of the experimental extruder data on 50 and 60 wt. % wood flour/vacuum bottoms slurries to commercial size units resulted in a reasonable number of extruder-feeders and at a reasonable cost for the projected 3,000 bbl per day crude wood oil plant. In fact, based on the fact that commercial extruders are available up to 24-inch diameter, it would be possible to handle the entire plant feedstock with one 21-inch diameter extruder-feeder. It would be equipped with a 10,000 Hp drive for handling 40 wt. % slurries, or 8,000 Hp drive for handling 60 wt. % wood flour slurries. Such drives could be either electric motor or steam turbine. Alternatively, one could handle the projected plant feedstock with either 2.2 extruders (16-inch diameter, same Hp) or 4 extruders (13-inch diameter, same Hp). The latter case would probably be preferable for the first commercial plant, using 2,500 Hp motors on each unit for handling any slurry concentrations in the range of 50 to 60 wt. % wood flour/vacuum bottoms.

The long-range significance of these findings is that as time progresses, and if biomass liquefaction plants larger than 3,000 bbl per day crude wood oil can be justified, then the economy of scale can be further utilized in the projected extruder-feeder-preheater-reactor system. It is visualized that eventually very large extruder-feeders would be designed specifically for these plants, being at least 24-inch in diameter and running at screw speeds higher than the 100 rpm specified in this report. Thus, there would be very high through-puts per unit of capital investment.

It should be emphasized that this preliminary economic evaluation was made in mid-1981, in justification for constructing an extruder-feeder biomass liquefaction unit at the University of Arizona. The DOE funding on this project was terminated effective October 1, 1988, before an up-to-date economic evaluation could be made based on the additional research between 1981 and 1988.

3.7 NOMENCLATURE

A	=	constant
b	=	Exponent for temperature dependence of the viscosity defined by $\mu = Ae^{-bT}$.
B	=	Channel depth and constant
C	=	Clearance between screw flgiht and barrel and heat capacity
C_p	=	Heat capacity
D	=	Diameter of screw
d	=	Width of gap and barrel diameter
D_b	=	Inside barrel diameter
e	=	Width of screw flights, perpendicular to the flights, cm
E	=	pitch = π(D-2c) tan θ
F_D	=	Drag flow shape factor
F_p	=	Pressure flow shape factor
H	=	Heat loss in extruder-feeder from radiation and conduction and channel depth
h	=	Heat transfer coefficient, cal/cm^2 °C sec
H_L	=	heat loss from radiation and conduction
k	=	Thermal conductivity
K_b	=	Viscosity at temperature, T_b
K_d	=	Die and valve characteristics
L	=	Length of screw
m	=	no. of parallel channels = 1 for the case at hand
N	=	Frequency of screw rotation, rpm
n	=	Flow index of power law fluid
p	=	Number of flights in parallel
P	=	pressure rise in extruder-feeder
P_w	=	mechanical power to screw
q	=	electric power to heaters
Q	=	Volumetric extrusion rate
Q_D	=	Drag flow
Q_L	=	Leakage flow
Q_p	=	Pressure flow
R	=	1.987 cal/g mol °K
S_R	=	Rotor rpm, 1/min.
t	=	Time, min.
T	=	Temperature
T(t)	=	Torque, m•kg
T_1	=	Intermediate temperature in Zone L_1
T_2	=	Output temperature
T_b	=	Temperature of barrel
T_i	=	Inlet melt temperature into metering section
To	=	Feed temperature
U	=	Velocity vector

U_z	=	Velocity
V	=	Maximum velocity of outer cylinder (inner cylinder is stationary)
V_{bz}	=	Velocity component of V_b in the down channel direction, cm/sec
W	=	total work, joule and width of channel
x	=	Coordinate in gap
Z	=	Rectangular coordinate (down channel direction) and mechanical power of screw
$\vec{\phi}_v$	=	Volumetric rate of conversion of mechanical energy into heat
$\underline{E}_T$	=	Activation energy
$\bar{\theta}$	=	Average helix angle
β	=	Modified Brinkman Number
δ_f	=	Flight clearance, cm.
η	=	Bulk viscosity
η'	=	Viscosity in the clearance
θ	=	Helix angle, radians
θ_b	=	helix angle at the barrel surface
μ	=	viscosity, dyne x sec/cm^2
μ_f	-	Viscosity in the flight clearance, dyne sec/cm^2
ρ	=	melt density
ψ	=	$(T_1-T_0)(T_2-T_0)$

3.8 REFERENCES FOR PART 3

Tadmar, Z. and I. Klein, "Engineering Principles of Plasticating Extrusion," Reinhold, New York, NY (1970).

McKelvey, J.M., "Polymer Processing," John Wiley & Sons, New York, NY (1962).

Middleman, S., "Fundamentals of Polymer Processing," McGraw-Hill, New York, NY (1977).

Bird, R.B., W.E. Stewart, and E.N. Lightfoot, "Transport Phenomena," John Wiley & Sons, Inc., New York, NY (1960).

Yang, L.C., "Rheology of Sawdust Filled Polymer," MS Thesis, Department of Plastics Engineering, University of Lowell (1981).

Glanvill, A., "The Plastics Engineer's Data Book," Industrial Press, New York, NY (1971).

Schenkel, G., "Plastics Extrusion Technology and Theory," American Elsevier (1966).

Pearson, J.R.A., "Mechanical Principles of Polymer Melt Processing," Pergamon Press (1966).

Harmann, D.V., and J.M. Harper, "Modeling of Forming Foods Extruder," J. Food Sci., 39, 1099 (1974).

Harmann, D.V., and J.M. Harper, "Effects of Extruder Geometry on Torque and Flow," Trans. ASAE, 1175 (1975).

Chung, C.I., "Frictional Behavior of Solid Polymers on a Metal Surface at Processing Conditions," Polymer Eng. Sci., 17, 1 (January 1977).

Mount, E.M., and C.I. Chung, "Melting Behavior of Solid Polymers on a Metal Surface at Processing Conditions," Polymer Eng. Sci., 18, 711 (July 1978).

Rust Engineering Company, Report on, "An Investigation of Liquefaction of Douglas Fir by a Process Developed at the Pittsburgh Energy Research Center as Modified by the Rust Engineering Company," (1981).

Schott, N.R., "Rheological Characteristics of LDPE and AC6 PE Mixtures by Extrusion Plastomer," A report submitted to the University of Arizona, Department of Chemical Engineering, Tucson, Arizona (1981).

Squires, P.H., "Extruding, Heating and Cooling Systems," Society of Plastics Engineers, 18th Annual Technical Conference, 10, p. 8 (1962).

Ecoenergy Associates, "A Technical and Economic Assessment of PERC and LBL Wood-to-Oil Conversion Processes," Contract No. 4-L40-0742M-1 (1980).

SRI International, "Assessment of the Biomass Liquefaction Facility in Albany, Oregon and Related Progresses Report," (1980).

APPENDIX A

EXPERIMENTAL DATA FOR WOOD FLOUR SLURRIES USING PRODEX EXTRUDER-FEEDER

APPENDIX A

EXPERIMENTAL DATA FOR WOOD FLOUR SLURRIES USING PRODEX EXTRUDER-FEEDER

The detailed data from 22 experimental runs upon the Prodex Extruder-Feeder are shown here in Appendix A. The feedstocks covered the full range of polyethylene *"model compounds,"* followed by various slurry concentrations of wood flour in either a specific polyethylene or in an Albany vacuum bottom as the fluid carrier. Detailed temperature data were acquired and printed out by the data acquisition system. Pressure generated was controlled by the setting of the valve on the outlet of the extruder-feeder.

Table A1. 100% LDPE (regrind), die removed.

RPM	Power	T_1	T_2	T_3	T_4	T_5	T_6	T_7	T_8	T_9	T_{b1}	T_{b2}	T_{b3}	T_{b4}	T_{b5}	T_{b6}	P_1	P_2	P_3	P_4	P_{die}	Output
l/min	watts	- - - - - - - - - - - - - - - - - - °F - - - - - - - - - - - - - - - - - -															- - - - - psi - - - -					g/min
	2200	329	344	372	317	377	331	176	86	84							52	339	427			145
40	2176	326	341	362	313	368	319	172	85	79	280	320	305	280	260	215	45	265	291	100		132
	2145	324	338	359	309	360	303	169	83	77							39	161	97			125
	3080	323	338	356	307	355	293	164	84	79							54	331	718	1340		195
50	2652	321	336	354	302	348	285	162	82	77	290	270	245	250	235	195	47	288	454	726		188
	2337	319	332	351	298	340	279	160	79	75							29	240	255	0		180
	4152	320	335	351	297	338	283	177	86	81							61	428	1071	1620		250
60	3672	319	334	351	296	337	282	161	84	78	300	315	290	250	215	210	61	416	1016	1500		245
	3287	317	332	350	296	336	280	165	83	76							61	404	960	1420		240
	4779	319	333	350	293	332	284	206	84	79							59	525	1455	2350		315
70	4420	318	331	348	291	330	282	295	82	77	300	300	280	265	250	235	58	495	1342	2203		312
	3957	315	330	345	287	326	281	183	81	75							54	449	1237	2060		310
	3998	319	334	348	291	327	288	207	85	79							64	520	1165	1920		335
80	3642	317	331	346	289	324	286	199	84	78	290	275	285	250	235	215	59	486	785	1137		330
	3160	314	329	343	287	321	283	192	82	77							54	424	430	500		325
	5040	318	335	349	289	323	289	186	87	79							66	476	996	1320		265
90	4779	316	334	347	288	320	286	182	85	78	300	320	290	250	235	215	55	450	814	1220		263
	4567	315	331	344	288	319	282	177	83	76							44	425	649	1120		260
	4714	317	336	352	288	319	291	174	84	79							61	482	909	1000		385
100	4473	316	335	349	288	318	287	172	82	78	305	310	290	250	240	210	58	468	650	727		378
	4000	315	334	347	287	317	284	170	81	75							56	443	449	500		375

Table A2. 100% LDPE (regrind), die removed.

RPM	Power	T_1	T_2	T_3	T_4	T_5	T_6	T_7	T_8	T_9	T_{b1}	T_{b2}	T_{b3}	T_{b4}	T_{b5}	T_{b6}	P_1	P_2	P_3	P_4	P_{die}	Output
l/min	watts	°F															psi					g/min
		329	344	363	317	377	330	176									54	339	427			
40	2169	326	341	362	313	368	319	172	85	78							47	249	247			125
		324	338	359	310	360	303	169									39	161	81			125
		322	337	356	307	355	293	163									54	331	718			195
50	2652	321	336	354	302	348	285	162	82	77							47	280	454			188
		319	332	351	298	340	280	160									29	240	253			180
60	3672	319	334	351	296	337	282	171	84	78							55	400	976	1238		245
		319	332	348	293	331	282	183	83	78							59	525	1445			315
70	4421	318	331	348	292	330	283	195	82	77							58	495	1344	2133		313
		315	330	345	289	326	283	206	81	77							54	449	1071			310
		319	334	348	290	327	288	204									64	520	1163			335
80	3642	316	331	346	289	324	286	199	84	77							59	486	785	1333		330
		316	324	347	288	322	285	192									54	424	430			325
		317	335	349	289	322	289	186									66	476	996		265	
90	4849	317	334	347	289	321	287	183	85	78							58	468	845	1220		265
		316	333	347	288	319	285	177									44	425	649			265
		317	336	352	288	319	291	174									61	484	909			
100	4630	316	335	349	288	318	287	173	83	78							59	468	650			375
		315	334	347	287	317	284	170									56	440	531			

Table A3. 100% LDPE (pellets), die valve partially open (10-1/2 turns).

RPM	Power	T_1	T_2	T_3	T_4	T_5	T_6	T_7	T_8	T_9	T_{b1}	T_{b2}	T_{b3}	T_{b4}	T_{b5}	T_{b6}	P_1	P_2	P_3	P_4	P_{die}	Output
l/min	watts	- - - - - - - - - - - - - - - - - - °F - - - - - - - - - - - - - - - - - -															- - - - - - psi - - - -					g/min
	3084	481	493	582	516	486	506	317									2253	2669	3592	4300		229
40	2757	448	464	459	487	462	462	274	94.0	92.9	411	425	410	460	400	340	1682	2207	3076	3867		200
	2588	413	445	519	466	444	420	221									607	1251	2562	3650		192
	3182	492	474	534	499	489	462	286									2117	2500	3386	4070		241
50	3109	489	461	510	483	472	429	275	87.5	86.0	365	410	419	388	345	282	2065	2440	3284	4027		238
	3023	486	449	488	468	446	399	266									2009	2376	3177	4000		235
	3832	478	432	459	437	450	358	259									2385	2713	3543	4290		273
60	3810	473	425	448	424	435	346	256	95.3	93.1	365	377	352	325	300	268	2362	2694	3486	4093		264
	3787	468	417	437	412	421	335	253									2328	2709	3431	3990		255
	4698	464	411	429	403	410	330	258									2736	3002	3984	4500		315
70	4677	460	407	424	397	403	328	256	92.7	87.7	331	341	337	305	285	257	2675	2941	3880	4470		308
	4650	455	403	420	392	397	326	254									2616	2867	3776	4430		306
	5434	454	400	417	389	393	327	263	97.5	96.2							2942	3193	4215	4850		358
80	5400	453	399	416	388	391	326	262	95.0	92.8	316	325	318	293	288	258	2937	3178	4200	4795		354
	5374	452	398	415	388	390	326	260	92.5	89.4							2932	3163	4185	4740		349
	5726	450	394	413	388	387	334	271			320	343	335	308	300	295	3050	3330	4367	5050		378
86	5712	449	393	413	387	387	332	269	94.1	92.7	320	334	317	306	298	270	2346	3214	4172	4950		368
	5701	449	393	412	386	386	331	268			320	325	300	305	297	265	1642	3011	3890	4900		362

Table A4. 100% LDPE (regrind), die valve partially open (10-1/2 turns).

RPM	Power	T_1	T_2	T_3	T_4	T_5	T_6	T_7	T_8	T_9	T_{b1}	T_{b2}	T_{b3}	T_{b4}	T_{b5}	T_{b6}	P_1	P_2	P_3	P_4	P_{die}	Output
l/min	watts	- - - - - - - - - - - - - - - - - - °F - - - - - - - - - - - - - - - - - -															- - - - - psi - - - - -					g/min
	3532	394	350	371	358	369	305	233	88								4678	4886	4873	4530		181
50	3483	394	349	370	356	364	305	233	87	303	304	311	270	250	234		4667	4872	4840	4495		173
	3452	393	348	369	354	379	304	232	86								4657	4860	4816	4470		169
	4007	399	351	372	355	358	308	241	89								4965	5100	5167	4680		217
60	3988	397	350	370	353	357	304	239	88	291	311	301	273	255	237		4947	5083	5106	4663		213
	3951	395	349	368	351	357	297	237	87								4933	5067	5073	4630		209
	4568	408	355	378	360	361	313	247	85								5132	5267	5600	4830		250
70	4502	408	354	377	359	359	312	245	84	311	312	301	277	268	247		5108	5258	5443	4825		240
	4436	407	352	376	357	357	310	243	82								5083	5250	5286	4820		228
	3433	368	346	369	342	326	274	226	88								5078	4984	4876	4410		282
80	4048	365	334	350	322	312	262	210	87	279	270	252	230	219	214		3582	3689	3352	3024		258
	4760	362	328	340	312	305	253	189	86								2504	2609	2151	1850		227
		359	325	337	315	312	278	238	86								4001	4097	3844	3440		313
90	4381	356	324	335	310	310	272	228	86	276	260	250	235	221	215		3852	3960	3723	3387		303
		352	322	331	299	304	270	224	86								3742	3840	3623	3330		292

Table A5. 25% LDPE/75% AC-6 (regrind), heaters off, die valve fully open.

RPM	Power	T_1	T_2	T_3	T_4	T_5	T_6	T_7	T_8	T_9	T_{b1}	T_{b2}	T_{b3}	T_{b4}	T_{b5}	T_{b6}	P_1	P_2	P_3	P_4	P_{die}	Output
l/min	watts	°F															psi					g/min
	2111	405	364	380	319	371	355	162			365	375	360	345	295	230	31	90	14			176
40	1910	402	358	367	308	360	324	154			352	360	345	318	272	220	30	90	12			176
	1518	400	351	354	292	346	290	147			340	345	330	290	250	210	29	89	11			175
		400	344	339	279	319	255	166			330	325	290	250	225	200	60	40	84	13		221
60	2317	398	342	338	372	306	250	154			318	310	272	240	218	198	60	38	77	10		205
		395	340	336	264	294	244	193			305	295	255	230	210	195	60	37	70	8		195
	2472	382	332	326	247	272	236	167	87	78							137	76	8			231
80	2472	377	325	314	238	262	234	166	86	77	295	260	240	220	205	195	134	76	8			223
	2471	372	318	309	230	252	232	166	86	76							130	75	8			215
	2606	361	301	290	216	237	229	170	85	77							42	71	13			290
100	2600	357	294	282	210	232	228	169	85	76	280	235	215	210	200	195	41	68	12			283
	2594	353	288	273	204	227	228	168	85	75							40	66	12			276
120	2841	340	269	255	194	218	226	171	84	76	245	220	205	210	200	195	41	66	13			315

Table A6. 25% LDPE/75% AC-6 (regrind), heaters off, die valve partially open.

RPM	Power	T_1	T_2	T_3	T_4	T_5	T_6	T_7	T_8	T_9	T_{b1}	T_{b2}	T_{b3}	T_{b4}	T_{b5}	T_{b6}	P_1	P_2	P_3	P_4	P_{die}	Output
l/min	watts	- - - - - - - - - - - - - - - - - - °F - - - - - - - - - - - - - - - - - -															- - - - - psi - - - - -					g/min
	2232	317	343	394	338	387	429	184	89	75							2970	2982	3025	2230		286
40	2212	306	338	380	332	384	415	178	87	73							2463	2656	2508	2230		286
	2194	295	339	368	328	381	403	172	86	71							2139	2568	2192	2230		286
	2233	339	332	361	325	385	396	191	89	75							2062	2432	2105	1600		176
50	2229	331	330	353	320	379	387	188	88	73	300	345	360	340	290	240	1770	2110	1805	1568		168
	2225	323	329	348	317	368	380	184	87	72							1659	1983	1672	1536		160
	2262	346	323	336	308	378	365	193	88	74							1450	1793	1454			
60	2258	344	323	334	306	376	352	194	88	73							1409	1733	1406	1290		115
	2254	341	323	332	305	374	359	194	87	72							1368	1673	1359			
	2281	355	321	327	300	369	351	194	88	74							1285	1580	1256	1080		74
70	2274	352	320	326	298	366	348	194	88	74	275	375	340	325	275	240	1200	1485	1186	1055		64
	2268	349	320	324	297	364	344	194	88	73							1115	1390	1116	1030		55
80	2295	361	321	324	297	364	344	194	88	73							1031	1332	1021	840		33
120	2468	373	317	313	283	345	325	197	89	77	255	305	310	280	270	230	784	1040	774	630		0

Table A7. 25% LDPE/75% AC-6 (regrind twice), die valve partially open (10-1/2 turns).

RPM	Power	T_1	T_2	T_3	T_4	T_5	T_6	T_7	T_8	T_9	T_{b1}	T_{b2}	T_{b3}	T_{b4}	T_{b5}	T_{b6}	P_1	P_2	P_3	P_4	P_{die}	Output
l/min	watts	- - - - - - - - - - - - - - - - - - °F - - - - - - - - - - - - - - - - - -															- - - - - psi - - - - -					g/min
	2155	368	318	307	240	266	226	167	88	80	285	275	235	225	195	185	250	455	350			131
40	2120	363	312	301	234	259	224	166	88	80	265	250	222	210	190	180	230	420	327	430		127
	2084	358	307	295	228	252	221	165	88	80	245	225	210	195	185	175	210	386	304			123
	2255	412	367	378	321	380	314	180	89	80	325	340	295	270	235	200	168	390	283	160		140
60	2224	411	360	364	305	358	268	178	88	78	290	325	280	258	225	200	86	250	207	160		137
	2181	410	352	351	287	335	192	176	87	77	255	310	265	245	215	200	10	78	110	160		136
80	2682	351	295	284	216	240	218	166	87	82	270	235	210	190	185	175	463	636	540	575		81
	2799	343	282	269	200	229	217	174	89	83	250	225	200	190	185	175	529	709	599	430		246
100	2764	338	275	261	196	225	217	172	89	82	242	218	200	190	185	175	421	614	492	385		221
	2728	334	268	253	193	221	217	170	89	80	235	210	200	190	185	175	313	520	386	340		206
																						290
120	2965	325	253	238	188	215	218	177	89	83							501	704	532	280		273
																						255
																				160		296
140											225	205	200	185	190	175				105		273
																				50		252
	3501	301	235	220	185	211	223	184	90	84							1135	1366	1162			270
160	3480	296	234	219	184	210	222	184	90	84	210	195	195	195	185	185	1036	1237	1046	30		244
	3460	292	233	218	184	210	220	183	89	83							938	1107	930			196

Table A8. 40% WF/15% LDPE/45% AC-6, regrind twice, die removed.

RPM	Power	T_1	T_2	T_3	T_4	T_5	T_6	T_7	T_8	T_9	T_{b1}	T_{b2}	T_{b3}	T_{b4}	T_{b5}	T_{b6}	P_1	P_2	P_3	P_4	P_{die}	Output
l/min	watts	- - - - - - - - - - - - - - - - - - °F - - - - - - - - - - - - - - - - - -															- - - - - psi - - - -					g/min
		351	295	305	259	295	255	166										142	33	10		145
40	1682	348	291	300	255	291	250	164	85	81	275	285	265	220	210	200	62	142	26	10		141
		346	287	296	250	286	245	162										142	16	10		137
	2336	344	279	288	241	275	240	176	84									142	15	10		199
60	2323	344	275	284	237	270	238	173	83		250	255	240	220	205	200	52	140	14	10		198
	2310	343	271	280	233	264	237	170	82									139	13	10		196
	2549	341	257	271	223	254	236	185									54	137	14	10		260
80	2538	340	254	265	218	249	236	182	85	84	245	245	225	215	190	185	52	135	14	10		248
	2527	339	252	258	213	244	236	180									51	133	14	10		235
	2782	337	244	248	205	236	235	189	86	84							52	131	15	10		290
100	2750	336	240	244	202	233	234	188	86	84	225	220	215	210	210	200	51	130	15	10		285
	2717	336	236	240	199	230	234	187	85	84							50	129	15	10		280
	3444	355	229	232	195	226	239	196	86	85							51	125	125	10		330
120	3369	334	228	230	195	225	237	194	86	83	220	220	220	210	210	190	48	120	22	10		328
	3349	333	227	227	195	224	235	192	85	81							46	116	18	10		325

Table A9. 40% WF/15% LDPE/45% AC-6 (regrind), die valve partially open.

RPM	Power	T_1	T_2	T_3	T_4	T_5	T_6	T_7	T_8	T_9	T_{b1}	T_{b2}	T_{b3}	T_{b4}	T_{b5}	T_{b6}	P_1	P_2	P_3	P_4	P_{die}	Output
l/min	watts	- - - - - - - - - - - - - - - - - - °F - - - - - - - - - - - - - - - - - -															- - - - - psi - - - - -					g/min
	2187	268	292	298	261	298	268	198	87	75							4964	4797	4678	3810		407
50	2169	268	287	293	258	295	267	195	86	75	275	265	270	255	240	220	4921	4792	4483	3783		405
	2141	267	282	288	256	293	266	191	86	75							4873	4783	4352	3770		400
	2379	266	279	283	252	290	268	201	87	73							4823	4767	4183	3590		367
60	2367	266	278	282	252	289	268	200	86	72	265	270	265	235	230	200	4796	4749	4154	3539		358
	2355	265	276	280	251	288	268	199	86	72							4768	4731	4124	3488		350
	2718	266	274	280	251	288	273	208	87	76							4740	4721	4078	3380		315
80	2712	262	273	280	251	288	272	207	87	76	250	290	270	260	240	225	4726	4718	4053	3345		310
	2705	258	272	279	251	288	270	206	87	75							4711	4716	4028	3310		304
	3119	262	263	280	254	291	274	212	87	75							4859	4804	4071			
100	3118	262	272	280	253	290	273	210	86	75	255	275	270	250	225	220	4847	4765	3918	2960		242
	3118	261	270	279	252	288	272	208	86	75							4835	4726	3765			
	3573	261	276	291	261	298	286	219	87	75							4631	4467	3397			
120	3544	260	274	288	258	296	284	217	87	74	265	295	270	260	255	235	4426	4247	3176	2320		132
	3516	259	273	285	256	293	281	215	87	74							4221	4027	2954			
	3942	261	279	297	271	304	294	222	86	73							4047	3885	2925			
140	3938	260	278	294	267	302	292	220	86	62	265	300	280	275	270	255	4042	3879	2876	2220		106
	3935	259	276	292	263	299	289	219	86	71							4037	3873	2828			

Table A10. 40% WF/15% LDPE/45% AC-6 (regrind twice), die valve partially open (10-1/2 turns).

RPM	Power	T_1	T_2	T_3	T_4	T_5	T_6	T_7	T_8	T_9	T_{b1}	T_{b2}	T_{b3}	T_{b4}	T_{b5}	T_{b6}	P_1	P_2	P_3	P_4	P_{die}	Output
l/min	watts	- - - - - - - - - - - - - - - - - - °F - - - - - - - - - - - - - - - - - -															- - - - - psi - - - -					g/min
	2138	390	373	403	360	434	370	190	89	85							764	985	817	410		150
40	2116	383	368	392	343	409	336	188	87	83	330	390	380	335	285	240	484	646	584	390		128
	2104	374	359	379	325	382	304	187	85	81							230	442	348	370		105
	2364	372	355	373	316	369	293	192	86	82							1371	1464	1312	1100	30	150
60	2343	370	352	369	312	363	289	190	86	82	325	345	330	275	245	230	1298	1446	1254	1055	30	148
	2322	368	350	365	308	357	285	188	86	81							1225	1428	1196	1010	30	145
	2702	364	345	356	298	343	276	199	87	82							2262	2332	2029	1850	71	190
80	2692	360	340	349	290	333	272	197	86	81	315	325	295	245	235	230	1890	2017	1728	1570	47	169
	2684	357	335	343	283	323	268	193	85	80							1476	1648	1387	1220	30	160
	2906	353	330	335	276	314	266	204	85	80							2794	2825	2448	2020	91	172
100	2948	350	325	329	272	308	265	202	85	79	300	300	280	235	230	225	2415	2542	2147	1740	61	159
	2974	347	321	324	268	303	264	200	85	79							1999	2097	1807	1550	41	130
	3322	341	320	321	266	299	278	212	85	80							4218	3973	3606	2460	125	360
120	3137	377	314	316	262	296	262	210	85	78	290	300	280	250	250	240	2851	2946	2460	1888	108	239
	2907	330	307	307	254	290	267	206	85	77							1528	1642	1363	1080	63	125

Table A11. 40% WF/15% LDPE/45% AC-6, die valve removed.

RPM	Power	T_1	T_2	T_3	T_4	T_5	T_6	T_7	T_8	T_9	T_{b1}	T_{b2}	T_{b3}	T_{b4}	T_{b5}	T_{b6}	P_1	P_2	P_3	P_4	P_{die}	Output
l/min	watts	°F															psi					g/min
40	1682	348	291	300	255	291	250	164	85	81							62	142	26	10		137
60	2323	344	275	284	237	270	238	173	83								52	140	14	10		196
80	2538	340	254	265	218	249	236	182	85	84							52	135	14	10		248
100	2750	336	240	244	202	233	234	188	86	84							51	130	15	10		285
120	3369	334	228	230	195	225	237	194	86	83							48	120	22	10		328
140	405	331	223	224	193	223	241	198	86	84							51	112	32	10		555

Table A12. 100% Vacuum bottoms, fresh, die valve fully open, heaters off.

RPM	Power	T_1	T_2	T_3	T_4	T_5	T_6	T_7	T_8	T_9	T_{b1}	T_{b2}	T_{b3}	T_{b4}	T_{b5}	T_{b6}	P_1	P_2	P_3	P_4	P_{die}	Output
l/min	watts								°F										psi			g/min
	2746	306		302	294	304	270	202		88							38	197	422	890	64	400
40	2683	304		296	287	298	268	199		87							35	185	336	830	60	383
	2615	302		290	287	293	265	197		86							30	174	261	770	55	355
	4040	290		283	282	314	381	220		91							70	343	936	1600		875
60	3900	288		280	278	306	272	195		89	223	237	241	236	226	199	18	301	730	1295		755
	3794	287		277	274	301	266	160		86							11	272	585	970		675
	4097	285		277	273	289	281	239		89							16	340	757	1500		700
80	3712	284		275	270	287	281	238		89							14	270	573	1300		649
	2927	283		272	268	286	280	236		88							11	216	235	1100		575
	3948	278		298	287	287	268	197		87							39	348	628	6000	72	625
60	3650	277		284	277	285	264	180		87	232	236	236	238	226	184	30	291	592	2652	50	550
	3374	276		279	271	283	261	164		86							15	266	533	1000	34	480
									Die valve partially closed													
	3072	299		281	271	290	270	223		86	223	235	238	230	201	202	2333	2686	3354	4300	74.0	325
40	3034	298		279	270	286	269	220		86							2262	2584	3271	4040	68	325
	2959	296		277	269	284	268	219		86							2177	2488	3190	3700	60	325
	3660	298		279	273	287	280	241		87	207	214	231	235			4829	4670	4645	5000	77	455
60	3100	297		279	270	286	275	237		87							3532	3781	3882	4240	60	292
	2669	296		278	268	284	270	233		86							2607	2874	3437	3900	48	55
	4582	284		272	266	284	280	235		86							2105	2343	2836	5000		710
80	4259	283		271	265	282	274	221		35							1236	1537	2060	2842		660
	3937	281		270	265	279	268	211		84							907	1227	1693	2200		600
	4575	287		272	268	286	284	244		85							1950	1984	2394	2400		685
90	4348	283		272	267	285	283	240		84							1410	1616	1996	2200		665
	4122	282		271	266	284	281	237		84							830	1182	1503	2000		65

Table A13. 100% VB-2, fresh, die valve fully then partially open.

RPM	Power	T_1	T_2	T_3	T_4	T_5	T_6	T_7	T_8	T_9	T_{b1}	T_{b2}	T_{b3}	T_{b4}	T_{b5}	T_{b6}	P_1	P_2	P_3	P_4	P_{die}	Output
l/min	watts	- °F -															- - - - - psi - - - - -					g/min
	2748	312	127	281	278	301	276	167		68							29	144	72			350
40	2450	307	126	276	271	292	260	163		65							28	135	65			347
	2256	290	125	264	256	275	235	161		64							28	131	50			345
	2971	313	-	286	274	294	260	198		86							2408	2494	2855			375
40	2648	303		276	267	290	260	171		86							790	1590	1670			353
	2256	290		264	256	276	259	164		85							690	925	817			325
	2894	286		275	280	301	279	192		90							1351	1631	1808	2200		400
40	2815	285		275	272	290	272	187		88	223	254	242	237	220	201	913	1230	1358	2195		387
	2661	284		269	260	276	254	179		86							576	830	909	2190		375
	3324	285		268	265	284	262	215		86							1663	2043	2474	3200		495
50	3258	284		266	262	281	262	208		86							625	1970	2348	2805		452
	3133	284		264	260	278	262	207		85							606	1905	2275	2470		435
	3426	284		260	255	272	263	236		86							2478	2682	3161	3490		475
60	3309	283		259	254	271	262	230		86	207	210	220	236	233	215	2299	2525	2916	3253		462
	3190	283		259	253	270	261	229		85							1995	300	2788	3040		450

Table A14. 100% VB-1 (coarse), die valve partially open (10-1/2 turns).

RPM	Power	T_1	T_2	T_3	T_4	T_5	T_6	T_7	T_8	T_9	T_{b1}	T_{b2}	T_{b3}	T_{b4}	T_{b5}	T_{b6}	P_1	P_2	P_3	P_4	P_{die}	Output
l/min	watts	- - - - - - - - - - - - - - - - - - °F - - - - - - - - - - - - - - - - - -															- - - - - psi - - - - -					g/min
	2894	285		278	280	301	279	198									1385	1667	1910	2440		400
40	2815	284		276	276	296	272	188			223	254	242	237	220	201	980	1248	1410	2277		387
	2661	284		273	271	292	266	179									576	830	909	2190		375
	3324	285		268	265	284	262	225									1736	2043	2474	3200		450
50	3214	284		265	258	279	260	218	8614	85.0							1653	1986	2351	2807		442
	3085	284		262	247	274	252	213									1606	1905	2246	2470		435
	3387	284		260	225	271	263	236		86							2478	2682	3162	3490		475
60	3231	283		260	255	270	262	234		86	207	210	220	236	233	215	2295	2600	2922	3202		460
	3117	283		259	254	270	262	232		85							2168	2556	2796	2900		445

Table A15. 10% WF, 90% VB-1, die valve fully open.

RPM	Power	T_1	T_2	T_3	T_4	T_5	T_6	T_7	T_8	T_9	T_{b1}	T_{b2}	T_{b3}	T_{b4}	T_{b5}	T_{b6}	P_1	P_2	P_3	P_4	P_{die}	Output
l/min	watts	- °F -															- - - - - psi - - - - -					g/min
	2488	297		377	344	329	379	190									68	283	197	70		350
40	2463	297		359	336	328	353	185	86.4	86.3	269	266	279	285	257	161	36	234	136	60		348
	2440	296		343	328	325	325	181									20	208	100	40		345
	2916	298		319	310	318	387	202		84							13	188	146	200		475
60	2893	296		314	305	314	282	200		84							13	186	140	195		458
	2870	295		310	300	310	376	199		84							13	184	135	190		450

Table A16. 10% WF, 90% VB-1, die valve partially open (10-1/2 turns).

RPM	Power	T_1	T_2	T_3	T_4	T_5	T_6	T_7	T_8	T_9	T_{b1}	T_{b2}	T_{b3}	T_{b4}	T_{b5}	T_{b6}	P_1	P_2	P_3	P_4	P_{die}	Output
l/min	watts	- - - - - - - - - - - - - - - - - - °F - - - - - - - - - - - - - - - - - -															- - - - - - psi - - - - -					g/min
	2809	298		281	271	283	256	207		84							1735	1974	2258	2700		300
40	2736	297		276	268	281	255	203		83	217	235	230	224	211	208	1487	1711	1928	2550		294
	2689	297		269	264	278	254	199		81							1267	1487	1642	2280		285
	3552	297		272	261	274	260	225		84							2329	2627	2986	3690		450
60	3376	296		270	260	273	258	219		83							2288	2615	2930	3273		441
	3246	296		269	259	271	255	211		82							2229	2597	2885	2930		435
	4042	296		267	259	272	265	236		82							2668	2842	3220	3360		550
80	4020	296		266	258	266	263	233		82	217	214	234	228	228	217	2626	2814	3148	3145		538
	3997	295		266	258	259	261	230		82							2585	2786	3076	2930		525

Table A17. 45% WF/55% VB-1, die valve partially open (9-1/2 turns).

RPM	Power	T_1	T_2	T_3	T_4	T_5	T_6	T_7	T_8	T_9	T_{b1}	T_{b2}	T_{b3}	T_{b4}	T_{b5}	T_{b6}	P_1	P_2	P_3	P_4	P_{die}	Output
l/min	watts	- °F -															- - - - - psi - - - - -					g/min
	2922	346		370	332	347	308	214		89							1625	4121	3920	1370		189
40	2695	342		348	330	345	300	202		89							1430	2159	1791	700		133
	2555	339		340	329	344	296	189		87							1270	1295	823	300		100
	3750	354		353	342	347	304	288		89							3193	3024	2691	4180		210
60	3476	349		348	339	343	299	265		88							2674	2576	2175	2055		167
	3189	344		341	332	340	292	232		85							1776	1804	1252	1200		150
	4258	359		364	352	354	308	316		88							3979	3257	3117	2400		275
80	4128	357		358	347	349	304	306		86							2935	2731	2314	1457		209
	3928	354		354	343	346	301	297		84							2145	2079	1597	700		135

Table A18. 50% WF, 50% VB-1, die valve fully open.

RPM	Power	T_1	T_2	T_3	T_4	T_5	T_6	T_7	T_8	T_9	T_{b1}	T_{b2}	T_{b3}	T_{b4}	T_{b5}	T_{b6}	P_1	P_2	P_3	P_4	P_{die}	Output
l/min	watts	- - - - - - - - - - - - - - - - - - °F - - - - - - - - - - - - - - - - - -															- - - - - - psi - - - -					g/min
	3583	371	336	368	367	390	357	224									811	1055	905	840		250
50	3514	360	332	364	365	389	353	208	88.3	87.0	290	327	323	321	306	278	763	1013	874	687		218
	3392	351	329	360	364	388	350	193									726	972	849	460		200
	4629	376	354	379	366	382	370	302									984	1177	1313	1390		285
60	4209	374	351	375	361	376	362	291		85	297	348	328	328	328	328	944	1161	1139	1287		275
	3773	373	349	369	355	371	352	277									865	1152	1031	1210		265
	4420	378	352	386	380	396	380	271									607	906	549	470		305
70	4095	378	348	380	376	393	374	254	89.3	88.0							674	869	523	430		281
	3859	378	343	374	371	390	366	237									649	844	497	400		259
	4512	384	366	401	392	407	392	305									698	911	680	480		344
80	4257	382	363	397	389	405	389	296	87.4	87.0	297	338	338	356	355	327	668	859	560	443		335
	4001	379	359	393	386	402	386	288									644	830	481	400		328
	5962	398	379	416	407	421	411	332									835	1064	871	470		397
90	5462	395	375	412	403	417	405	324		83							748	973	730	455		380
	4952	391	372	408	400	414	400	314									689	898	625	440		362

Table A19. 50% WF, 50% VB-1, die valve partially open (9 turns).

RPM	Power	T_1	T_2	T_3	T_4	T_5	T_6	T_7	T_8	T_9	T_{b1}	T_{b2}	T_{b3}	T_{b4}	T_{b5}	T_{b6}	P_1	P_2	P_3	P_4	P_{die}	Output
l/min	watts	- - - - - - - - - - - - - - - - - - °F - - - - - - - - - - - - - - - - - -															- - - - - - psi - - - -					g/min
	3902	384	388	423	421	447	422	342	88.8	87.1							1929	2281	2778	3950		240
40	3639	378	385	422	420	445	418	338	88.7	87.0	348	368	379	374	352	342	1840	2237	2588	3462		262
	3273	370	380	421	419	443	415	331	88.6	86.8							1759	2206	2168	3040		285
	4934	396	390	424	419	441	424	369									1662	2199	2805	3220		295
50	4813	393	389	422	417	440	420	362	87.6	86.0	298	347	348	381	371	341	1596	2125	2694	3110		311
	4713	389	389	421	416	439	413	346									1544	2064	2547	2950		355

Table A20. 50% WF, 50% VB-2, die valve partially open (9 turns).

RPM	Power	T_1	T_2	T_3	T_4	T_5	T_6	T_7	T_8	T_9	T_{b1}	T_{b2}	T_{b3}	T_{b4}	T_{b5}	T_{b6}	P_1	P_2	P_3	P_4	P_{die}	Output
l/min	watts	- - - - - - - - - - - - - - - - - - °F - - - - - - - - - - - - - - - - - -															- - - - - psi - - - -					g/min
	4539	396	369	406	385	402	399	300									1351	2019	3167	4800	182	
40	4268	386	365	401	382	395	396	252	84.3	83.7	305	350	322	340	340	312	1098	1730	2639	4200	145	352
	4021	376	362	395	377	385	390	202									766	1357	2240	3770	96	
	4525	414	368	397	388	409	398	343									1208	1695	2231	3090	98	
50	4418	410	366	396	386	407	397	333	88.2	87.1							1108	1580	2010	2627	87	375
	4288	403	364	394	383	405	396	321									1051	1498	1837	2390	67	

Table A21. 50% WF, 50% VB-2, die valve partially open (9-1/2 turns)

RPM	Power	T_1	T_2	T_3	T_4	T_5	T_6	T_7	T_8	T_9	T_{b1}	T_{b2}	T_{b3}	T_{b4}	T_{b5}	T_{b6}	P_1	P_2	P_3	P_4	P_{die}	Output
l/min	watts	- - - - - - - - - - - - - - - - - - °F - - - - - - - - - - - - - - - - - -															- - - - - psi - - - - -					g/min
	4680	432	416	446	446	470	438	346									1690	2661	3211	4040		340
40	4344	413	393	445	435	459	428	304	86.8	86.1	370	388	392	395	365	325	1911	2406	3010	3742		310
	4147	390	288	444	413	439	411	243									2237	2174	2570	3410		280
	4787	410	452		445	468	438	366														335
50	4648	404	434		442	464	437	366	88.4	87.0							2424	2796	2967	3000		318
	4509	399	415		439	461	436	365														310

Table A22. 45% WF, 45% VB-1, die valve fully open.

RPM	Power	T_1	T_2	T_3	T_4	T_5	T_6	T_7	T_8	T_9	T_{b1}	T_{b2}	T_{b3}	T_{b4}	T_{b5}	T_{b6}	P_1	P_2	P_3	P_4	P_{die}	Output
l/min	watts	- °F -															- - - - - psi - - - -					g/min
	3195	375		328	316	319	303	226									552	809	1030	800	348	275
40	3889	368		326	313	316	296	217	89.4	89.2	261	259	249	248	238	213	481	702	535	200	316	214
	2725	363		324	310	312	292	203									422	633	293	0	286	165
	3307	380		332	317	320	293	241		91							499	655	337	60	216	310
60	3262	378		331	317	319	292	232		90	274	265	254	250	241	228	430	541	275	20	211	281
	3212	377		329	316	319	291	226		90							353	481	223	0	202	210
	4685	406		328	318	320	278	235		90							389	343	82	0	121	250
80	4087	400		327	316	319	273	204		89	256	262	257	237	228	195	338	305	69	0	105	235
	3401	391		326	314	318	270	179		88							272	265	55	0	90	200

APPENDIX B

CALCULATIONS OF THE MODIFIED BRINKMAN NUMBER

APPENDIX B

CALCULATIONS OF THE MODIFIED BRINKMAN NUMBER

Numerical calculations of the modified Brinkman Number are given for two case studies and the results were discussed in Part 3, Section 3.2.3. The two cases were: (1) LDPE, (2) 40 wt. % wood flour and 60 wt. % of a mixture of LDPE (25 wt. %) and AC6 PE (75 wt. %).

Case 1

Extrusion of polyethylene at 370°F using some data from the literature (Glanvil, 1971, p. 43 and p. 66):

N	=	100 rpm
k	=	8×10^{-4} cal/cm^2-s-°C/cm
	=	4.18×10^{-2} lb$_f$/s-°F
n	=	0.57
b	=	0.0118^{K-1}
B	=	0.0775 in
U_z	=	9.17 in/s

The shear rate at 100 rpm is:

$$\dot{\gamma} = \frac{\pi DN}{B} = \frac{\pi(1.75)(1.67)}{0.0775} = 118.5\ s^{-1}$$

The viscosity for LDPE at this shear rate is:

$$K_b = 2.6x10^6\ \frac{dyne}{cm^2}\ \frac{1}{118.5\ s^{-1}} = 2.19x10^4\ poise$$

$$K_{b_{corr}} = (2.19x10^4)\left[\frac{(4)(0.57)}{3(0.57)+1}\right] = 1.84x10^4\ poise$$

$$= 38.43\ \frac{lb_f\text{-}s}{ft^2}$$

$$= 0.267 \quad lb_f/in^2$$

$$\beta = 0.0118°K^{-1} \left| \frac{0.267\, lb_f\text{-}s}{in^2} \right| \frac{(9.18in)^{0.57+1}}{s^2} \left| \frac{s\text{-}°F}{4.18HO^{-2}lb_f} \right| \frac{1°K}{1.8°F} \left| \frac{1}{(0.0775in)^{-0.43}} \right.$$

$$= \frac{(0.0118)(0.267)(32.5)}{(4.18x10^{-2})(1.8)} (0.333)$$

$$= 4.53x10^{-2} = 0.453$$

Case 2

Extrusion of 40% wood flour/60% (25% LDPE, 75% AC6 PE), using experimental data generated at the University of Arizona and the University of Lowell (White et al. 1981).

N	=	100 rpm
k_{PE}	=	$8x10^{-4}$ cal/cm^2-s-°C/cm
	=	$4.18x10^{-2}$ lb$_f$/s-°F
$k_{wood\ flour}$	=	$43x10^{-4}$ cal/cm^2-s-°C/cm
n	=	0.43
b	=	0.056°K^{-1}
B	=	0.0775 in
U_z	=	9.18 in/s

For the slurry, the thermal conductivity is estimated by a rule of mixtures as:

k_s	=	$(0.60)(8x10^{-4}) + (0.4)(43x10^{-4})$
	=	$22x10^{-4}$ cal/cm^2-s-°C/cm
	=	$115x10^{-3}$ lb$_f$/s-°F

One must also estimate the viscosity of the slurry in the screw channel. From an experimental run, the viscosity of a 40% slurry was found to be

$$20x10^{-4} \frac{lb_f\text{-}s}{in^2}$$

at a shear rate of 7235 s^{-1}.

The viscosity in the metering section is:

$$K_b = 20x10^{-4} \left|\frac{118.5}{7235}\right|^{0.43-1} = 2.08x10^{-2}\ \frac{lb_f\text{-}s}{in^2}$$

Thus:

$$\beta = 0.056°K^{-1} \left|\frac{2.08x10^{-2}lb_f\text{-}s}{in^2}\right| \left|\frac{9.18in)^{0.43+1}}{s^2}\right| \left|\frac{s\text{-}°F}{115x10^{-3}lb_f}\right| \left|\frac{1°K}{1.8°F}\right| \frac{1}{(0.0775in)^{-0.43}}$$

$$= \frac{(0.56)(2.08x10^{-2})(9.18)^{1.43}}{(115x10^{-3})(1.8)(0.0775)^{-0.57}} = 0.031$$

APPENDIX C

CALCULATION FOR SCALE-UP FOR EXTRUDER-FEEDER

APPENDIX C

CALCULATION FOR SCALE-UP FOR EXTRUDER-FEEDER

The experimental data on the extruder-feeder and those experimental results on which this scale-up was based are as follows:

N	= 40 rpm	P_4	= 6,470 psi
D_b	= 1.75"	P_1	= 5,020 psi
θ	= 17.7°	T	= 367°F = 457°K
W	= 1.67"	ΔZ	= 12.5"
H	= 0.078"	ρ	= 0.77 g/cc
F_d	= 0.95	Q	= 175 g/min

Calculation of F_p

Using the above data and the appropriate conversion factors we obtain

$$F_p = \left(\frac{Q}{0.77 \cdot 28317 \cdot 60} - \frac{\pi}{2} \cdot \frac{N}{60} \cdot \frac{1.75}{12} \cdot 0.95 \cdot \frac{1.67}{12} \cdot \frac{0.078}{12} \cdot 0.9\right)$$

$$x \; \frac{12\mu \; \frac{12.5}{12}}{\frac{1.67}{12} \cdot \left(\frac{0.078}{12}\right)^3 \cdot \Delta P}$$

$$F_p = (7.64x10^{-7} Q - 2.95x10^{-6} N) \; x \; 3.271 \; x \; 10^8 \frac{\mu}{\Delta P}$$

where Q is in g/min, N is in RPM, β is in $lb_f \cdot s/ft^2$, and $\Delta P = lb_f/ft^2$.

Calculate ΔP

ΔP = (6470-5020) = 1450 psi
= 208800 lb_f/ft^2

Calculate μ

First we have to calculate the shear rate $\dot{\gamma}$

$$\dot{\gamma} = \frac{\pi DN}{H} = \frac{\pi \cdot 1.75 \cdot 40}{0.078 \cdot 60} = 45.8 s^{-1}$$

From $\dot{\gamma}$ we calculate $E_{\dot{\gamma}}$ by equation

$$\dot{\gamma} = 2.025 x 10^{7} e^{-1.669 E_{\dot{\gamma}}}$$

and we get $E_{\dot{\gamma}} = 7{,}800$ cal/g moles

For T = 457°K we calculate μ by the equation

$$\mu = 548.85 \exp(E_{\dot{\gamma}}/RT)$$

$$= 548.85\ e^{\frac{7800}{1.987 \cdot 457}} = 2.95 x 10^{6}\ cp$$

$$= 2.95 x 10^{6} \cdot 2.089 x 10^{-5} = 61.6\ \frac{lb_f s}{ft^2}$$

Substituting in Equation 8 for Q, N, μ, and ΔP we get $F_p = 1.53$.

Alternative Method of Calculating Viscosities

Using Equation 3.17:

$$\mu = \frac{Kd \cdot \Delta P}{Q}$$

A sample calculation will be made for one case of vacuum bottoms. Virgin vacuum bottoms and 10.5 closure turns on die valve.

N	=	40 RPM
Q	=	365 g/min
P	=	1101 psi
o	=	1.2 g/cm^3
K_d	=	0.00033 cm^3

Using these values and the appropriate conversion factors we obtained:

$$\mu = K_d \frac{\Delta P}{Q} = \frac{0.00033}{38317} \cdot \frac{\frac{1101 \cdot 144}{365}}{1.2 \cdot 28317 \cdot 60}$$

$$= 21.5 \frac{lb_f s}{ft^2} = 1{,}030{,}000\ cp$$

Numerical Example for Calculating ΔP_{max}

$$\Delta P_{max} = \frac{6\pi \cos\theta_b N D_b \mu l}{H^2 \sin\theta}$$

$$\frac{6 \cdot 0.95\ 1 \cdot \frac{1.75}{12} \cdot 100{,}000 \cdot 1.4504 x 10^{-7} (\frac{15}{12})}{0.29 \cdot (\frac{0.082}{12})^2}$$

$$= 3496\ psi$$

where:

θ	=	$\frac{\theta_b + \theta_s}{2}$; Assume $\theta_b = \theta_s = \theta = 17.7°$
N	=	60
RPM	=	1 rps
D_b	=	1.75"
μ	=	100,000 C_p
1 cp	=	1.4504 10^{-7} $\frac{lb_f s}{in^2}$
l	=	15"
H	=	0.082"

Calculation of Temperature Rise (ΔT) Due to Viscous Dissipation

In this case we calculate the ΔT obtained due to viscous dissipation and then P_{wvs}, the power needed for that purpose.

The data used were obtained from our experimental work as follows:

B	=	-0.39 cm^3
A	=	5.05 cm^3
K	=	0.00033 cm^3
C_p	=	0.75 cal/g°C
ρ	=	0.77 g/cm^3
N	=	40 rpm
Z	=	15"
b	=	4254°K
μ	=	61.6 $\frac{lb_f s}{ft^2}$

The ΔT we calculate as follows:

$$Evaluate \quad N_1 = \frac{B}{K} = \frac{-0.39}{0.00033} = -1182$$

$$Evaluate \quad N_2 = \frac{A \rho C_p}{NZ\mu_Q b E}$$

where:

$$b = -\frac{E_{\dot{\gamma}}}{R T^2} = \frac{4254\ °K}{T^2}$$

for

$E_{\dot{\gamma}}$	=	8.453
T	=	457°K

and

$$E = \frac{\pi^3 D^3 \sin\theta}{H + \delta_f}(1 + 3\cdot\sin^2\theta)$$

δ = clearance distance

$$E = \pi^3 \frac{1.75^3 \cdot 0.30 \cdot 12}{12^3 \cdot (0.0078 + 0.0030)}(1 + 3 \cdot 0.09) = 4127$$

Substituting in equation for N_2 we get:

$$N_2 = \frac{5.05 \cdot 0.77 \cdot 0.75}{\frac{40}{60} \cdot \frac{15}{12} \cdot 61.6 \frac{4254}{4572}} \frac{f_1}{f_2} = 1.95$$

$$f_1 = \frac{1}{252}\ Btu/cal$$

$$f_2 = \frac{1}{778}\ Btu/ft.lb_f$$

N_1 = 0
N_2 = 1.95

We obtain from the correlation between X and N_1 and N_2 by Middlemen (1977):

X = 1.5

From the Equation $X = e^{b\Delta t}$ or, $\log X = b\Delta t$

$$\Delta T = \frac{\log X}{b} = \frac{\log 1.5}{\frac{4254}{4572}} = 19.9°C$$

Calculation of Power Required for Viscous Dissipation

The power used for the viscous dissipation P_{wvs} can be calculated using equation:

$$P_{wvs} = QC_p\Delta T$$

where:

ΔT = temperature rise due to the viscous dissipation and Q, and C_p are the same as in the energy balance calculation.

P_{wvs} = $195 \cdot 0.75 \cdot 19.9 = 2910$ cal/min $= \frac{2910}{252.60} = 0.19$ Btu/s $= 0.9 \cdot 1054.35 = 203$ Watts $= 0.272$ Hp.

Reference

Middleman, S., "Fundamentals of Polymer Processing," McGraw-Hill, New York, NY (1977).

DISTRIBUTION

No. of Copies

OFFSITE

12 DOE/Office of Scientific and Technical Information

R. Annan
Office of Solar Energy Conversion
U.S. Department of Energy
Forrestal Building (CE-13)
1000 Independence Avenue
Washington, D.C. 20585

J. Allsup
Office of Alternative Fuels
U.S. Department of Energy
Forrestal Building (CE-33)
1000 Independence Avenue
Washington, D.C. 20585

W. Ayres
Pyrotech, Inc.
8016 Stateline
Suite 101
Leawood, KS 66208

S. Babu
Institute of Gas Technology
IIT Center
3424 South State Street
Chicago, IL 60616

P. Badger
Southeastern Regional Biomass Energy Program
Tennessee Valley Authority
CEB 4W 436A-M
Muscle Shoals, AL 35660

N. Banns
Onsite*Ofsite, Inc.
2500 East Foothill Blvd.
Suite 201
Pasadena, CA 91107

No. of Copies

K. Birkinshaw
California Energy Commission
1516 - 9th Street, MS-43
Sacramento, CA 95814

H. Clark
American Society of Mechanical Engineers
1825 K Street N.W., Suite 216
Washington, D.C. 20006-1202

R. Costello
Biofuels Systems Division
U.S. Department of Energy
Forrestal Building (CE-331)
1000 Independence Avenue
Washington, D.C. 20585

J. Diebold
Solar Energy Research Inst.
1617 Cole Blvd.
Golden, CO 80401

K. Durai-Swamy
Manufacturing and Technology Conversion International, Inc.
13080 Park Street
Santa Fe Springs, CA 90670

V. Flanigan
223 Engineering Research Lab.
University of Missouri-Rolla
Rolla, MO 65401

G. Fleischman
Bureau of Energy
Idaho Department of Water Resources
1301 N. Orchard St.
Boise, ID 83706

No. of
Copies

P. Fox
Pacific Northwest and Alaska
Regional Biomass Energy
Program
Bonneville Power
Administration
P.O. Box 3621
Portland, OR 97208

S. Friedrich
Waste Material Management
Division
U.S. Department of Energy
Forrestal Building (CE-222)
1000 Independence Avenue
Washington, D.C. 20585

B. Goodman
Solar Energy Research
Institute
1617 Cole Blvd.
Golden, CO 80401

S. Gronich
Solar Thermal & Biomass Power
Division
U.S. Department of Energy
Forrestal Building (CE-132)
1000 Independence Avenue
Washington, D.C. 20585

J. Hamrick
Aerospace Research Corporation
5454 Jae Valley Rd., S.E.
Roanoke, VA 24014

W. Densmore Hunter
Manager, Energy Technology
Department
Weyerhaeuser Company
WTC-1B-30
Tacoma, WA 98477

J. Kadyszewski
Winrock International
611 Kent St. Suite 600
Arlington, VA 22209-2134

No. of
Copies

J. Kerstetter
Washington State Energy Office
State of Washington
809 Legion Way S.E., ER-11
Olympia, WA 98504-1211

D. Kirchgessner
Global Warming Control Branch
U.S. Environmental Protection
Agency
Research Triangle Park, NC
27711

D. Klass
Institute of Gas Technology
IIT Center
3424 South State Street
Chicago, IL 60616

F. Kuzel
Council of Great Lakes
Governors
310 South Michigan Ave.
Chicago, IL 60604

E. Larson
Center for Energy and
Environmental Studies
Engineering Quadrangle
Princeton University
Princeton, NJ 08544-5263

M. Mansour
Manufacturing & Technology
Conversion International,
Inc.
P.O. Box 21
Columbia, MD 21044

P. Mathusa
Program Director
New York State Energy Research
and Development Authority
2 Rockefeller Plaza
Albany, NY 12223

No. of Copies

T. Miles
Consulting Engineer
5475 S.W. Arrowwood Lane
Portland, OR 97225

T. Milne
Solar Energy Research Institute
1617 Cole Blvd.
Golden, CO 80401

R. Moorer
Biofuels Systems Division
U.S. Department of Energy
Forrestal Building (CE-331)
1000 Independence Avenue
Washington, D.C. 20585

R. O'Connell
CONEG Policy Research Center, Inc.
400 N. Capital Street, NW
Washington, DC 20001

D. O'Neil
Georgia Tech Research Institute
Georgia Institute of Technology
Atlanta, GA 30332-0420

R. Overend
Solar Energy Research Institute
1617 Cole Blvd.
Golden, CO 80401

M. Paisley
Battelle-Columbus Division
505 King Avenue
Columbus, OH 43201

J. Roethell
Office of Critical Materials
U.S. Department of Agriculture
342 Aerospace Building
Washington, DC 20250-2200

No. of Copies

R. San Martin
Deputy Assistant Secretary
Office of Utility Technology
Forrestal Building
1000 Independence Avenue, SW
Washington D.C. 20585

M. Scheve
Solar Thermal & Biomass Power Division
U.S. Department of Energy
Forrestal Building (CE-132)
1000 Independence Avenue
Washington, DC 20585

G. Simons
California Energy Commission
1516 - 9th Street, MS-43
Sacramento, CA 9581

S. Sobczynski
Division of Improved Energy Productivity
U.S. Department of Energy
Forrestal Building CE-231
1000 Independence Avenue
Washington, DC 20585

D. Stevens
Cascade Research, Inc.
2952 George Washington Way
Richland, WA 99352

C. Sullivan
Electric Power Research Institute
P. O. Box 10412
Palo Alto, CA 94303

D. Swanson
Western Regional Biomass Energy Program
Western Area Power Administration
P.O. Box 3402
Golden, CO 80401

No. of Copies

E. Taylor
Corporate Manager,
Energy & Environmental Affairs
Louisiana-Pacific Corporation
P.O. Box 158
Samoa, CA 95564

C. Wallace
Solar Energy Research Institute
409 12th St. S.W., Suite 710
Washington, DC 20024

D. Walter
Waste Material Management Division
U.S. Department of Energy
Forrestal Building (CE-222)
1000 Independence Avenue
Washington, D.C. 20585

E. Wan
Science Applications International Corporation
1710 Goodridge Drive
McLean, VA 22102

25 D. White
Department of Chemical Engineering
University of Arizona
Geology Building
Tucson, AZ 85721

R. Williams
Center for Energy and Environmental Studies
Princeton University
Princeton, NJ 08544

No. of Copies

FOREIGN

D. Asplund
Valtion Teknillinen Tutkimuseskus
Statens Tekniska Forskningscentral
Technical Research Centre of Finland
P.O. Box 221
SF-40101 Jyvaskyla 10
FINLAND

T. Bridgwater
The University of Aston in Birmingham
Dept. of Chemical Engineering
Gosta Green
Birmingham
ENGLAND B4 7ET

J. Fredriksson
Department of Thermal Engineering
The Royal Institute of Technology
S-100 44 Stockholm,
SWEDEN

E. Rensfelt
Department of Fuel Technology
Studsvik Energiteknik AB
S-611 82 Nykoping,
SWEDEN

ONSITE

DOE Field Office, Richland

E. Norman A5-10

10 Pacific Northwest Laboratory

D. Elliott K2-40
M. Gerber P8-38
G. Schiefelbein (2) P8-38
Publishing Coordination
Technical Report Files (5)

END

DATE FILMED

01/24/92